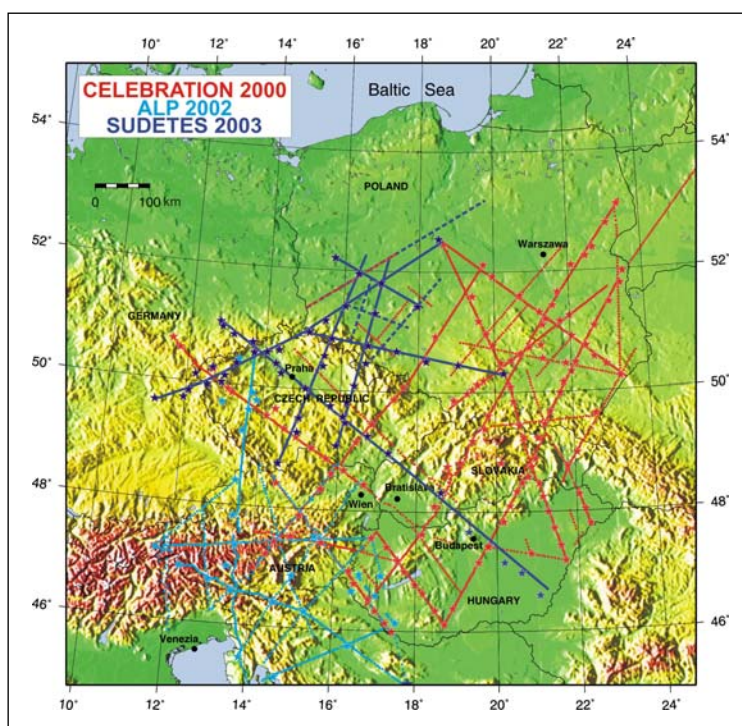Charles University in Prague
Faculty of Mathematics and Physics

PhD. THESIS

Crustal Structure of the Bohemian Massif Based on Seismic Refraction Data

RNDr. Pavla Hrubcová

Supervisor: RNDr. Václav Vavryčuk, DrSc.

January 2010

To my parents

Contents

Preface

Presented thesis includes my work over several last years during which I have been involved in the acquisition, processing and interpretation of seismic refraction data. The thesis summarizes results presented in six papers published in the impacted scientific journals. In four of them, I was the first principal author. In two other papers, I was the second and third author with the essential contribution.

The overall aim of the thesis is to interpret the seismic refraction and wide-angle reflection data and supply the answers on the crustal and uppermost mantle velocities of the Bohemian Massif. So far, the Bohemian Massif has been studied mainly to show the depth of the Moho. New insight into its deep configuration can help to complement this knowledge, determine the crustal thickness and show the velocity differences within its individual and surrounding units. The contrasts in seismic velocities together with the depth of the Moho discontinuity reflect the compositional and structural variances resulting from the crust-forming processes during tectonic development.

In all papers forming the thesis, the results are based on the interpretation of the refraction and wide-angle reflection data acquired during the CELEBRATION 2000, ALP 2002 and SUDETES 2003 seismic experiments carried out in central Europe and targeted the Bohemian Massif. Three of the papers focus on the interpretation of the data recorded along profiles. The refraction and wide-angle reflection modelling is supplemented by other methods such as the reflectivity or gravity modelling. This reduces the ambiguity of the interpretation and gives the additional constraints on seismic velocity models. The fourth paper focuses on a comparison of the results from the seismic refraction modelling with the results from other experiments, namely the receiver functions interpretation. The goal is to show and discuss the ways how to combine different methods in a complex interpretation. The last two papers in the thesis deal with the crustal anisotropy of the Bohemian Massif. The anisotropy is inferred from the seismic refraction data and its knowledge is necessary for assessing the limits of applicability of the standard isotropic approach.

Abstract

The deep structure of the Bohemian Massif, the largest stable outcrop of the Variscan rocks in central Europe, was studied using the data of the international seismic refraction and wide-angle reflection experiments CELEBRATION 2000, ALP 2002 and SUDETES 2003. The data were interpreted by seismic tomographic inversion and by 2-D trial-and-error forward modelling of the P and S waves. Above, additional constraints on the crustal structure were imposed by reflectivity or gravity modelling, and by receiver function interpretation. Knowledge of the crustal velocity structure in the Bohemian Massif was complemented by its azimuthal variation. Though consolidated, the Bohemian Massif can be subdivided into several tectonic units separated by faults, shear zones, or thrusts reflecting varying influence of the crust forming processes. The resultant velocity models determined different types of the crust-mantle transition reflecting variable crustal thickness and delimiting contacts of these tectonic units at depth.

Abstrakt

Český masív je jedním z největších souvisle vystupujících fragmentů původně rozsáhlého variského orogenu ve střední Evropě. Na základě současné koncepce deskové tektoniky je možné interpretovat Český masív jako heterogenní celek složený ze čtyř samostatných regionálních jednotek s rozdílným vývojem i tektonickým omezením vůči svému okolí. Ke studiu hlubinné stavby tohoto komplexu byla použita data z mezinárodních seismických reflexních a refrakčních experimentů CELEBRATION 2000, ALP 2002 a SUDETES 2003. Tato data byla interpetována pomocí seismické tomografie a modelována s využitím paprskových metod pro vlny typu *P* a *S*. K omezení mnohoznačnosti řešení bylo použito reflektivity, modelování tíhových účinků i interpretace s využitím dalších metod, zejména receiver function. Rozložení seismických rychlostí v kůře Českého masívu bylo studováno podél profilů i doplněno o azimutální, mimoprofilovou závislost. Výsledné rychlostní modely ukazují rozdílné mocnosti kůry i různé typy přechodu na hranici kůra–plášť, což umožňuje vymezit kontakt jednotlivých jednotek ve větších hloubkách. Rozložení rychlostí pak odráží geotektonický vývoj dílčích jednotek Českého masívu.

Main theme

Crustal Structure of the Bohemian Massif Based on Seismic Refraction Data

1. Geology and tectonic settings of the Bohemian Massif

The Bohemian Massif is one of the largest stable outcrops of pre-Permian rocks in central and western Europe. It forms the easternmost part of the Variscan Belt, which developed approximately between 500 and 250 Ma during a stage of large-scale crustal convergence, collision of continental plates and microplates and possibly also subduction [*Matte et al.,* 1990]. It consists mainly of low- to high-grade metamorphic and plutonic Palaeozoic rocks. The area of the Bohemian Massif can be subdivided into various tectonostratigraphic units separated by faults, shear zones or thrusts. They trend roughly SW-NE and reflect varying influence of the Cadomian and Variscan orogenies: the Saxothuringian in the NW, the Teplá-Barrandian, the Moldanubian and the Moravo-Silesian in the SE (see Figure 1). Geographically, it comprises the area of the Czech Republic, partly Austria, Germany and Poland. It borders the Eastern Alps to the south, and submerges beneath the Carpathians to the southeast. The northern termination of the Bohemian Massif at the contact with the Palaeozoic Platform is still not well recognized. While the post-collisional history of the Variscan Bohemian Massif is relatively clear, the kinematics of plate movements before and during collision is a subject of ongoing debates.
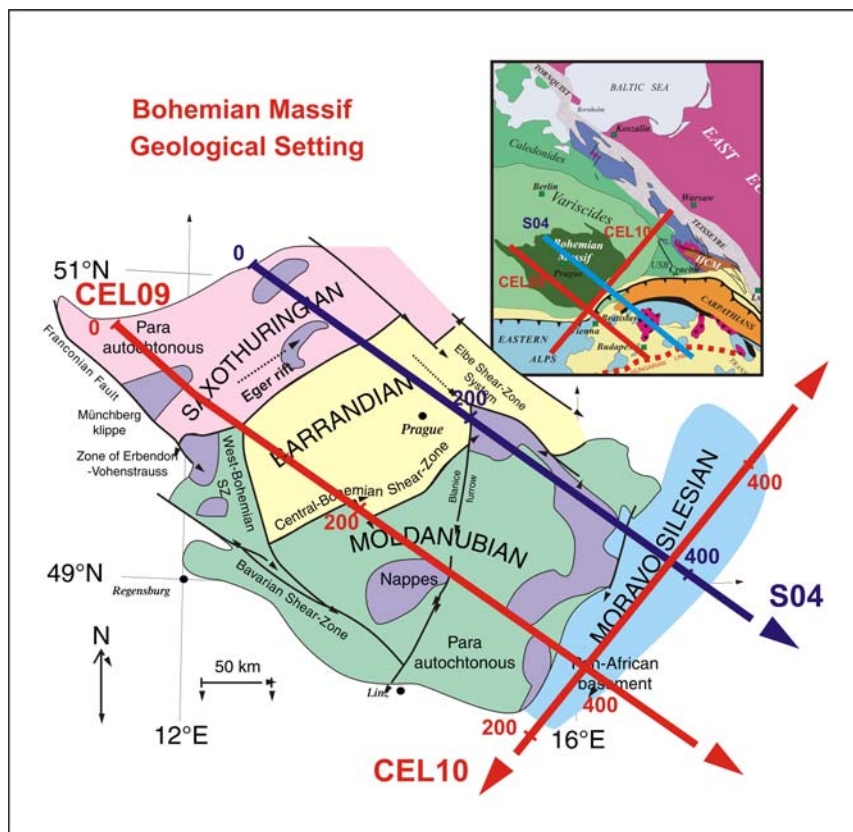

Figure 1. Major tectonic units of the Bohemian Massif and its setting within the European Variscides with the location of the profiles CEL09, CEL10, ALP04, and S04.

2. Refraction experiments

As a result of a massive international cooperative effort in central Europe, the Bohemian Massif was covered by several seismic experiments CELEBRATION 2000, ALP 2002, and SUDETES 2003. These experiments resulted in a network of seismic refraction and wide-angle reflection profiles covering not only the Bohemian Massif but extending from the East European Craton to the Bohemian Massif, through the Carpathians and the Eastern Alps to the Pannonian Basin (Figure 2). Total length of the interlocking profiles was about 16 500 km and about 230 shots were fired along most of them. All together they enabled to obtain dense ray coverage for a subsequent 3-D modelling. The shooting was both in drill holes and quarry blasts; the prevalent shot point charges in the Bohemian Massif were about 210 kg in drilled holes, shots in quarry blasts ranged from 400 kg to ~10 t. Single channel recorders were of the Texan type (RefTek 125, Refraction Technology, Inc.) and employed 4.5 Hz vertical geophones. The average distance between shots was 30 km with the average station spacing of ~3 km for the high density profiles or ~6 km for the additional low density ones. The positions of shot points and stations were measured by GPS; the origin time was controlled by a GPS-controlled blasting device. Details of the experiments are given in *Guterch et al.* [2003a], *Guterch et al.* [2003b], *Brűckl et al.* [2003], and *Grad et al.* [2003].

The data from the experiments were recorded with the sampling rate of 100 Hz in the recording time window of 300 s for each shot. For local studies (the experiment in paper **P6**), the sampling rate was increased to 250 Hz. Data processing included shot-time corrections and band-pass filtering of the whole data set (usually 2-15 Hz) in order to remove low- and high-frequency noise. Recordings were sorted into shot gathers in the SEGY format; seismic sections were trace-normalized to the maximum amplitude along the trace and cut to a length of 100 s starting at the zero reduced time.

The seismic data had, in general, a good signal-to-noise ratio and allowed several *P*-wave phases to be correlated. In the first arrivals, we could distinguish refraction from the upper/middle crust marked as the *Pg* phase, and refractions from the upper mantle marked as the *Pn*. The refracted waves from the sedimentary cover (*Psed*) were observed in a vicinity of the shot points in the east. In later arrivals, the reflections from the Moho discontinuity (*PmP*) were usually the strongest phases. In some sections, reflections from the mid-crustal discontinuities or reflections from the top of the lower crust were also visible. Clearly visible arrivals of the refracted and reflected waves from the crystalline crust and the upper mantle were typically observed up to the offsets of 250 – 300 km.

The refraction and wide-angle reflection data were analysed in the 2-D and 3-D geometry. The main 2-D profiles (Figure 2) in the Bohemian Massif showed the crustal and uppermost mantle structure together with the surrounding complexes and continuation of the tectonic units at depths. The profile CEL09 of the CELEBRATION 2000 experiment (paper **P1**) was in a favourable position to all key tectonic units of the Bohemian Massif (the Saxothuringian, the Barrandian, the Moldanubian, and the Moravo-Silesian) traversing the massif in the NW-SE direction. The SW-NE orientated line of the integrated profiles CEL10 and ALP04 (CELEBRATION 2000 and ALP 2002 experiments, respectively) dealt with the interpretation

of the crustal and uppermost mantle structure at the eastern margin of the Bohemian Massif (the Moravo-Silesian unit) and its southern and northern tectonic neighbours, the Eastern Alps and the Palaeozoic Platform, respectively (paper **P2**). The NW-SE oriented S04 profile acquired during the international SUDETES 2003 seismic experiment (paper **P4**) was parallel to the CEL09 profile at about 90 km to the north. It crossed all main tectonic units of the Bohemian Massif and showed its contact with the Carpathian orogenic belt. In the 3-D interpretation, the refraction data were analyzed to show the crustal azimuthal variations (paper **P5** and **P6**).
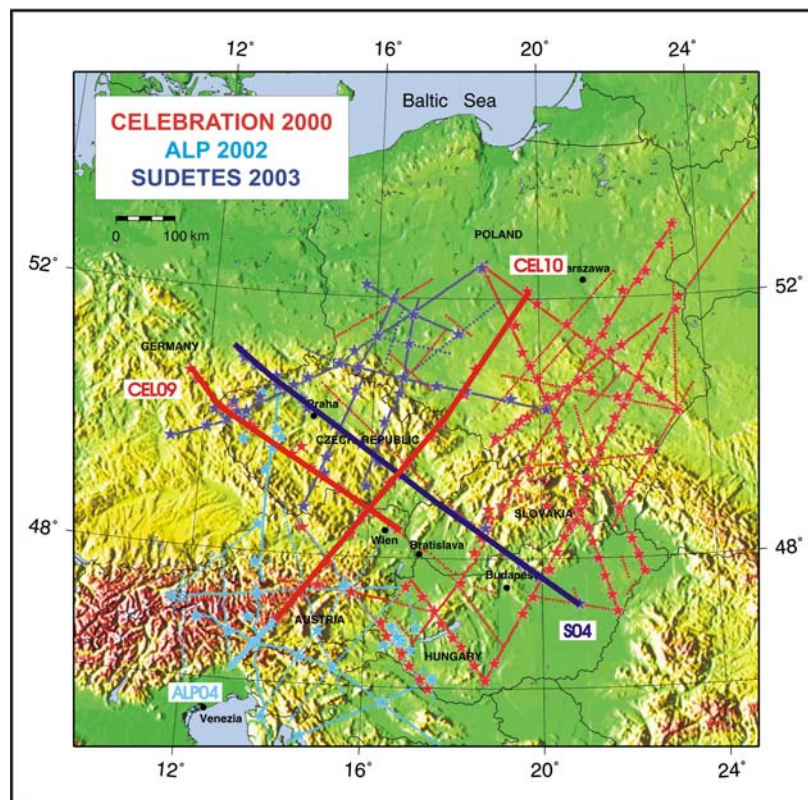

Figure 2. Geographical setting of the CELEBRATION 2000 (red), ALP 2002 (light blue), and SUDETES 2003 (dark blue) refraction experiments in central Europe. Stars mark the positions of the shot points; lines mark the positions of the receivers. The interpreted profiles CEL09, CEL10, ALP04, and S04 are highlighted.

3. Interpretation of the seismic refraction data

3.1. Modelling strategy

Modelling is an essential part of the investigation. In the modelling, a particular type of a structural model of the subsurface is chosen and then it is used to predict waveforms, which are compared with the actual waveforms recorded. The model is then adjusted to get the best fit between the predicted (modelled) and observed waveforms. The fit depends on both the signal-to-noise ratio of the waveforms and, in some cases, on the starting model used. The modelling can be done in 2-D or 3-D configurations. In the 2-D approach, the results of modelling are usually displayed as cross-sections through the structure under investigation.

In principle, the modelling of seismic data can be carried out in two possible ways. First, a new modelling and/or inversion method can be developed and tested on the existing data. Second, the existing methods can be applied to achieve results suitable for further geological/tectonic interpretations. Obviously, both approaches can be combined. Though, in either case, it is necessary to be careful about the amount and quality of the data and about the limitations, drawbacks and applicability of each method applied.

For the interpretation of the refraction and wide-angle reflection data in the Bohemian Massif we decided to follow the second concept and applied several existing methods to get the most complex knowledge of the structure. First, we applied the tomographic inversion routine of *Hole* [1992] for inverting the first P-wave arrivals for the velocity model. The stability of the inversion requires the resultant model to be sufficiently smooth. Since this condition is not fully satisfied in the crustal velocity models, the tomographic inversion was just used as a tool to determine a preliminary seismic velocity distribution in the Bohemian Massif. In the next step, the preliminary velocity distribution was further improved by applying a 2-D trial-and-error forward modelling using the ray-tracing algorithm [*Červený and Pšenčík*, 1984]. This approach exploited information on later arrivals of waves in the observed wave fields. It was applied to both the refracted and reflected P waves, and, in some parts of the massif, to the modelling of the S waves, too. Details of individual crustal blocks of the Bohemian Massif were further investigated by a modelling of the seismic wave field with the reflectivity method [*Fuchs and Müller*, 1971]. The velocity analysis was complemented by the gravity modelling. The resultant profile models were interpreted geologically, tectonically and lithologically. Such approach was adopted in the case of the profiles CEL09, CEL10 and S04 (papers **P1**, **P2**, and **P4**, respectively) where the final simplified tectonic schemes served as a basis for further integrated geophysical and tectonic analyses of the Bohemian Massif. The profile interpretations were supplemented by an analysis of the off-line data in order to study the azimuthal variations of the seismic velocities in the Bohemian Massif (discussed in papers **P5** and **P6**).

3.2. Seismic tomography of the first arrivals

In the first modelling step, we applied tomographic inversion. The tomography (from the Greek tomos "to slice" and graphein "to write") is an inverse technique of determining a velocity model from path-dependent properties such as attenuation, travel time, or source intensity [*Aster et al.*, 2005]. The tomographic inversion usually exploits techniques of geometric ray theory, which describes the high-frequency approximation of the wave equation. Consequently, wave energy travelling between a source and a receiver is assumed to propagate along narrow ray paths. The density of the ray path coverage may vary significantly throughout the area under study. Thus, it may provide much better constraints on physical properties in some densely sampled regions than in other sparsely sampled ones. The ray paths can change directions due to the refraction and/or reflection. And since these paths depend on model parameters (i.e., velocity distribution) the inverse problem is non-linear.

In papers **P1** and **P2** we applied the tomographic travel time inversion of the first *P*-wave arrivals developed by *Hole* [1992]. The essential part of the inversion was the backprojection algorithm [*Humphreys and Clayton*, 1988] based on linearization of the non-linear relation between the travel time and the slowness. The model was defined in an equidistant rectangular grid with the *Vp* velocities defined at the grid nodes. In the forward step, the travel times were calculated using a finite difference algorithm for solving the eikonal equation [*Vidale*, 1990]. In the inverse step, the slowness perturbations were calculated by uniformly distributing the travel time residuals along a ray. The perturbations were summed up for all rays, smoothed and added to the original model. The procedure was repeated iteratively until the model with a satisfactory level of the travel time residuals was obtained.

The tomographic inversion required specifying an initial 1-D model. In the Bohemian Massif, the initial 1-D model for the upper crust was calculated by inverting the average *Pg* travel time curve using the Wiechert-Herglotz formula [*Aki and Richards*, 1980]. The initial model for the lower crust and mantle was derived from smoothed average crust and mantle velocity values of *Christensen and Mooney* [1995]. The computation was usually carried out for the model grid size of 1x1 km in 5 subsequent steps, gradually enlarging the data offsets (50, 100, 150, 200 and 400 km) and thus enlarging the maximum depth of the ray penetration with several iterations at each step. The smoothing was performed by a moving average filter with the cell sizes of 40x10, 20x4 and 10x2 km. The resolution of the algorithm increased gradually and stabilized the inversion. The calculation was controlled by minimizing the root-mean-square (RMS) travel time residuals.

Due to a high near-surface velocity gradient with denser ray coverage followed by a low gradient in the middle crust, the turning points of the *Pg* rays in the crystalline rocks of the Bohemian Massif were at shallow depths. The rays concentrated in parts with high velocity gradients and left the deeper parts of the crust practically unconstrained. Thus, the middle and lower crust lacked the velocity differentiation in the tomographic model. Moreover, due to the smoothing performed during the inversion and model parameterization, the velocity discontinuities were smoothed into broad gradient zones. For this reason, the depth of the Moho boundary could not be reliably estimated from such model. In such a way, the

tomographic models served just as the approximate preliminary 2-D velocity models which had to be further improved.

3.3. Trial-and-error forward modelling using the ray tracing

As discussed above, the smooth velocity model resulting from the tomographic inversion of the first arrivals yielded only an approximate distribution of the velocities in the crust and mantle and was not sufficient to describe correctly the structure. On the other hand, variations in the amplitude, travel time and duration of both refracted and reflected seismic phases in the crust and uppermost mantle gave more constraints on the velocity differentiation and location of the seismic discontinuities. Obviously, the modelling of all phases could produce a more detailed velocity image with delineation of the reflecting interfaces, including the Moho discontinuity.

In papers **P1**, **P2**, and **P4**, we applied an iterative travel time fitting to further refine the preliminary models obtained from the tomographic inversion. We used the ray-tracing program package *SEIS83* [*Červený and Pšenčík*, 1984] supplemented by an interactive graphical interface *MODEL* [*Komminaho*, 1997] and *ZPLOT* [*Zelt*, 1994] with modifications by *Środa* [1999]. The models consisted of layers separated by velocity discontinuities. The initial velocity distributions were based on models from the tomographic inversion, the layering was derived mainly according to the reflected phases. In each layer, the *P*-wave velocity was specified in an irregular rectangular grid and interpolated by the bicubic splines. The *SEIS83* algorithm calculated ray paths, travel times and synthetic seismograms. The solution was sought iteratively; the travel times of the refracted and reflected waves were calculated for a current *Vp* model and compared with the observed travel times. Then the *Vp* model was modified in order to minimize the misfit.

This ray-tracing modelling also involved a calculation of the sections of the synthetic waveforms and a qualitative comparison of the amplitudes of synthetic and observed seismograms. Since the amplitudes of the seismic waves are very sensitive to the velocity gradients and velocity contrasts at discontinuities, the synthetic seismograms of both reflected and refracted seismic waves were used as an additional constraint on the velocity distribution.

3.4. Analysis of S waves

Some of the recorded seismic data showed a distinct *S*-wave signal for the refracted crustal phases (*Sg*) and reflected phases from the Moho (*SmS*) so that we could also apply a modelling of the *S* waves. The *S* waves were mostly interpreted in the records of the vertical component since the three-component recordings were available for a small number of stations, only. Despite, the vertical recordings of the *S* waves were usually clear enough to be interpreted as is often the case with crustal refraction data where waves propagate over large horizontal distances [see, e.g., *Thybo et al.*, 2003].

In paper **P1**, the best branches of correlated *S*-wave travel times were used for the forward modelling to provide another constraint in discriminating different tectonic areas. In the first approximation, the *S*-wave velocity models were adopted from the *P*-wave velocity models by calculating the *Vs* velocities using the standard ratio of *Vp/Vs* = 1.73 [e.g., *Christensen*, 1996]. Lack of the reflected crustal arrivals, as well as the refractions from the upper mantle, together with the limited number of good quality travel time picks did not allow detailed *S*-wave modelling. The resulting accuracy was not enough to determine fine variations of the *Vp/Vs* ratio for different parts of the Bohemian Massif.

3.5. Evaluation of anisotropy from non-profile data

To assess the limits of applicability of the standard isotropic approach used in the analysis of the profile data knowledge of a crustal anisotropy was necessary. In general, a medium is anisotropic if the seismic velocities are directionally dependent. The crustal anisotropy can be caused by an intrinsic crystallographic anisotropy of minerals in rocks or by a preferred orientation of structural complexities in the crust such as inclusions, cracks, fractures or aligned small scale inhomogeneities [*Lay and Wallace*, 1995]. The horizontal directional dependence of the velocity is called the azimuthal anisotropy.

Papers **P5** and **P6** were devoted to the evaluation of the strength of anisotropy and its parameters in the crust of the Bohemian Massif. We interpreted regional as well as local non-profile refraction data to reveal a possible azimuthal variation of the *Pg* waves. The regional azimuthal velocity variation of the *Pg* waves was studied based on the analysis of the 3-D cross-profile data from the CELEBRATION 2000 experiment (paper **P5**). The interpretation revealed a systematic azimuthal dependency indicating a weak regional-scale intrinsic or effective anisotropy [*Lay and Wallace*, 1995].

Since the Bohemian Massif consists of several tectonic units, the next step in discriminating the azimuthal variations led to a closer investigation of one of them. We chose the Moldanubian unit, a crystalline segment within the whole Bohemian Massif, to study the horizontal anisotropy on a local scale (paper **P6**). For this reason, a special multi-azimuthal common-shot experiment with two offsets was performed as a part of the ALP 2002 refraction experiment. To eliminate the effect of heterogeneities, the layout was carried out in a two-circle arrangement. The interpretation displayed similar azimuthal variation with similar values of anisotropy strength and direction of the symmetry axis as in the case of the regional scale interpretation.

Results of the local and regional azimuthal anisotropy indicated that the horizontal anisotropy pattern within the Bohemian Massif for the upper crust is likely stable with no distinct lateral or vertical variations. Moreover, strength of anisotropy was rather low, thus it was possible to accept the isotropic approach for the interpretation of the refraction data along profiles. Nevertheless, in detailed analyses it was necessary to bear in mind that the profiles CEL09 and S04 (papers **P1** and **P4**, respectively) are perpendicular to the high-velocity direction, while the profile CEL10 (paper **P2**) coincides with the fast velocity direction of the *Pg* waves.

4. Analysis of accuracy, resolution and uncertainties

The analysis of accuracy, resolution and uncertainties is an important part of the interpretation. Errors in refraction modelling result from a combination of several factors: data timing errors, misidentification of seismic phases, travel time picking, inaccuracy of modelling (misfit between the recorded and modelled travel times), and the 2-D geometry of the experiment, not accounting for the 3-D effects or for the anisotropy. Some errors are introduced by the interpreter during phase correlation and are not easy or even possible to be quantified. Their magnitude decreases with the increasing quality and quantity of the data.

In papers **P1**, **P2**, **P3**, and **P4**, we attempted to evaluate the errors resulting from the picking accuracy and from the misfit between the data and a response from the model. Also, in the process of modelling, the limitations of the ray theory had to be kept in mind. In addition, the 2-D modelling did not take into account the out-of-plane refracted and reflected arrivals, which must have occurred particularly in a structurally complex area and on the contacts of several units. In the interpreted data set, the major seismic phases in the wave field were correlated with a considerable confidence, increased by an independent phase picking by different interpreters and by checking the reciprocity. The picking accuracy was usually about $\pm 0.05 - 0.1$ s for the *Pg* phases (smaller especially for the near-offset arrivals) and about $\pm 0.1 - 0.2$ s for the reflected phases (*PmP*, and mid-crustal reflections) and for the *Pn* phases. The calculated travel times fitted the observed travel times with the accuracy of ± 0.2 s on average for both the refracted and reflected phases (details in paper **P2**).

During the ray-tracing modelling, we analyzed travel time curves rather than single arrivals. In such cases, typical velocity errors were in a range of 0.1 km s^{-1} and the errors in the boundary depth determination were of the order of 1 km. However, in complicated or poorly constrained parts of the model, the errors might increase up to 0.2 km s^{-1} and 2 km, respectively. Above, the resolution depended on the frequency content of the analyzed waves. The typical frequencies of waves generated in the controlled source experiments covered the range of several Hz. This represented the wave lengths from several hundred meters to about 1 km and gave a limiting factor on the resolution of interfaces. In details, it was discussed in paper **P3** together with other theoretical and methodological constraints of the refraction method.

The velocity results from both the inversion and the ray tracing modelling were calculated together with the ray coverage and the final travel time residuals to evaluate the misfit between the observed and calculated travel times. The final models usually showed the average of the residuals close to zero implying no or very low systematic deviations of the model parameters with respect to the data. In addition, synthetic seismograms generally showed a good qualitative agreement with the relative amplitudes of the observed refracted and reflected phases.

Another important issue was to assess a reliability of the modelling results. It was particularly essential in parts where a sufficient amount of data was missing. In such a case, it was necessary to show the parts of the model where rays were calculated. In paper **P4**, this

concerned the contact of the Bohemian Massif with the Western Carpathians where the ray coverage was poor and the resolution decreased.

5. Comparison with outcomes from other profiles and/or other independent methods

5.1. Previous refraction and reflection profiles

To decrease the ambiguity of the interpretation, the modelled velocities were compared with the results of previous geophysical investigations. Their beginnings in the Bohemian Massif were associated with the deep seismic sounding profiles and indicated a position of the Moho discontinuity [*Beránek and Zátopek*, 1981]. The refraction measurements were complemented by other geophysical methods [*Bucha and Blížkovský*, 1994] as well as by the interpretation of the reflection profiles 9HR, 8HR, GRANU'95 or MVE'90 [*Tomek et al.*, 1997; *Enderle et al.*, 1998; *DEKORP Research Group*, 1994].

To compare results from the reflection profiling, it was necessary to be aware that the reflection and refraction seismics are complementary methods. The refraction study gives large lateral and vertical resolution that cannot be obtained from the reflection seismics. The reflection profiles provide an instant qualitative image of the subsurface being especially useful when imaging sedimentary sequences. However, mapping the reflected phases into the actual depths is more complicated because it requires knowledge of the average background seismic velocity. Since the reflection seismic data are sensitive to the background velocity, a typical reflection profiling suffers from the trade-off between the seismic velocities and the reflector depths. This trade-off can be resolved with the use of the refraction and wide-angle data.

Papers **P1** and **P3** showed a combined interpretation of the reflection and refraction seismics in the Saxothuringian unit of the Bohemian Massif. The reflection profiles 9HR and MVE'90 were compared with the results of the refraction CEL09 profile. The MVE'90 imaged a highly reflective layer at the base of the crust with the uppermost mantle more or less without reflections. The Moho was interpreted at the base of this layer at a depth where the strong reflectivity disappeared. Similarly, the refraction velocity study of the CEL09 profile revealed a lower crustal layer with a velocity gradient. In the refraction seismic sections, the strong reflection in the lower crust was not attributed to the Moho discontinuity though it was the strongest reflected phase and based on its amplitude and shape it could have been interpreted as the Moho reflection. According to the ray-tracing and reflectivity analyses, this reflection was attributed to the top of a highly reflective lower crust where a long-coda wave masked a relatively weak reflection from the Moho.

5.2. Additional refraction profiles

To further constrain the velocities and to reduce the ambiguity, the interpretations of other refraction and wide-angle reflection profiles, namely from the CELEBRATION 2000, ALP 2002, and SUDETES 2003 experiments, were incorporated. A high number of transects in the Bohemian Massif gave an advantage for the interpretation at the intersections.

The benefit from having independent information in different directions proved during the interpretation of the lower crust at the intersection of the perpendicular profiles CEL09 and CEL10 in the Moravian unit. The Moho was interpreted as a broad crust/mantle transition zone with gradually increasing velocities detected along both profiles (see paper **P2**). Imaging the lower crust by the high velocity gradients with no distinct Moho interface is not very common but there it was justified by the interpretations of the data from both profiles.

By contrast, the interpretation of the lower crust at the crossing point of the CEL10 and S04 profiles in the Moravo-Silesian unit was more complex. According to the results from the CEL10 profile (paper **P2**), a broad crust-mantle transition zone with the elevated gradient velocities was interpreted along the whole eastern edge of the Bohemian Massif because the data did not indicate a sharp Moho discontinuity. On the other hand, the interpretation of the data along the perpendicular S04 profile (paper **P4**) was more ambiguous involving options both consistent and different from the CEL10 interpretation. In order to decide, which interpretation of the S04 profile was more plausible, a response from phases originating from the first order Moho discontinuity with a sharp velocity contrast was compared with a response from phases originating from the gradient crust-mantle transition zone (as was the case of the perpendicular profile CEL10). The calculated travel times and the synthetics indicated that both interpretations satisfied, to some extent, the data along the S04 profile. Though usually an agreement for the interpretations on crossing profiles is preferred, we decided to keep the first order Moho discontinuity for the S04 profile for the following reasons. Unlike CEL10, the S04 profile was in a more favourable position to the configuration of the tectonic units. In such a case, when two interpretations along the S04 profile were equally satisfactory in terms of uncertainties, a structure with the minimum complexities was the preferred one. Nevertheless, this was a complicated tectonic area and we admit that the proposed interpretation of the S04 profile at the crossing point with the CEL10 profile may be a matter of debates in future studies.

5.3. Reflectivity method

During the forward modelling, we observed differences in the amplitudes and coda length of some deeper reflected phases that were not possible to analyze by the ray method. To explain the dynamic characteristics of these phases, we applied the reflectivity method of *Fuchs and Müller* [1971]. In this method, the numerical integration of the reflectivity of a layered 1-D medium model was carried out over a horizontal wavenumber. The multiplication with a source spectrum and the subsequent inverse Fourier transform yielded the computed full waveform seismograms that were compared with the observed seismic data. The reflectivity method was used to simulate more accurately the observed seismic data than the ray method and, especially, to study the character of the lower crustal and the Moho reflections.

In paper **P1**, the representative 1-D velocity models obtained by the ray-tracing modelling in different tectonic areas of the Bohemian Massif were tested for the existence of laminated layers and for high-gradient zones in the lower crust. The procedure comprised the calculation of synthetic seismograms and the comparison of these seismograms with the data. The most important results were achieved in the Saxothuringian unit (NW), where the high-amplitude

long-coda reflections were attributed to the strong reflectivity in the lower crust. The lower crustal layering with sections of randomly alternating high and low velocities masked a relatively weakly reflected phase from the Moho.

5.4. Receiver functions

The receiver function method is based on an analysis of the teleseismic recordings of the three-component broad-band seismological stations and reveals the relative response of the Earth's structure near the receiver [*Kind et al.,* 1995]. It analyses the seismic phases converted from the *P* to *S* waves at discontinuities underneath the receiver where the strongest *P*-to-*S* conversions with a positive polarity (indicating a velocity increase with the depth) are often attributed to the Moho discontinuity. The arrival time of the *P*-to-*S* converted phases is measured in relation to the *P* waves and depends on the depth of the discontinuity and on the *S*-wave velocity above it. The amplitudes depend on the contrast of seismic velocities, densities and on the incidence angle of the impinging *P* wave.

In paper **P3**, the interpretations of the receiver functions are compared with the refraction and wide-angle reflection measurements to investigate the depth and the character of the Moho in the western part of the Bohemian Massif. Both methods found some indications for a major discontinuity near the base of the crust but differed partly in the depth determination and in the characterization of the crust-mantle transition. The discrepancies could be partly attributed to a different theoretical background and methodology of both approaches as well as to their spatial resolution. The uncertainty in knowledge of the *Vp/Vs* ratio and the different frequency band of waves used in both methods could also play an important role. Furthermore, the methods sampled the boundary at slightly different places. However, these methodological aspects were not enough to explain the observed discrepancies. New synthetic modelling for both methods was necessary with the aim to find some indicators for a more complex interpretation.

Paper **P3** describes several synthetic tests that were carried out. First, 1-D velocity profiles from the CEL09 ray-tracing model were extracted at places close to the receiver functions and there were calculated synthetic receiver function responses for such velocities. Since it was not possible to get a reasonable fit of the receiver function data with the response from the CEL09 ray-tracing model, the other step was to alternate the velocity structure. The receiver function responses were calculated for models ranging from the first-order Moho discontinuity to different gradient zones. In the same way, it was necessary to alternate the ray-tracing velocity model to match the result from the receiver functions. Finally, a reasonable fit for both methods was achieved for a model with a thin lower crustal layer between the depth of 26 and 30 km and a thin Moho transition layer at the depth from 30 to 32 km.

5.5. Gravity modelling

The gravity modelling was used to test the seismic velocity models and to obtain additional geophysical constraints on the crustal structure and its composition. It was applied to the profiles CEL09 and S04 (papers **P1** and **P4**). In the case of the CEL09 profile (paper **P1**), the *P*-wave velocity models were converted into the density blocks using the seismic velocity-density relation of *Thybo and Schönharting* [1991]. Slightly different approach was applied to the S04 profile (paper **P4**), where the velocities were converted into densities using the velocity-density relation of *Christensen and Mooney* [1995] for the crustal and upper mantle velocities (6-8 km s^{-1}) and the velocity-density relation of *Ludwig* [1971] for the velocities of sediments. Both approaches resulted in the initial density models. Using the 2-D modelling software GRAVMOD developed by *C. Zelt* (internet freeware code, paper **P1**), or GRDGRAVITY developed by *I. Trinks* (internet freeware code, paper **P4**), the gravity effect of the initial density models was compared with the Bouguer anomalies along the profile. Then, the densities in the models were modified by the trial-and-error approach in order to obtain a better fit with the experimental gravity data.

The analysis of the gravity response for the initial models indicated that the seismic models agreed with the Bouguer anomalies in terms of the large-scale and deep structure, because the calculated gravity effect resembled a long-wavelength, smoothed version of the experimental gravity data. The most prominent discrepancies in the initial models (about 50 mGal) occurred in the areas of the negative anomalies and coincided with the location of low density granites of the Karlovy Vary Pluton and the Krušné hory Mts. These discrepancies were probably due to greater density differences between low density granites and surrounding rocks than estimated from the seismic velocities. Another contributing factor might be a 3-D influence of the density anomalies, not taken into account by the 2-D velocity modelling. Since the aim was to test the 2-D velocity models, the gravity modelling was confined to two dimensions, only. The other prominent discrepancy occurred at the contact of the Bohemian Massif with the Carpathians and was attributed to the low-density foredeep and flysch sedimentary successions not properly resolved from the seismic data.

6. Summary of the main interpretation results in the Bohemian Massif

The results of the interpretations were based on the modelling of the refraction and wide-angle reflection data and were related to the key units of the Bohemian Massif. They comprised the analysis of the *P* and *S*-wave velocity distribution, the character of the lower crust and the Moho topography, the surface geology and the results from the other reflection and refraction profiles, especially CEL09 and CEL10, S01, S02 and S03, S04, 9HR, MVE-90, GRANU'95, 8HR, and MT-15. Above, additional constraints on the crustal structure were given by the reflectivity or the gravity modelling, and by the receiver function interpretation. The resultant velocity models determined different types of the crust-mantle transition reflecting variable crustal thickness and delimiting contacts of the tectonic units at depth. Knowledge of the crustal velocity structure in the Bohemian Massif was complemented by its azimuthal variations. Due to the ambiguity of the modelling and data, there could have been several possible interpretations. But because of all aforementioned mentioned reasons and constraints the proposed interpretations gave one of the most plausible solutions. Main features of the interpretations are summarized below. Detailed reasoning with geotectonic implications are discussed in the respective papers.

6.1. Profile CEL09

The interpreted profile CEL09 (paper **P1**) of the NW-SE direction crossed all main tectonic units of the Bohemian Massif. In the west, in the Saxothuringian unit, a highly reflective lower crustal layer above the Moho was detected with a strong velocity contrast at the top of this layer. This reflective laminated lower crust (also discussed in paper **P3**) showed the gradually increasing velocities from 6.9 to 7.5 km s^{-1} and was characteristic for the Saxothuringian unit, which was subject to the eastward subduction. The Moldanubian unit in the central part was characterized by the deepest (39 km) and the most pronounced Moho within the whole Bohemian Massif with a strong velocity contrast from 6.9 to 8.1 km s^{-1}. A thick crust-mantle transition zone in the SE, with the velocity increase from 6.8 to 7.8 km s^{-1} over a depth range of 23 – 40 km, seemed to be a characteristic feature of the Moravian unit overthrusted by the Moldanubian unit during the Variscan collision.

6.2. Profiles CEL10 and ALP04

The perpendicular integrated profiles CEL10 and ALP04 (paper **P2**) sampled the crustal structure along the eastern margin of the Bohemian Massif (the Moravo-Silesian unit) and its contact with the Alps and Baltica. In the upper crust of the Bohemian Massif, the velocities ranged from 5.0 to 5.6 km s^{-1} down to a depth of 5 km and represented the SE prolongation of the Elbe Fault Zone. The lower crust was characterized by elevated velocities and by a high *Vp* gradient, which seemed to be characteristic for the Moravo-Silesian unit. Slightly different properties of the Moravian and Silesian units were attributed to varying distances of the profile from the Moldanubian Thrust front, as well as different type of contact of the

Brunovistulian with the Moldanubian units and with its northern root sector. The north-eastern termination of the high velocity lower crust in the Bohemian Massif could be seen as the termination of the Variscan collision tectonics on a crust/mantle level. South of the Bohemian Massif, the Moho was dipping to the depth of 43 – 45 km reaching its maximum in the Eastern Alps. To the north, at the Palaeozoic Platform, the Moho was interpreted as the first-order discontinuity at a depth of 30 km.

6.3. West Bohemian region

Different seismic methods, namely the reflection, the receiver function and the refraction and wide-angle reflection measurements, sampled the crust-mantle boundary in the West Bohemian region (paper **P3**). These methods found some indications for a major discontinuity near the base of the crust but differed partly in the determination of the depth and in the characterization of the crust-mantle transition. The discrepancies could be partly attributed to different theoretical backgrounds of the methods and their resolution but could not fully explain them. New synthetic modelling for the receiver functions and the ray-tracing (paper **P3**) amended the interpretation and revealed that both data sets could be explained by a lower crustal layer or by a crust-mantle transition zone with the maximum thickness of 5 km. The top of the lower crust was interpreted at a depth of 28 km, where highly reflective lower crustal layer could mask the Moho reflection from the depth of 32 – 33 km.

6.4. Profile S04

The interpretation along the S04 profile (paper **P4**) focused on the tectonic units of the Bohemian Massif in the NW-SE direction. In the Saxothuringian unit, higher near-surface velocities represented the Palaeozoic metamorphic rocks alternating with lower velocities at the contact of the Saxothuringian and Barrandian units caused by low density granites. The contrast was even more pronounced in densities than in seismic velocities suggesting deeper seated granites than ensued from the seismic modelling. The lower crust in the northern part of the Saxothuringian unit exhibited a complicated structure, ranging from the high-velocity lower crust and double Moho to the Moho with some lateral topography. The Moho at the northern rim of the Moldanubian unit was modelled as the first order discontinuity at a slightly shallower depth of 33 km than in the central part of the Moldanubian, where it reached the depth of 39 km (paper **P1**). The lower crust in the Moravo-Silesian unit showed slightly elevated velocities though it was not modelled by a gradient zone as in the case of the perpendicular profile CEL10 (paper **P2**). The Moho at the contact of the Bohemian Massif with the Western Carpathians disclosed strong lateral variations in a depth range of 26 – 37 km with an abrupt change from a depth of 26 km followed by a steeply dipping Moho at a depth of 37 km. This abrupt change of the crustal thickens can represent the contact of different tectonic plates at the lower crustal level. Low velocities of 4 km s^{-1} at a depth of 6 km at the contact with the Carpathians represented sedimentary successions of the Carpathian Flysch, a source of the pronounced gravity low. The Moho in the Carpathians was modelled as the first first-order discontinuity at the depth of 32 – 33 km.

6.5. Non-profile interpretations

An overall azimuthal velocity variation in the Bohemian Massif was studied in paper **P5**. The observed travel times at regional distances were inverted for parameters of a velocity model formed by an isotropic low-velocity subsurface layer with a varying depth lying on a homogeneous transversely isotropic half-space with a horizontal axis of symmetry. The recovered velocity displayed a systematic azimuthal variation indicating a regional-scale intrinsic or effective anisotropy in the Bohemian Massif. The Pg velocity values ranged from 5.98 to 6.10 km s^{-1}, indicating the anisotropy of 1.5 – 2.5%. The direction of the maximum propagation velocity was to the NE (35°).

Additionally, the local azimuthal velocity variation was studied in the Moldanubian unit (paper **P6**) using the data from a multi-azimuthal common-shot experiment performed as a part of the ALP 2002 refraction experiment. To eliminate the effect of heterogeneities, the layout was carried out in a two-circle arrangement. The interpretation in the Moldanubian unit displayed similar azimuthal variation indicating the anisotropy of 2% with minimum and maximum velocity values of 5.83 and 5.95 km s^{-1}, respectively. The local-scale direction of the maximum velocity was to the NE (50°), characterizing the horizontal anisotropy of the uppermost crust and being consistent with the overall upper crustal anisotropy of the entire Bohemian Massif.

6.6. Lithology

Part of the interpretation leading to the geological and/or tectonic realizations was the evaluation of the seismic velocities in terms of their lithological representations. The interpretation of crustal lithologies was based on the *P*-wave velocities obtained from the 2-D ray-tracing modelling. The most plausible lithologies were inferred from the modelled *Vp* values and they were compared with global [*Christensen and Mooney*, 1995; *Weiss et al.*, 1999] and regional [*Christensen*, 1974; *Mueller*, 1995; *Grégoire et al.*, 2001] laboratory data for various crustal rock assemblages. Laboratory data were considered at the depths of 5 km (upper crust) and 25-30 km (lower crust), and compared with modelled velocities at the same depth levels. Resultant lithologies for the upper and lower crust for different parts of the Bohemian Massif were discussed in papers **P2** and **P4**.

Acknowledgements

List of papers P1 – P6 included in the thesis

P1: Hrubcová P., P. Środa, A. Špičák, A. Guterch, M. Grad, R. Keller, E. Brückl and H. Thybo. Crustal and uppermost mantle structure of the Bohemian Massif based on data from CELEBRATION 2000 Experiment, *J. Geophys. Res., 110*, B11305, doi:10.1029/2004JB003080, 2005.

P2: Hrubcová P., P. Środa, and CELEBRATION 2000 Working Group. Crustal structure at the easternmost termination of the Variscan belt based on CELEBRATION 2000 and ALP 2002 data, *Tectonophysics*, 460, 55-75, doi:10.1016/j.tecto.2008.07.009, 2008.

P3: Hrubcová, P., and W.H. Geissler. The Crust-Mantle Transition and the Moho beneath the Vogtland/West Bohemian Region in the Light of Different Seismic Methods, *Stud. Geophys. Geod.*, 53, 275-294, 2009.

P4: Hrubcová, P., P. Środa, M. Grad, W.H. Geissler, A. Guterch, J. Vozár, E. Hegedűs, and Sudetes 2003 Working Group. From the Variscan to the Alpine Orogeny – crustal structure of the Bohemian Massif and Western Carpathians in the light of the SUDETES 2003 seismic data, *Geophys. J. Int.*, submitted.

P5: Růžek, B., V. Vavryčuk, P. Hrubcová, J. Zedník, and the CELEBRATION Working Group. Crustal anisotropy in the Bohemian Massif, Czech Republic: Observations based on Central European Lithospheric Experiment Based on Refraction (CELEBRATION) 2000, *J. Geophys. Res., 108(B8)*, 2392, doi:10.1029/2002JB002242, 2003.

P6: Vavryčuk, V., P. Hrubcová, M. Brož, J. Málek, and the ALP 2002 Working Group. Azimuthal variation of Pg velocity in the Moldanubian, Czech Republic: observations based on a multi-azimuthal common-shot experiment, *Tectonophysics, 387*, 189-203, 2004.

In papers **P1** – **P4**, I was the first principal author with the principal contribution; in papers **P5** – **P5**, I was not the first author but I had the essential contribution to the article. The participation in each paper is endorsed in Supplement 1. Papers are enclosed in Supplement 2.

References

Aki, K., and P.G. Richards, 1980. *Quantitative seismology, theory and methods*. Columbia University.

Aster, R.C., B. Borchers, and C.H. Thurber, 2005. *Parameter estimation and inverse problems*. International Geophysical Series, Volume 90, Elsevier Academic Press.

Beránek, B., and A. Zátopek, 1981. Earth's crust structure in Czechoslovakia and central Europe by methods of explosion seismology, in *Geophysical Synthesis in Czechoslovakia*, edited by A. Zátopek, Veda, Bratislava, Slovakia, 253–264.

Brűckl, E., T. Bodoky, E. Hegedűs, P. Hrubcová, A. Gosar, M. Grad, A. Guterch, Z. Hajnal, G.R. Keller, A. Špičák, F. Sumanovac, H. Thybo, F. Weber, and ALP 2002 Working Group, 2003. ALP 2002 seismic experiment, *Stud. Geophys. Geod., 47*, 671–679, doi:10.1023/A:1024780022139.

Bucha, V., and M. Blížkovský (Eds.), 1994. *Crustal Structure of the Bohemian Massif and the West Carpathians*, Academia Praha, Prague.

Červený V., and I. Pšenčík, 1984. SEIS83 – numerical modelling of seismic wave fields in 2-D laterally varying layered structures by the ray method. In: Engdal, E.R. (Ed.), *Documentation of Earthquake Algorithms. Rep. SE-35*, World Data Cent. A for Solid Earth Geophysics, Boulder, Colo., 36–40.

Christensen, N. I., 1974. Compressional wave velocities in possible mantle rocks to pressures of 30 kbars, *J. Geophys. Res.*, 79, 407–412.

Christensen, N. I., 1996. Poisson's ratio and crustal seismology, *J. Geophys. Res., 101*, 3129–3156.

Christensen, N. I., and W. D. Mooney, 1995. Seismic velocity structure and composition of the continental crust: A global view, *J. Geophys. Res., 100*, (B6), 97619788, doi:10.1029/95JB00259.

DEKORP Research Group, 1994. The deep seismic reflection profiles DEKORP 3/MVE-90, *Z. Geol. Wiss., 22* (6), 623–825.

Enderle, U., K. Schuster, C. Prodehl, A. Schulze, and J. Bribach, 1998. The refraction seismic experiment GRANU95 in the Saxothuringian belt, southeastern Germany, *Geophys. J. Int., 133*, 245–259, doi:10.1046/j.1365-246X.1998.00462.x.

Fuchs, K., and G. Mülller, 1971. Computation of synthetic seismograms with the reflectivity method and comparison with observations, *Geophys. J. R. Astron. Soc., 23*, 417–433.

Grad, M., A. Špičák, G. R. Keller, A. Guterch, M. Brož, and E. Hegedűs, 2003. SUDETES 2003 seismic experiment, *Stud. Geophys. Geod., 47*, 681–689, doi:10.1023/A:1024732206210.

Grégoire, M., I. Jackson, S. Y. O'Reilly, and J. Y. Cottin, 2001. The lithospheric mantle beneath the Kerguelen Islands (Indian Ocean): petrological and petrophysical characteristics of mantle mafic rock types and correlation with seismic profiles, *Mineral Petrology, 142*, 244–259.

Guterch, A., M. Grad, A. Špičák, E. Brűckl, E. Hegedűs, G. R. Keller, H. Thybo, and CELEBRATION 2000, ALP 2002, SUDETES 2003 Working Groups, 2003a. An overview

of recent seismic refraction experiments in central Europe, *Stud. Geophys. Geod., 47*, 651–657, doi:10.1023/A:1024775921231.

Guterch, A., M. Grad, G. R. Keller, K. Posgay, J. Vozár, A. Špičák, E. Brűckl, Z. Hajnal, H. Thybo, O. Selvi, and the CELEBRATION 2000 Experiment Team, 2003b. CELEBRATION 2000 seismic experiment, *Stud. Geophys. Geod., 47*, 659–669, doi:10.1023/A:1024728005301.

Hole, J.A., 1992. Non-linear high-resolution three-dimensional seismic travel time tomography, *J. Geophys. Res., 97*, 6553–6562.

Humphreys, E., and R. W. Clayton, 1988. Adaptation of backprojection tomography to seismic travel time problems, *J. Geophys. Res., 93*, 1073–1085.

Kind, R., G.L. Kosarev, and N.V. Petersen, 1995. Receiver functions at the Stations of the German Regional Seismic Network (GRSN), *Geophys. J. Int., 121*, 191–202.

Komminaho, K., 1997, Software manual for programs MODEL and XRAYS − A graphical interface for SEIS83 program package*, Rep. 20, 31, Dep. of Geophysics Univ. of Oulu, Oulu, Finland.

Lay, T., and T.C. Wallace. *Modern Global Seismology*, International Geophysical Series, Volume 58, Academic Press, 1995.

Ludwig, W.J., J.E. Nafe, and C.L. Drake, 1971. Seismic refraction. In Maxwell, A. E. (Ed.), *The sea, v. 4*, New York, (Interscience), 53–84.

Mueller, H.J., 1995. Modelling of the lower crust by simulation of the in situ conditions: an example from Saxonian Erzgebirge, *Phys. Earth Planet. Inter., 92*, 3–15.

Środa, P., 1999. Modifications of Software Package ZPLOT by C. Zelt, *Inst. Geophys. Pol. Acad. Sci.*, Warsaw.

Thybo, H., and G. Schönharting, 1991. Geophysical evidence for early Permian igneous activity in a transtensional environment, Denmark, *Tectonophysics, 189*, 193–208.

Thybo, H., T. Janik, V. D. Omelchenko, M. Grad, R. G. Garetsky, A. A. Belinsky, G. I. Karatayev, G. Zlotski, M. E. Knudsen, R. Sand, J. Yliniemi, T. Tiira, U. Luosto, K. Komminaho, R. Giese, A. Guterch, C.-E. Lund, O. M. Kharitonov, T. Ilchenko, D. V. Lysynchuk, V. M. Skobelev, and J. J. Doody, 2003. Upper lithospheric seismic velocity structure across the Pripyat Trough and the Ukrainian Shield along the EUROBRIDGE'97 profile, *Tectonophysics, 371*, 41–79.

Tomek, C., V. Dvořáková, and S. Vrána, 1997. Geological interpretation of the 9HR and 503 M seismic profiles in western Bohemia, *J. Geol. Sci. Prague, 47*, 43–51.

Vidale, J.E., 1990. Finite-difference calculation of travel times in three dimensions. *Geophysics, 55*, 521–526.

Weiss, T., S. Siegesmund, W. Rabbel, T. Bohlen, and M. Pohl, 1999. Seismic velocities and anisotropy of the lower continental crust: a review, *Pure Appl. Geophys., 156*, 97–122.

Zelt, C., 1994. ZPLOT − An interactive plotting and picking program for seismic refraction data, report, Bullard Lab., Univ. of Cambridge, Cambridge, U.K.

Supplement 1

Authorship contribution

Authorship contribution

I acknowledge that Pavla Hrubcová was the first principal author and had the principal contribution to the articles:

Hrubcová P., P. Środa, A. Špičák, A. Guterch, M. Grad, R. Keller, E. Brückl and H. Thybo, Crustal and uppermost mantle structure of the Bohemian Massif based on data from CELEBRATION 2000 Experiment, *J. Geophys. Res.*, *110*, B11305, doi: 10.1029/2004JB003080, 2005.

Dr. Piotr Środa
Geophysical Institute
Księcia Janusza 64
01-452 Warsaw
Poland

Dr. Aleš Špičák
Institute of Geophysics
Boční II /1401
142 31 Prague 4
Czech Republic

Hrubcová P., P. Środa, and CELEBRATION 2000 Working Group, Crustal structure at the easternmost termination of the Variscan belt based on CELEBRATION 2000 and ALP 2002 data, *Tectonophysics*, 460, 55-75, doi:10.1016/j.tecto.2008.07.009, 2008.

Dr. Piotr Środa
Geophysical Institute
Księcia Janusza 64
01-452 Warsaw
Poland

Hrubcová, P., and W.H. Geissler. The Crust-Mantle Transition and the Moho beneath the Vogtland/West Bohemian Region in the Light of Different Seismic Methods, *Stud. Geophys. Geod.*, 53, 275-294, 2009.

Dr. Wolfram Geissler
Alfred Wegener Institute for Polar and Marine Research
Am Alten Hafen 26
D-27568 Bremerhaven
Germany

Hrubcová, P., P. Środa, M. Grad, W.H. Geissler, A. Guterch, J. Vozár, E. Hegedűs, and Sudetes 2003 Working Group. From the Variscan to the Alpine Orogeny – crustal structure of the Bohemian Massif and Western Carpathians in the light of the SUDETES 2003 seismic data, *Geophys. J. Int.*, submitted.

Dr. Piotr Środa
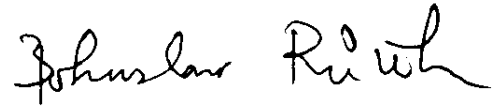Geophysical Institute
Księcia Janusza 64
01-452 Warsaw
Poland

Prof. Marek Grad
University of Warsaw
Pasteura 7
02-093 Warsaw
Poland

I acknowledge that Pavla Hrubcová had the essential contribution to the articles:

Růžek, B., V. Vavryčuk, P. Hrubcová, J. Zedník, and the CELEBRATION Working Group. Crustal anisotropy in the Bohemian Massif, Czech Republic: Observations based on Central European Lithospheric Experiment Based on Refraction (CELEBRATION) 2000, *J. Geophys. Res., 108(B8)*, 2392, doi:10.1029/2002JB002242, 2003.

Dr. Bohuslav Růžek
Institute of Geophysics
Boční II /1401
142 31 Prague 4
Czech Republic

Dr. Václav Vavryčuk
Institute of Geophysics
Boční II /1401
142 31 Prague 4
Czech Republic

Vavryčuk, V., P. Hrubcová, M. Brož, J. Málek, and the ALP 2002 Working Group. Azimuthal variation of Pg velocity in the Moldanubian, Czech Republic: observations based on a multi-azimuthal common-shot experiment, *Tectonophysics, 387*, 189-203, 2004.

Dr. Václav Vavryčuk
Institute of Geophysics
Boční II /1401
142 31 Prague 4
Czech Republic

Dr. Milan Brož
Institute of Rocks and Mechanics
V Holešovičkách 41
182 09 Prague 8
Czech Republic

Prague, February 3, 2010

Supplement 2

Papers included in the thesis

List of papers P1 – P6

P1: Hrubcová P., P. Środa, A. Špičák, A. Guterch, M. Grad, R. Keller, E. Brückl and H. Thybo. Crustal and uppermost mantle structure of the Bohemian Massif based on data from CELEBRATION 2000 Experiment, *J. Geophys. Res.*, *110*, B11305, doi:10.1029/2004JB003080, 2005.

P2: Hrubcová P., P. Środa, and CELEBRATION 2000 Working Group. Crustal structure at the easternmost termination of the Variscan belt based on CELEBRATION 2000 and ALP 2002 data, *Tectonophysics*, 460, 55-75, doi:10.1016/j.tecto.2008.07.009, 2008.

P3: Hrubcová, P., and W.H. Geissler. The Crust-Mantle Transition and the Moho beneath the Vogtland/West Bohemian Region in the Light of Different Seismic Methods, *Stud. Geophys. Geod.*, 53, 275-294, 2009.

P4: Hrubcová, P., P. Środa, M. Grad, W.H. Geissler, A. Guterch, J. Vozár, E. Hegedűs, and Sudetes 2003 Working Group. From the Variscan to the Alpine Orogeny – crustal structure of the Bohemian Massif and Western Carpathians in the light of the SUDETES 2003 seismic data, *Geophys. J. Int.*, submitted.

P5: Růžek, B., V. Vavryčuk, P. Hrubcová, J. Zedník, and the CELEBRATION Working Group. Crustal anisotropy in the Bohemian Massif, Czech Republic: Observations based on Central European Lithospheric Experiment Based on Refraction (CELEBRATION) 2000, *J. Geophys. Res., 108(B8)*, 2392, doi:10.1029/2002JB002242, 2003.

P6: Vavryčuk, V., P. Hrubcová, M. Brož, J. Málek, and the ALP 2002 Working Group. Azimuthal variation of Pg velocity in the Moldanubian, Czech Republic: observations based on a multi-azimuthal common-shot experiment, *Tectonophysics, 387*, 189-203, 2004.

P1

Hrubcová P., P. Środa, A. Špičák, A. Guterch, M. Grad, R. Keller, E. Brückl and H. Thybo

Crustal and uppermost mantle structure of the Bohemian Massif based on data from CELEBRATION 2000 Experiment

Crustal and uppermost mantle structure of the Bohemian Massif based on CELEBRATION 2000 data

P. Hrubcová,[1] P. Środa,[2] A. Špičák,[1] A. Guterch,[2] M. Grad,[3] G. R. Keller,[4] E. Brueckl,[5] and H. Thybo[6]

[1] The deep structure of the Bohemian Massif (BM), the largest stable outcrop of Variscan rocks in central Europe, was studied using the data of the international seismic refraction experiment Central European Lithospheric Experiment Based on Refraction (CELEBRATION) 2000. The data were interpreted by seismic tomographic inversion and by two-dimensional (2-D) trial-and-error forward modeling of P and S waves. Additional constraint on crustal structure was given by amplitude modeling using the reflectivity method and gravity modeling. Though consolidated, the BM can be subdivided into several tectonic units separated by faults, shear zones, or thrusts reflecting varying influence of the Cadomian and Variscan orogeneses: the Saxothuringian, Barrandian, Moldanubian, and Moravian. Velocity models determine three types of crust-mantle transition in the BM reflecting variable crustal thickness and delimiting contacts of tectonic units in depth. The NW area, the Saxothuringian, has a highly reflective lower crustal layer above Moho with a strong velocity contrast at the top of this layer. This reflective laminated lower crust reaches depths of 26–35 km and is characteristic for the Saxothuringian unit, which was subject to eastward subduction. The Moldanubian in the central part is characterized by the deepest (39 km) and the most pronounced Moho within the whole BM with a strong velocity contrast 6.9–8.1 km s^{-1}. A thick crust-mantle transition zone in the SE, with velocity increase from 6.8 to 7.8 km s^{-1} over the depth range of 23–40 km, seems to be the characteristic feature of the Moravian overthrusted by the Moldanubian during Variscan collision.

1. Introduction

[2] The Bohemian Massif is a large complex terrain consolidated in the Paleozoic, located on the territory of the Czech Republic, partly Germany, Poland, and Austria. It forms the easternmost rim of the Variscan belt, a Paleozoic chain extending from southern Iberia to the Bohemian Massif in central Europe. Its configuration is the result of convergence and collision between two main continents, Laurentia-Baltica-Avalonia and Gondwana, after the closure of various oceanic basins, followed by obduction, continental collision, continental subduction, and strike-slip faulting between 500 and 250 Ma. While the postcollisional history

of the Variscan Bohemian Massif is relatively clear, the kinematics of plate movements before and during collision is still subject of debates.

[3] The fan-like shape of the Variscan belt mainly in the east European part shows that the key mechanism of its evolution was two-sided lithospheric subduction [*Matte*, 1991]. This subduction was accompanied by crustal stacking and thickening mainly at the crust-mantle boundary with production of various granitoids by melting of the middle and lower parts of the crust. Also, *Meissner and Wever* [1986], studying the deep structure of the European Variscan crust showed that the pre-Permian thrusts outcropping at the surface are rooted in the lower crust, at Moho, or in the mantle. Thus the Bohemian Massif as a stable exposure of pre-Permian rocks offers the evidences of the Variscan tectonic development. Studying the deep structure of the Bohemian Massif can bring the verification of the subduction-collision processes and better delineation of subduction zones with depth.

[4] In our paper, we present the crustal and uppermost mantle structure in different parts of the Bohemian Massif based on the interpretation of seismic data along the refraction and wide-angle reflection profile CEL09 of the Central European Lithospheric Experiment Based on

[1]Geophysical Institute, Academy of Sciences of the Czech Republic, Prague, Czech Republic.
[2]Institute of Geophysics, Polish Academy of Sciences, Warsaw, Poland.
[3]Institute of Geophysics, University of Warsaw, Warsaw, Poland.
[4]Department of Geological Sciences, University of Texas at El Paso, El Paso, Texas, USA.
[5]Vienna University of Technology, Vienna, Austria.
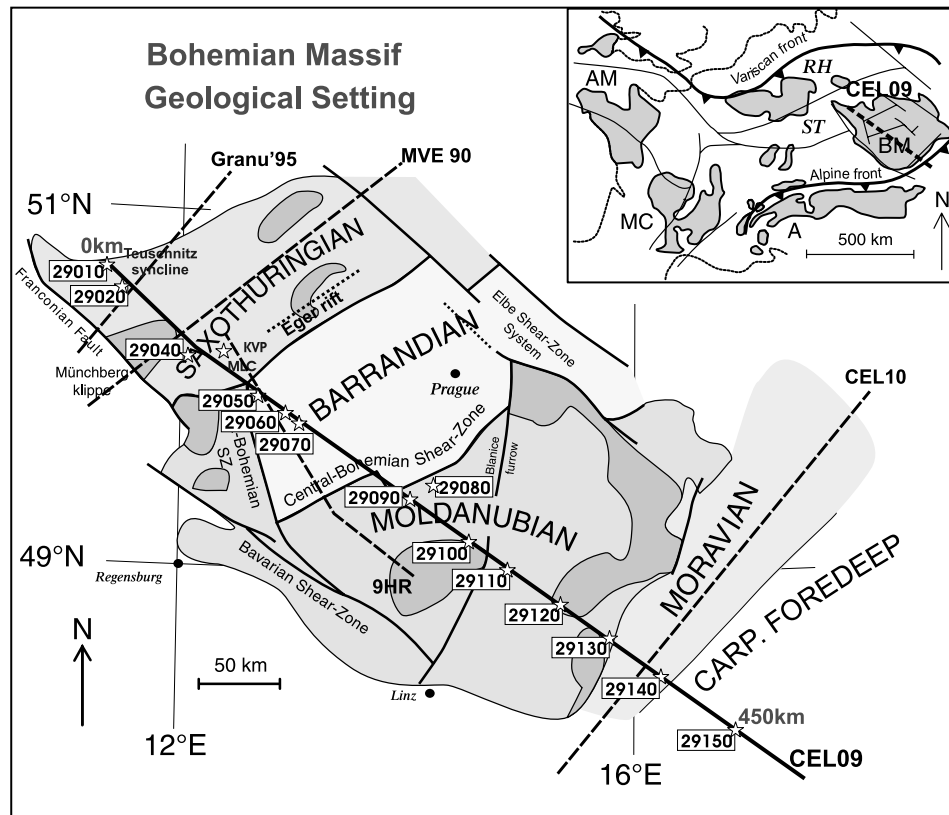[6]Geological Institute, University of Copenhagen, Copenhagen, Denmark.

Figure 1. Major tectonic units of the Bohemian Massif and its setting within the European Variscides with the CELEBRATION 2000 CEL09 line. BM, Bohemian Massif; AM, Armorican Massif; MC, Massif Central; A, Alps; ST, Saxothuringian Zone; RH, Rhenohercynian Zone [after *Pitra et al.*, 1999; *Franke et al.*, 2000]. MLC, Mariánské Lázně Complex; KVP, Karlovy Vary Pluton. Stars mark positions of the individual shot points along the profile. Intersections with other seismic refraction and reflection experiments (Granu'95, MVE 90, 9HR, CEL10) are marked.

Refraction (CELEBRATION) 2000 experiment [*Guterch et al.*, 2003]. This profile traverses the whole Bohemian Massif in NW-SE direction and in the SE it continues to the west Carpathians (Figure 1). For the interpretation we chose the tomographic inversion routine of *Hole* [1992] as a tool to determine the preliminary seismic *P* wave velocity distribution in the crust using first arrivals. The resulting tomographic model was further improved by two-dimensional (2-D) trial-and-error forward modeling using a ray-tracing algorithm [*Červený and Pšenčík*, 1984] for *P* and *S* refracted and reflected waves. The differences in the properties of individual crustal blocks of the Bohemian Massif were further studied by modeling of the seismic wave field with the reflectivity method [*Fuchs and Müller*, 1971]. Gravity modeling complemented the velocity analysis. In this study we concentrate on velocity variations along the profile; azimuthal anisotropic studies are a matter of other investigations [e.g., *Růžek et al.*, 2003; *Vavryčuk et al.*, 2004; *Plomerová et al.*, 1984].

[5] So far, the Bohemian Massif has been studied mainly to show the depth of the Moho discontinuity. New insight into the deep structure of the Bohemian Massif can help to complement this knowledge, determine the crustal thickness and show the differences in crustal and upper mantle

structures in three areas pertaining to different Paleozoic regimes. Contrasts in seismic properties reflect compositional variances resulting from crust-forming processes during the Paleozoic tectonic development.

2. Geology and Tectonic Evolution of the Region

[6] The Bohemian Massif is one of the largest stable outcrops of pre-Permian rocks in central and western Europe. It forms the easternmost part of the Variscan Belt, which developed approximately between 500 and 250 Ma during a period of large-scale crustal convergence, collision of continental plates and microplates and subduction [*Matte et al.*, 1990]. It consists mainly of low- to high-grade metamorphic and plutonic Paleozoic rocks. On the basis of the respective effects of the Cadomian and Variscan orogenesis, the area of the Bohemian Massif can be subdivided into several tectonostratigraphic units, the Saxothuringian, Barrandian, Moldanubian and Moravian, separated by faults, shear zones or thrusts (see Figure 1).

[7] The Moldanubian unit represents a major crystalline segment within the Bohemian Massif and its boundary with the Saxothuringian in the NW is regarded to be a suture-type discontinuity. A structurally higher unit, the Barrandian, has been thrust over the Saxothuringian rocks toward

the northwest, while in the SE it has been thrust in southerly direction over the Moldanubian. It is separated from the latter by a major NE-SW trending Variscan dextral fault, the Central Bohemian Shear Zone (CBSZ), obscured by the intrusion of the Central Bohemian Pluton [*Dallmeyer et al.*, 1994]. The Moldanubian/Moravian boundary in the east has the character of a ductile shear zone with significant translation of the Moldanubian over the Moravian unit. According to *Finger and Steyrer* [1995], Moldanubian overthrust was the final stage of the subduction of the oceanic crust and subsequent Variscan collision between Moldanubian and Moravian units. The Moravian unit consists of a Cadomian basement overlain by the Moravicum and Silesicum nappes and to the east it submerges beneath the Carpathian Foredeep, where it forms the basement reactivated during the Alpine orogeny.

[8] The mafic Mariánské Lázně Complex (MLC), situated between the Saxothuringian and Barrandian, represents an important suture comprising segments of oceanic crust, which were subducted and metamorphosed during the Variscan orogeny and later thrust over the SE margin of the Saxothuringian [*Vrána et al.*, 1997]. This complex probably represents a boundary between two different Variscan tectonic regimes and a zone, which was reactivated later by younger tectonic movements [*Babuška and Plomerová*, 2000]. In the NE it adjoins the intrusion of the granitoid Karlovy Vary Pluton (KVP).

[9] From a tectonic point of view, one of the major deformation events occurred during the Variscan orogeny. Then the Bohemian Massif was sandwiched between high-grade Variscan metamorphic areas, represented by two opposing subduction zones, at first of an oceanic, then of a continental character [*Matte*, 2001]. The oldest deformational structures occur in the Barrandian and are associated with the earliest stages of the Saxothuringian eastward subduction and shortening of the plate. The upper plate developed into a lithospheric-scale arc system, which was manifested by the intrusion of the Central Bohemian Pluton, steeply dipping to the east along the eastern boundary of the Barrandian [*Schulmann et al.*, 2002].

3. Previous Geophysical Studies in the Area

[10] The beginning of the investigation of the Bohemian Massif and its deep structure is associated with the deep seismic sounding profiles recorded on the territory of the Czech Republic as a part of the international "Upper Mantle Project" [*Beránek and Zounková*, 1977]. The interpretation of these refraction measurements indicated the position of the Moho discontinuity with a maximum depth of 39 km in the central part of the Bohemian Massif and a less pronounced Moho at a depth of about 32 km at the eastern edge of the Bohemian Massif [*Beránek and Zátopek*, 1981].

[11] Later, these measurements were complemented by reflection profiling, as well as by other geophysical methods [see, e.g., *Bucha and Bližkovský*, 1994]. The deep seismic reflection profile 9HR extending from SE Germany to southern Bohemia (Figure 1) showed a crustal thickness increasing from 31 km in the NW to 39 km in the south. Combined seismic and gravity interpretation [*Tomek et al.*, 1997; *Švancara and Chlupáčová*, 1997] delimited the thickness of granitoid plutons and mafic intrusions, and

showed overthrusting along a SE dipping contact zone in western Bohemia.

[12] The most recent research has been done in the NW of the Bohemian Massif, in Germany. There, the seismic refraction and wide-angle reflection profile GRANU'95 [*Enderle et al.*, 1998] and deep reflection profile MVE 90 as part of the DEKORP investigation [*DEKORP Research Group*, 1994] showed the velocity structure of the Saxothuringian belt in SE Germany, where laminated lower crust was indicated by MVE 90 data.

[13] Continuous monitoring of seismic activity in the western part of the Bohemian Massif shows frequent occurrence of intraplate earthquake swarms with magnitudes up to 4.5. According to *Horálek et al.* [1996] and *Fischer and Horálek* [2003], the hypocenters of these earthquake swarms are located in the upper and middle crust down to about 20 km depth with the majority between 5 and 15 km. This seismic area, also characteristic of numerous mineral springs and CO_2 emissions, encompasses the western termination of the Eger Rift (see Figure 1), a geodynamically active zone of the European Cenozoic Rift System [*Prodehl et al.*, 1995].

4. Data Acquisition and Processing

[14] The deep structure of the Bohemian Massif was studied along the refraction and wide-angle reflection profile CEL09 using the data of the international seismic refraction experiment Central Europe Lithospheric Experiment Based on Refraction 2000 (CELEBRATION) [*Guterch et al.*, 2003]. The NW-SE oriented profile CEL09 starts in the Saxothuringian in the NW, intersects the Mariánské Lázně amphibolite complex and continues to the Barrandian. Then it crosses the granitoid intrusions spreading along the Central Bohemian Shear Zone and continues to the Moldanubian and Moravian. Farther to the SE, it continues across the Vienna Basin into the Carpathians. The interpreted part of the profile in this paper is 450 km long and ends at the contact of the Bohemian Massif with the Carpathian Foredeep (Figure 1).

[15] Along the interpreted part of the profile, 20 shots were fired, with charges ranging from 210 kg to 10 000 kg of explosives. Some of the shots (5 in all) were shot twice and the recordings were stacked in order to improve the signal-to-noise ratio. The average distance between the shots was 30 km with a station spacing of 2.7 km. The positions of the shot points and stations were measured by GPS; the origin time was controlled by a DCF77 timer with an accuracy of 3 ms [see also *Málek et al.*, 2001]. For more details on the geometry of the experiment refer to *Guterch et al.* [2003] and *Růžek et al.* [2003].

[16] Refraction and wide-angle reflection data were sampled at intervals of 10 ms and were recorded mainly by one-component stations REFTEK-125 (TEXAN), complemented by three-component REFTEK and PDAS stations. The station sensors were 4.5 Hz geophones. Data processing included shot time corrections and band-pass filtering of the whole data set (usually 2–15 Hz) in order to remove low- and high-frequency noise. The frequency content of the seismic data was highly variable for different shot points, probably due to the varying local environment and due to different shooting techniques (drill hole shots,

quarry blasts). Thus the filter window was determined interactively during data interpretation, depending on the data quality and the frequency content. Recordings were sorted into shot gathers; seismic sections were trace normalized to the maximum amplitude along the trace and plotted with a reduction velocity of 8 km s^{-1}.

5. Seismic Wave Field

[17] Refraction and wide-angle reflection data used for the interpretation allow several seismic P wave phases to be correlated (see Figures 2–4). In the first arrivals, we can distinguish refractions from the upper/middle crust, marked as the Pg phase, and refractions from the upper mantle marked as Pn. Refracted waves from the sedimentary cover (P_{sed}) are observed in the vicinity of shot points in the SE. The first arrivals can usually be correlated up to a distance of 250–300 km. In later arrivals, we observe reflections from the Moho discontinuity (PmP) usually as the strongest, reflections from midcrustal discontinuities (PiP) and from the top of the lower crust (PcP). At large offsets, a reflection from an upper mantle discontinuity ($P1$) can be identified in few shot points. Figures 2a–2c give examples of the whole seismic sections in different parts of the Bohemian Massif, while Figures 3a, 3b, 4a, and 4b show details of the seismic wave field with representative features of the Bohemian Massif, to which we will refer in our following explanation.

5.1. Pg Phase

[18] The Pg phase has an apparent velocity of 5.8–6.2 km s^{-1} along the whole profile except at its ends, reflecting the presence of the consolidated Paleozoic basement outcropping at the surface. At the NW end of the profile (0–50 km), lower apparent velocities increasing from 5.0 to 5.9 km s^{-1} are observed with strong Pg arrivals (Figure 2a). Similarly, at the SE end (SP 29150, Figure 4b) the first arrivals at offsets smaller than 30 km display an apparent velocity of 2.5–5.5 km s^{-1} reflecting several kilometers of sedimentary cover in the Carpathian Foredeep and Neogene basins. Apparent velocities higher than average occur at locations of specific near-surface geological structures, e.g., the apparent velocity of about 6.1 km s^{-1} correlates with the mafic Mariánské Lázně Complex at a distance of 115 km along the profile.

[19] For most of the sections from the Bohemian Massif we observe a relatively fast decrease of the Pg amplitude (e.g., Figure 2c). At offsets of 80–120 km, the Pg wave becomes either very weak or completely disappears. This phenomenon is visible not only in the trace-normalized sections but also in the true-amplitude sections. Therefore it cannot be explained by the normalization of sections to the maximum trace amplitude, which can make first arrivals hardly visible if they are followed by very strong PmP reflections. This fact indicates a very small vertical gradient of the P wave velocity in the upper crust, except in its uppermost (1–2 km thick) part or the existence of a low-velocity zone (LVZ). Another factor contributing to the decaying amplitudes can be relatively high attenuation in the upper crust.

[20] The rate of Pg amplitude decrease varies. Figure 3a shows an example of a seismic section where the Pg phase vanishes at about 80 km offset, while for the data from other locations (Figure 3b), the Pg phase, though weak, continues at least to 120 km. The first example might be an indication for a LVZ. However, to prove the existence of a low-velocity zone definitely, it should be possible to detect a later phase, corresponding to rays refracted at (or reflected from) the base of the potential LVZ, with an accuracy allowing precise velocity determination. Modeling of such a phase provides a criterion for deciding if a layer with a velocity decrease is really necessary, and for estimating the average velocity in that layer. The later phase visible in Figure 3a is not clear enough to determine its apparent velocity with confidence. Therefore we decided not to introduce a LVZ explicitly and to explain the behavior of the Pg phase by a very small (close to zero) vertical gradient of the V_p velocity.

[21] Similar variations of the Pg amplitudes were observed in other Variscan areas: the Saxothuringian and Moldanubian in Germany [*Enderle et al.*, 1998; *DEKORP Research Group*, 1988; *Zeis et al.*, 1990], the Massif Central in France [*Zeyen et al.*, 1997], Ireland [*Masson et al.*, 1998] or SW Poland [*Grad et al.*, 2003]. In some cases, they were interpreted as an indication of the existence of a LVZ. Contrasting properties of the Pg phase (strong amplitudes up to 200 km offset) were observed, e.g., in the crystalline crust of the east European Craton [*Šroda and Polonaise Profile P3 Working Group*, 1999; *Czuba et al.*, 2002; *Thybo et al.*, 2003].

[22] Some sections indicate the continuation of the Pg phase as secondary arrivals, especially for shots in the middle part of the profile (Figures 2b and 2c). This indicates a low-velocity gradient in the middle crust, which confines refracted arrivals to shallow depth.

5.2. Crustal Phases in Later Arrivals and PmP Phase

[23] Besides crustal refracted phases, we also observed reflected waves recorded in later arrivals. Intracrustal reflections (PiP) can be observed in several seismic sections, but some of them cannot be traced consistently in more than one section, which makes their interpretation ambiguous. The most widely observed intracrustal reflections occur at offsets of 70–130 km and are thought to originate from a discontinuity at some 15–20 km depth.

[24] In the sections from the NW part of the profile, we observe a clear reflected PcP phase as the reflection from a deep intracrustal interface, the top of the lower crust (SP 29040, Figures 4a and 2a). This is the strongest reflected phase in these sections, and based on its amplitude and shape it might be interpreted as a reflection from the Moho (PmP). Nevertheless, we disallow this interpretation because the arrival time of the observed Pn wave does not fit the critical point of the discussed phase, as should be the case for refraction and reflection from the same discontinuity. In our data, Pn phase occurs 1 s later and PcP phase obscures relatively weak PmP arriving 0.5–1.0 s later. Also, forward modeling confirmed that hypothesis. Similar observations can be seen in some sections from the GRANU'95 profile [*Enderle et al.*, 1998], which crosses CEL09 at its NW end in the Saxothuringian.

[25] The PmP phase is the best visible in the central part of the profile roughly corresponding to the Moldanubian unit (SP 29050, 29060 and 29100, Figures 2b and 2c). The critical point, where the PmP amplitude reaches its maxi-
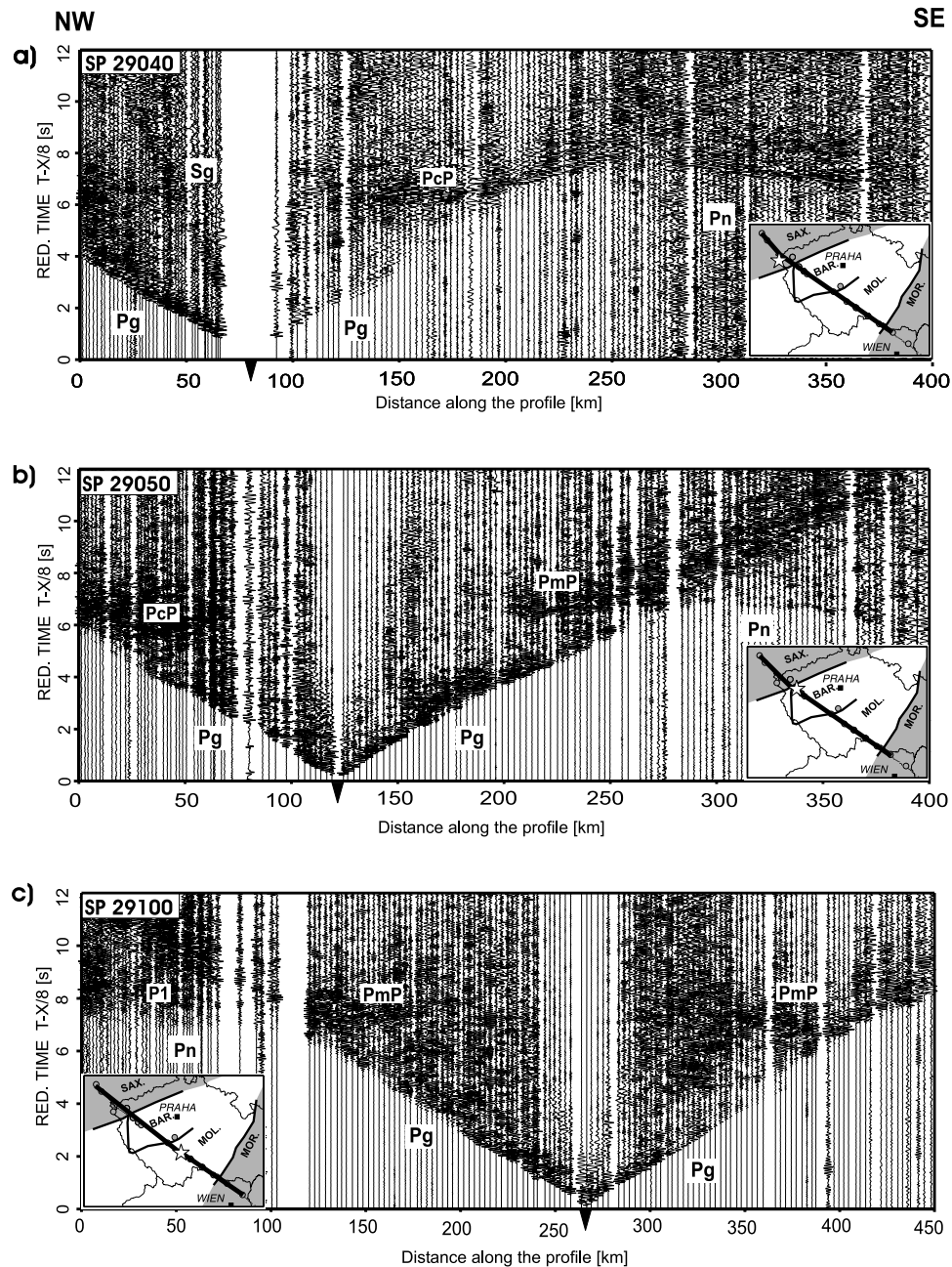
Figure 2. Amplitude-normalized vertical component seismic sections for shot points in different parts of the Bohemian Massif plotted with reduction velocity of 8.0 km s^{-1}, along with the identifications of the main seismic phases (RED, reduced). *P* waves are *Pg*, refraction within the crust; *Pn*, refraction from the uppermost mantle; *PmP*, reflection from the Moho discontinuity; *PcP*, reflection from the top of the lower crust; and *P*1, mantle reflection. *S* waves are *Sg*, refraction within the crust. Data have been bandpass filtered from 2 to 15 Hz. Locations of major tectonic units and shot points are indicated. (a) SP 29040 (Saxothuringian), strong first *Pg* arrivals in NW, strong *PcP*, weak *PmP* phase in the SE. *Pn* phase is weak but observable. (b) SP 29050 (Moldanubian), no *PmP* observed in the NW, sharp *PmP* and no *PcP* in SE. (c) SP 29100, weak *PmP* phase, scattered reflectivity in the crust, *P*1 phase observed.

mum, occurs at an offset of about 90–110 km. At larger offsets (up to 250 km), strong overcritical *PmP* arrivals are often observed. In other areas, the *PmP* is weak or not visible (in the NW and SE). This suggests a well-defined Moho discontinuity in the central part of the profile and a transition zone or Moho with relatively low-velocity contrast in other parts. In the NW part of the profile (the Saxothuringian), the *PmP* is probably masked by a preceding phase (*PcP*) with much higher amplitude and long coda. The SE end of the profile (beneath the Moravian unit and at the contact of the Bohemian Massif with the Carpathians) exhibits no Moho reflections, no intracrustal reflections (SP
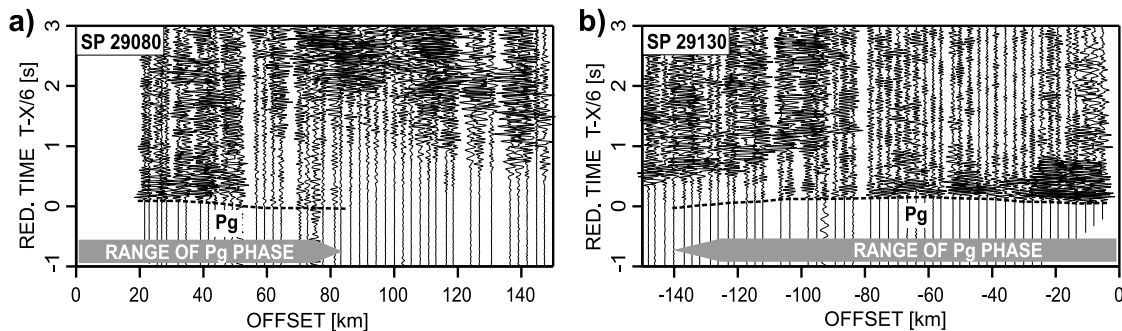
Figure 3. Examples of true amplitude vertical component seismic record sections for shot points 29080 and 29130 illustrating differences in the decay rate of the *Pg* amplitude. (a) Fast decaying *Pg* phase (visible up to 80 km offset). (b) Slowly decaying *Pg* wave (observable up to 130 km offset). Reduction velocity is 6.0 km s^{-1}, with distance exponent 1.

29150) and strong mantle refraction. This suggests the existence of a zone with gradually increasing velocities, rather than the Moho discontinuity. In this area, the first arrivals display a long coda with high-amplitude oscillations observable within several seconds after the first arrivals. The comparison of the wave field for SP 29150 and SP 29140 (Figure 4b) reveals completely different images: very strong *Pg* and *Pn* phases for the first section and clear *Pg*, very strong *PiP* and weak *Pn* for the second section. Taking into account that the distance between the shot points is only 40 km, an abrupt change of the deep crustal structure must occur in this area.

5.3. Mantle Phases

[26] The *Pn* phase can be identified as first arrivals usually at offsets of 130–230 km, sometimes up to 300 km (Figure 4b) with an apparent velocity of 8 km s^{-1} on average. In some sections (e.g., SP 29100, 29110, Figure 2c), a reflected phase following the *Pn* phase can be observed at offsets greater than 190 km. We interpreted it as a reflection from a discontinuity in the upper mantle (*P1*). Though mantle phases are visible only in large distances, the *P1* phase is not observed in all sections with large offsets (e.g., SP 29150, Figure 4b). Thus the corresponding mantle discontinuity seems to be confined to the central part of the Bohemian Massif.

6. *P* Wave Modeling
6.1. Seismic Tomography of the First Arrivals

[27] First, we applied the tomographic inversion of *Hole* [1992] in order to invert the first arrival travel times and determine a smooth 2-D *P* wave velocity model. This is a fast tool to asses a preliminary velocity model in the crust. The procedure uses the single backprojection algorithm [*Humphreys and Clayton*, 1988], based on the linearization of the nonlinear relation between the travel time t and the slowness u = 1/V_p. The model is defined on an equidistant rectangular grid; the V_p velocities are defined at the grid nodes. In the forward step, the travel times are calculated using a finite difference algorithm for solving the eikonal equation [*Vidale*, 1990], adapted for media with arbitrary velocity variations. The travel time residuals measure the misfit of the model. In the inverse step, the slowness

perturbations are calculated by uniformly distributing the travel time residual along a ray. The perturbations are then summed up for all rays, smoothed and added to the original model. The procedure is repeated iteratively until a model with satisfactory travel time residuals is obtained.

[28] For the inversion, we used 2202 first arrival picks with an uncertainty of ∼50 ms for most of the *Pg* and *Pn* phases. The initial 1-D model for the upper crust was calculated by inverting an average travel time curve of *Pg* arrivals by the Wiechert-Herglotz formula [*Aki and Richards*, 1980]; for the lower crust and mantle, a smooth user-defined velocity-depth curve was derived. The 2-D model was calculated for a profile length of 450 km in a uniform grid of 1 × 1 km. The computation was carried out in 6 subsequent steps gradually enlarging the offsets (50, 100, 150, 200, 300, and 400 km) and thus the maximum depth of ray penetration. At each step, several iterations were made with decreasing size of the smoothing area. The smoothing was performed by a moving average filter with cell sizes of 40 × 2 × 10, 20 × 2 × 4 and 10 × 2 × 2. The resolution of the algorithm thus increased gradually and the inversion was stable. The calculation was controlled by the root-mean-square (RMS) travel time residual, which amounted to 80 ms for the final model, exceeding the level of the estimated picking uncertainty by about 50% (Figure 5a).

[29] The residuals, ray coverage, and the resulting tomographic model are presented in Figures 5a–5c. The crust is characterized by an almost uniform velocity distribution throughout most of the Bohemian Massif, except the NW end. The upper crust exhibits a relatively high V_p gradient in the first 3 km with velocities ranging from 5.6 to 6.0 km s^{-1} and a very low gradient in the deeper parts with V_p velocities of 6.0–6.1 km s^{-1} down to about 15 km depth. This V_p distribution corresponds to an almost missing sedimentary cover and outcropping metamorphic and plutonic Paleozoic rocks at the surface. Considerably lower velocities in the upper crust in the range of 3.0–5.0 km s^{-1} for depths down to 10 km delimit the beginning of the Carpathian Foredeep in the SE. Because of the high near-surface velocity gradient followed by a low gradient in the upper crust, the turning point of the *Pg* rays is at shallow depths (Figure 5b). The rays travel almost horizontally and leave the deeper parts of the crust practically unconstrained.
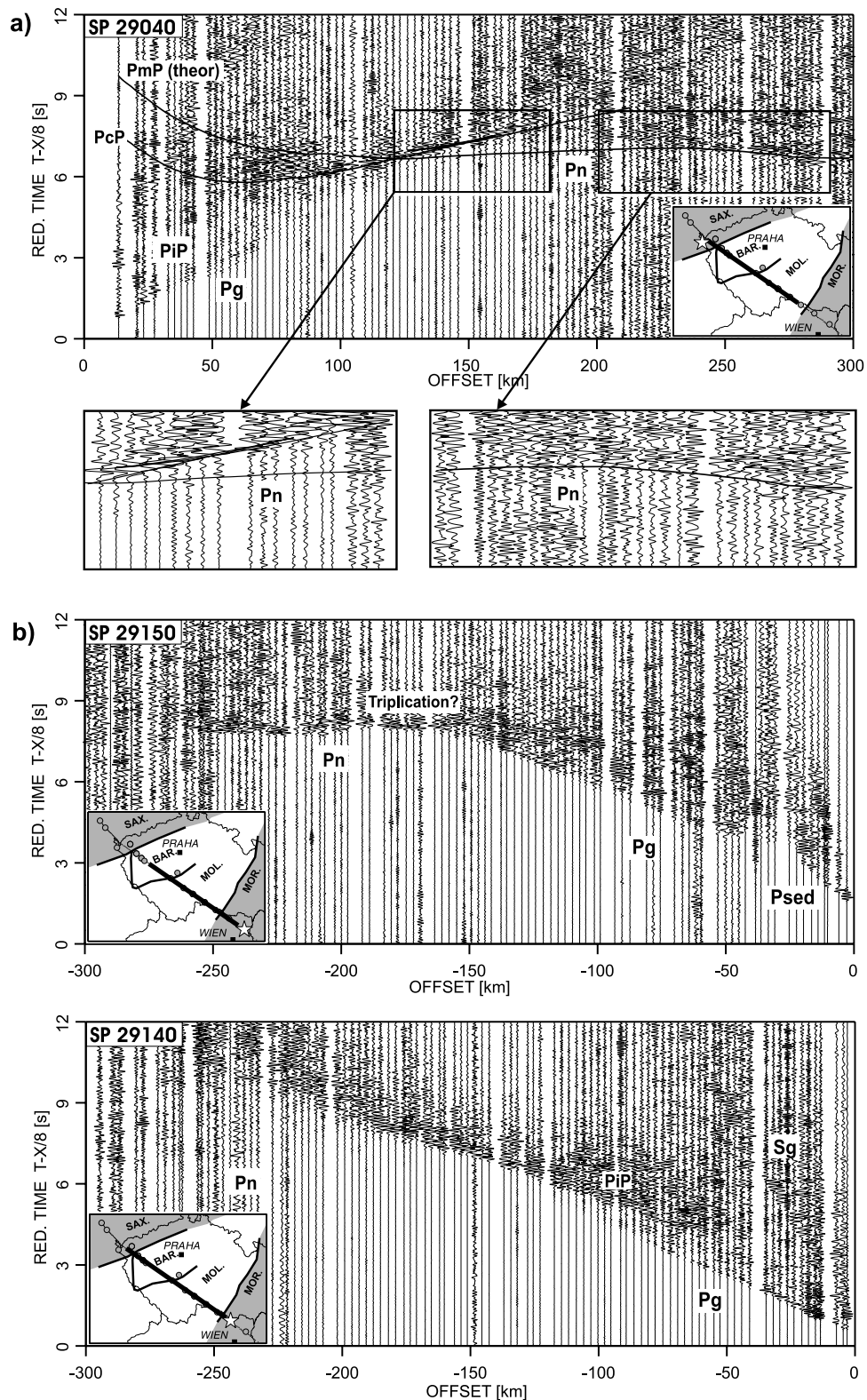
Figure 4. Details of amplitude-normalized vertical component seismic sections. (a) SP 29040 in the Saxothuringian, strong *PcP* with long coda obscuring the relatively weak *PmP* phase. (b) SE end, SP 29150, high-amplitude *Pn* phase, *PmP* not observed, scattered reflectivity in the crust; SP 29140, no *PmP* phase observed, strong *PiP*. Description of phases is as in Figure 2, and P_{sed}, refracted arrivals from the sedimentary cover; *PiP*, intracrustal reflection. Reduction velocity is 8.0 km s^{-1}.
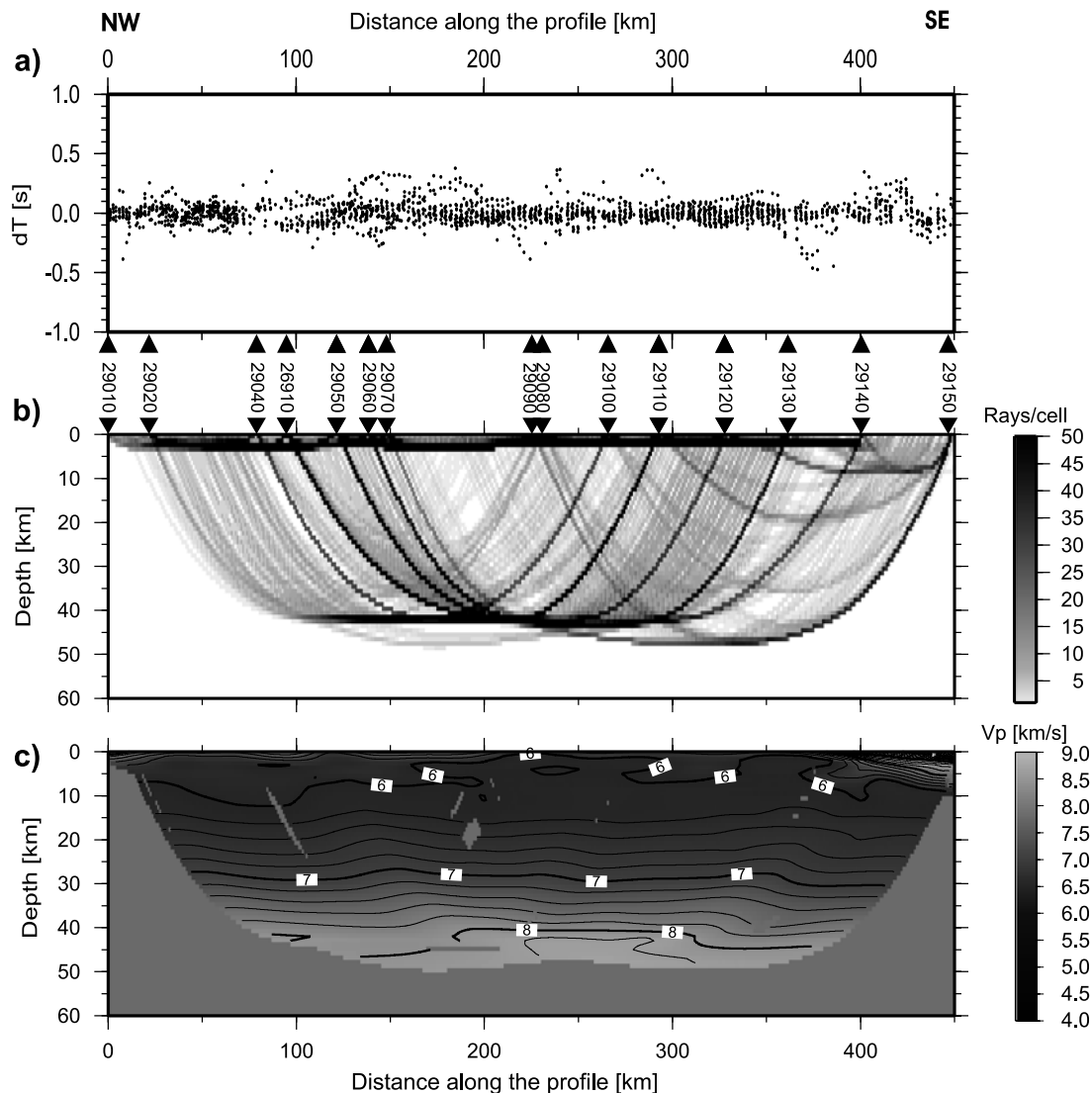
Figure 5. Results of 2-D seismic tomography. (a) Misfit between observed and calculated travel times. (b) Ray coverage for the model. (c) Model of *P* wave velocity. Triangles indicate shot point positions.

For this reason the middle and lower crust lack any differentiation of velocities in the tomographic model (Figure 5c). Because of the nature of the tomographic algorithm applied, the smoothing performed during the inversion and model parameterization, the velocity discontinuities are smoothed into broad gradient zones and, e.g., the depth of the Moho boundary cannot be reliably estimated.

6.2. Trial-and-Error Forward Modeling

[30] The smooth velocity model resulting from the tomographic inversion of the first arrivals (Figure 5) gives only an approximate distribution of velocities in the crust and mantle. On the other hand, modeling of the entire wave field enables a more detailed velocity resolution including velocity contrasts at interfaces and identification of the Moho discontinuity. We thus further refined the 2-D tomographic model by trial-and-error forward modeling using the

SEIS83 program package [*Červený and Pšenčík*, 1984]. In this modeling approach, to obtain the *P* wave velocity distribution, we used not only the first arrivals but also further phases (reflected waves and available refractions in later arrivals). The modeling also involved the calculation of synthetic sections and qualitative comparison of amplitudes of synthetic and observed seismograms. Since the amplitudes of seismic waves are very sensitive to velocity gradients and velocity contrasts at discontinuities, synthetic seismograms of both reflected and refracted seismic waves were useful tools in obtaining additional constraints on the velocity distribution.

[31] The SEIS83 algorithm calculated ray paths, travel times and synthetic seismograms in the high-frequency approximation. The model consisted of layers separated by velocity discontinuities. In each layer, the *P* wave velocity was specified in an irregular rectangular grid and interpolated by bicubic splines. The solution was
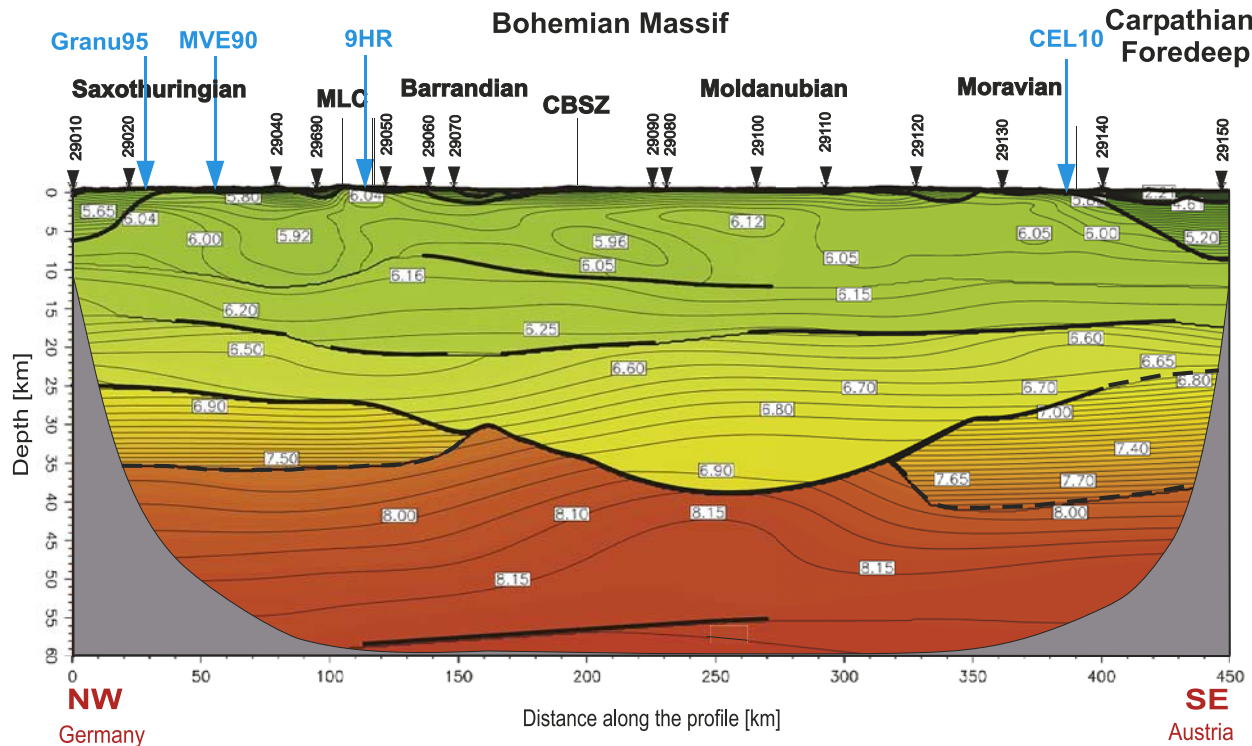
Figure 6. The 2-D model of the *P* wave velocity along the CEL09 profile developed by forward ray-tracing modeling (with SEIS83). The gray covers the unconstrained parts of the model. Bold lines mark boundaries constrained by reflections and well-constrained interfaces in the uppermost crust; dashed bold lines mark layer boundaries where no reflections were observed. Thin lines represent velocity isolines spaced at intervals of 0.05 km s^{-1}. Triangles show projections of the shot points. Arrows show the locations of other refraction and reflection profiles. MLC, Mariánské Lázně Complex; CBSZ, Central Bohemian Shear Zone. Vertical exaggeration is 1:3.

sought iteratively: the travel times of the refracted and reflected waves were calculated for the current V_p model and compared with the observed travel times. Then the V_p model was changed in order to minimize the misfit.

[32] The final 2-D model of the *P* wave velocity distribution is presented in Figure 6. In accordance with the tomography model, the upper crust of the Bohemian Massif displays a relatively high V_p gradient in a near-surface 2–3 km thick zone with velocities of 5.8–6.0 km s^{-1}, except at its NW end. The first, high-gradient layer with velocities of 5.8–6.0 km s^{-1} is the most pronounced in the Barrandian and Saxothuringian, while the Moldanubian and Moravian units show an almost constant near-surface velocity of 6.0 km s^{-1}. Lower V_p velocities, characteristic for sedimentary rocks with velocities ranging from 5.0 to 6.0 km s^{-1} to ~6 km depth, occur in the NW. Mafic Mariánské Lázně Complex exhibits near-surface velocity of V_p 6.05 km s^{-1} at a distance of 115 km along the profile. The SE part of the profile from 400 km onward reflects a sedimentary cover of the Carpathian Foredeep at the eastern edge of the Bohemian Massif with velocities in the range of 2.5–5.5 km s^{-1} to a depth of about 10 km.

[33] Deeper parts of the upper crust, not resolved properly by the tomography, exhibit a very low vertical gradient with the V_p velocity of 6.0–6.1 km s^{-1} down to about a depth of 13 km. This low gradient is evidenced

by the fast decrease of *Pg* wave amplitude for most of the shot points. The alternative solution may involve introduction of a low-velocity layer in the upper crust, however, in our opinion the data did not allow the evaluation of the amount of velocity decrease, and therefore we decided not to propose it. In the middle crust, we identified two reflectors with a velocity contrast of 0.15–0.3 km s^{-1} in the depth ranges of 8–13 km and 17–20 km (*PiP* phases). The upper one is limited to the central part of the Bohemian Massif, to distances among 150–270 km along the profile, slightly dipping to the SE. The lower one is detectable with gaps almost throughout the whole massif.

[34] The most distinct lateral differences in V_p velocities in the Bohemian Massif can be distinguished in the lower crust. According to its properties and the character of the crust-mantle transition zone, the investigated area can be divided into three areas: (1) the central part of the Bohemian Massif, which correlates with the extent of the Moldanubian, (2) the NW part in the Saxothuringian, and (3) the SE part beneath the Moravian.

[35] In the Moldanubian, the *PmP* phase is the most pronounced in terms of high amplitude and short pulse length, and Moho is interpreted as a first-order discontinuity (from 6.9 to 8.1 km s^{-1}, see Figure 7a). The maximum Moho depth is 39 km. The V_p velocity in the middle and lower crust increases gradually from 6.5 km s^{-1} at 19 km
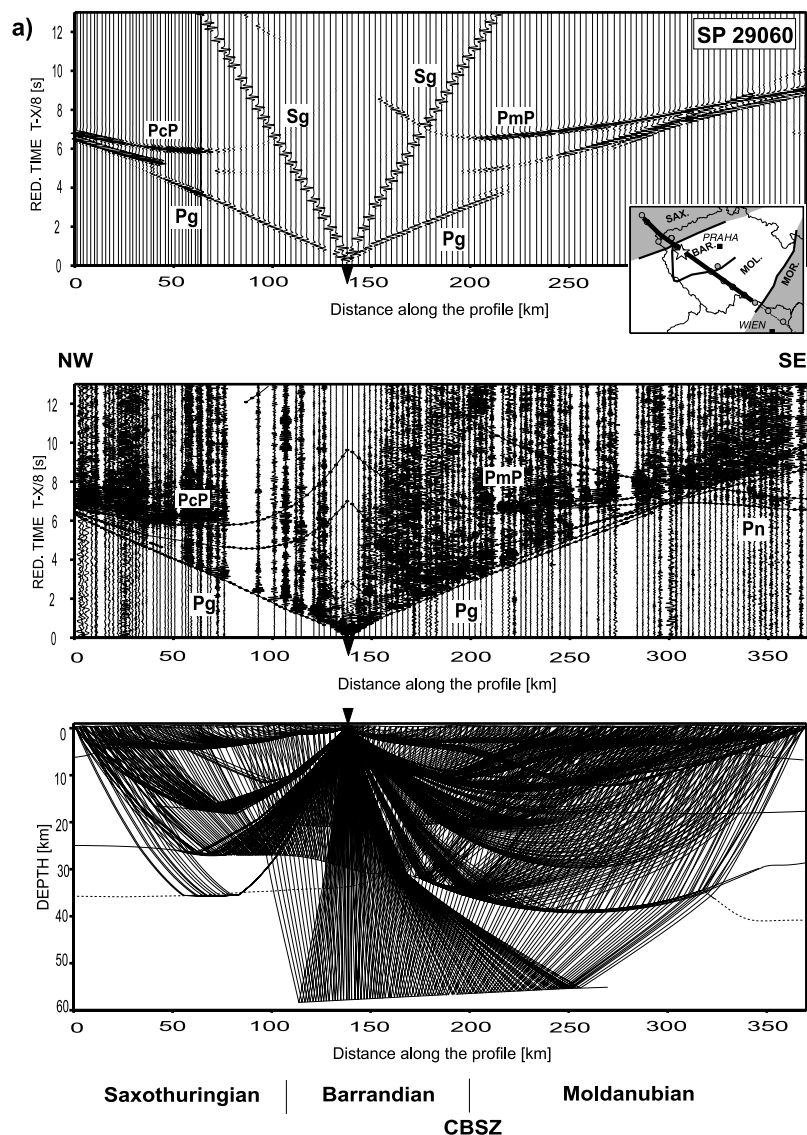
Figure 7. Examples illustrating forward modeling for selected shot points. (bottom) Model and ray paths, (middle) seismic record sections with superimposed calculated travel time curves (solid lines) for final model, and (top) synthetic seismic sections. (a) SP 29060, documentation of the Moho discontinuity in the Moldanubian, (b) SP 29150 documentation of gradient zone in the SE, and (c) SP 29110 and 29100, documentation of the mantle reflector. Reduction velocity is 8 km s^{-1}.

depth to 6.9 km s^{-1} above Moho, without any pronounced discontinuities in this depth range. The upper mantle velocities of 8.0–8.15 km s^{-1} are higher than in the neighboring units.

[36] In the Saxothuringian and partly beneath the Barrandian in the NW to a distance of 150 km along the profile, a lower crustal layer with a velocity gradient from 6.9 to 7.5 km s^{-1} can be inferred above the Moho. The character of the reflection from the top of the lower crust (*PcP* phase) with the long and irregular coda indicates that the layer is highly reflective, probably due to the presence of thin layers of material with contrasting seismic velocities. The properties of this layer were investigated in detail by synthetic seismogram modeling using the reflectivity method and will be discussed later. The top of this layer is located at a depth of 25–27 km

and is explained by the interface with a velocity contrast of 0.3 km s^{-1}. The bottom is interpreted to have a smaller velocity contrast at the Moho in order to obtain low amplitudes of the *PmP* phase as compared to the *PcP*, as observed in the data (Figures 2a and 4a). Since no refracted phase from this layer is observed and the *PmP* phase is poorly visible, the velocities in the lower crust are not well constrained and they are inferred only by modeling of the amplitude relation of the *PcP* to Moho reflections.

[37] The Moravian unit exhibits no distinct intracrustal reflectors except for the discontinuity at a depth of 18 km, which is the most pronounced at a distance of about 350 km along the profile and which produces a very strong reflection for SP 29140. The Moho reflection, however, is not visible (Figure 4b). The section in the very SE (SP 29150)
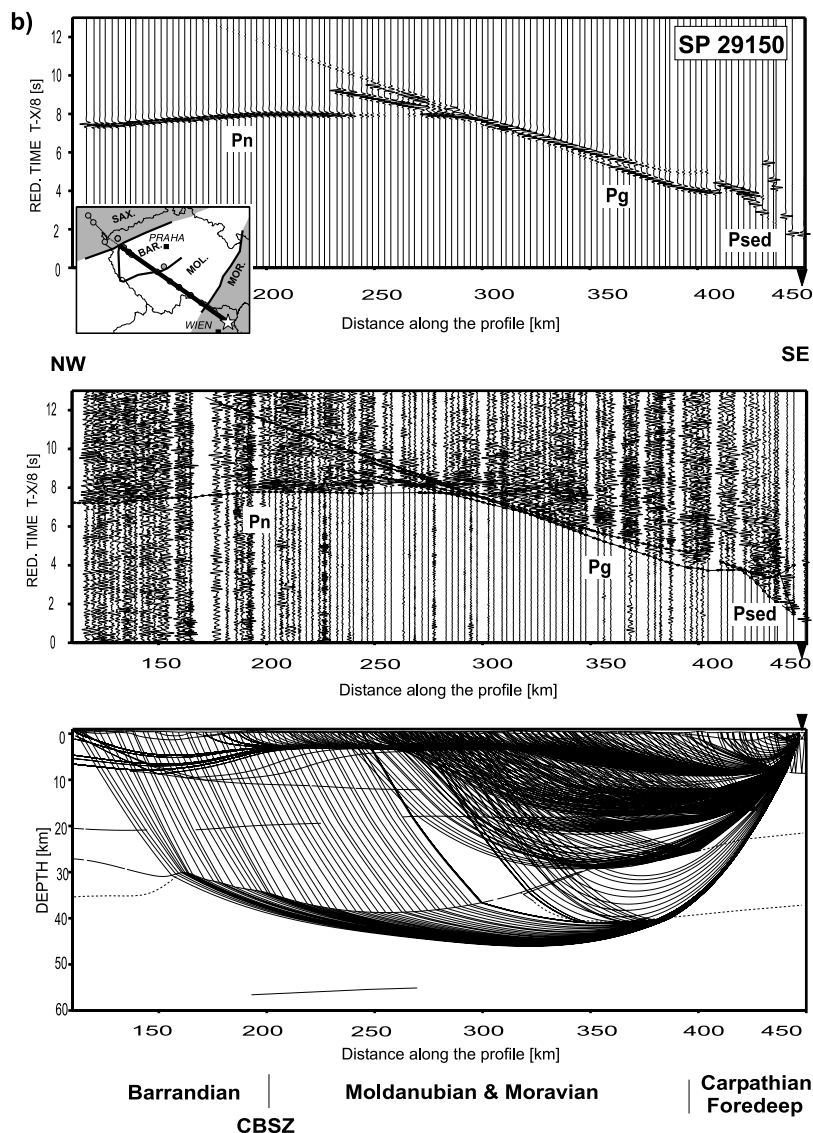
Figure 7. (continued)

exhibits quite unusual character: only the first arrivals can be clearly identified as a strong Pg turning into a very strong Pn phase. Apart from this, we identified a weak phase with a high apparent velocity in a short offset interval (140–180 km), immediately after the bending point of the first arrivals (place where Pg phase turns into Pn phase), forming a triplication. Travel time curves have this shape in media without velocity discontinuities but with a vertical gradient increase at some depth. Therefore, on the basis of the results of 1- and 2-D modeling of travel times and amplitudes, we suggest that the lower crust and crust-mantle transition in this area is a 17 km thick gradient zone at depths of 23–40 km with V_p velocities ranging from 6.8 to 7.8 km s^{-1} (Figure 7b). The top and bottom of this zone are interpreted with no distinct velocity discontinuities, especially in the very SE part. Therefore in this part of the model there is no Moho discontinuity but a thick crust-mantle transition zone. The uppermost mantle displays a velocity of 7.9 km s^{-1}.

[38] Mantle velocities in the Bohemian Massif range from 7.85–8.15 km s^{-1}, with the highest and well-constrained values in the central part in the Moldanubian. Upper mantle velocities of about 7.9 km s^{-1} in the NW and 8.0 km s^{-1} in the SE were derived with higher uncertainty. A local mantle reflector (at a distance of 115–265 km), slightly dipping to the NW, is visible at a depth of 55–58 km (Figure 7c). Velocities beneath this reflector are not constrained, as no arrivals are observed from below it.

6.3. Analysis of Resolution and Uncertainties

[39] Uncertainties for any 2-D seismic velocity model are due to a combination of several factors. Some amount of subjectivity cannot be avoided but the model accounts for the major features observed in the seismic data. Errors and uncertainties originate in travel time picking errors, misinterpretation of seismic phases and inaccuracy of modeling (misfit between data and modeled travel times), amount of data, geometry of the experiment and simplification of the
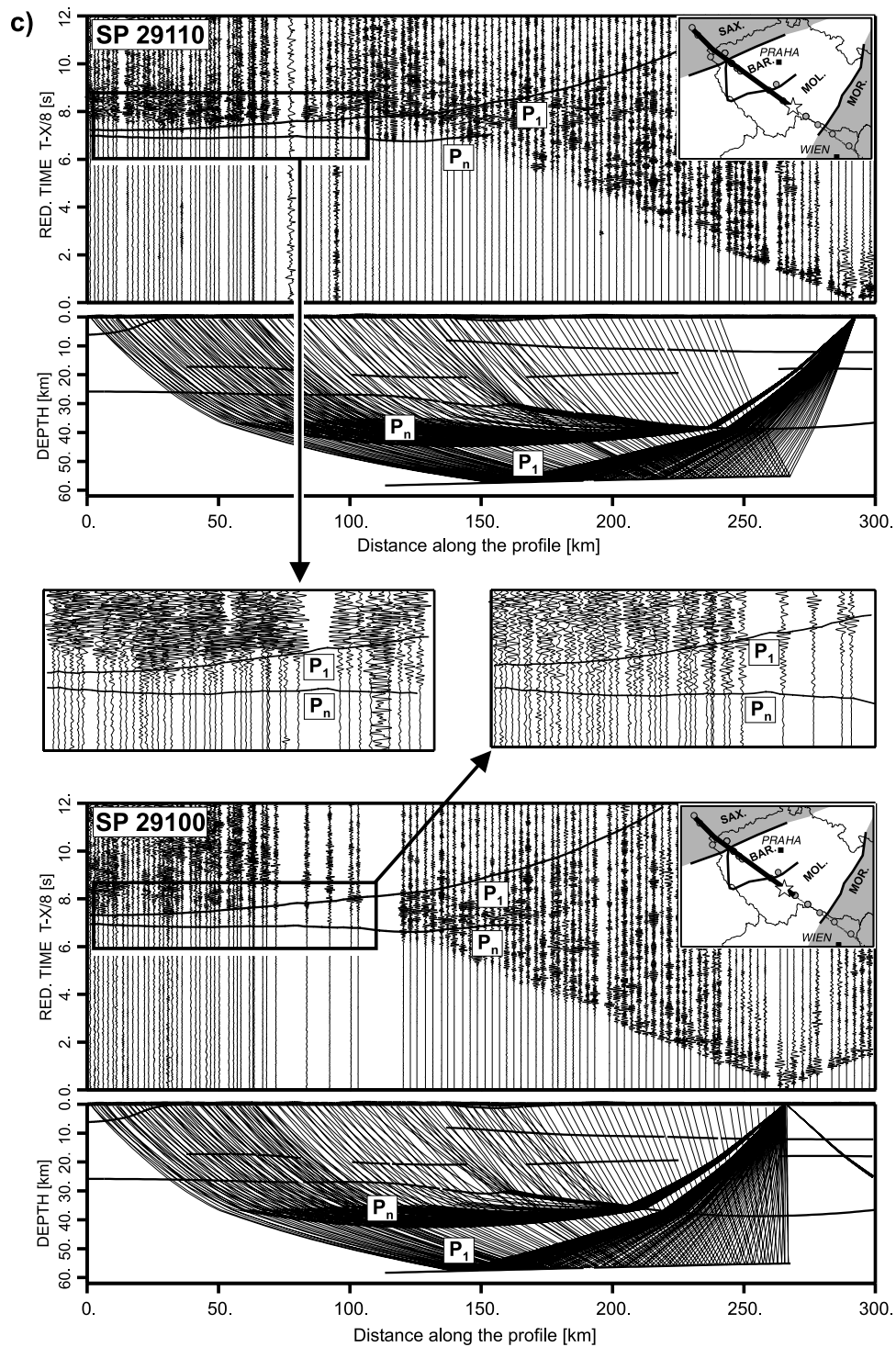
Figure 7. (continued)

model where 3-D effects or anisotropy are not considered. Also, the limitations of the ray theory must be kept in mind. Since the errors introduced by the interpreter during correlation and interpretation of seismic phases are subjective and impossible to quantify, it is not possible to perform a systematic error analysis.

[40] Figure 8a shows an approximate estimation of the differences in the calculated travel times of Pg waves.

The response of the presented model (Figure 6) and the response for the model with the Pg velocity perturbations of ± 0.2 km s^{-1} (about 3%) are depicted. Figure 8b shows an approximate estimation of the differences in the calculated travel times of PmP waves. It is clear that the uncertainties of the apparent velocity determination based on the first arrivals are much less than ± 0.2 km s^{-1}, and similarly, this suggests that the uncertainties in the
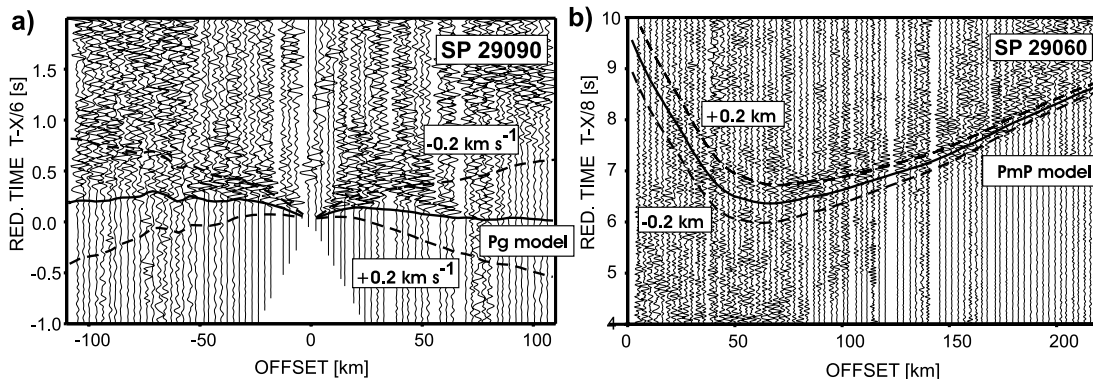
Figure 8. Estimation of model uncertainties. (a) Seismic section for shot point SP 29090 with calculated travel times for the *Pg* phase with velocity model shown in Figure 6 (solid line) and differences in travel times for the model with the upper crustal velocity different by ±0.2 km s^{-1} (dashed lines). Reduction velocity is 6.0 km s^{-1}. (b) Seismic section for shot point SP 29060 with calculated travel times for the *PmP* phase with the velocity model shown in Figure 6 (solid line) and differences in travel times for the model with the location of Moho different by ±2 km (dashed lines). Reduction velocity is 8.0 km s^{-1}.

depth of Moho (and intracrustal reflectors) are less than ±2 km.

7. Analysis of *S* Waves

[41] Some of the recorded seismic data show an *S* wave signal for refracted crustal phases (*Sg*) and reflected phases from Moho (*SmS*). Seismic sections show recordings with clear arrivals of *Sg* phase with an apparent velocity of 3.5 km s^{-1} and *SmS* waves up to an epicentral distance of 230–350 km. Neither intracrustal and mantle reflections nor Moho refraction, could be reliably identified (Figure 9). Altogether, refracted and reflected *S* wave arrivals have been correlated in 15 seismic sections. The recordings of the vertical component were used for *S* waves interpretation, as the horizontal component was recorded by a small number
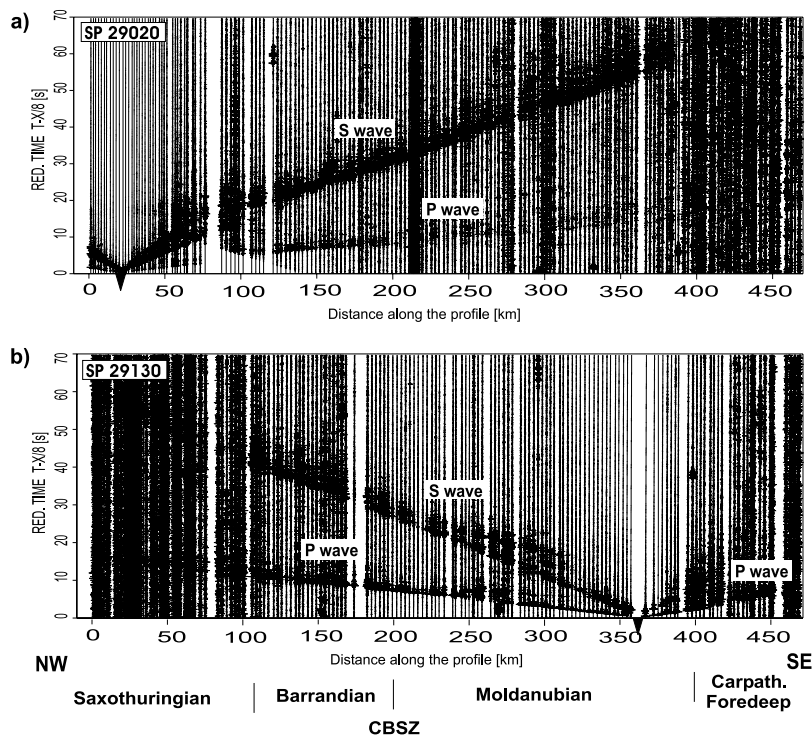

Figure 9. Examples of amplitude-normalized vertical component seismic sections for (a) SP 29020 and (b) SP 29130, along with the identifications of the main seismic phases of *P* and *S* waves. Reduction velocity is 8.0 km s^{-1}. A 2–10 Hz band-pass filter was applied.
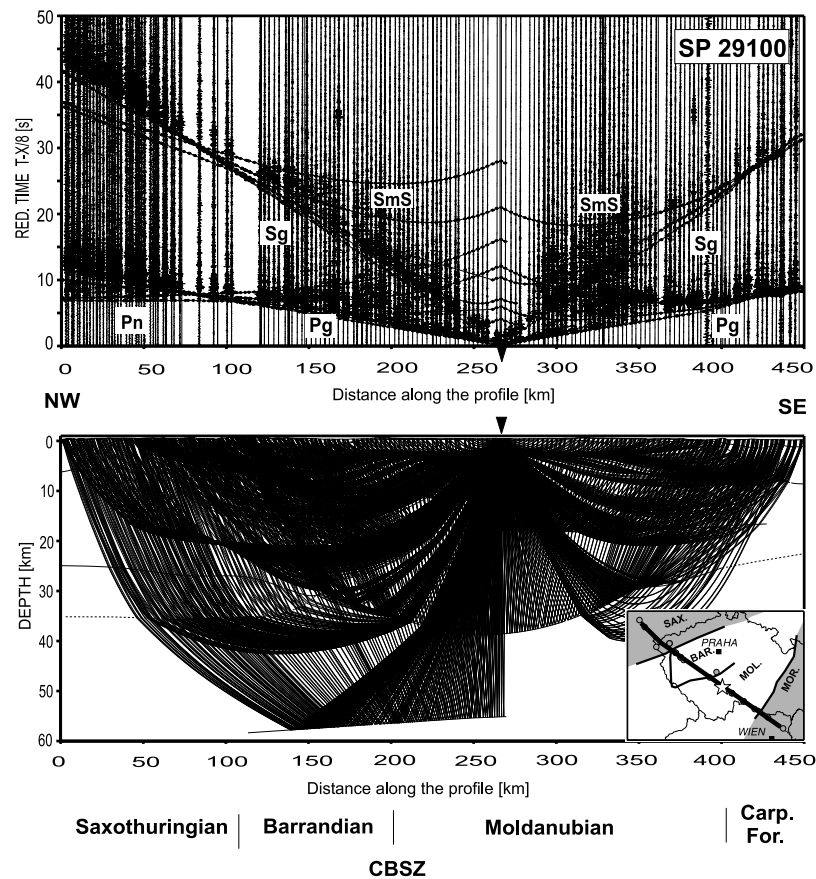
Figure 10. Example of *P* and *S* wave forward modeling for shot point SP 29100. (top) Model and ray paths; (bottom) seismic record sections with superimposed calculated travel time curves (solid line) for the final model. V_p/V_s ratio is 1.73. Seismic data section is shown with the same parameters and phase description as in Figure 2. Reduction velocity is 8 km s^{-1}.

of stations. Nevertheless, the vertical component shows as clear shear wave arrivals as the horizontal components, which is often the case with crustal refraction data [see, e.g., *Thybo et al.*, 2003]. In the middle part of the Bohemian Massif, the observed first *S* wave arrivals (*Sg*) at larger offsets (80–150 km) are weak compared to *S* wave reflected arrivals, which is similar to the effect of the *Pg* phase in that area. Similar to the *P* wave, it again indicates a small velocity gradient in the upper crustal parts. In the NW, we can observe *ScS* phase (reflection from the top of the lower crust) with a long coda, indicating that the lower crust is reflective for *S* waves too.

[42] The best branches of correlated *S* wave travel times were used for forward modeling to provide another constraint in discriminating different tectonic areas. The *S* wave velocity model in the first approximation was adopted from the *P* wave model and converted into the V_s velocity model using the standard ratio of $V_p/V_s = 1.73$ [e.g., *Christensen*, 1996]. Lack of reflected crustal arrivals, as well as refractions from the upper mantle, together with the limited number of good quality travel time picks obtained did not allow detailed *S* wave modeling, and thus the obtained accuracy did not enable fine variations of the V_p/V_s ratio to be determined throughout the model. Forward modeling of the *S* wave travel times for available refracted (*Sg*) and reflected (*SmS*) phases for the given model did not indicate

that V_p/V_s differs substantially from 1.73 along the profile (Figure 10). The only exception can be found for the upper crust at the distance of 150–230 km along the profile, where slightly higher values of the V_p/V_s ratio (1.76) can be observed. Such lower *S* velocity values may suggest slightly higher density of cracks or fluid-filled fractures in that area roughly spreading along the Central Bohemian Shear Zone (at the distance of 200 km along the profile).

8. Modeling of Lower Crustal and Moho Characteristics by the Reflectivity Method

[43] During forward modeling we observed differences in the amplitudes and coda length of some reflected phases that were not possible to analyze by the ray-tracing modeling. Therefore we used the reflectivity method by *Fuchs and Müller* [1971] to simulate the variability of the character of the lower crust and Moho reflections assuming a 1-D seismic velocity-depth structure. On the basis of the result of 2-D forward modeling we took representative 1-D functions from three different areas and tested them for the existence of features such as laminated layers with alternating high and low velocities or high gradient zones. For three representative seismic sections (SP 29040, 29050, and 29150), we calculated synthetic seismograms and compared the seismic data with these synthetic seismograms (see Figure 11).
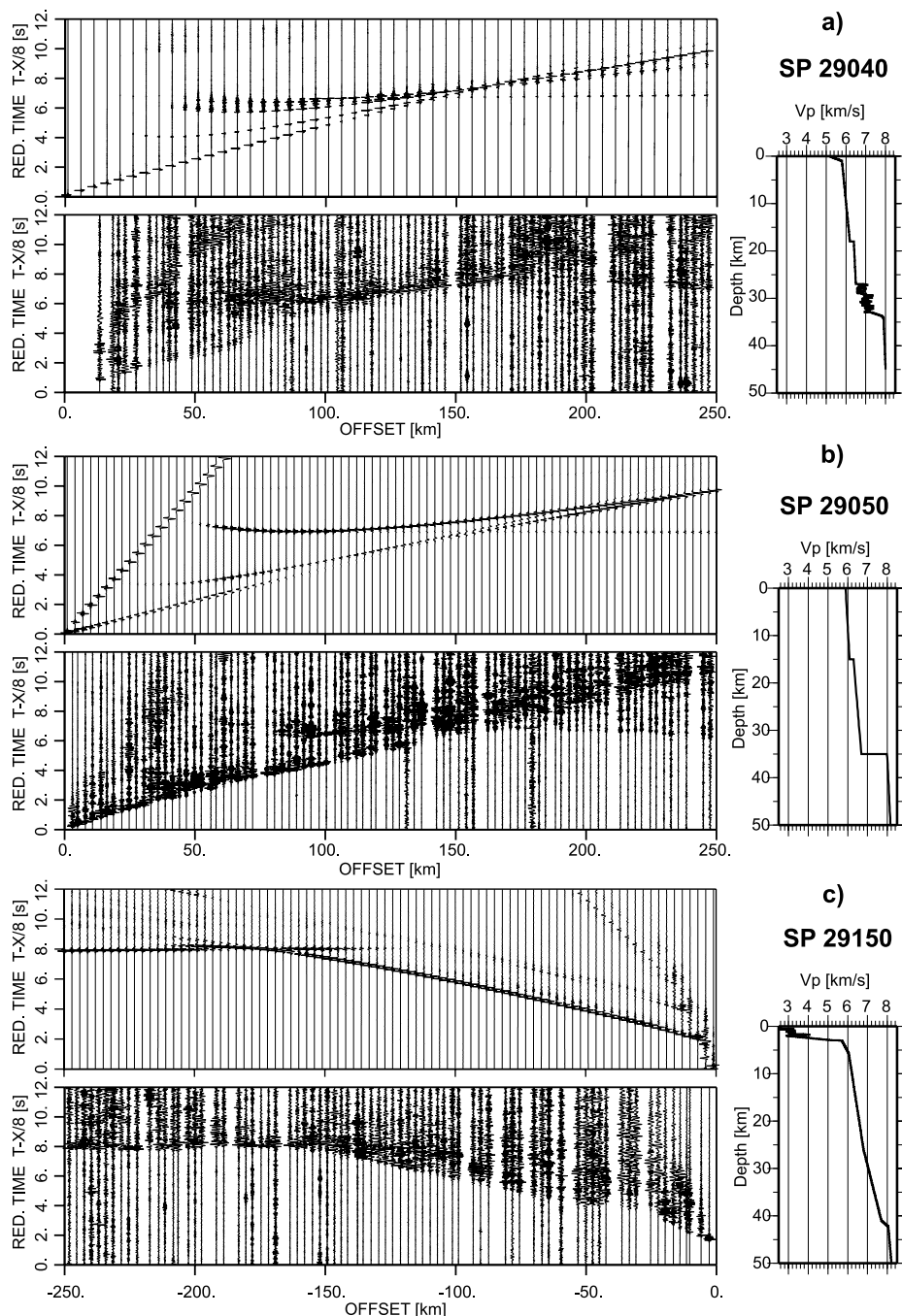
Figure 11. Modeling of the lower crustal and Moho characteristics using the reflectivity method. (top) Synthetic reflectivity seismograms and (bottom) seismic data; (right) 1-D velocity model. Seismograms and seismic data sections are shown with the same scaling parameters as in Figure 2. (a) SP 29040, Saxothuringian area (NW). Strong reflections form the top of the lower crust (*PcP*) and from the laminated lower crust, with the coda obscuring the *PmP* phase, weak *Pn*. (b) SP 29050, Moldanubian area. No *PcP* phase, sharp Moho reflection (*PmP*), no evidence of the laminated lower crust. Interpreted as strong Moho discontinuity with the velocity contrast. (c) SP 29150, SE edge of the Bohemian Massif. Very strong and ringing first arrivals (*Pg* and *Pn*). Interpreted as a thick gradient zone.

[44] Section 29040 (Figure 11a), recorded in the area of the Saxothuringian (NW), displays a high-amplitude reflection from the top of the lower crust, with a long coda suggesting strong reflectivity of the lower crustal layer. The coda obscures a relatively weak *PmP* phase. The *Pn* phase is weak, but observable. The proposed 1-D model explains it by the existence of the lower crustal layer with a background V_p velocity of 6.9–7.3 km s^{-1}, consisting of layers of randomly alternating high and low velocities with a standard deviation of 4% and correlation length of 300 m. Moho is interpreted as a 1 km thick gradient zone at a depth of 33 km with velocities increasing gradually from 7.3 to 7.9 km s^{-1}, which produces a refracted phase weak enough to fit the data.

[45] The section from SP 29050 (Figure 11b), located in the Moldanubian area, shows relatively sharp onsets of the *PmP* phase and a clear *Pn* phase. The high-velocity reflective lower crust is absent in the model and Moho is suggested to be a discontinuity with a velocity contrast from 6.8 to 8.1 km s^{-1}.

[46] The section from SP 29150 (Figure 11c), recorded at the SE edge of the Bohemian Massif, differs from all other data along the profile, and bears some resemblance to few sections from the CEL10 profile of the CELEBRATION 2000 experiment (under interpretation). Strong first arrivals, including the *Pn* phase, were observed up to the offsets of 300 km, but the *PmP* phase is not visible. Also no clear intracrustal reflections are visible. Thus the lower crust is interpreted as a thick layer with a high gradient of V_p velocities from the lower crust to the uppermost mantle. Such a gradient zone may represent a broad transition zone between the crust and mantle. The overall ringing character of the data and long coda (high amplitude oscillations observable within a few seconds after the first arrivals) may be explained by a high reflectivity caused by small-scale velocity fluctuations in the thick sedimentary sequences beneath the shot point. The long coda can also be explained as due to the overall increased reflectivity of the Moravian basement.

9. Gravity Modeling

[47] After interpretation of seismic velocities, we used gravity modeling to test the seismic model and to obtain additional geophysical constraints on the crustal structure and composition. In the first approximation we converted the *P* wave velocity model (Figure 6) into density blocks using a velocity-density relation of *Thybo and Schönharting* [1991] and created an initial density model. Using the 2-D modeling software GRAVMOD developed by *Zelt* [1994], we compared the gravity effect of this initial density model with Bouguer anomalies along the profile. We then modified the densities in model blocks where needed by trial-and-error in order to obtain a better fit to experimental gravity data.

[48] Figure 12a shows Bouguer anomalies together with the gravity response of the initial density model and resulting final model. The analysis of the gravity response for the initial model (Figure 12b) indicates that the seismic model agrees with Bouguer anomalies in terms of the large-scale and deeper structure because the calculated gravity effect resembles a long-wavelength, smoothed version of the

experimental gravity values. The most prominent discrepancy (about 50 mGal) occurs in the distance range of 60–120 km along the profile, where the negative anomaly reaches −60 mGal. This minimum coincides with the location of the granitoid Karlovy Vary Pluton, mostly located slightly to the NE of the CEL09 profile. Therefore the discrepancy for the initial model is probably due to the larger density difference between the Karlovy Vary granites and surrounding rocks than estimated from seismic velocities. Another contributing factor might be a 3-D influence of the density anomalies, not taken into account by the 2-D velocity modeling. However, the aim was to test 2-D velocity results, therefore we confined the gravity modeling to two dimensions.

[49] The final density model (Figure 12c) explains discrepancies in the short-wavelength anomalies, which results in a better fit of the corresponding gravity curve. The modifications were mostly confined to the upper crust, with the biggest changes in the Karlovy Vary area. There, the difference between the granitoids and neighboring metamorphic rocks is more pronounced in density (about 0.1 g cm^{-3}) than in seismic velocities, consistently with the results of *DEKORP Research Group* [1994]. Other, smaller corrections (positive and negative) were made in most parts of the upper crust, explaining the anomalies caused by numerous granitoid plutons, as well as mafic rocks, occurring along the profile or in its close vicinity and producing a gravity effect not accounted for by velocity modeling.

10. Interpretation and Discussion of the Results

[50] The CELEBRATION 2000 profile CEL09 was designed to cross the key tectonic units of the Bohemian Massif. Figure 13 summarizes the main interpreted features of the crust and uppermost mantle together with the 1-D velocity characteristics for different parts of the Bohemian Massif and suggests possible tectonic interpretation of velocity and gravity models that we discuss in detail in this section. In general, the average overall compressional velocity of the crust in the Bohemian Massif is about 6.3 km s^{-1} and is slightly lower than the crustal average of 6.45 km s^{-1} presented by *Christensen and Mooney* [1995] for the continental crust. Even then, it is still higher than the average of 6.0–6.2 km s^{-1} observed in the Moldanubian and Saxothuringian in SW Germany [*Giese*, 1976].

10.1. Upper Crust

[51] The upper crust shows relatively small lateral variations of V_p (except for younger formations at both ends of the profile); nevertheless, the large-scale velocity anomalies may be correlated with the composition of the individual tectonic units. We believe that in this case even relatively small velocity differences may be meaningful because the uppermost part of the model is best resolved due to the maximum ray density in this depth range.

[52] In the uppermost crust, the Barrandian and Saxothuringian show a high-gradient layer with velocities of 5.8–5.9 km s^{-1} down to a depth of 3 km, which may be connected with volcano-sedimentary and sedimentary Lower Paleozoic rocks. The metamorphic rocks and Variscan granitoid intrusions in the Moldanubian are characterized by a similar velocity increase of 5.9–6.0 km s^{-1} down
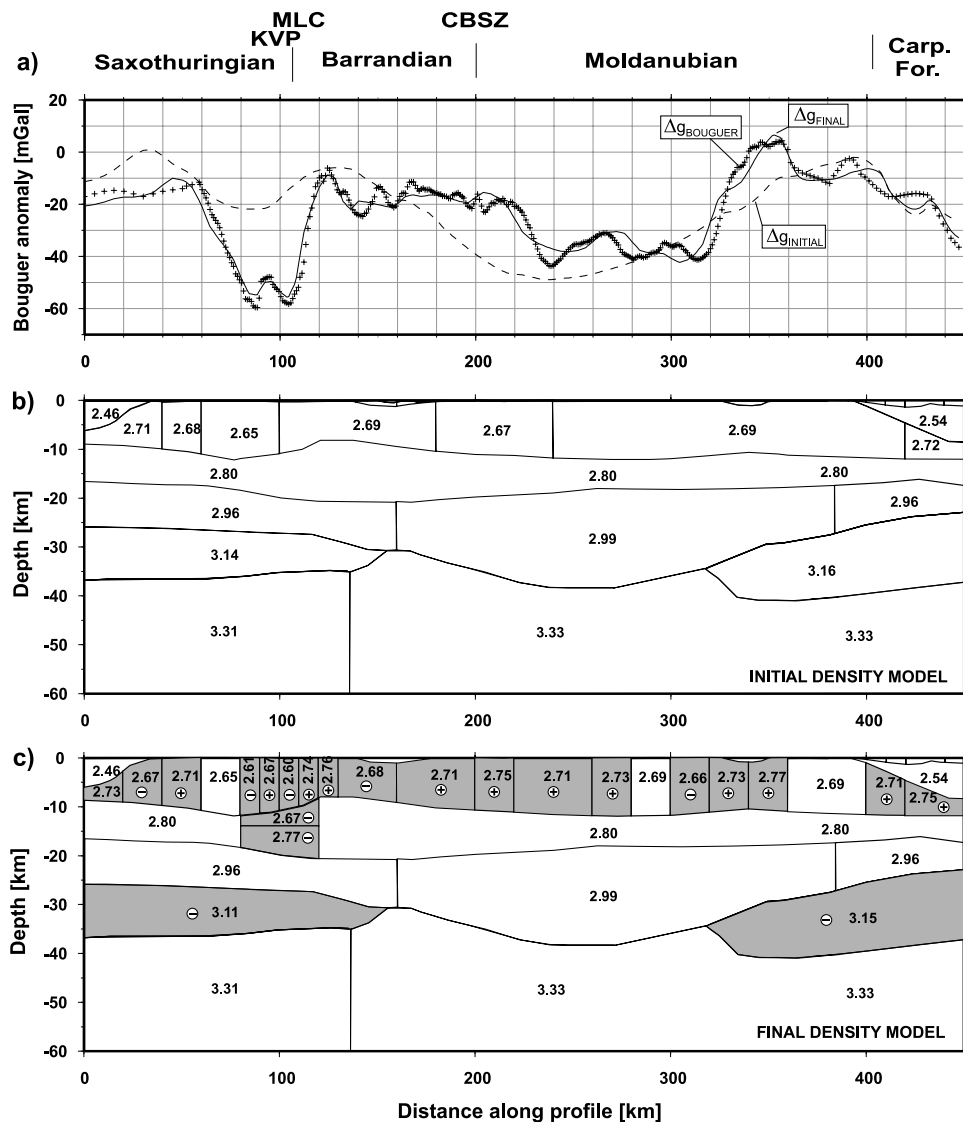
Figure 12. Gravity modeling. (a) Bouguer anomaly (crosses), calculated gravity effect from initial density model (dashed line) and from final density model (solid line). (b) Initial gravity model converted from seismic velocity model in Figure 6. (c) Final gravity model. Blocks with densities different from initial model are marked in gray. Signs in circles represent positive or negative density modifications. Numbers in blocks indicate densities in g cm^{-3}. Geological abbreviations are MLC, Mariánské Lázně Complex; KVP, Karlovy Vary Pluton; CBSZ, Central Bohemian Shear Zone.

to a depth of 2 km due to the closing of microcracks under increasing pressure [*Pros et al.*, 1998]. In deeper parts of the upper crust down to about 13 km, the vertical velocity gradient is very small (velocity increase of 0.05–0.1 km s^{-1} over an interval of 10 km), as indicated by a fast decay of the Pg wave amplitude. In terms of horizontal variability, a slightly smaller V_p velocity (5.9–6.0 km s^{-1}) characterizes the Saxothuringian Paleozoic sediments, and possibly also the granitoids of the Karlovy Vary intrusion at a distance of around 90 km along the profile. The latter, even if not as pronounced in terms of velocities, produces a significant (about 0.1 g cm^{-3}) density contrast with respect to neighboring areas. Similar V_p velocities characterize the upper crust of the Barrandian unit. Slightly higher velocities occur in the Moldanubian, especially in its central part (up to 6.1 km s^{-1}), abundant in high-grade gneisses and

migmatites of the crystalline basement. Lower velocities (5.95 km s^{-1}) at a distance of 200–230 km along the profile and depth of 10 km may be connected with the intrusion of the granitoid Central Bohemian Pluton.

[53] Local near-surface velocities of 6.05 km s^{-1} and densities with a density contrast of 0.1 g cm^{-3} observed in the area of the amphibolite Mariánské Lázně Complex at the boundary between the Saxothuringian and Barrandian are smaller than those expected for a body of mafic composition. Possible reason is that the profile crosses only a thin portion of the complex at its NE end, and thus it has only a moderate influence on the apparent velocities of the refracted arrivals.

[54] More pronounced V_p variations in the upper crust were observed in the NW part of the Saxothuringian. They show velocities of 5.0 km s^{-1} at the surface increasing
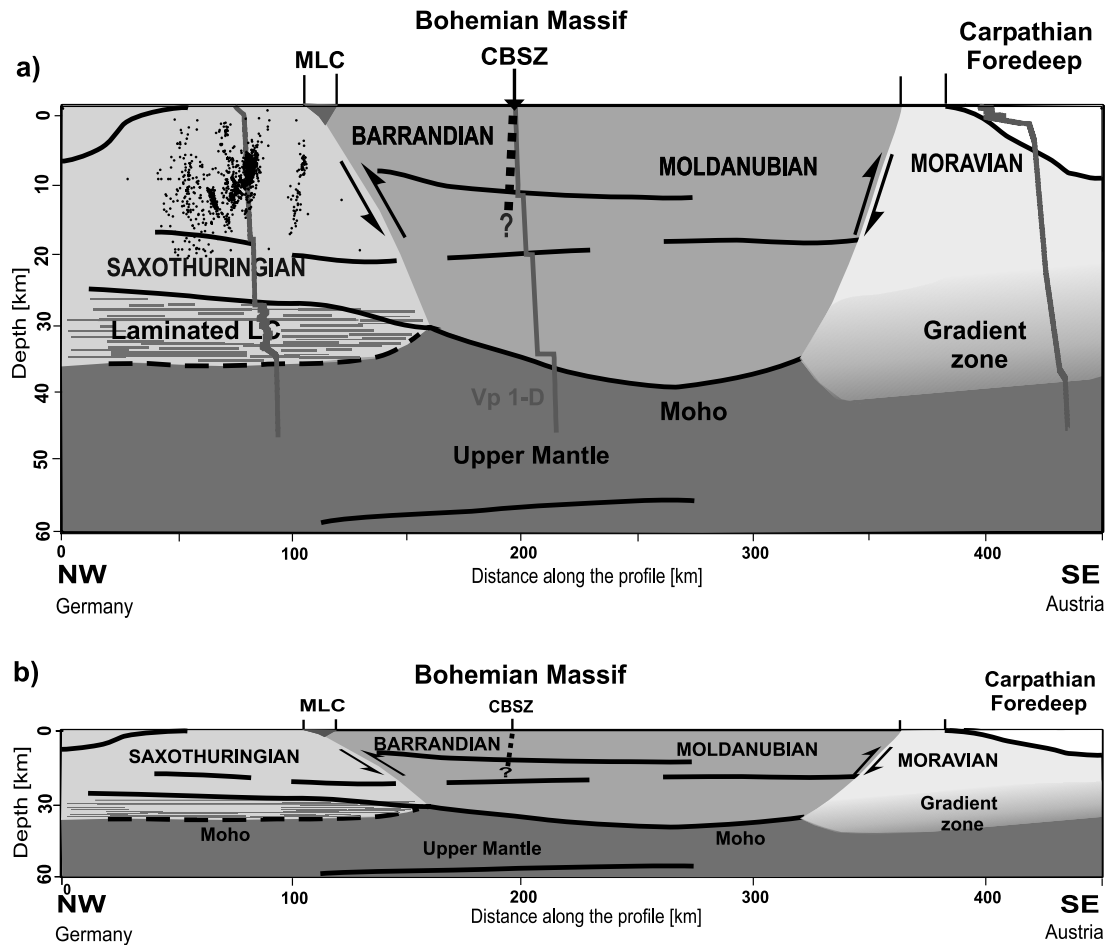
Figure 13. Schematic tectonic representation along profile CEL09. Dots show locations of hypocenters of the earthquake swarms in the west Bohemia/Vogtland area. Superimposed are 1-D velocity characteristics showing differentiation in the lower crust for different parts of the Bohemian Massif (from left): the Saxothuringian with laminated lower crust dipping SE; high-velocity contrast at Moho in the Moldanubian; the Moravian with whole crustal gradient zone. Arrows indicate relative movement along contact zones. MLC, Mariánské Lázně Complex; CBSZ, Central Bohemian Shear Zone. (a) Vertical exaggeration of 1:3. (b) Without vertical exaggeration.

rapidly to 6.0 km s^{-1} at a depth of 6 km and correlate on the surface with the Carboniferous flysch of the Teuschnitz syncline (see Figure 1). Considerably lower velocities (2.5–5.5 km s^{-1}) occur in the SE part of the profile beyond a distance of 400 km, where the Carpathian Foredeep forms an up to 10 km thick sedimentary complex.

[55] Since the profile CEL09 crosses the seismically active west Bohemian region, Figure 13 shows also locations of hypocenters of the earthquake swarms recorded between 1985 and 1998 overlain on the sketch of the crustal structure. In this projection, only hypocenters with the distance smaller than 20 km from the profile were selected. Comparison with the velocity model shows that the hypocenters are located in the upper and middle crustal layer, the majority occurring in the upper crust. The seismically active region coincides well with the location of the lower velocity (5.9 km/s) region in the upper crust at distances 50–120 km along the CEL09 model, at 0–12 km depth (see Figure 6). According to *Špičák and Horálek* [2001] this activity may be caused by emission of fluids released by ongoing

magmatic activity and/or fracturing of the crust. As both phenomena decrease seismic velocities, low V_p may be due to the same factors that cause the seismic activity of the region. However, the relation of velocity decrease to the seismically active area is still a matter of further investigation.

10.2. Middle Crust

[56] In the middle crust two reflectors with a velocity contrast of 0.2 km s^{-1} were observed in a depth range of 7–12 km and 17–20 km. The first is confined to the area of the Barrandian and partly Moldanubian units, dipping to the SE. The deeper reflection can be traced with few gaps throughout the whole model, and is the most pronounced at a distance of about 350 km, producing very strong reflections for SP 29140 (Figure 4b). The V_p velocities in the middle crust are in the range of 6.15–6.25 km s^{-1} and display no horizontal variability, as this part of the model is constrained mainly by the reflections from the interface at a depth of 16–20 km.

10.3. Lower Crust

[57] In the deeper parts, three different types of lower crust and uppermost mantle can be distinguished. The central part, corresponding to the Moldanubian unit, is characterized by the wave field with sharp onsets of PmP phases and a clear Pn phase. The lower crust displays average velocities of 6.8 km s^{-1} and a strong velocity contrast at Moho modeled as a first-order discontinuity (6.8–8.1 km s^{-1}). The Moho depth reaches 39 km and it is the deepest and the most pronounced Moho within the whole Bohemian Massif. This area also correlates with the area of minimum heat flow value (<50 mW m^{-2}) [*Hurtig et al.*, 1992] and may represent a part of the relatively cold and strong Moldanubian lithosphere [*Babuška and Plomerová*, 2000]. The crustal thickness also agrees with previous seismic results [e.g., *Beránek and Zátopek*, 1981; *Bucha and Blížkovský*, 1994].

[58] The NW part, in the Saxothuringian and partly beneath the Barrandian to a distance of ~150 km along the profile, shows high-amplitude reflections from the top of the lower crust with a long coda suggesting strong reflectivity in this layer. The Pn phase is weak but visible. The area is interpreted with a highly reflective layer above the Moho, producing a long coda, which obscures a relatively weak PmP phase. There is a strong velocity contrast at the top of this layer (0.3 km s^{-1}) as compared to the contrast at the Moho. The velocities in the lower crust range from 6.9 to 7.3 km s^{-1}, and its upper boundary is in the depth range of 25–27 km. Moho is represented by a thin (about 1 km) gradient zone where the velocity increases from 7.3 to 7.9 km s^{-1} at a depth of 34–35 km. The correlation length of the velocity fluctuations in the lower crust was roughly estimated to be 300 m. The lamella thicknesses, reported in Variscan areas by other authors, are, e.g., 120 m in Germany [*Sandmeier and Wenzel*, 1990] or 100–300 m in Poland [*Jensen et al.*, 1999].

[59] CEL09 results in the NW area can be compared with those determined along the perpendicular wide-angle refraction and reflection profiles GRANU'95 and MVE 90 (see Figure 1). The GRANU'95 experiment indicate a velocity increase from 6.5 km s^{-1} in the middle crust to an average value of 7.0 km s^{-1} at a depth of 24 km interpreted as the top of the lower crust [*Enderle et al.*, 1998]. The MVE 90 shows a highly reflective layer in this area at 8–10 s of two-way travel time corresponding to the depth range of 24–32 km [*DEKORP Research Group*, 1994], which may be viewed as the laminated lower crust found in several Variscan areas. Average V_p velocities in the lower crust and upper mantle along CEL09 (7.1 and 7.9 km s^{-1}, respectively) are consistent with the velocities along GRANU'95 and MVE 90 (7.0 and 7.9–8.1 km s^{-1}, respectively). However, CEL09 crustal thickness is a little larger than in case of GRANU'95 and MVE 90 (30 and 33 km).

[60] According to *Enderle et al.* [1998], elevated lower crustal velocities seem to be characteristic for the Saxothuringian unit. The change of the lower crustal velocities at a distance of ~150 km along the CEL09 profile may mark the SE extent of the Saxothuringian lower crust (Figure 13). It correlates with the interpretation of the 9HR [*Tomek et al.*, 1997] and DEKORP 4 profiles [*Vollbrecht et al.*, 1989] where the contact between the Saxothuringian and the units

in the SE is interpreted as a SE dipping overthrust, reaching the base of the crust about 50–80 km to the SE of the contact zone at the surface.

[61] Such a highly reflective lower crust is a phenomenon frequently observed in Caledonian and Variscan areas. It was also found along the deep reflection profiles crossing CEL09 in the Saxothuringian: the MVE 90 and locally 9HR. The most common explanations assume that bands of reflections result form densely spaced layering, produced by igneous intrusions of mafic melt from the upper mantle, subhorizontal ductile shear zones, or layers with higher fluid content [*Warner*, 1990]. Here, the explanation involving the presence of fluids in the lower crust is not likely, as the S wave reflections from the lower crust display very much the same characteristics as the P wave in terms of the length of the coda and amplitudes relative to the Moho reflection. Therefore we suggest that lower crustal reflectivity may be caused by mafic intrusions, possibly stretched and arranged horizontally during postorogenic extension.

[62] The SE end of the profile shows strong first arrivals and high reflectivity in the whole crust without any strong intracrustal reflections and with missing PmP phase. The overall ringing character of the data and a long coda after the first arrivals is explained by the high reflectivity caused by the small-scale velocity fluctuations in the thick sedimentary sequences of the Carpathian Foredeep. On the basis of the travel time and amplitude character of the data, the lower and middle crust of the Cadomian basement seems to form a thick gradient zone starting at a distance of some 330 km along the profile, with velocities of 6.8–7.8 km s^{-1} ranging in a depth of 23–40 km. Such a velocity structure is quite unusual for a relatively old Cadomian unit and its origin is difficult to interpret. It may represent gradual changes of the lower crustal composition, with the percentage of mafic/ultramafic material increasing with depth. Alternative explanation may involve a change in metamorphic grade with an incomplete phase transition of mafic (gabbroic) rocks from amphibolite to eclogite facies. This process is likely to occur continuously over a wide range of pressure, producing a gradual increase of seismic velocities with depth [*Furlong and Fountain*, 1986]. *Hurich et al.* [2001], studying properties of rock samples of eclogite facies, report velocities and densities for HP granulites in the range of 7.0–7.7 km s^{-1} and 3.05–3.3 g cm^{-3}, respectively, depending on the metamorphic grade. Complete eclogitization is unlikely, as it would result in too high densities (3.3–3.5 g cm^{-3}) compared to the model.

[63] During previous investigations, the Moho depth in the SE was not resolved [*Beránek and Zátopek*, 1981], or was approximated by a discontinuity at a depth of 32–35 km [*Bucha and Blížkovský*, 1994]. We do not see any evidence for a discontinuity, but our model is consistent with these results, because the overall seismic travel time or gravity effect of the gradient layer will be similar to the effect of a discontinuity located at the center of the layer, given the same average velocity.

10.4. Mantle

[64] The local mantle reflector at a depth of 55–58 km in the central part of the Bohemian Massif (distance 115–265 km) dips slightly to the NW. Its position corresponds to the mantle reflector located on the 9HR profile [*Tomek et*

al., 1997] in the cross section with CEL09. Geologically it can be viewed either as a first-order discontinuity or a shear zone with properties different from the neighboring mantle.

11. Summary and Conclusions

[65] Seismic data of high quality for interpretation of both the *P* and *S* wave velocity structure was acquired during the CELEBRATION 2000 experiment along a 450 km long, NW-SE striking profile across the Bohemian Massif. The data have been interpreted by seismic tomography inversion of the travel times of first arrival *P* waves, by two-dimensional ray-tracing of travel times of first and later arrivals of *P* and *S* waves, as well as by calculation of two dimensional synthetic seismograms for the *P* wave arrivals. Additional constraint on the crustal structure was given by gravity modeling. Our effort to model these data provides us with the conclusions that are summarized in the tectonic sketch in Figure 13.

[66] The presented crustal model across the Bohemian Massif supplements previous results of geophysical investigations and provides new important information about the structure of the Bohemian Massif, particularly about lower crustal properties and the character of the crust-mantle transition. It helps to verify hypotheses concerning the tectonic evolution of the area during the Paleozoic. Previous wide-angle seismic data provided only generalized information about the velocity distribution (mainly in the upper crust) and about crustal thickness, using methods of kinematic modeling. Our research supplements the kinematic modeling with analysis of the amplitude and character of the seismic wave field and thus gives better insight into the properties of the crust and upper mantle. The boundaries of the main crustal blocks of the Bohemian Massif (Saxothuringian, Barrandian, Moldanubian, Moravian) were previously traced on the surface, based predominantly on the available geological data, whereas the locations of their contact zones at depth were only partially constrained. Our results show differentiation of the structure not only in the upper crustal parts, but mainly at lower crust and upper mantle level, which gives some indications for tracing of crust-forming processes during the Variscan orogeny.

[67] Seismic reflection data along profile 9HR indicated that the Saxothuringian has been underthrusted beneath the Barrandian/Moldanubian along a SE dipping thrust zone. The new CEL09 model supports these results and provides additional information for locating the Saxothuringian/ Barandian contact at the lower crustal level. Its location is inferred from the differences between high-velocity, strongly reflective lower crust, which we attribute to the Saxothuringian unit, and moderate-velocity unreflective lower crust and sharp Moho characteristics for the Barrandian/ Moldanubian unit. The latter is connected with the crustal thickening of the crystalline segment, the Moldanubian, characterized by the deepest and the most pronounced Moho within the whole Bohemian Massif.

[68] The deep structure of the Moravian unit and its contact with the Moldanubian were, up to now, not constrained by any wide-angle or reflection seismic data. New CELEBRATION 2000 data suggest a peculiar lower crustal/ upper mantle structure beneath this region, where a thick crust-mantle transition zone occurs. We postulate that it may

be a characteristic feature of the Moravian unit, and that the western termination of this transition zone may delimit the NW extent of the Moravian lower crust, reaching ~40 km farther to the NW than the Moldanubian thrust on the surface. The contact of the above units would form a NW dipping whole crustal zone with the dip of 45° and may represent underthrusting of the Moravian beneath the Moldanubian during the Variscan collision.

References

Aki, K., and P. G. Richards (1980), *Quantitative Seismology, Theory and Methods*, W. H. Freeman, New York.

Babuška, V., and J. Plomerová (2000), Saxothuringian-Moldanubian suture and predisposition of seismicity in the western Bohemian Massif, *Stud. Geophys. Geod.*, *44*, 292–306.

Beránek, B., and A. Zátopek (1981), Earth's crust structure in Czechoslovakia and central Europe by methods of explosion seismology, in *Geophysical Synthesis in Czechoslovakia*, edited by A. Zátopek, pp. 253–264, Veda, Bratislava, Slovakia.

Beránek, B., and M. Zounková (1977), Investigations of the Earth's crust in Czechoslovakia using industrial blasting, *Stud. Geophys. Geod.*, *21*, 273–280.

Bucha, V., and M. Blížkovský (Eds.) (1994), *Crustal Structure of the Bohemian Massif and the West Carpathians*, Academia Praha, Prague, Czech Republic.

Červený, V., and I. Pšenčík (1984), SEIS83—Numerical modelling of seismic wave fields in 2–D laterally varying layered structures by the ray method, in *Documentation of Earthquake Algorithms*, edited by E. R. Engdal, *Rep. SE-35*, pp. 36–40, World Data Cent. A for Solid Earth Geophys., Boulder, Colo.

Christensen, N. I. (1996), Poisson's ratio and crustal seismology, *J. Geophys. Res.*, *101*, 3129–3156.

Christensen, N. I., and W. D. Mooney (1995), Seismic velocity structure and composition of the continental crust: A global view, *J. Geophys. Res.*, *100*, 9761–9788.

Czuba, W., M. Grad, U. Luosto, G. Motuza, V. Nasedkin, and POLONAISE P5 Working Group (2002), Uppercrustal seismic structure of the Mazury complex and Mazowsze massif within East European Craton in NE Poland, *Tectonophysics*, *360*, 115–128.

Dallmeyer, D., W. Franke, and K. Weber (1994), *Pre-Permian Geology of Central and Eastern Europe*, Springer, New York.

DEKORP Research Group (1988), Results of the DEKORP 4/KTB Oberpfalz deep seismic reflection investigations, *J. Geophys.*, *62*, 69–101.

DEKORP Research Group (1994), The deep reflection seismic profiles DEKORP 3/MVE-90, *Z. Geol. Wiss.*, *22*(6), 623–824.

Enderle, U., K. Schuster, C. Prodehl, A. Schultze, and J. Briebach (1998), The refraction seismic experiment GRANU'95 in the Saxothuringian belt, southeastern Germany, *Geophys. J. Int.*, *133*, 245–259.

Finger, F., and H.-P. Steyrer (1995), A tectonic model for the eastern Variscides: Indications from a chemical study of amphibolites in the southeastern Bohemian Massif, *Geol. Carpathica*, *46*(3), 137–150.

Fischer, T., and J. Horálek (2003), Space-time distribution of earthquake swarms in the principal focal zone of the NW Bohemia/Vogtland seismoactive region: Period 1985–2001, *J. Geodyn.*, *35*, 125–144.

Franke, W., V. Haak, O. Oncken, and D. Tanner (Eds.) (2000), *Orogenic Processes: Quantification and Modelling in the Variscan Belt*, Geol. Soc. Spec. Publ., *179*, 464 pp.

Fuchs, K., and G. Müller (1971), Computation of synthetic seismograms with the reflectivity method and comparison with observations, *Geophys. J. R. Astron. Soc.*, *23*, 417–433.

Furlong, K. P., and D. M. Fountain (1986), Continental crustal underplating: Thermal considerations and seismic-petrologic consequences, *J. Geophys. Res.*, *91*, 8285–8294.

Giese, P. (1976), Results of the generalized interpretation of the deep-seismic sounding data, in *Explosion Seismology in Central Europe*, edited by P. Giese, C. Prodehl, and A. Stein, pp. 201–214, Springer, New York.

Grad, M., et al. (2003), Crustal structure of the Trans-European suture zone region along POLONAISE'97 seismic profile P4, *J. Geophys. Res.*, *108*(B11), 2541, doi:10.1029/2003JB002426.

Guterch, A., et al. (2003), CELEBRATION 2000 Seismic Experiment, *Stud. Geophys. Geod.*, *47*, 659–670.

Hole, J. A. (1992), Non-linear high-resolution three-dimensional seismic travel time tomography, *J. Geophys. Res.*, *97*, 6553–6562.

Horálek, J., A. Boušková, F. Hampl, and T. Fischer (1996), Seismic regime of the west-Bohemian earthquake swarm region: Preliminary results, *Stud. Geophys. Geod.*, *40*, 398–412.

Humphreys, E., and R. W. Clayton (1988), Adaptation of backprojection tomography to seismic travel time problems, *J. Geophys. Res.*, *93*, 1073–1085.

Hurich, C. A., S. J. Deemer, A. Indares, and M. Salisbury (2001), Compositional and metamorphic controls on velocity and reflectivity in the continental crust: An example from the Grenville Province of eastern Québec, *J. Geophys. Res.*, *106*, 665–682.

Hurtig, E., , V. Čermák, R. Haenel, and V. I. Zui (Eds.) (1992), *Geothermal Atlas of Europe*, set of 36 maps and explanatory note, 156 pp., Hermann Haack Verlagsgesellsch., Geogr.-Kartogr. Anstalt, Gotha, Germany.

Jensen, S. L., T. Janik, H. Thybo, and POLONAISE Working Group (1999), Seismic structure of the Palaeozoic Platform along POLONAISE'97 profile P1 in northwestern Poland, *Tectonophysics*, *314*, 123–144.

Málek, J., M. Brož, T. Fischer, J. Horálek, P. Hrubcová, J. Janský, O. Novotný, and B. Růžek (2001), Seismic measurements along short profiles in western Bohemia during the CELEBRATION 2000 experiment, *Acta Mont., Ser. A*, *18*(121), 15–28.

Masson, F., B. Jacob, C. Prodehl, P. Readman, P. Shannon, A. Schulze, and U. Enderle (1998), A wide-angle seismic traverse through the Variscan of SW Ireland, *Geophys. J. Int.*, *134*, 689–705.

Matte, P. (1991), Accretionary history and crustal evolution of the Variscan belt in western Europe, *Tectonophysics*, *196*, 309–337.

Matte, P. (2001), The Variscan collage and orogeny (480–290 Ma) and the tectonic definition of the Armorica microplate: A review, *Terra Nova*, *13*, 122–128.

Matte, P., H. Maluski, P. Rajlich, and W. Franke (1990), Terrane boundaries in the Bohemian Massif: Result of large-scale Variscan shearing, *Tectonophysics*, *177*, 151–170.

Meissner, R., and T. Wever (1986), Nature and development of the crust according to deep reflection data from the German Variscides, in *Reflection Seismology: A Global Perspective*, Geodyn. Ser., vol. 13, edited by M. Barazangi and L. Brown, pp. 31–42, AGU, Washington, D. C.

Pitra, P., J. P. Burg, and M. Guiraud (1999), Late Variscan strike-slip tectonics between the Tepla-Barrandian and Moldanubian terranes (Czech Bohemian Massif): Petrostructural evidence, *J. Geol. Soc. London*, *156*, 1003–1020.

Plomerová, J., V. Babuška, and L. Ruprechtová (1984), Velocities of seismic waves propagating through the Bohemian Massif from foci in Poland, *Stud. Geophys. Geod.*, *28*, 56–66.

Prodehl, C., S. Mueller, and V. Haak (1995), The European Cenozoic Rift System, in *Continental Rifts: Evolution, Structure, Tectonics*, *Dev. Geotectonics*, vol. 25, edited by K. H. Olsen, pp. 133–212, Elsevier, New York.

Pros, Z., T. Lokajíček, R. Přikryl, A. Špičák, V. Vajdová, and K. Klíma (1998), Elastic parameters of West Bohemian granites under hydrostatic pressure, *Pure Appl. Geophys.*, *151*(2-4), 631–646.

Růžek, B., V. Vavryčuk, P. Hrubcová, J. Zedník, and CELEBRATION Working Group (2003), Crustal anisotropy in the Bohemian Massif, Czech Republic: Observations based on Central European Lithospheric

Experiment Based on Refraction (CELEBRATION) 2000, *J. Geophys. Res.*, *108*(B8), 2392, doi:10.1029/2002JB002242.

Sandmeier, K.-J., and F. Wenzel (1990), Lower crustal petrology from wide-angle *P*- and *S*-wave measurements in the Black Forest, *Tectonophysics*, *173*, 495–505.

Schulmann, K., J. Plomerová, V. Babuška, and O. Lexa (2002), A kinematic model of the structural development of the Moldanubian root during the Variscan orogeny based on correlation of crustal and mantle lithosphere fabrics, *Geolines*, *14*, 82–84.

Špičák, A., and J. Horálek (2001), Possible role of fluids in the process of earthquake swarm generation in the West Bohemia/Vogtland seismoactive region, *Tectonophysics*, *336*, 151–162.

Šroda, P., and POLONAISE Profile P3 Working Group (1999), *P*- and *S*-wave velocity model of the southwestern edge of the Precambrian East European craton; POLONAISE'97, profile P3, *Tectonophysics*, *314*, 175–192.

Švancara, J., and M. Chlupáčová (1997), Density model of geological structure along profile 9HR, *J. Geol. Sci. Prague*, *47*, 32–36.

Thybo, H., and G. Schönharting (1991), Geophysical evidence for early Permian igneous activity in a transtensional environment, Denmark, *Tectonophysics*, *189*, 193–208.

Thybo, H., et al. (2003), Upper lithospheric seismic velocity structure across the Pripyat Trough and the Ukrainian Shield along the EUROBRIDGE'97 profile, *Tectonophysics*, *371*, 41–79.

Tomek, C., V. Dvořáková, and S. Vrána (1997), Geological interpretation of the 9HR and 503 M seismic profiles in western Bohemia, *J. Geol. Sci. Prague*, *47*, 43–51.

Vavryčuk, V., P. Hrubcová, M. Brož, J. Málek, and ALP 2002 Working Group (2004), Azimuthal variation of *Pg* velocity in the Moldanubian, Czech Republic: Observations based on a multi-azimuthal common-shot experiment, *Tectonophysics*, *387*, 189–203, doi:10.1016/j.tecto.2004.06.015.

Vidale, J. E. (1990), Finite-difference calculation of travel times in three dimensions, *Geophysics*, *55*, 521–526.

Vollbrecht, A., K. Weber, and J. Schmoll (1989), Structural model for the Saxothuringian-Moldanubian suture in the Variscan basement of the Oberpfalz (northeastern Bavaria, F. R. G.) interpreted from geophysical data, *Tectonophysics*, *157*, 123–133.

Vrána, S., J. Cháb, and V. Štědrá (1997), Main results of the project, *J. Geol. Sci. Prague*, *47*, 15–23.

Warner, M. R. (1990), Basalts, water or shear zones in the lower continental crust?, *Tectonophysics*, *173*, 163–173.

Zeis, S., D. Gajewski, and C. Prodehl (1990), Crustal structure of southern Germany from seismic refraction data, *Tectonophysics*, *176*, 59–86.

Zelt, C. A. (1994), ZPLOT—An interactive plotting and picking program for seismic data, Bullard Lab., Univ. of Cambridge, Cambridge, U. K.

Zeyen, H., O. Novak, M. Landes, C. Prodehl, L. Driad, and A. Hirn (1997), Refraction-seismic investigations of the northern Massif Central, *Tectonophysics*, *275*, 99–117.

————————————

E. Brueckl, Vienna University of Technology, Gusshausstrasse 27-29, A-1040 Vienna, Austria. (ebrueckl@luna.tuwienac.at)

M. Grad, Institute of Geophysics, University of Warsaw, Pasteura 7, PL-02-093 Warsaw, Poland. (mgrad@mimuw.edu.pl)

A. Guterch and P. Šroda, Institute of Geophysics, Polish Academy of Sciences, Ks. Janusza 64, PL-04-152 Warsaw, Poland. (aguterch@igf.edu.pl)

P. Hrubcová and A. Špičák, Geophysical Institute, Academy of Sciences of the Czech Republic, Bocni II/1401, 141 31 Prague 4, Czech Republic. (pavla@ig.cas.cz)

G. R. Keller, Department of Geological Sciences, University of Texas at El Paso, El Paso, TX 79968, USA. (keller@geo.utep.edu)

H. Thybo, Geological Institute, University of Copenhagen, Oster Voldgade 10, DK-1350 Copenhagen, Denmark. (thybo@geol.ku.dk)

P2

Hrubcová P., P. Środa,
and CELEBRATION 2000 Working Group

Crustal structure at the easternmost termination of the Variscan belt
based on CELEBRATION 2000 and ALP 2002 data

Crustal structure at the easternmost termination of the Variscan belt based on CELEBRATION 2000 and ALP 2002 data

P. Hrubcová [a,*], P. Środa [b]
CELEBRATION 2000 Working Group [1]

[a] Institute of Geophysics, Academy of Sciences of the Czech Republic, Prague, Czech Republic
[b] Institute of Geophysics, Polish Academy of Sciences, Warsaw, Poland

ARTICLE INFO

ABSTRACT

The eastern margin of the Variscan belt in Europe comprises plate boundaries between continental blocks and terranes formed during different tectonic events. The crustal structure of that complicated area was studied using the data of the international refraction experiments CELEBRATION 2000 and ALP 2002. The seismic data were acquired along SW–NE oriented refraction and wide-angle reflection profiles CEL10 and ALP04 starting in the Eastern Alps, passing through the Moravo-Silesian zone of the Bohemian Massif and the Fore-Sudetic Monocline, and terminating in the TESZ in Poland. The data were interpreted by seismic tomographic inversion and by 2-D trial-and-error forward modelling of the P waves. Velocity models determine different types of the crust–mantle transition, reflecting variable crustal thickness and delimiting contacts of tectonic units in depth. In the Alpine area, few km thick LVZ with the Vp of 5.1 km s^{-1} dipping to the SW and outcropping at the surface represents the Molasse and Helvetic Flysch sediments overthrust by the Northern Calcareous Alps with higher velocities. In the Bohemian Massif, lower velocities in the range of 5.0–5.6 km s^{-1} down to a depth of 5 km might represent the SE termination of the Elbe Fault Zone. The Fore-Sudetic Monocline and the TESZ are covered by sediments with the velocities in the range of 3.6–5.5 km s^{-1} to the maximum depth of 15 km beneath the Mid-Polish Trough. The Moho in the Eastern Alps is dipping to the SW reaching the depth of 43–45 km. The lower crust at the eastern margin of the Bohemian Massif is characterized by elevated velocities and high Vp gradient, which seems to be a characteristic feature of the Moravo-Silesian. Slightly different properties in the Moravian and Silesian units might be attributed to varying distances of the profile from the Moldanubian Thrust front as well as a different type of contact of the Brunia with the Moldanubian and its northern root sector. The Moho beneath the Fore-Sudetic Monocline is the most pronounced and is interpreted as the first-order discontinuity at a depth of 30 km.

1. Introduction

The tectonic evolution of the Variscan orogenic belt is related to amalgamation of various continental crustal blocks previously situated between Baltica in the NE and Gondwana in the SW during the Devonian and Late Carboniferous (Matte et al., 1990). This belt is characterized by the Ibero-Armorican spread from north Africa to the Bohemian Massif in central Europe.

The eastern termination of the Variscan belt comprises plate boundaries between continental blocks and terranes formed during different tectonic events. Its south-eastern margin was influenced and modified by large movements between Africa and Europe resulting in the Alpine deformation. On the other hand, the north-eastern termination of the Variscan orogen is obliquely cut off and offset by large transcurrent dextral faults parallel with the TESZ (like the Elbe zone or the Odra Fault zone) considered by some authors as forming the southern boundary of the East European Craton (e.g., Dallmeyer et al., 1995; Winchester et al., 2002; Dadlez et al., 2005). The nature and position of boundaries between these units have been interpreted by several investigators, sometimes controversially (e.g. Matte et al., 1990; Fritz et al., 1996; Schulmann and Gayer, 2000; Edel et al., 2003) and are still a matter of ongoing debates. Recent ideas about tectonic history of Central European Variscides have been presented by e.g. Winchester et al. (2006) and Franke (2006).

The Variscan Belt as a prominent structure in Europe has been subject of a vast amount of geophysical investigations and interpretations

* Corresponding author.
  E-mail address: pavla@ig.cas.cz (P. Hrubcová).
[1] Celebration 2000 Working Group: A. Guterch[a], M. Grad[b], T. Janik[a], G.R. Keller[c], E. Hegedüs[d], J. Vozár[e], A. Špičák[f], E. Brückl[g], H. Thybo[h]. [a]Institute of Geophysics, Polish Academy of Sciences, Poland. [b]Institute of Geophysics, University of Warsaw, Poland. [c]Department of Geological Sciences, University of Texas at El Paso, USA. [d]Eötvös Loránd Geophysical Institute, Budapest, Hungary. [e]Geological Survey, Bratislava, Slovak Republic. [f]Geophysical Institute Academy of Sciences, Prague, Czech Republic. [g]Vienna University of Technology, Austria. [h]University of Copenhagen, Denmark.

over decades. Starting in Iberia (Simancas et al., 2003; Carbonell et al., 2004), through western to central Europe (British Institutions Reflection Profiling Syndicate (BIRPS) and Étude Continentale et Océanique par Réflexion et Refraction (ECORS), 1986; Deutches Kontinentales Reflektionsseismisches Programm (DEKORP) Research Group, 1985, 1988; Aichroth et al., 1992; Onken et al., 2000) it includes also the CELEBRATION 2000 and SUDETES 2003 experiments at its eastern termination (Guterch et al., 2003; Grad et al., 2003b). The EUROPROBE project (Gee and Zeyen, 1996), investigating evolution of the European lithosphere, targeted also the Variscan areas.

The most eastern part of the Variscan orogen is constituted of the Bohemian Massif, a large stable outcrop of pre-Permian rocks. Eastern sectors of the Bohemian Massif comprise the Moldanubian and the Moravo-Silesian zones, the last one having a completely different tectonic history as a part of a separate micro-continent (e.g. Winchester et al., 2002). The development in this region is a result of oblique collision between the Moldanubian terrane and the Brunovistulian micro-continent to the east (Dudek, 1980), where the Moldanubian is viewed as a Variscan orogenic root thrust over the Brunovistulian forming together the Moravo-Silesian zone (Matte, 1991; Schulmann et al., 2005).

The Moravo-Silesian zone is an appropriate area to study tectonic development due to a superposition of three structural levels corresponding to three orogenic cycles (e.g., Grygar et al., 2002). The lowermost cycle represents the Pan-African (Cadomian) Brunovistulian foreland terrane, which determined and influenced complex geological development of the second cycle, the Variscan accretion wedge, represented by volcano-sedimentary formations of the Rhenohercynian foredeep and the Sub-Variscan foreland. Finally, sequences of the West Carpathian foredeep and the Outer West Carpathian nappes formed the Alpine accretion wedge. The Brunovistulicum is the oldest crustal segment and represents a foreland of both the above-mentioned accretionary wedges: the older Variscan one with generally NE directed kinematics and the younger Alpine wedge with northward tectonics. The goal of this study includes supplying answers on the crustal and upper mantle structure of this area together with delimitation of the contact with the Eastern Alps and the north-eastern continuation of the Brunovistulian beneath the Fore-Sudetic Monocline and the TESZ.

To investigate the area, we are using refraction and wide-angle reflection data along the CEL10 profile from CELEBRATION 2000 experiment (Guterch et al., 2003) and ALP04 profile of the ALP 2002 experiment (Brückl et al., 2003). The SW–NE orientated line of joint profiles CEL10 and ALP04 starts in the Central to Eastern Alps, continues along the eastern edge of the Bohemian Massif and ends at the Mid-Polish Trough (MPT) — a part of the Trans-European Suture Zone (TESZ) forming the SW margin of the East European Craton (see Fig. 1). For the interpretation, we choose the tomographic inversion routine of Hole (1992) as a tool to determine a preliminary model of seismic P-wave velocity in the crust using first arrivals. The resulting tomographic model is further improved by two-dimensional (2-D) trial-and-error forward modelling of the refracted and reflected P waves using a ray-tracing algorithm (Červený and Pšenčík, 1984). In this study, we concentrate on velocity variations along the profile; azimuthal anisotropic studies are a matter of other investigations (e.g., Plomerová et al., 1984; Růžek et al., 2003; Vavryčuk et al., 2004).

2. Geology and tectonic evolution of the region

The easternmost termination of the Variscan belt in central Europe comprises the Bohemian Massif, which developed approximately between 480 and 290 Ma (Matte, 2001) and played an important role in the development of the Variscan orogen. At the eastern margin of the Bohemian Massif, the Moldanubian root was thrust over the Brunovistulian foreland along a major dextral transpressional zone during the imbrication of the Brunovistulian, forming the Moravo-

Silesian zone (Fritz et al., 1996). The Moravo-Silesian is a 50 km wide and 300 km long NE–SW-trending zone of sheared and metamorphosed Brunia-derived rocks and represents an interface between the upper Moldanubian terrane and the undeformed rocks of the Brunovistulian foreland covered by Devonian to Carboniferous sediments (Schulmann and Gayer, 2000) (see Fig. 1).

The Moravo-Silesian zone of the Bohemian Massif can be followed from Krems in Austria to the NE, where it is often thought to extend to the Odra Fault Zone (OFZ) in Poland. The northern termination of the Moravo-Silesian zone is still not well recognized and is a matter of debates (e.g. Matte, 1986). In this part, the external belt of the Variscan orogen extends beneath the Fore-Sudetic Monocline and continues to the presumed assemblage of suspect terranes accreted to Baltica in the Early Paleozoic called the Trans-European Suture Zone (TESZ) (Berthelsen, 1992; Dadlez et al., 2005). To the SE, the Cadomian Brunia continent submerges beneath the Carpathian Foredeep and the Outer Carpathians, where it may form a basement reactivated during the Alpine orogen (Dallmeyer and Urban, 1994; Fritz et al., 1996). To the south, the belt was influenced by the Alpine orogen, when the Alpine nappes were thrust northwards onto the European foreland including the Bohemian Massif. Most of the basement of the Eastern Alps corresponds to the internal parts of the Variscan belt.

The Moravo-Silesian zone can be divided into two parts — the southern and northern segments referred to as the Moravian and Silesian units, respectively. The boundary between these two segments corresponds to a wide, repeatedly rejuvenated NW–SE transverse dextral fault zone representing the eastern part of the Elbe Fault Zone (EFZ) (Dallmeyer et al., 1995; Edel et al., 2003). In both the southern and northern segments, it is possible to discern autochthonous and the allochthonous domains. The southern part consists of two elongated tectonic windows emerging through high-grade rocks of the Moldanubian (Fritz et al., 1996; Schulmann and Gayer, 2000). The northern, Silesian unit contains Devonian and early Carboniferous mafic volcanic rocks (Dallmeyer et al., 1995). The intensity of the Variscan deformation decreases eastwards; the western part of the Moravo-Silesian zone, close to the boundary with the overriding Moldanubian zone, is composed of a number of allochthonous thrusts sheets, while the east part are mostly in autochthonous position (Dallmeyer et al., 1995; Mazur et al., 2006). The classical tectono-stratigraphic zones of the Variscan orogen have recently been considered to represent separate terranes (e.g., Matte et al., 1990; Franke et al., 2000; Winchester et al., 2002) usually correlated with Armorica and interpreted to form the Armorican Terrane Assemblage (Belka et al., 2000; Tait et al., 2000; Finger et al., 2000; Belka et al., 2002).

The tectonics of the Alpine–Carpathian system was controlled during Tertiary by the N–S convergence of the Adriatic and European plates. The resulting collision caused thrusting and crustal thickening during the continental collision. The Tertiary deformation of the northern Eastern Alps was characterized by northward thrusting and dextral wrenching along WNW-trending strike-slip faults. Presently, in the northern part of the Eastern Alps, the Northern Calcareous Alps, built up by thick Permomesozoic carbonatic layers, are the highest tectonic unit thrust over the Flysch-Helvetic zone and the Molasse zone outcropping in the northern rim of the Eastern Alps. The Molasse zone lies autochthonously on the European foreland in its lower part and partly allochthonously below the Alpine nappes (Reinecker and Lenhardt, 1999).

3. Previous geophysical studies in the area

The attempts to reveal a crustal structure of this region were usually associated with the investigation of the Bohemian Massif (Beránek and Zátopek, 1981) or with the investigation of the Carpathian foreland (Majerová and Novotný, 1986; Bielik et al., 2004). The interpretation of the refraction measurements indicated the pronounced Moho discontinuity at a maximum depth of 39 km in
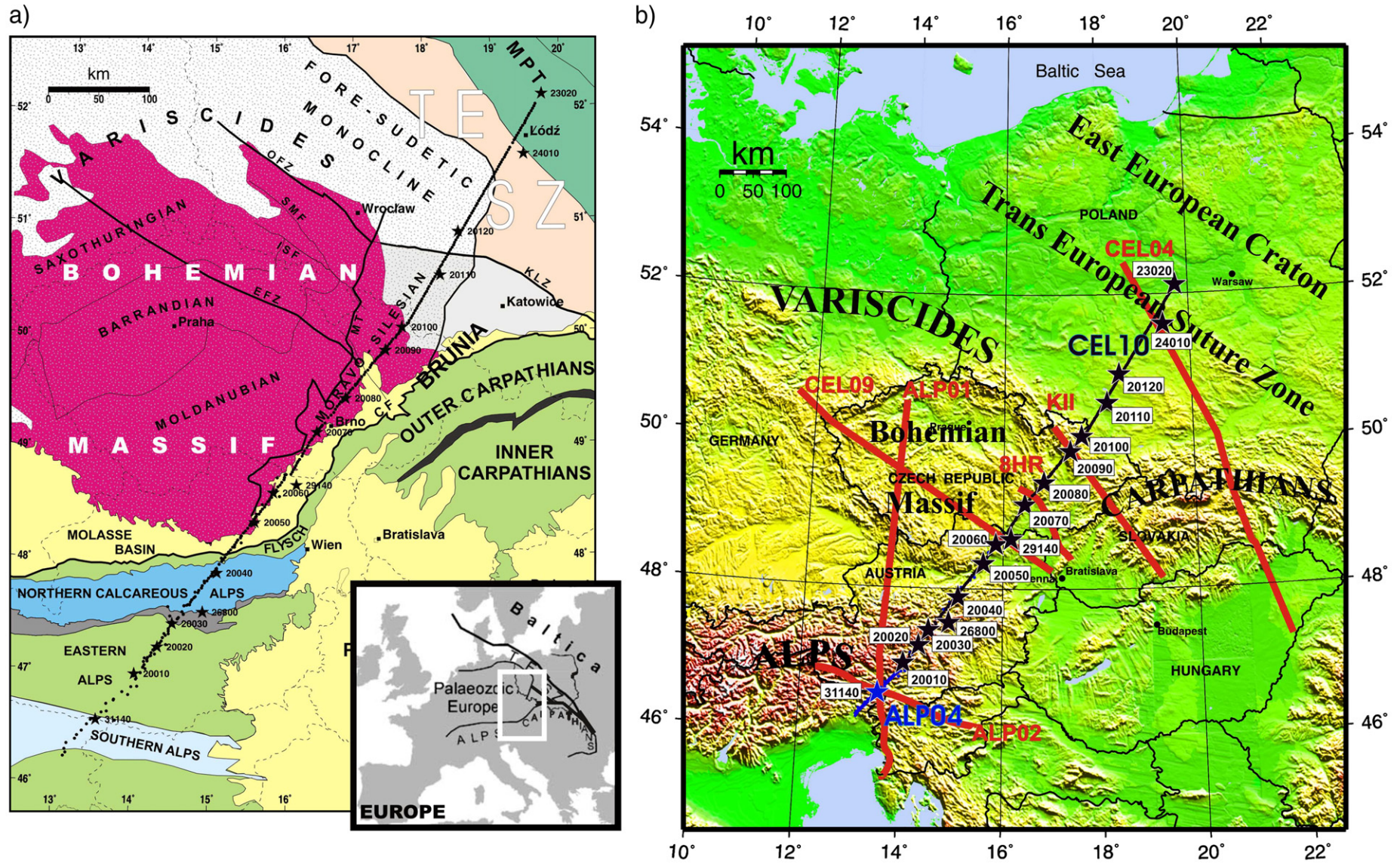
Fig. 1. (a) Location of the profile CEL10 and ALP04 together with the main basement units. The insert shows the study area on a simplified map of Europe. EFZ, Elbe Fault Zone; ISF, Intra-Sudetic Fault; SMF, Sudetic Marginal Fault; OFZ, Odra Fault Zone; KLZ, Kraków-Lubliniec Zone; MT, Moldanubian Thrust; CF, Carpathian Flysch; TESZ, Trans-European Suture Zone; MPT, Mid-Polish Trough. (b) Geographical setting of profile CEL10 and ALP04. Black stars mark positions of individual shot points along the CEL10 profile, blue star refers to the ALP04 shot point. Other seismic refraction and reflection profiles (ALP01, ALP02, CEL09, 8HR, KII, and CEL04) are marked by red solid lines.

the central part of the Bohemian Massif and a less pronounced Moho at a depth of about 32 km at the eastern margin of the Bohemian Massif at its contact with the Carpathians (Beránek and Zounková, 1977). In general, the interpreted profiles were of NW–SE direction, perpendicular to the CEL10 profile. The important contribution to understanding of the geological structure on the contact of the Bohemian Massif and the Carpathians was the interpretation of the regional refraction profile KII extending from the border of the Czech Republic and Poland to Slovakia. In the Silesian zone, the two bands of reflections suggested the Moho located at 36–37 km depth and rising towards the SE to 30–32 km (Majerová and Novotný, 1986). Reflection profile 8HR further to the south (see Fig. 1b), crossing CEL10 at 440 km distance in the Moravian zone, indicated the Moho at 35–37 km depth.

Within the frame of the CELEBRATION 2000 experiment, a refraction and wide-angle reflection profile CEL09, traversing the whole Bohemian Massif, was modelled. Beneath the Moravian unit (360 km along the CEL10 profile), CEL09 data indicate a broad crust–mantle transition zone and suggest a thrusting of the Moldanubian over the Moravian unit in depth (Hrubcová et al., 2005).

The Polish Variscides and the TESZ were broadly investigated during the last 20 years, except for the easternmost termination of the Variscides, corresponding to the location of the NE part of the CEL10 profile. The POLONAISE'97 experiment and earlier deep seismic sounding studies with TTZ and LT profiles provided a good regional picture of crustal structure in western and NW Poland (Guterch et al., 1999; Grad et al., 2003a, 2005). The Variscan crust in this area is 30–35 km thick (e.g., Wilde-Piórko et al., 2005) with a two-layer seismic structure characterized by low P-wave velocities down to the Moho discontinuity (<6.7 km s^{-1}) (Grad et al., 2002; Majdański et al., 2006, 2007) and crustal thickening in the TESZ (Dadlez et al., 2005).

Crustal structure of the Eastern Alps was studied along the N–E oriented TRANSALP profile (Bleibinhaus and Gebrande, 2006) and during the ALP2002 experiment (Brückl et al., 2007), when two crossing profiles ALP01 and ALP02 were interpreted. These investigations reveal deepening of the Moho from the North Calcareous Alps to the south from 38 km to 47 km depth and reflect a crustal thickening during the Alpine orogeny.

4. Data acquisition and processing

The seismic data along two refraction and wide-angle reflection profiles CEL10 and ALP04 were acquired during the international
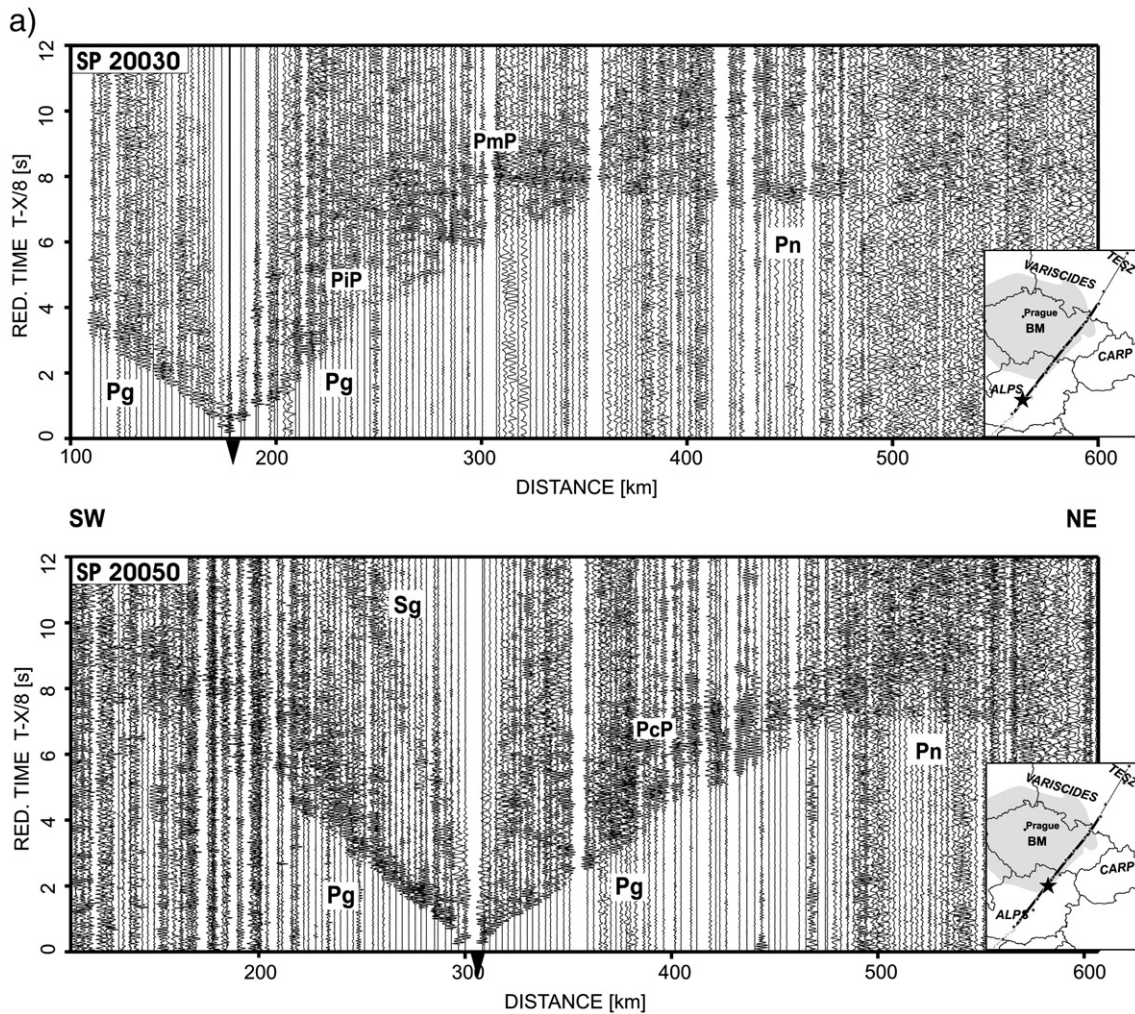

Fig. 2. Examples of amplitude-normalized vertical component seismic sections from different parts along the profile CEL10 plotted with the reduction velocity of 8 km s^{-1} (Fig. 2a–c) and 6 km s^{-1} (Fig. 2d). Identification of main seismic phases: Pg, refraction within the crust; Psed, refraction from the sedimentary cover; Pn, refraction from the uppermost mantle; PmP, reflection from the Moho discontinuity; PcP, reflection from the top of the lower crust; PiP, reflection in the crust. Data have been band-pass filtered from 2–15 Hz. Locations of major tectonic units and shot points are indicated. (a) SP 20030 and 20050 in the SW. Note strong PmP in the Alpine area, vanishing of PmP beneath the Bohemian Massif (SP 20050) and Pn visible to 350 km offset (SP 20030). (b) SP 20080 and 20090 in the Bohemian Massif. Note strong variability of the wave field within individual shot points: SP 20080 — high amplitude Pg phase to the SW, highly reflective crust, and strong decrease of Pg amplitudes to the NE suggesting the existence of very low or negative gradient (LVZ) with corresponding effect on SP 20090. (c) SP 20100 and 20120 in the NE. Note strong PmP with short impulse duration for SP 20120 from the Fore-Sudetic Monocline. (d) SP 24010 and 23020 in the NE with the reduction velocity of 6 km s^{-1}. Note Psed with the apparent velocity of 4.5–5.0 km s^{-1} in the TESZ.
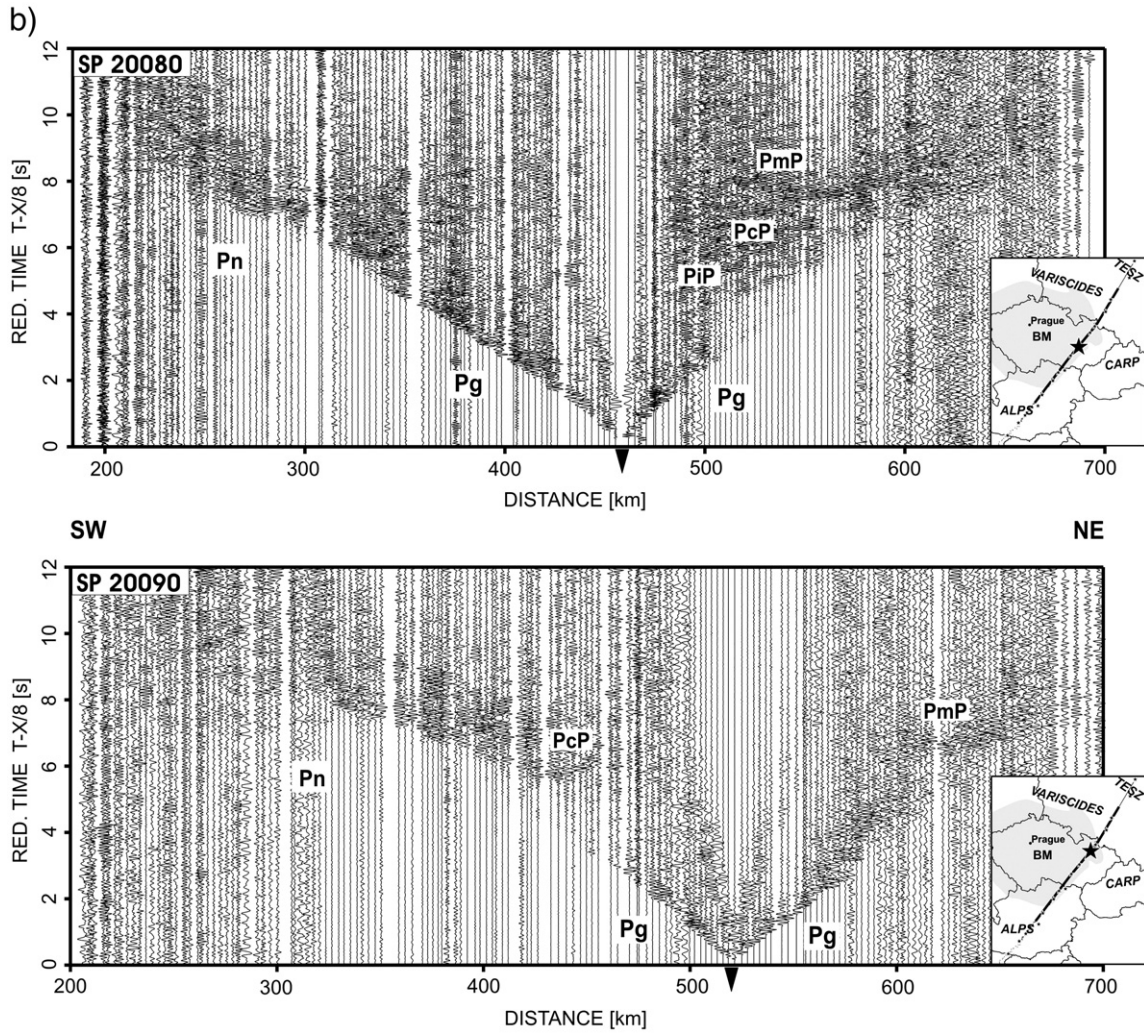
Fig. 2 (*continued*).

seismic experiments CELEBRATION 2000 (Guterch et al., 2003) and ALP 2002 (Brückl et al., 2003). The SW–NE oriented transects CEL10 starts in the Eastern Alps, continues through the Moravo-Silesian zone of the Bohemian Massif, where it strikes the Moravian granitoids and further to the NE the Devonian and Carboniferous Paleozoic cover, continues through the Fore-Sudetic Monocline, and terminates in the TESZ and the Mid- Polish Trough. This profile is 710 km long and comprises 16 shot points. To extend the knowledge of the Eastern Alps and its Variscan basement, profile ALP04 was designed as the extension of CEL10 line to the SW across the Eastern Alps. One shot point was registered along 360 km long profile where 250 km overlapped the CEL10 line (Fig. 1). Thus, the interpreted joint SW–NE oriented profile was 820 km long.

Three shots along CEL10 transects were fired twice or three times and the recordings were stacked in order to improve the signal-to-noise ratio. The average distance between the shots was 30 km with a station spacing of 2.7 km (6 km for ALP04, respectively). The charges amounted to 200 kg on average, for some shot points a charges of 1000–1200 kg were fired. The non-overlapping part of the profile ALP04 comprises 1 shot point with the charge of 300 kg. The positions of shot points and stations were measured by GPS; the origin time was controlled by a DCF77 timer with an accuracy of 3 ms. For more details on geometry of both experiments refer to Málek et al. (2001), Brückl et al. (2003), Guterch et al. (2003), and Růžek et al. (2003). The data from both experiments were sampled at intervals of 10 ms and were recorded mainly by one-component stations REFTEK-125 (TEXAN),

complemented by three-component REFTEK and MK-4P stations. The station sensors were 4.5 Hz geophones (1 Hz geophones for three-component stations). Data processing included shot-time corrections and band-pass filtering of the whole data set (usually 2–15 Hz) in order to remove low- and high-frequency noise. The frequency content of the seismic data was highly variable for different shot points, probably due to varying local environment and due to different shooting techniques (borehole shots, quarry blasts). Thus, the filter window was determined interactively during the interpretation, depending on the data quality and the frequency content. Recordings were sorted into shot gathers; seismic sections were trace-normalized to the maximum amplitude along the trace and plotted with a reduction velocity of 8 km s^{-1}.

5. Data description

The seismic data used for the interpretation have good signal-to-noise ratio and allow several P-wave phases to be correlated (see Fig. 2a–d). In the first arrivals, we can distinguish refraction from the upper/middle crust, the Pg phase, and refractions from the upper mantle marked as Pn. Refracted waves from the sedimentary cover (Psed) are observed in the vicinity of shot points in the NE. Clear arrivals of refracted and reflected waves from the crystalline crust and the upper mantle are typically observed up to the offsets of 250–300 km. In later arrivals, we observe the reflections from the Moho discontinuity (PmP) usually as the strongest phase, especially in the
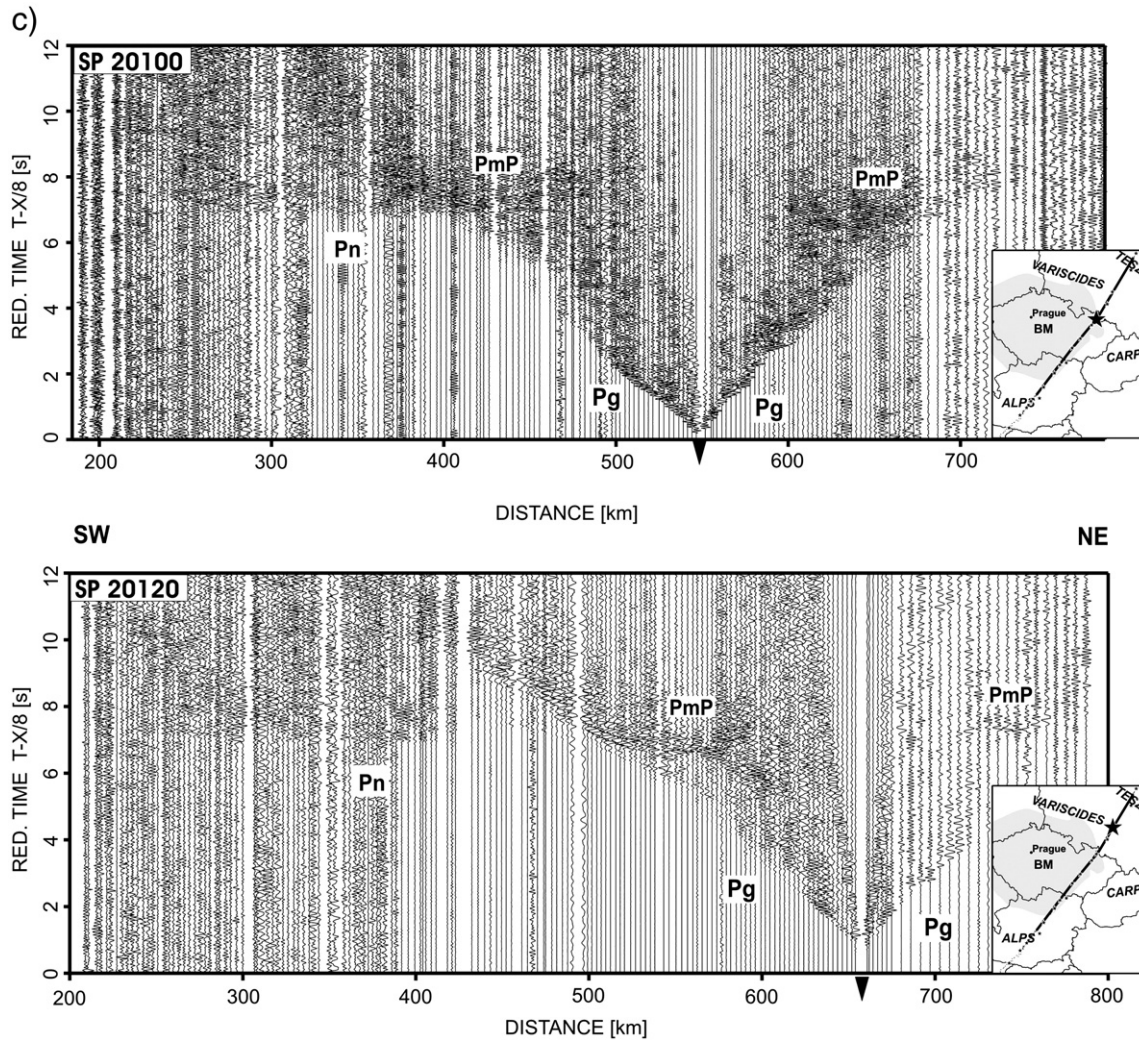
Fig. 2 (*continued*).

NE part of the profile. Reflections from mid-crustal discontinuities are marked as PiP, or PcP for reflections from the top of the lower crust. Fig. 2a–d give the examples of seismic sections in different part along the profile.

5.1. Pg phase

The Pg phase with the apparent velocity of 5.8–6.1 km s^{-1} is usually possible to correlate up to the 100–120 km offsets. The abrupt anomalies of Pg phase reflect the existence of near-surface velocity inhomogeneities. Slightly higher apparent velocities (about 6.2 km s^{-1}) correlate with the mafic volcanic rocks of the Silesian unit at a distance of 510–550 km along the profile.

In the Alpine area (SW part of the profile), SP 20020, 20030, 26800 and reciprocally SP 20050 and 20060 show a jump of 0.35 s on the Pg phase at 235 km along the profile that indicates low velocity zone (LVZ) beneath near-surface rocks at that distance. Moreover, in seismic sections of SP 20020 and 20030 the Pg phase vanishes at about 80 km offsets. The deeper phase P1 has small apparent velocity and thus it cannot be satisfactorily modelled without assuming LVZ at a distance of 180–230 km. The data suggest that the LVZ outcrops at the surface at 250 km distance and dips to the SW (see Figs. 2a, 5). Forward modelling confirmed that hypothesis.

In the middle part of the profile, in the Bohemian Massif, the SP 20080 displays strong differences in the wave field with a high ampli-

tude Pg phase in the SW and a strong decrease of the Pg amplitude with highly reflective middle/lower crust in the NE. The corresponding effect is visible on SP 20090 and 20100 (see Figs. 2b,c, 6) with a Pg amplitude decrease at the offsets between 50–130 km and with a strong intracrustal reflection in later arrivals. It cannot be the effect of trace normalization (a decrease of the Pg amplitudes due to the relatively higher amplitudes of later arrivals, mainly PmP), because amplitude decrease is also observed in the true amplitude scaling. Thus it may suggest the existence of very low or negative gradient zone in the upper crust in that area.

For shot points in the NE (SP 23020, 24010), first arrivals at offsets smaller than 60 and 30 km, respectively show the apparent velocity of 4.5–5 km s^{-1} marked as Psed (see Fig. 2d). This reflects a few to over 10 km thick sedimentary cover in the Fore-Sudetic Monocline and particularly in the TESZ zone.

5.2. Lower crust and mantle phases, PmP reflections

At the lower crustal and uppermost mantle level we can distinguish following differences. While in the Bohemian Massif the crossover distance between the crust and mantle refractions is 160 km and sometimes the Pn is missing, in the SW, in the Alps, the crossover distance is 180 km, indicating a very deep crust. Unfortunately, the most SW section of the profile (SP 31140 from ALP 2002 experiment) enables to correlate the Pg only up to 70 km offset and no Moho
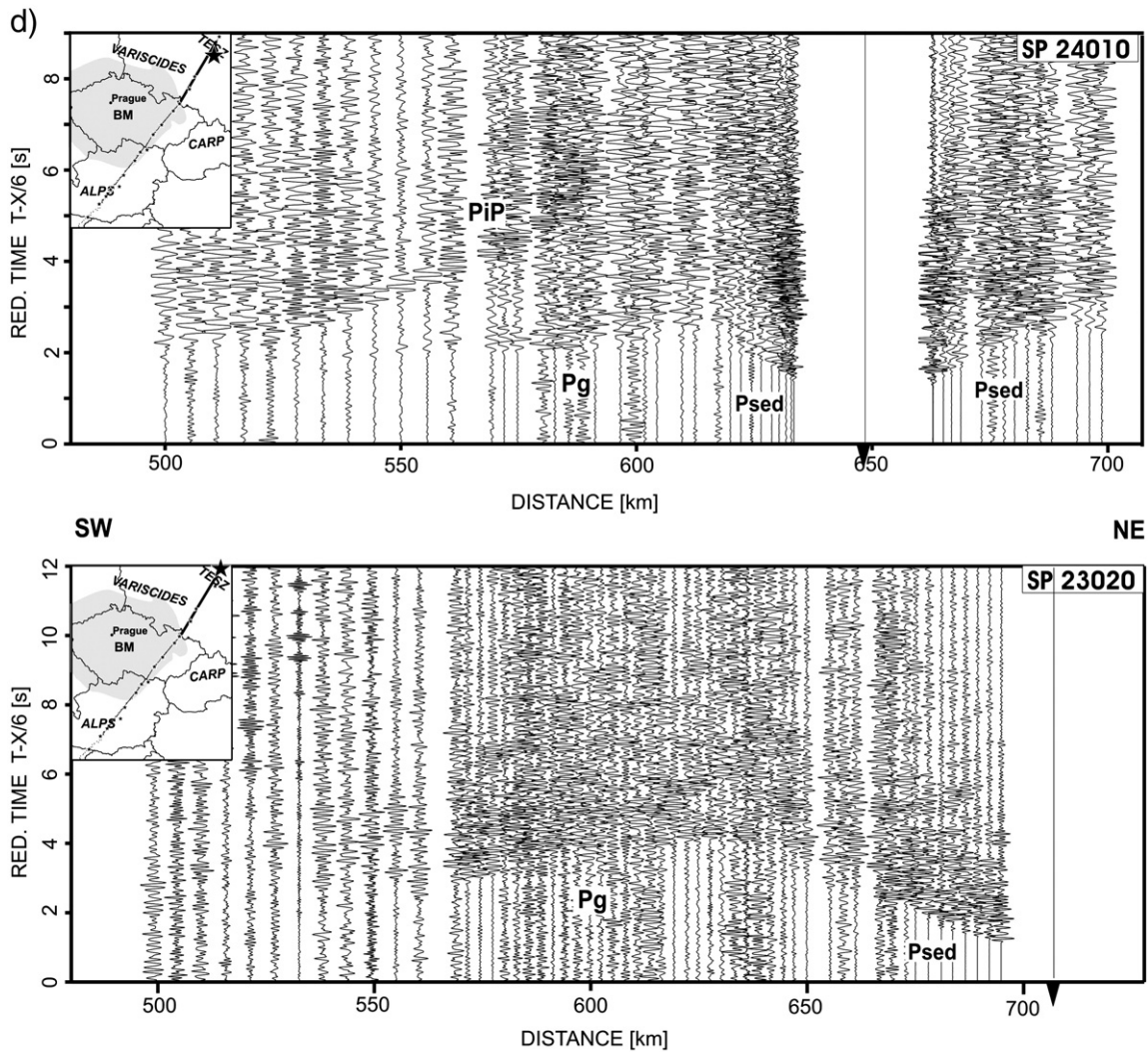
Fig. 2 (*continued*).

reflections are observed, which does not allow for any differentiation of the velocity structure in the deeper crust at the SW termination of the profile.

The Bohemian Massif in the central part of the profile shows strongly reflecting crust with a long coda, while the Moho reflections are not well pronounced (SP 20050, 20060; see Fig. 2a). The local intracrustal reflectors are sometimes hard to correlate in-between shot points. Thus, it is sometimes impossible to perform the reciprocity checking necessary for depth/dip location of the reflectors. Nevertheless, in the middle crust, one consistent reflector is possible to correlate in the SE and central part of the Bohemian Massif. In the NE part of the Bohemian Massif, we can observe a clear PcP phase, interpreted as the reflection from the top of the lower crust (SP20070, 20080 right and SP 20100 left, Figs. 3bc, 6, 7). It is the strongest reflection in these sections and due to its long coda and high amplitude it masks the much weaker PmP reflection.

In the NE, the crossover distance is the shortest and is about 140 km. There, the PmP reflections are the most pronounced compared to other areas along the profile. This suggests a well-defined Moho discontinuity beneath the Fore-Sudetic Monocline and the TESZ, while the weaker PmP phase in the Bohemian Massif indicates the Moho with a relatively low velocity contrast (Figs. 2c, 7).

The Pn phase can be identified as the first arrivals usually at the offsets of 130–230 km, sometimes up to 300 km with an apparent velocity of 8 km s^{-1} on average. It is usually visible in the SW and NE

part of the profile, while in the Bohemian Massif it is mostly missing. This enhances the idea of a well-defined Moho in the SW and NE parts of the profile and a less pronounced transition zone in the central part of the profile.

6. P-wave velocity models

6.1. Seismic tomography model

In the first modelling step, we applied the tomographic travel time inversion of the first P-wave arrivals (Hole, 1992) to assess a preliminary 2-D velocity model in the crust. The procedure uses the backprojection algorithm (Humphreys and Clayton, 1988), based on the linearization of the non-linear relation between the travel time and the slowness. The model is defined on an equidistant rectangular grid with the Vp velocities defined at the grid nodes. In the forward step, the travel times are calculated using a finite difference algorithm (Vidale, 1990). In the inverse step, the slowness perturbations are calculated by uniformly distributing the travel time residual along a ray.

For the inversion, the initial 1-D model for the upper crust was calculated by inverting the average Pg travel time curve by the Wiechert–Herglotz formula (Aki and Richards, 1980); for the lower crust and mantle, a smooth arbitrary velocity–depth curve was derived. In total, 1546 first arrival picks from 21 shots were selected
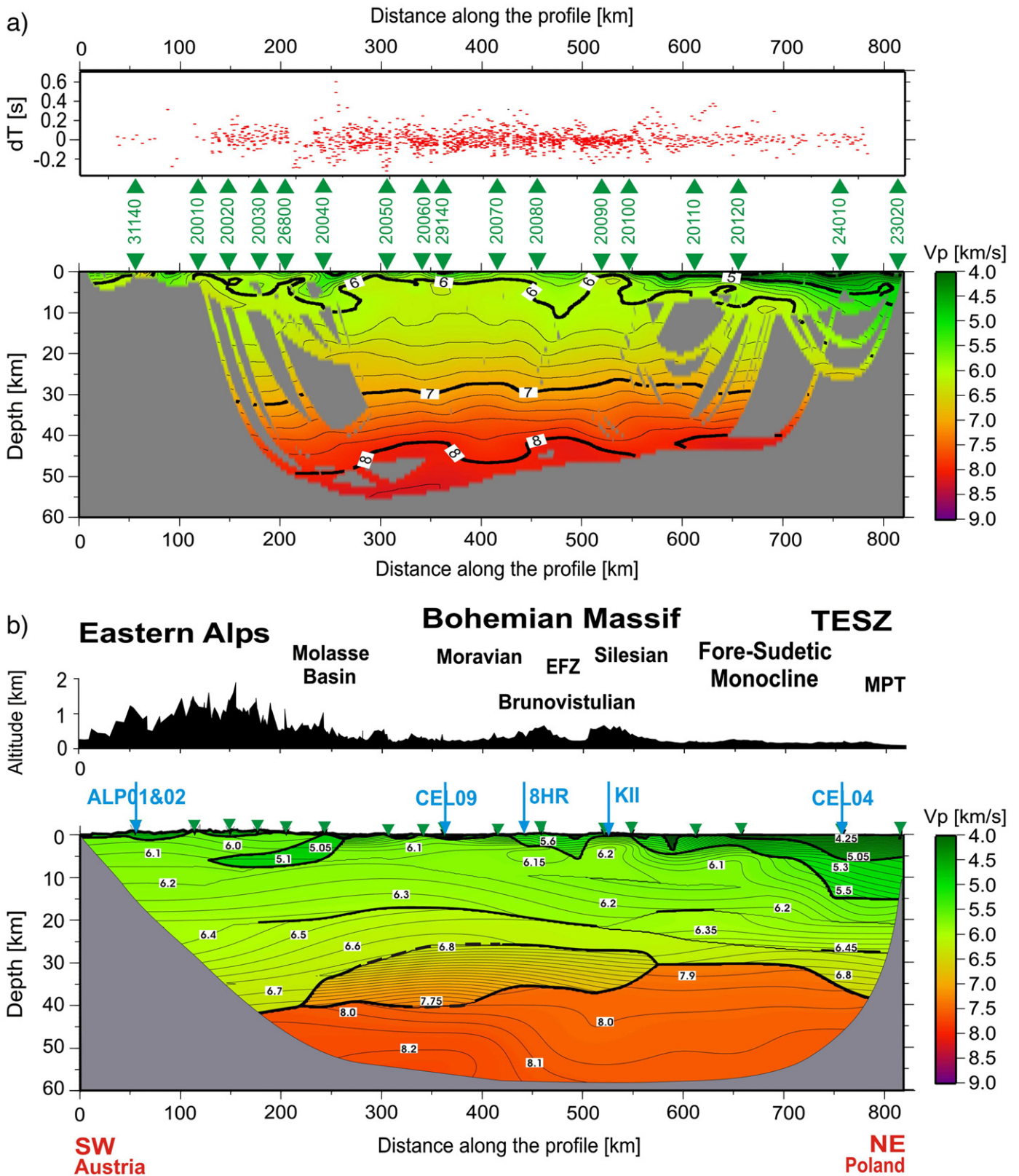
Fig. 3. Two-dimensional P-wave velocity models for the joint profile CEL10 and ALP04. a) Results of 2-D seismic tomography of J. Hole (1992) together with a misfit between the observed and calculated travel times. Numbers represents P-wave velocities in km s^{-1}. b) Results of forward ray-tracing modelling with SEIS83 package (Červený and Pšenčík, 1984) with elevations on the top. The grey covers the unconstrained parts of the model. Thick lines mark discontinuities constrained by the reflections and well-constrained interfaces in the uppermost crust; dashed thick lines mark the layer boundaries where no reflections were observed. Thin lines are the isovelocity contours spaced at the intervals of 0.05 km s^{-1}. Numbered triangles refer to the shot points, arrows show locations of other refraction and reflection profiles. EFZ, Elbe Fault Zone; TESZ, Trans-European Suture Zone; MPT, Mid-Polish Trough. Vertical exaggeration is 1:4.

for the inversion. Picks which could not be reliably identified as first arrivals were not included. The computation was carried out for a model grid size of 1 × 1 km in 5 subsequent steps, gradually enlarging the data offsets (50, 100, 150, 200 and 400 km) and thus the maximum depth of ray penetration, with several iterations at each step. The smoothing was performed by a moving average filter with cell sizes of 40 × 10, 20 × 4 and 10 × 2. The resolution of the algorithm thus

increased gradually and stabilized the inversion. The calculation was controlled by the root-mean-square (RMS) travel time residuals, which amounted to 92 ms for the final model, exceeding approximately twice the level of the estimated picking uncertainty.

The resulting tomographic model and the final travel time residuals are presented in Fig. 3a. The velocity variations in the upper and middle crust indicate differences in the structure of the tectonic

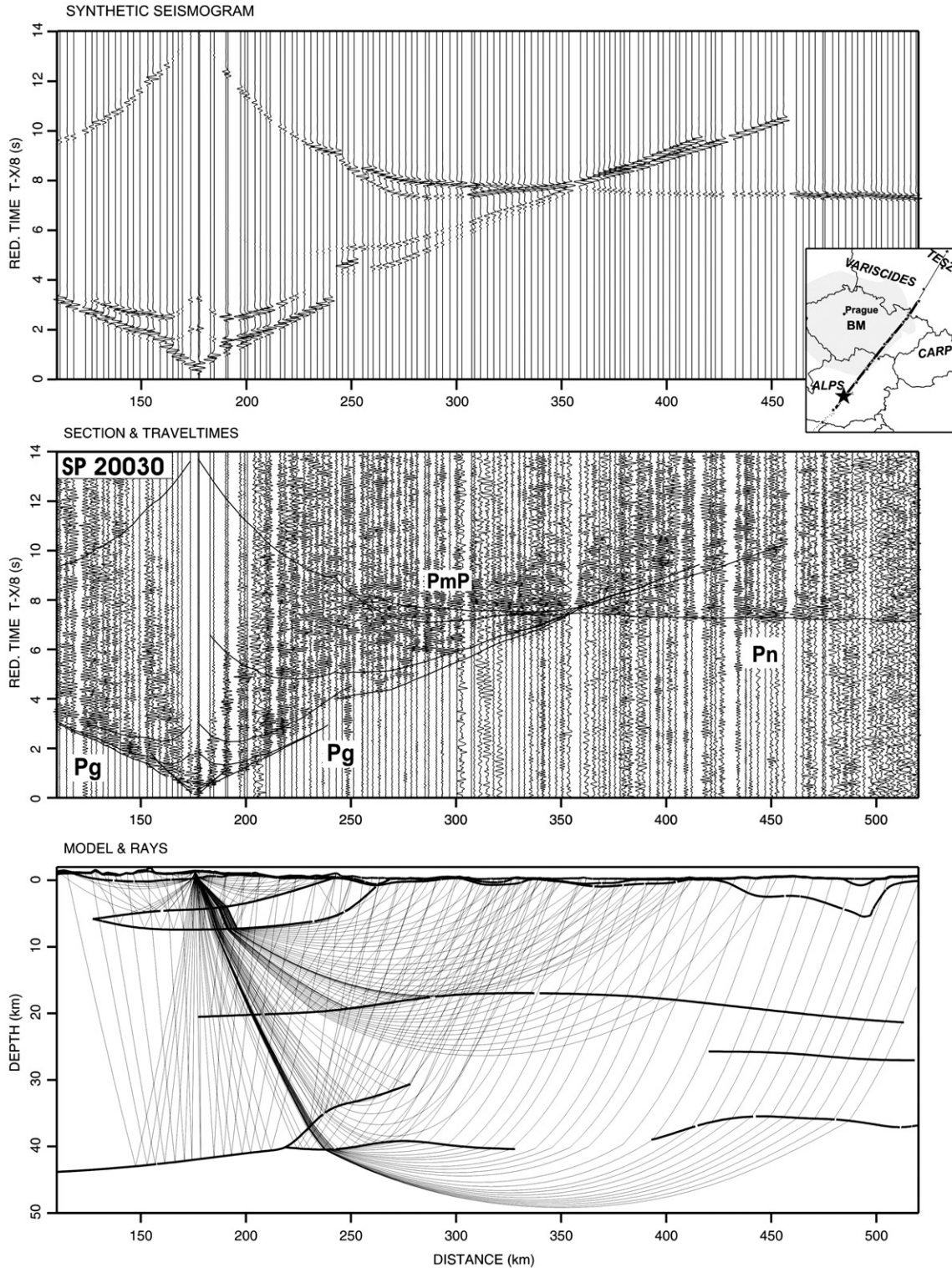**Fig. 4.** Example illustrating forward modelling for the SP 20030 from the Eastern Alps area. Top — synthetic section, middle — amplitude-normalized seismic section with calculated travel times, bottom — model and calculated raypaths. Reduction velocity is 8 km s^{-1}, locations of major tectonic units and shot points are indicated. Note strong Pn detected up to 350 km offset in the Bohemian Massif.

units crossed by the profile. The upper crust in the Alpine area at a distance of 150–260 km exhibits the alternations of higher and lower velocities. In the Bohemian Massif, a high near-surface velocity gradient followed by a low gradient in the upper/middle crust is observed. Lower velocities of 5.4–5.8 km s^{-1} down to a depth of 10 km occur near the contact of the Moravian and Silesian units. Considerably lower velocities in the upper crust in the range of 3.0–5.5 km s^{-1} for depths down to 15 km delimit the Mid-Polish Trough of the TESZ in the NE.

In the Bohemian Massif, due to a higher near-surface velocity gradient followed by a low gradient in the middle crust for crystalline rocks, the turning point of the Pg rays is at shallow depths. The rays concentrate in the parts with high velocity gradients and leave the deeper parts of the crust practically unconstrained. For this reason the middle and lower crust with the sparse ray coverage are poorly constrained and lack the velocity differentiation in the tomographic model. Due to the smoothing performed during the inversion and model parameterization, the velocity discontinuities are smoothed into broad gradient zones and the depth of the Moho boundary cannot be reliably estimated from this model.

6.2. Forward modelling results

The smooth tomographic model (Fig. 3a) gives only an approximate distribution of velocities in the crust and mantle and is not sufficient to describe the structure. On the other hand, variations in amplitude, travel time and duration of both the refracted and reflected seismic phases from the crust and uppermost mantle give more constraints on the velocity variations and location of the seismic discontinuities. Modelling of all phase allows for a more detailed velocity image, and for delineation of the reflecting interfaces, including the Moho discontinuity. Thus, we applied the iterative travel time fitting to further refine the tomographic model using the ray-tracing program package SEIS83 (Červený and Pšenčík, 1984) supplemented by

interactive graphical interface MODEL (Komminaho, 1997) and ZPLOT (Zelt, 1994). The initial velocity model was based on the final model from the tomographic inversion, and the overall layering was derived mainly according to reflected phases. The modelling also involved the calculation of synthetic sections and qualitative comparison of the amplitudes of synthetic and observed seismograms. Since the amplitudes of seismic waves are very sensitive to the velocity gradients and velocity contrasts at discontinuities, synthetic seismograms were used as an additional constraint. Fig. 4 shows an example of the forward modelling approach for SP 20030 in the Alpine area with calculated travel times and synthetic section, where strong Pn in the Bohemian Massif was detected up to 350 km offset.

The final 2-D velocity model is presented in Fig. 3b. Starting in the SW, in the Alpine area, a higher near-surface velocity of 6 km s^{-1} at 190–220 km distance along the profile corresponds to higher velocities of the Northern Calcareous Alps. They are underlain by a few km thick low velocity zone (LVZ) with the Vp of 5.1 km s^{-1} outcropping at the surface at 250 km distance and dipping to the SW to the maximum depth of 7 km (Fig. 5). It is interpreted as the Molasse and Helvetic Flysch sediments overthrust by the Northern Calcareous Alps extending from 130 to 300 km distance along the profile.

In Fig. 5, two shot points (SP 20030 and 26800) give an example of LVZ modelling below the rocks with higher velocities. It is evidenced by high apparent velocity of the Pg (~6 km s^{-1}) close to the shot points and quick decrease of the Pg amplitude, particularly to the NE. Later arrivals, observed at the offsets beyond 30 km, are delayed by about 2 s with respect to the first arrivals up to 12 km offset generated by the top layer. These delayed arrivals were attributed to the basement, which is separated from the high velocity limestone/dolomite layer by a few km thick low velocity zone. According to the velocity, the low velocity layer can be interpreted as the Molasse and/or Helvetic rocks and/or Flysch underlying the Northern Calcareous Alps with higher velocity values.

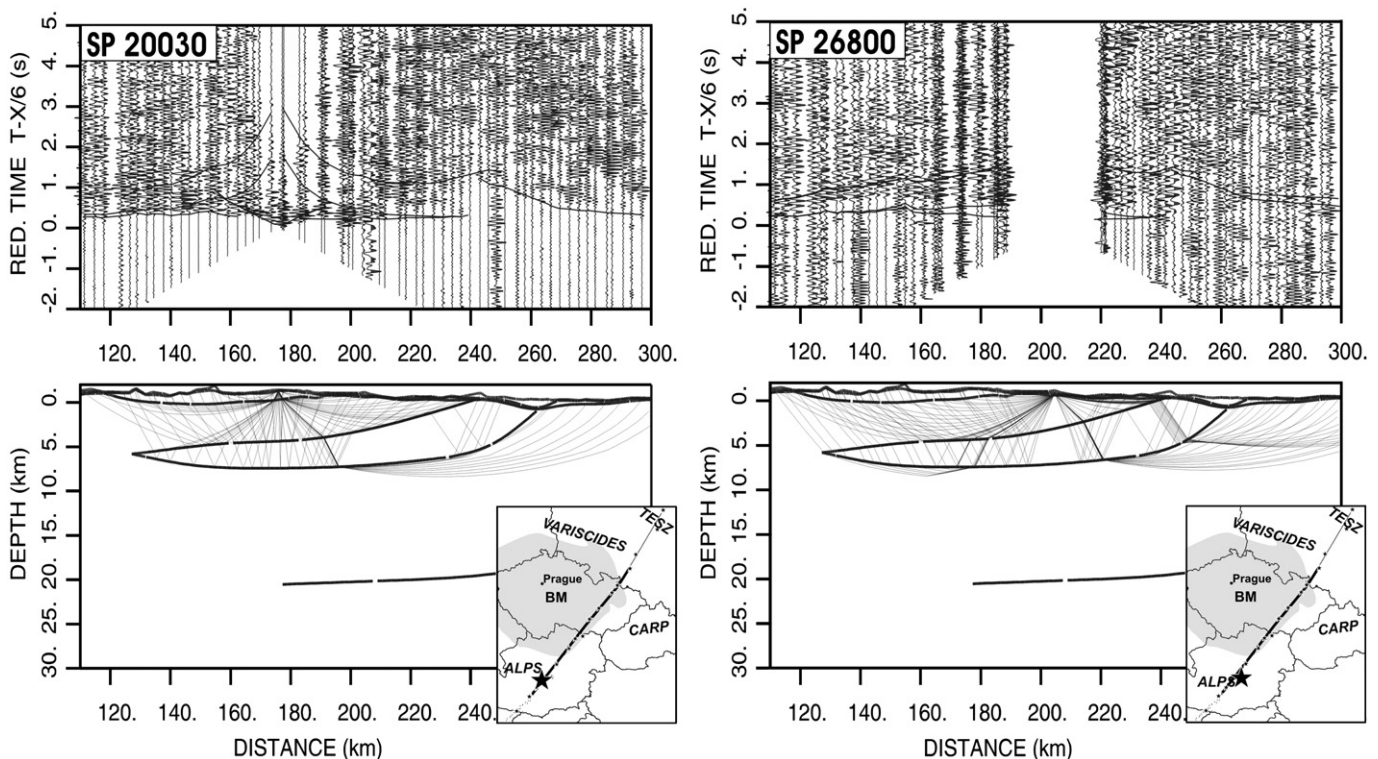**Fig. 5.** Examples of forward modelling of the overthrust low velocity zone (LVZ) in the area of the Northern Calcareous Alps. Right – SP 20030, left – SP 26800. Reduction velocity is 6 km s^{-1}, locations of major tectonic units and shot points are indicated. Note high apparent velocity of the Pg (~6 km s^{-1}) close the shot points and fast decrease of Pg amplitude, particularly to the NE.

In the Bohemian Massif, the interpretation along its whole eastern margin is influenced by the fact that this is the area of the Variscan nappes formation, compensated by large faults and shear zones. As such, it represents quite a complicated system and the seismic wave field irregularities reflect the existence of not only velocity inhomogeneities along the profile but also the ones generated by off-line sources. The upper crust of the Bohemian Massif displays a relatively high Vp gradient in the near-surface 2–3 km thick zone with the velocities of 5.8–6.0 km s^{-1} except at its NE end. An almost constant near-surface velocity of 6.0 km s^{-1} is typical especially for the Moravian unit, while the Silesian unit in the NE shows lower Vp velocities with higher gradient. Such feature is characteristic for
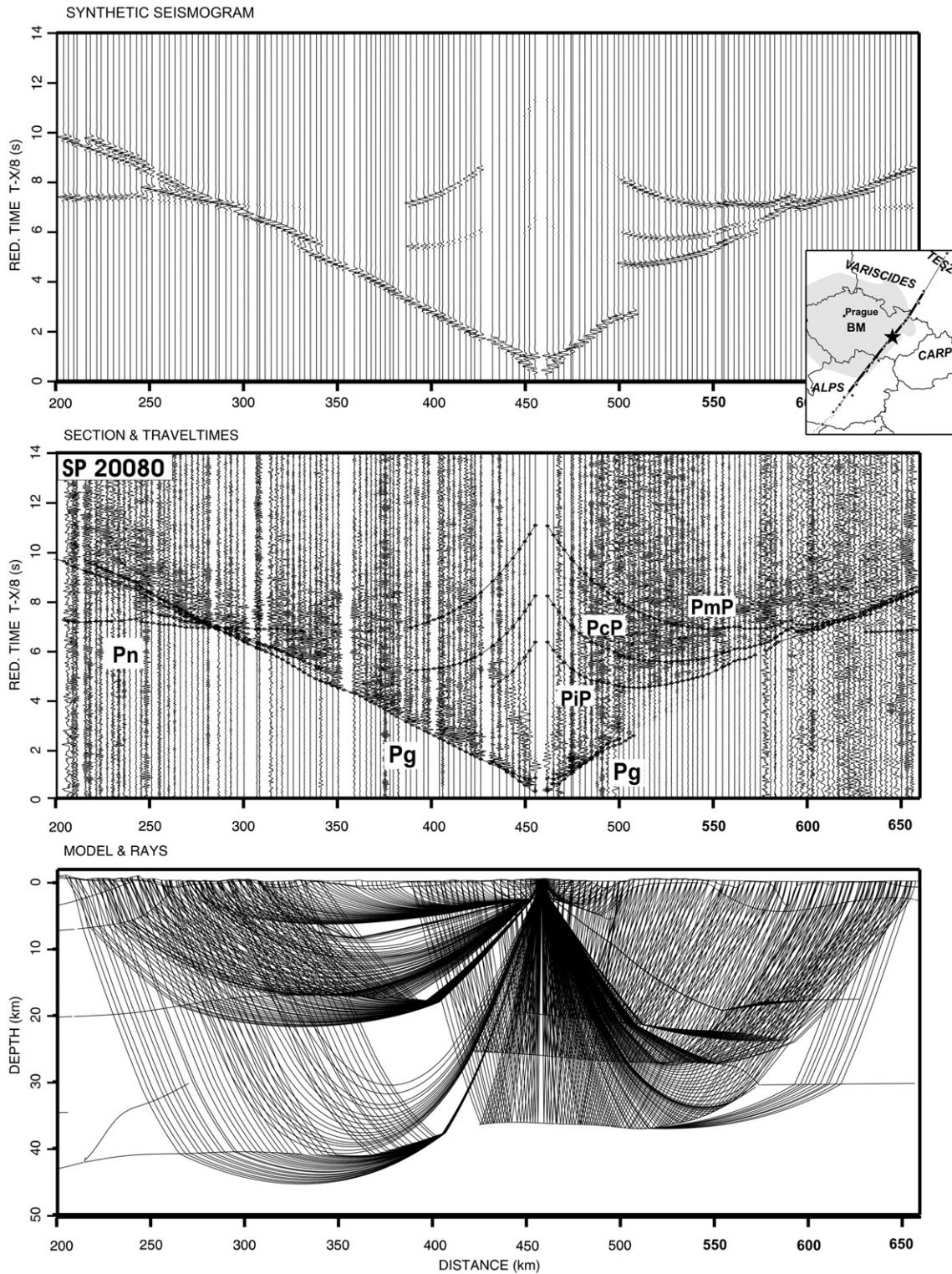
Fig. 6. Example of forward modelling for the SP 20080 illustrating different character of the wave field for two parts of the Bohemian Massif. The SW part shows pronounced, highly reflective Pg phase corresponding to higher velocity gradient (5.8–6.0 km s^{-1}) and no visible reflections from the crust/mantle transition. More to the NE, the fast decrease of Pg wave indicates low gradient. PiP, intracrustal reflection, PcP, reflection from the top of the lower crust. Top — synthetic section, middle — amplitude-normalized seismic section with calculated travel times, bottom — model and calculated raypaths. Reduction velocity is 8 km s^{-1}, locations of major tectonic units and shot points are indicated.

sedimentary rocks and their velocities are in the range from 5.0 to 6.0 km s^{-1} to about 6 km depth. Lower velocities in the range of 5.0–5.6 km s^{-1} down to a depth of 5 km correspond to the Paleozoic sediments on the contact of the Moravian and Silesian units at a distance of 470–510 km along the profile. Very low velocities of 3.9 km s^{-1} to the depth of 0.5 km at the distance of 480 km represent the Neogene sediments of a promontory of the Carpathian foreland. The higher near-surface Vp velocity of 6.2 km s^{-1} at a distance of 510–550 km along the profile coincides with the volcano-sedimentary complex of the Silesian unit (Nízký Jeseník Mts.).

In the NE part of the profile, from 640 km onward, upper crust comprises sediments of the Fore-Sudetic Monocline and the TESZ with velocities in the range of 3.6–5.5 km s^{-1} and maximum depth of about 15 km beneath the Mid-Polish Trough. Significantly lower velocities of 3.7–4.3 km s^{-1} at a distance of 590 km along the profile to a depth of 3 km coincide with the south-eastern extension of the Odra Fault Zone.

In the Bohemian Massif beneath the Paleozoic sediments, the deeper parts of the upper crust are not resolved properly by the tomography and exhibit a very low vertical gradient with the Vp velocity of 6.0–6.1 km s^{-1} from 3 km down to about 10 km depth. Instead of a low gradient, an alternative solution may be to introduce a low velocity layer in the upper crust at a distance of 400–480 km along the profile. However, in our opinion, the data cannot constrain the decrease in the velocity, partly because this area borders with lower velocities (5.0–5.6 km s^{-1}) from the surface down to a depth of 5 km at a distance of 470–510 km along the profile. Therefore we do not describe a LVZ in this part of the Bohemian Massif. In the middle crust, we identified a reflector with a velocity contrast of 0.2 km s^{-1} at a depth range of 17–22 km (PiP phases). It is detectable throughout the whole Bohemian Massif; shallower in the Moravian and dipping in the Silesian units, where it features a higher velocity contrast resulting in the reflected phases with high amplitudes (see Fig. 6).

At the lower crustal/upper mantle depths, the Vp features lateral variations, and the seismic signature of the crust/mantle transition suggests differences in its structure in the Bohemian Massif and its neighbouring units. In the Eastern Alps, the Moho is dipping to the SW reaching the depth of 43–45 km. Similar to the interpretation of profiles ALP01 and ALP02 (Brückl et al., 2007), the lower crustal velocities are within the range of 6.6–6.8 km s^{-1} with a velocity
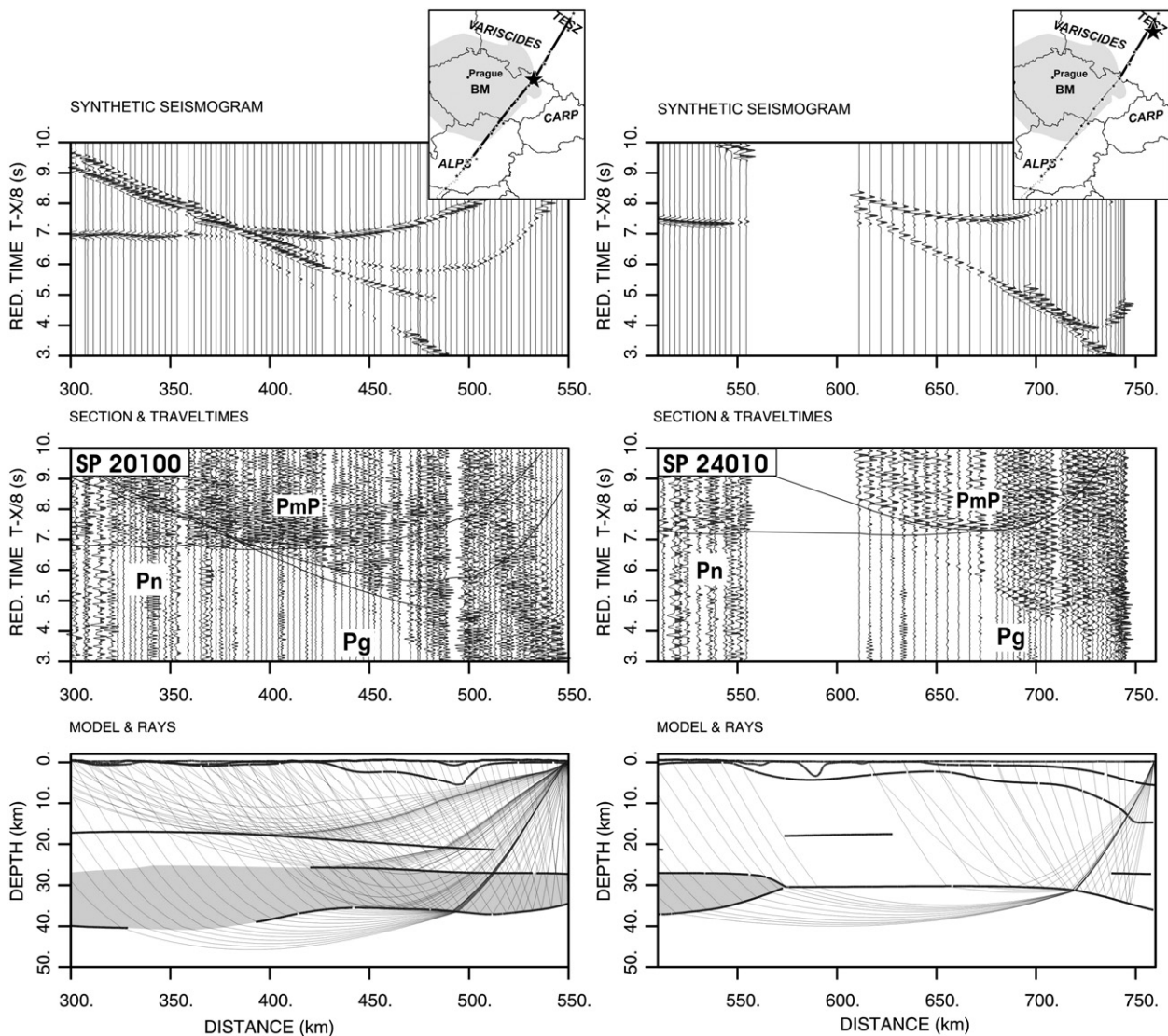
Fig. 7. Examples of forward modelling for SP 20100 and 24010, illustrating the difference in the character of the crust–mantle transition. Note high apparent velocity and long coda of the PmP for the area with high gradient crust–mantle transition zone (SP 20100) and lower apparent velocity and sharp onsets of the PmP for the "normal" Moho discontinuity with high velocity contrast. Top — synthetic sections, middle — amplitude-normalized seismic sections with calculated travel times, bottom — models and calculated raypaths for both shot points. High velocity zone in the Bohemian Massif marked in grey. Reduction velocity is 8 km s^{-1}, locations of major tectonic units and shot points are indicated.

contrast to 8.1 km s^{-1}. The increase in the Moho depth at the distances of 0–220 km along the profile reflects a crustal thickening beneath the Alpine area.

In the deeper parts of the Bohemian Massif's crust, instead of a sharp Moho, we interpreted a lower crustal high velocity layer spreading from 230 to 570 km along the profile. Though, the high velocity lower crustal zone can be viewed as a common feature along the whole eastern margin of the Bohemian Massif, the slightly different character of the wave field suggests differences between the Moravian and Silesian units, crossed by the profile. Beneath the Moravian unit in the SW, a strong lower crustal reflectivity with a long coda and a weak or null PmP phase suggests the existence of a highly reflective zone with high Vp gradient and continuous increase in the Vp from 7.0 to 7.9 km s^{-1} over a depth range of 28–40 km. This gradient zone has no distinct velocity contrast either on the top or in the bottom of this zone. More to the NE, beneath the Silesian unit, the PmP is more pronounced, though it is usually not the strongest reflection. In some sections (SP 20070, 20080, 20090 and 20100, see Figs. 2b,c, 6 and 7), it is masked by stronger reflections at the depths of 26–28 km interpreted as originating at the top of the lower crust. This discontinuity extends from 420 to 570 km distance with a velocity contrast of 0.4 km s^{-1}. Moreover, some sections show a pronounced mid-crustal reflection at 17–21 km depth in this area (Fig. 6). The Moho boundary is modelled with lower velocity contrasts at 35–38 km depth. Velocities in the uppermost mantle are within the range of 7.9–8.1 km s^{-1} with higher values in the SW but they are not well-constrained since the Pn phase is missing in some sections.

Beneath the Fore-Sudetic Monocline, where the PmP phase is the most pronounced in terms of high amplitude and short coda, the Moho is interpreted as a first-order discontinuity at a depth of 30 km with a sharp velocity increase from 6.75 to 7.9–8.0 km s^{-1}. Fig. 7 illustrates the differences in the character of the crust–mantle transition. It compares the PmP with long coda and high apparent velocity originating from high gradient crust–mantle transition zone in the Silesian unit (SP 20100) on one side. On the other side there is the PmP with sharp onsets and lower apparent velocity originating from the "normal" Moho discontinuity with high velocity contrast in the Fore-Sudetic Monocline (SP 24010). Intracrustal interfaces are practically not observed in this area. The Vp velocity in the middle and lower crust increases from 6.6 km s^{-1} at 19–21 km depth to 6.85 km s^{-1} above the Moho, which is in agreement with the velocities along a perpendicular profile (Środa et al., 2006), where the Moho is located at a depth of 35 km with a velocity increase from 6.80 km s^{-1} to 8.15 km^{-1}. The Moho reaches 40 km depth beneath the axial zone of the TESZ, the Mid-Polish Trough (MPT), where the upper mantle velocities are in the range of 7.9–8.1 km s^{-1}.

7. Analysis of accuracy, resolution and uncertainties

Errors of modelling result from combination of several factors: data timing errors, misidentification of seismic phases, travel time picking, inaccuracy of modelling (misfit between data and modelled travel times) and 2-D geometry of the experiment, not accounting for 3-D effects or anisotropy. Some errors are subjective, introduced by
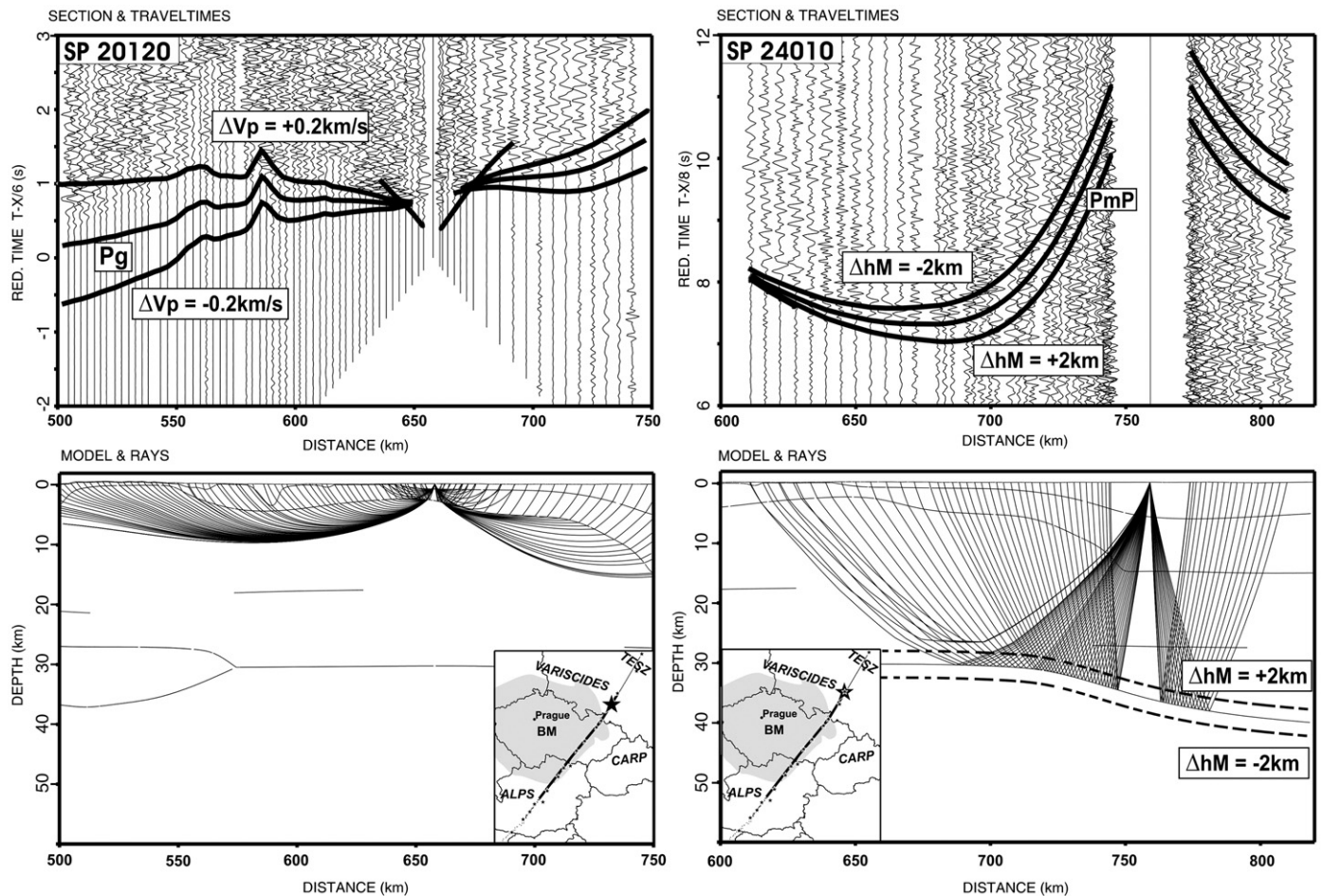
Fig. 8. Example of the arrival times of the Pg phase (Vp ~ 6.0 km s^{-1}) for SP 20120 with velocity perturbations of +/−0.2 km s^{-1} and the arrival times of the Moho reflections PmP (depth ~ 30 km) for SP 24010 together with the perturbations of the Moho depth of +/−2 km. Reduction velocity is 6 km s^{-1} (SP 20120), and 8 km s^{-1} (SP 24010). Locations of major tectonic units and shot points are indicated.

the interpreter during phase correlation, and are not possible to quantify. Their magnitude decreases with increasing quality and quantity of data. Due to the subjective errors, it is not possible to produce a full and systematic error analysis. In this study we attempt to evaluate the errors resulting from picking accuracy and from the misfit between the model and the data. Also, in the process of modelling, the limitations of ray theory must be kept in mind. In addition, two-dimensional modelling does not take into account out-of-plane refracted and reflected arrivals, which must have occurred particularly in such a structurally complex area on the contacts of several units.

In the interpreted data set, there were enough data/shots to correlate the major phases with considerable confidence, increased by comparisons of phases picked independently by different interpreters and with the help of reciprocity checking. The calculated travel times fit the observed travel times with accuracy for both refracted and reflected phases of ±0.1 s. The picking accuracy was usually about ±0.05–0.1 s for the Pg phases and about ±0.1–0.2 s for the reflected phases (PmP, mid-crustal reflections) and the Pn. In addition, synthetic seismograms generally showed good qualitative agreement with the relative amplitudes of the observed refracted and reflected phases.

Based on the error analyses for wide-angle data of similar density and quality from the CELEBRATION 2000 experiment (Środa et al., 2006), we assume a standard deviation of the first arrival times to be ~0.1 s or 0.05 s, if we consider near-offset arrivals. For the reflected phases, PmP, which are much harder to correlate, the standard deviation might be as high as 0.2 s. Residuals in the final tomographic models seem to confirm these estimates. In the ray-tracing modelling, we analyze travel time curves rather than single arrivals. In such cases, typical velocity errors, as shown, e.g., by Janik et al. (2002) and Grad

et al. (2003a), are in the range of 0.1 km s^{-1} and errors in the boundary depth are of the order of 1 km; however, in complicated parts of the model, they might increase up to 0.2 km s^{-1} and 2 km, respectively. In Fig. 8, we show the arrival times of the Pg phase with the velocity perturbations of +/−0.2 km s^{-1} where the perturbed Pg arrivals are either too late or too early, which illustrates that the velocity in the upper crust can be determined with an accuracy of +/−0.1 km s^{-1}. In a similar way, the arrival times of the Moho reflections PmP are shown together with the perturbations of the Moho depth of +/−2 km.

8. Geological interpretation and discussion

In the following discussion, we propose a general tectonic/geological interpretation for the velocity model along CEL10 and ALP04 profiles at the eastern termination of the Variscan belt. We discuss namely the Moravo-Silesian zone of the Bohemian Massif, and its contact with the Eastern Alps and the TESZ based on the Pg velocity distribution, character of the lower crust and Moho topography, surface geology and results from other profiles, especially ALP01 and ALP02, CEL09, 8HR, and KII.

8.1. Lithology

Interpretation of crustal lithologies along the profile is based on the P-wave velocities obtained by the 2D ray-tracing modelling. The most plausible lithologies are inferred from modelled Vp values compared to global and regional laboratory data for various rock assemblages in the crust (Christensen and Mooney, 1995; Mueller, 1995). Laboratory data are considered at 15 km and 30 km depth, shaded areas represent modelled Vp velocities beneath the interpreted profiles (Fig. 9). In the upper crust, in the Bohemian Massif; the modelled Vp velocities
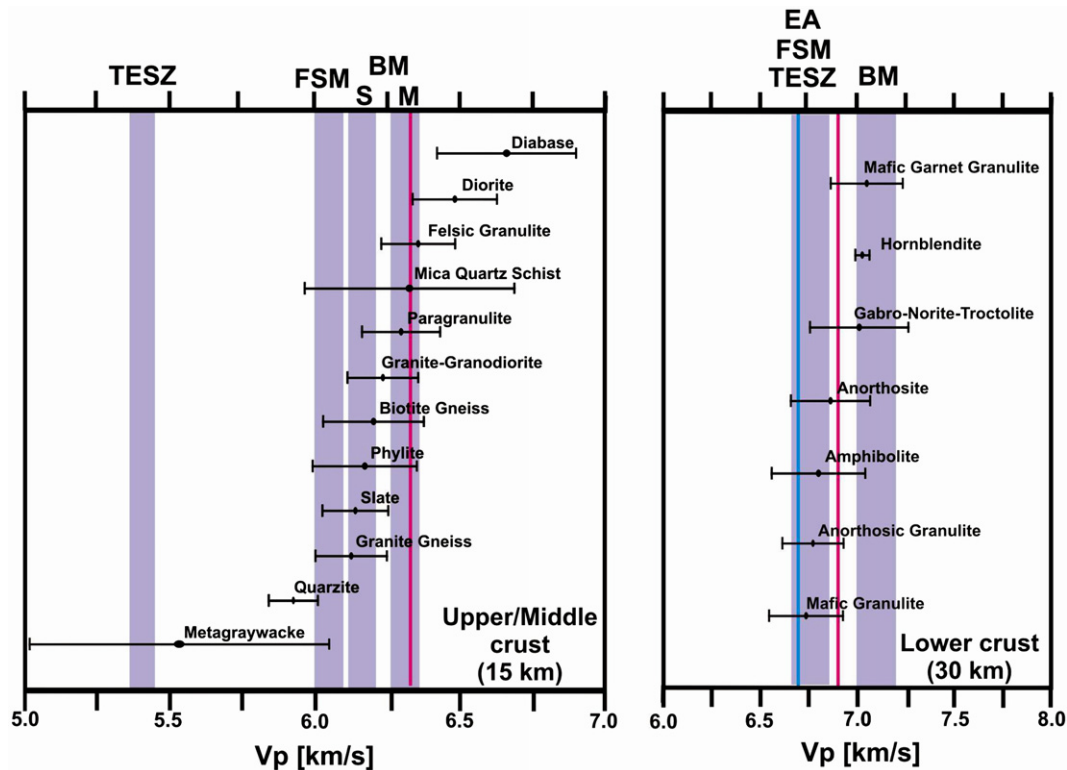

Fig. 9. Comparison of the Vp velocities observed along the joint profile CEL10 and ALP04 with laboratory data according to Christensen and Mooney (1995). Modified after Malinowski et al. (2005). Anisotropy has been neglected. Laboratory data for various rock assemblages in the crust are shown at 15 km (a) and 30 km depth (b). Shaded areas represent modelled Vp velocities beneath the interpreted profiles, and in the upper/middle crust they are 6.3 km s^{-1} for the Moravian (M) and 6.15 km s^{-1} for the Silesian (S) (both the Bohemian Massif BM); 6.05 km s^{-1} for the Fore-Sudetic Monocline (FSM); 5.4 km s^{-1} for the TESZ. In the lower crust they are 7.2 km s^{-1} for the BM and 6.75 km s^{-1} for the Alps, FSM and TESZ. The shaded areas are shown with the estimated uncertainty of the velocity values of ±0.05 km s^{-1} for the upper/middle crust and ±0.1 km s^{-1} for the lower crust. Vertical lines represent calculated velocities for the extended crust − BM (6.31±0.32 km s^{-1} for 15 km depth, 6.89±0.40 km s^{-1} for 30 km depth) (Christensen and Mooney, 1995).

are 6.3 km s^{-1} for the Moravian and 6.15 km s^{-1} for the Silesian; 6.05 km s^{-1} for the Fore-Sudetic Monocline; and 5.4 km s^{-1} for the TESZ. In the lower crust they reach 7.2 km s^{-1} for the Bohemian Massif and 6.75 km s^{-1} for the Alps, the Fore-Sudetic Monocline and the TESZ. The shaded areas are shown with the estimated uncertainty of the velocity values of ±0.05 km s^{-1} for the middle crust and ±0.1 km s^{-1} for the lower crust. Bars represent published standard deviations for laboratory data. Anisotropy has not been taken into account, however it might reach values from 1–5% (e.g. igneous rocks, gneiss, quartzite, granulites, eclogite), to even 10–20% (e.g. phylite, mica schist, amphibolite) (Christensen and Mooney, 1995).

The upper crust in the Bohemian Massif shows velocities typical for granitoids and gneisses, which corresponds to the abundance of plutonic basement rocks of Cadomian age in the Moravo- Silesian unit. Although they occur directly at the surface only in a minor part in tectonic windows, they are known from drillings and geophysical research to occupy at least one third of the entire basement (Dallmeyer et al., 1995). Cadomian plutons are bodies of granitoid gneisses with more granitic composition in the S, while to the N they change to the rocks of intermediate to basic composition as e.g. the intrusions of diorites exposed at the surface at around 420 km along the profile. The velocities in the Silesian unit at the upper/middle crustal level are comparable to that of the Moravian unit which points to a similar origin. Uppermost crustal velocities of about 5.5 km s^{-1} represent the Culm sediments. The velocity model evidences higher velocities of 6.2 km s^{-1} in the upper crust at around 530–540 km along the profile, which can be attributed to basalts of neo-volcanics, though their occurrence is much more limited to a smaller area. The anomalous low velocity upper crust of the TESZ can be interpreted as an extensive pile of sediments and low-grade metasediments (e.g. metapellites, meta-graywacke) (Grad et al., 2002, in press). Modelled lower crustal Vp velocities for the Alps, FSM and TESZ are 6.7–6.8 km s^{-1}, which may correspond with gabbros and granulites. On the other hand, for the Moravian and Silesian, the Vp in the lower crust is in the range of 6.8–7.8 km s^{-1}, which can be explained by the presence of mafic garnet granulite, assuming that its content in the lower crust increases with depth as a result of phase transition of rocks with gabbroic composition. Large differences in lower crustal velocities between the Bohemian Massif and the surrounding areas with possibly similar composition may have resulted from a different tectonic evolution and different *P–T* conditions.

Christensen and Mooney (1995) divided the crust into five tectonic provinces, where central Europe belongs to the extended crust. If we compare their weighted calculated velocities for the extended crust (6.31±0.32 km s^{-1} for 15 km depth, 6.89±0.40 km s^{-1} for 30 km depth; vertical lines in Fig. 9), the modelled lower crustal velocities in the Bohemian Massif are slightly higher (7.1 km s^{-1}).

8.2. Eastern Alps

During the formation of the Eastern Alps, northward thrusting of nappes occurred along the northern rim of the orogen. Thus, the alternation of higher and lower velocities dipping SW in the upper crust is interpreted as the Molasse and Helvetic Flysch sediments beneath the Northern Calcareous Alps (LVZ at 130–260 km distance along the profile). The interpreted result corresponds with Giese and Prodehl (1976), where they describe an overthrusting of Permome-sozoic Northern Calcareous Alps over the Flysch-Helvetic and Molasse outcropping in the northern rim of the Eastern Alps. According to e.g. Reinecker and Lenhardt (1999), the Molasse is detectable not only on the surface but lies allochthonously below the Alpine nappes and its lower velocities alternate with higher velocities of the thick carbonate layers of the Northern Calcareous Alps (Figs. 3, 12). It also corresponds with the results of Behm et al. (2007), where lower velocities of the Molasse Flysch shift in the southern direction with the increasing depth.

We interpreted the base of the Northern Calcareous Alps at 2–5 km depth with the SW dip and Vp of 5.9–6.1 km s^{-1}. The thickness of limestones and dolomites in the Northern Calcareous Alps was interpreted by Giese and Prodehl (1976) and resulted in about 3 km with the P-wave velocities from 5.5 km s^{-1} at the surface to more than 6.5 km s^{-1} at the base. The difference in the velocity compared to our results might be explained by the fact that Giese and Prodehl's results concern the area located about 100 km to the west from the CEL10 profile.

Beneath the Flysch/Molasse low velocity layer, velocities of 6.2 km s^{-1} represent Palaeozoic rocks of the Bohemian Massif, overthrust by the Alpine units and forming their basement. From our data, it was not possible to determine how far to the south the Bohemian basement continues beneath the Alps, but it probably underlies at least the whole lower velocity layer, which extends to the south to a distance of 150 km along the profile.

Beneath the Eastern Alps, the crust thickens and the south-westward dip of the Moho continues to reach the maximum thickness of 40–44 km closer to the axis of the Eastern Alps. The velocity contrast at the Moho is from 6.7 km s^{-1} in the lower crust to 8.2 km s^{-1} in the upper mantle. This interpretation correlates with the results of the interpretation along the ALP01 and ALP02 profiles from ALP 2002 experiment (Brückl et al., 2007), which interpreted the Moho at 43 km and a velocity contrast from 6.6 km s^{-1} to 8.2 / 8.0 km s^{-1}, respectively. Behm et al. (2007) in determination of the Moho show a deeper Moho at the Alpine root compared to a shallower Moho in the Bohemian Massif. Such results reflect the thickening of the crust in a conse-quence of large-scale collision of the Adriatic and European plates during the Tertiary.

8.3. Bohemian Massif

8.3.1. Upper crust of the Bohemian Massif

The Moravian unit in the SW consists of the metamorphic rocks intruded by Cadomian granitoids and is characterized by a velocity of 5.9–6.0 km s^{-1} down to a depth of 2–3 km. This velocity gradient in the crystalline rocks is usually due to the closing of micro-cracks under increasing pressure. The Cadomian granitoids of the Brunovistulian block in deeper parts of the upper crust show very small, sometimes even negative, vertical gradients as indicated by fast decay of the Pg phase amplitude.

More to the NE, in the Silesian unit, the high velocity gradient in the upper crust is related to the sedimentary rocks of Devonian and Carboniferous deposits covering the Brunovistulian foreland. Higher near-surface velocities at a distance of 500–550 km along the profile can be explained by the occurrence of the Devonian and early Carboniferous mafic volcanic intrusions (Dallmeyer et al., 1995), which increase the average Vp of the sedimentary layer to 6.2 km s^{-1}. A major concentration of volcanic bodies exposed on the surface lies in the vicinity of Bruntál in the Nízký Jeseník Mts. (535 km along the profile) and they are documented also in mines and by geophysical investigations (Gruntorád and Lhotská, 1973). Also, this area coincides with the location of the Quaternary volcanoes.

Lower velocities in the range of 5.0–5.6 km s^{-1} down to a depth of 5 km at a distance of 465–500 km along the profile might represent the SE extension of the Elbe Fault Zone (EFZ) (e.g., Mazur et al., 2006), the crustal scale NW–SE trending zone separating the northerly Sudetic realm from the main part of the Bohemian Massif (e.g. Schulmann et al., 2005) and limiting the contact of the Moravian and Silesian units (Dallmeyer et al., 1995). It is also the area of the increased tectonic activity manifested by the increased seismicity in the eastern part of the Bohemian Massif. Špaček et al. (2006) showed that the majority of seismic activity of swarm-like sequences is concentrated in a 40–60 km wide zone of generally NW–SE trend, crossing the profile in the 465–500 km distance range, which represents a regional zone of weakness. These authors also attribute

this zone to the continuation of the Elbe Fault Zone (EFZ), where the increased tectonic activity can be interpreted as a result of the abundance of faults and their interconnection into major fault systems, together with the neo-volcanic activity in the Nízký Jeseník Mts. in the vicinity.

The northern termination of the Bohemian Massif is often thought to be docked by the Odra Fault Zone, a few-km-wide vertical zone liable to the interpretation as a major wrench compatible with the EFZ (Elbe Fault Zone) (Dallmeyer et al., 1995). Low upper crustal velocities of 3.5 km s^{-1} at a distance of 590 km along the profile may represent the south-eastern extension of this Odra Fault Zone and the extension of the Variscan basement exposed at the surface.

8.3.2. Lower crust of the Bohemian Massif

Along the whole eastern margin of the Bohemian Massif, the lower crust is characterized by elevated the velocities of 6.8 to 7.8 km s^{-1}; however, its properties differ between the Moravian and Silesian units along the profile. At the base of the crust in the Moravian area, we do not observe a regular Moho discontinuity with a velocity contrast. The lower crustal arrivals with a long coda and a weak PmP phase with high apparent velocity suggest a high gradient (6.9–7.9 km s^{-1}) reflective layer extending from the middle crust to the mantle, in the depth range of 26–40 km. This layer represents a broad crust–mantle

transition zone spreading in the range of 230–400 km along the profile, with no distinct velocity contrast either on the top or bottom. Such a result is consistent with the interpretation of the SE part of CEL09 profile from the CELEBRATION 2000 experiment, where no Moho is imaged as a first-order discontinuity. Hrubcová et al. (2005) interpreted the Moho along the perpendicular CEL09 profile as a broad crust/mantle transition zone with the velocities increasing gradually from 6.8 to 7.8 km s^{-1} over a depth range of 23–40 km (Fig. 10).

More to the NE beneath the Silesian unit, a strong reflector at the depths of 26–28 km represents the top of the lower crust extending from 420 to 560 km along the profile with the velocity contrast of 0.4 km s^{-1} (SP 20080, 20090 and 20100, Figs. 2b,c 6, 7). This reflector is the highest amplitude event within the crust in this area and, together with the poorly pronounced Moho at 35–38 km depth, delimits the lower crustal layer. These results support the interpretations along two perpendicular lines, the reflection profile 8HR and the refraction profile KII. The reflection profile 8HR, which crosses the CEL10 transect in the Brno massif at a distance of 440 km, showed the Moho at 35–37 km (Hubatka and Švancara, 2002a). The KII profile, which crosses the CEL10 transect at 530 km distance, images a strong reflector in the lower crust (28–30 km depth) dipping towards the SE and two bands of reflections at a depth of 36 and 37 km, rising towards the SE to 30–32 km (Majerová and Novotný, 1986; Hubatka and Švancara, 2002b). A
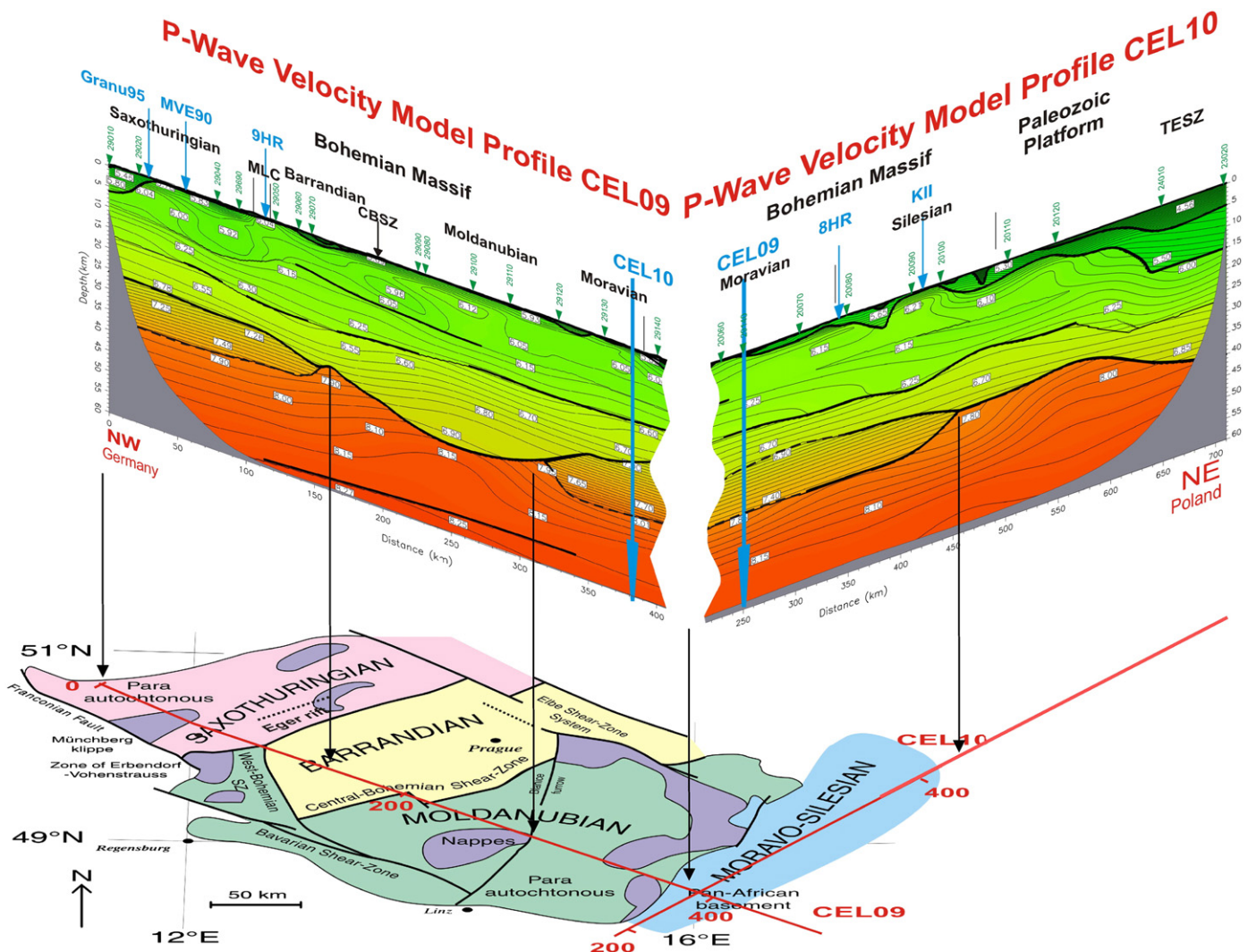

Fig. 10. P-wave velocity models along the profiles CEL10 and CEL09 (Hrubcová et al., 2005) at the crossing point of both profiles, superimposed on a schematic map of major tectonic units of the Bohemain Massif. In the Moravian, the Moho is viewed as a broad crust/mantle transition zone with velocities increasing gradually from 6.8 to 7.8 km s^{-1} over a depth range of 23–40 km.

similar lower crustal layer with the same velocity (in the range of 7.1–7.2 km s^{-1}) was also interpreted by Malinowski et al. (2005) for the Upper Silesian Block, about 100 km to the east. Though their results of the interpretation (along CEL02 profile) differ in having much thicker middle crust (velocities of 6.5 km s^{-1}) compared to the results in our part of the Silesian unit (velocities of 6.2 km s^{-1}), both profiles show similar lower crust with high P-wave velocities.

The origin of the high gradient reflective lower crustal zone might represent gradual changes of the lower crustal composition, with the percentage of mafic/ultramafic material increasing with depth. Alternative explanation may involve a change in metamorphic grade with an incomplete phase transition of granulitic rocks from amphibolite to eclogite facies (e.g. Thybo et al., 2003), where velocities can range from 7.0 to 7.7 km s^{-1} depending on the metamorphic grade, composition and P–T conditions (Furlong and Fountain, 1986; Hurich et al., 2001). Such metamorphic processes are commonly associated with lithospheric plate boundaries, where the interactions between plates can produce sufficient heat for metamorphism of the crustal rocks on a large-scale. The lower crustal zone might be also affected by solidified intrusions most probably of amphibole rich composition, which is commonly considered as the magmatic underplating (e.g., Furlong and Fountain, 1986), where seismic velocities might be in the range from values intermediate between crustal and mantle values (7.1–7.5 km s^{-1}) to values typically interpreted to represent mantle material with velocities greater than 7.8 km s^{-1} (Furlong and Fountain, 1986). Magmatic underplating can be attributed to subhorizontal laminae of the dense mafic rocks or melt within felsic granulites (Handy and Streit, 1999), or represented by garnet pyroxene granulites (Morozov et al., 2001).

Schulmann et al. (2008) suggest that the orogenic lower crust in the Bohemian Massif represents Neoproterozoic-Cambrio-Ordovician continental crust that experienced a major thermal reworking during the Devonian where also mantle was involved during Carboniferous. This led to continuous convergent motion of the Brunia continent towards velocities of Moldanubian and a major shortening with extrusion of the granulized lower crust to higher crustal levels. Thus the metamorphic change with possible perturbations of the granulized lower crust is the most probable cause of the high gradient reflective lower crust.

The structural complexity of the Bohemian Massif and adjacent areas led some authors to propose a small-scale mosaic of microplates (e.g. Oliver et al., 1993) but the detailed evaluation of the new findings showed that the north and east parts of the Bohemian Massif are attributed to one Variscan orogenic cycle. Variscan convergence resulted in the Devonian subduction and the early Carboniferous collision. Tectonic structure reveals an overthrusting directed to the NE at the southern flank of the Variscides. The crystalline basement of the whole area is composed of the Brunovistulian and the Moravo-Silesian zone can be seen as a zone of deformation along the Moldanubian Thrust where the Brunovistulian rocks emerge through it in some tectonic windows (e.g., Schulmann et al., 2005, 2008). From this point of view, it is not possible to discern the contact of the Moravian and Silesian units in the depth and the difference can be seen only on the surface, where the area east of the Moldanubian Thrust is covered by clastic sediments of the Culm.

The differences in the character of the lower crust and the Moho between the Moravian and Silesian units might be attributed to the differences in a distance of the profile from the Moldanubian Thrust front, which is oblique to the CEL10 transect. The studied part of the Moravian unit in the SW is located close to this major contact thrust zone. Strong metamorphism and tectonic deformations at this contact zone might contribute to transformation of the original lower crustal architecture into a high Vp and high gradient layer. The Silesian part of the profile in the NE is more distant from the Moldanubian Thrust front and might be less affected by the tectonic processes, which resulted in retaining a more typical character at the lower crust

and Moho level with more pronounced velocity discontinuities. Schulmann et al. (2005) show a different type of contact of the Brunia promontory in the southern and northern parts of the Bohemian Massif. As discussed above, the contact with the Moldanubian resulted in the underthrusting of the Brunia promontory beneath the Moldanubian. In contrast, the Brunia continent was not underthrust beneath the orogenic root in the northern sector which might contribute to different character of the lower crust beneath Silesian.

Schulmann et al. (2008) in discussing the characteristics of the lower crust at the eastern sector of the Variscan orogenic belt suggest vertical exhumation of a deep orogenic lower crust followed by subhorizontal escape. They conclude that this early exhumation was kinematically related to the Saxothuringian continental subduction to the east, creating a convergent accretionary wedge west of the Silesian. Fig. 11 shows the comparison of 1-D velocity models for the Silesian and the Saxothuringian crusts. The 1-D velocity characteristics for the Silesian unit was taken from the profile CEL10 at 465 km distance, 1-D velocity characteristics for the Saxothuringian unit was derived from the profile CEL09 at 105 km distance in the west part of the Bohemian Massif (according to the interpretation of Hrubcová et al., 2005). The similarities of the Vp velocities for both these regions can suggest that the Silesian crust is roughly similar to that of the Saxothuringian, especially in its lower parts. This might show some affinity of the Silesian and the Saxothuringian zone as proposed also by e.g. Edel et al. (2003) though more detailed analysis is beyond the scope of this study.

Franke and Żelaźniewicz (2002) and also Mazur et al. (2006) mention the record of the Moravo-Silesian belt that has much in common with that of the Rhenohercynian Belt: Devonian rifting and mafic volcanism, Middle and Late Devonian Reef carbonates, as well as Early and Late Carboniferous deposits. They discuss that the high pressure rocks contained in the structurally highest unit of Jeseniky segment represent deeper parts of the Rhenohercynian / Moravo-
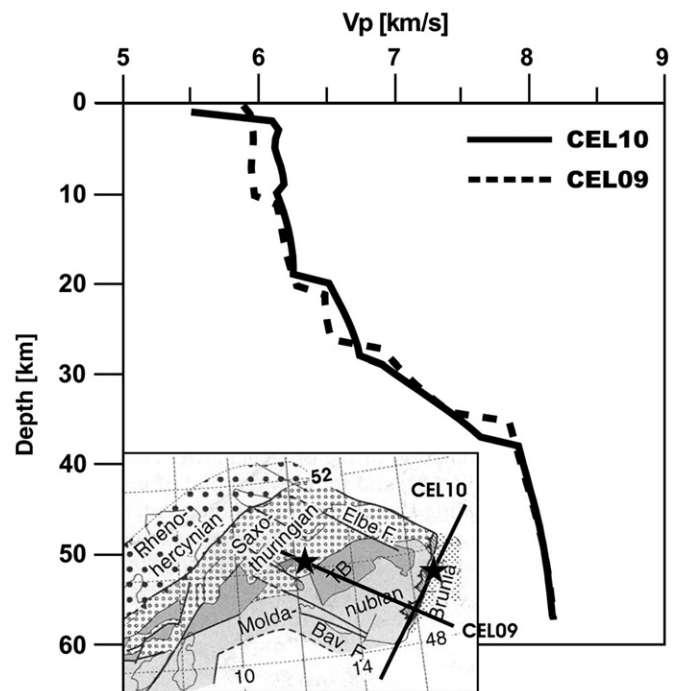

Fig. 11. Comparison of a velocity/depth curve for the Silesian and Saxothuringian units. Solid line: 1-D velocity characteristic for the Silesian taken from the profile CEL10 at a distance of 465 km. Dashed line: 1-D velocity characteristic for the Saxothuringian taken from the profile CEL09 at a distance of 105 km in the west part of the Bohemian Massif (according to the interpretation of Hrubcová et al., 2005). Note similarities of Vp velocities for both these regions especially in their lower parts. The insert modified after Schulmann et al. (2008), stars represent locations of 1-D models.

Silesian basin, which were subducted, then exhumed and overthrust on the Moravo-Silesian foreland and only later affected by the N–S trending Moldanubian Thrust. Also, paleomagnetic studies (e.g. Krs et al., 1995) show unequivocal evidence for rotation of the Moravo-Silesian Belt to the SE of the Moldanubian Thrust, which has been rotated clockwise through at least 90o (with respect to the Rhenohercynian Belt in Germany) since the Devonian.

The high velocity lower crust beneath the Bohemian Massif (velocities within the range of 6.8–7.8 km s^{-1} over a depth range of 28–40 km) terminates at 575 km along the profile. It is in contrast with the Moho in the Fore-Sudetic Monocline interpreted as the first-order discontinuity at 30 km depth. If we think of the gradient zone of the lower crust as a characteristic feature of the Bohemian Massif in this area, then the termination of the high velocity lower crust can be considered as a north-eastern termination of the Bohemian Massif at a crust/mantle level affected by eastward collisional tectonics and probably also rotation.

8.4. Fore-Sudetic Monocline and TESZ

The northern Variscan foreland represented by the TESZ has a structure that corresponds to the previous studies (Grad et al., 2002; Środa et al., 2006; Grad et al., in press). The upper crust of the Fore-Sudetic Monocline has slightly different velocity than that of the Bohemian Massif (Fig. 4). But it has noticeably different crust from that of the Mid-Polish Trough and thus it most probably belongs to the Variscan orogen. Compared to the Bohemian Massif, the area of the Fore-Sudetic Monocline displays considerably lower velocities in the upper crust beyond a distance of 600 km along the profile. There, the Lower Paleozoic metamorphic basement is overlain by largely flat lying
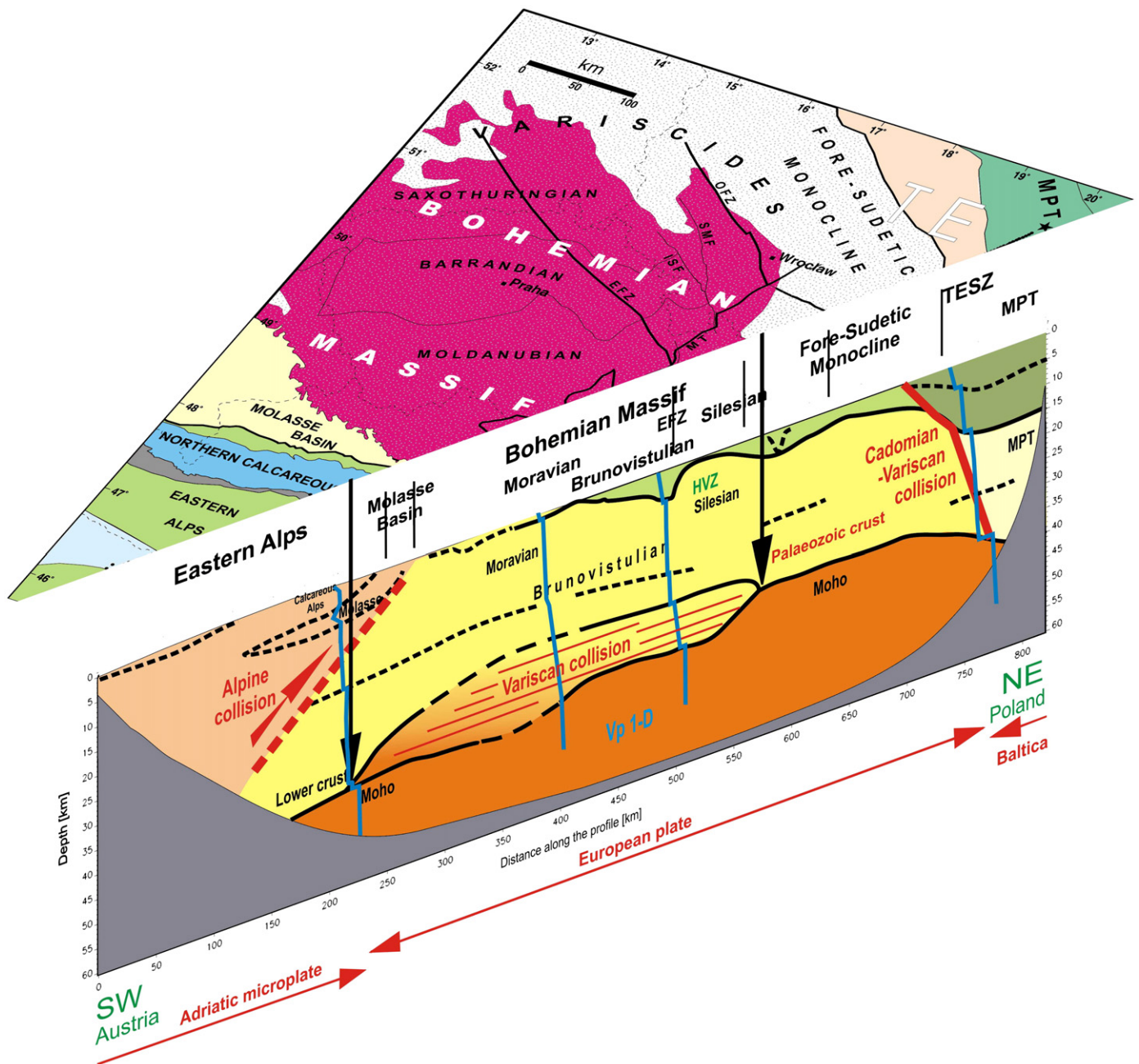

Fig. 12. Schematic geological/tectonic representation along joint profile CEL10 and ALP04 with simplified tectonic map. Black vertical arrows mark the extension of the lower crustal gradient zone of the Bohemian Massif at the surface. Superimposed, there are 1-D velocity characteristics for different parts of the profile: Eastern Alps, Moravian, Silesian, TESZ. Vertical exaggeration is 1:4. EFZ, Elbe Fault Zone; MPT, Mid-Polish Trough; HVZ, high velocity zone; TESZ, Trans-European Suture Zone.

sedimentary rocks with velocities of 3.7–5.3 km s^{-1} to the depths of 3–6 km. Underneath this cover, the upper crust has relatively low P-wave velocities of 5.9–6.05 km s^{-1}. Similar upper crustal velocities were also found in the Paleozoic part of the P1 and P4 profiles (Guterch et al., 1986; Jensen et al., 1999). Dadlez et al. (2005) showed that in the Variscan Belt the lower crust has velocities of 6.5–6.6 km s^{-1} and the middle crust is in the range of 6.2–6.3 km s^{-1}, which corresponds to the velocity range detected from our data beneath the Fore-Sudetic Monocline. Further to the NE, the velocities of 3.6–5.5 km s^{-1} at the depths of 15 km correspond to Permian to Mesozoic sediments and low-grade metasediments of the Mid-Polish Trough, as well as to older metasedimentary sequences. Similar low velocities (<6.4 km s^{-1}) to the depths of about 20 km are observed on several other seismic profiles in the TESZ area, e.g. Grad et al. (2002).

The Moho in the Fore-Sudetic Monocline is interpreted as a first-order discontinuity with a velocity jump from 6.7 to 7.9–8.0 km s^{-1} at a depth of 30 km and is in sharp contrast with the high velocity lower crust of the Bohemian Massif. The deepening of the Moho towards the axial zone of the TESZ, the Mid-Polish Trough, to the depth of about 40 km is in agreement with other investigations of the TESZ as a transition zone between the Paleozoic Platform and the East European Craton (e.g., Grad et al., 2003a; Grad et al., 2007). There are still debates on the location of the boundary between the internal and external Variscides, which is supposed to be somewhere in the Fore-Sudetic Monocline between 620 and 650 km along the profile (e.g., Mazur et al., 2006). Some authors, e.g. Franke and Żelaźniewicz (2002), consider continuation of the Silesian as far as the Krakow–Lubliniec Zone where the contact of the Silesian and the Fore-Sudetic Monocline is located on the surface. Our results do not help in answering these questions, as there is no differentiation in the seismic model observed in this area.

9. Summary and conclusions

High quality seismic data were acquired during the CELEBRATION 2000 and ALP 2002 experiments along 820 km long, SW–NE striking profile at the easternmost margin of the Variscan belt and on the contact with the Alps and Baltica. The data have been interpreted by tomographic inversion of the first arrival travel times and by two-dimensional ray-tracing of the first and later arrivals, as well as by calculation of synthetic seismograms for the P-wave arrivals. Our effort to model these data provides us with the conclusions that are summarized in Fig. 12. We show differentiation of the structure both in the upper crustal parts and also at lower crust and upper mantle levels, which gives some indications for tracing of crust-forming processes during the Variscan and Alpine orogeny.

In the SW, the N–S directed Tertiary orogeny resulted in northward thrusting of the Eastern Alpine nappes along the northern rim of the Alps. The interpretation of joint ALP04 and CEL10 models shows the lower velocities of the Molasse and Helvetic Flysch sediments detectable not only on the surface but dipping SW below the Alpine nappes, where they alternate with higher velocities of the thick carbonatic layers of the Northern Calcareous Alps. Beneath the Eastern Alps, the crust thickens and the south-westward dip of the Moho continues to reach the maximum thickness of 40–44 km closer to the axis of the Eastern Alps. This reflects the thickening of the crust in a consequence of large-scale collision of the Adriatic and European plates during the Tertiary.

The eastern margin of the Bohemian Massif, represented by the Moravo-Silesian zone, provides a detailed picture of geological inventory as a zone of sheared and metamorphosed Brunia-derived rocks. These rocks emerge through the Moravo-Silesian in the tectonic windows along the deformation zone, the Moldanubian Thrust. Three orogenic cycles in this area, the lowermost cycle represented by the Pan-African (Cadomian) Brunovistulian foreland terrane, the Variscan accretion wedge and the Alpine accretion wedge, influenced the

tectonic development. The lower crust in this area is characterized by high velocities with no distinct Moho interface. The high velocity gradient lower crust seems to be a characteristic feature of the Moravo-Silesian overthrust by the Moldanubian unit. Slightly different properties of the crust in the Moravian and Silesian units might be attributed to the variation in distance from the Moldanubian Thrust front as well as the different type of contact of the Brunia with the Moldanubian and its northern root sector and thus resulting in different degree of metamorphism and/or deformation during tectonic processes. The north-eastern termination of the high velocity lower crust in the Bohemian Massif could be seen as the termination of the Variscan collision tectonics on a crust/mantle level.

Lower velocities in the upper crust in the Fore-Sudetic Monocline represent the Lower Paleozoic metamorphic basement overlain by largely flat lying sedimentary rocks. The Moho in the Fore-Sudetic Monocline interpreted as a first-order discontinuity is in a sharp contrast with the high velocity lower crust of the Bohemian Massif. It might reflect different tectonic regime compared to the eastern Bohemian Massif. The deepening of the Moho towards the axial zone of the TESZ, the Mid-Polish Trough, to the depth of about 40 km is in agreement with other investigations of the TESZ as a transition zone between the Paleozoic Platform and the East European Craton.

References

Aichroth, B., Prodehl, C., Thybo, H., 1992. Crustal structure along the Central Segment of the EGT from seismic-refraction studies. Tectonophysics 207, 43–64.

Aki, K., Richards, P.G., 1980. Quantitative seismology, theory and methods. Columbia University.

Behm, M., Brückl, E., Chwatal, W., Tybo, H., 2007. Application of stacking and inversion techniques to three-dimensional wide-angle reflection and refraction seismic data of the Eastern Alps. Geophys. J. Int. 170 (1), 275–298. doi:10.1111/j.1365-246X.2007.03393.x.

Belka, Z., Ahrendt, H., Franke, W., Wemmer, K., 2000. The Baltica–Gondwana suture in central Europe: evidence from K-Ar ages of detrital muscovites and biogeographic data. In: Franke, W., Haak, V., Oncken, O., Tanner, D. (Eds.), Orogenic Processes: Quantification and Modelling in the Variscan Belt. Geol. Soc., London, Spec. Publ., vol. 179, pp. 87–102.

Belka, Z., Valverde-Vaquero, P., Ahrendt, H., Wemmer, K., Franke, W., Schäffer, J., 2002. Accretion of first Gondwana derived terranes at the margin of Baltica. In: Winchester, J.A., Pharaoh, T.C., Verniers, J. (Eds.), Paleozoic Amalgamation of Central Europe. Geol. Soc., London, Spec. Publ., vol. 201, pp. 19–36.

Beránek, B., Zátopek, A., 1981. Earth's crust structure in Czechoslovakia and Central Europe by methods of explosion seismology. In: Zátopek, A. (Ed.), Geophysical Synthesis in Czechoslovakia. Veda, Bratislava.

Beránek, B., Zounková, M., 1977. Investigations of the Earth's crust in Czechoslovakia using industrial blasting. Stud. Geophys. Geod. 21, 273–280.

Berthelsen, A., 1992. From Precambrian to Variscan Europe. In: Blundell, D.J., Freeman, R., Muller, S. (Eds.), A Continent Revealed—The European Geotraverse. Cambridge Univ. Press, New York, pp. 153–164.

Bielik, M., Šefara, J., Kováč, M., Bezák, V., Plašienka, D., 2004. The Western Carpathians—interaction of Hercynian and Alpine processes. Tectonophysics 393, 63–86.

Bleibinhaus, F., Gebrande, H., 2006. Crustal structure of the Eastern Alps along the TRANSALP profile from wide-angle seismic tomography. Tectonophysics 414 (1–4), 51–69. doi:10.1016/j.tecto.2005.10.028.

British Institutions Reflection Profiling Syndicate (BIRPS) and Étude Continentale et Océanique par Réflexion et Refraction (ECORS), 1986. Deep seismic reflection profiling between England, France and Ireland. J. Geol. Soc. London 143, 45–52.

Brückl, E., Bodoky, T., Hegedüs, E., Hrubcová, P., Gosar, A., Grad, M., Guterch, A., Hajnal, Z., Keller, G.R., Špičák, A., Sumanovac, F., Thybo, H., Weber, H., ALP 2002 Working Group, 2003. ALP 2002 seismic experiment. Stud. Geophys. Geod. 47, 671–679.

Brückl, E., Bleibinhaus, F., Gosar, A., Grad, M., Guterch, A., Hrubcová, P., Keller, G.R., Majdański, M., Sumanovac, F., Tiira, T., Yliniemi, J., Hegedus, E., Thybo, H., 2007. Crustal structure due to collisional and escape tectonics in the Eastern Alps region based on profiles Alp01 and Alp02 from the ALP 2002 seismic experiment. J. Geophys. Res. 112, B06308. doi:10.1029/2006JB004687.

Carbonell, R., Simancas, F., Juhlin, C., Pous, J., Pérez-Estaún, A., Gonzalez-Lodeiro, F., Muñoz, J., Heise, W., Ayarza, P., 2004. Geophysical evidence of a mantle derived intrusion in SW Iberia. Geophys. Res. Lett. 31, L11601. doi:10.1029/2004GL019684.

Červený, V., Pšenčík, I., 1984. SEIS83 — numerical modelling of seismic wave fields in 2-D laterally varying layered structures by the ray method. In: Engdal, E.R. (Ed.), Documentation of Earthquake Algorithms. Rep. SE-35, World Data Cent. A for Solid Earth Geophysics, Boulder, Colo. , pp. 36–40.

Christensen, N.I., Mooney, W.D., 1995. Seismic velocity structure and composition of the continental crust: a global view. J. Geophys. Res. 100, 9761–9877.

Cohen, J.K., Stockwell Jr., J.W., 1997. CWP/SU: Seismic Unix Release 30: a free package for seismic research and processing. Center for Wave Phenomena, Colorado School of Mines.

Dadlez, R., Grad, M., Guterch, A., 2005. Crustal structure below the Polish Basin: is it composed of proximal terranes derived from Baltica? Tectonophysics 411, 111–128.

Dallmeyer, R.D., Urban, M., 1994. Evolution of Variscan (Hercynian) and comparable Palaeozoic orogenic belts. J. Czech Geol. Soc. 39, 21–22.

Dallmeyer, D., Franke, W., Weber, K. (Eds.), 1995. Pre-Permian Geology of Central and Eastern Europe. Springer, New York.

Deutches Kontinentales Reflektionsseismisches Programm (DEKORP) Research Group, 1985. First results and preliminary interpretation of deep-reflection seismic recording along profile DEKORP 2-South. J. Geophys. 57, 137–165.

Deutches Kontinentales Reflektionsseismisches Programm (DEKORP) Research Group, 1988. Results of the DECORP 4/KTB Oberpfalz deep seismic reflection investigation. J. Geophys. 62, 69–101.

Dudek, A., 1980. The Crystalline Basement Block of the Outer Carpathians in Moravia-Brunovistulicum. Rozpravy Československé Akademie věd, Řada matematika-přírodní vědy, vol. 90, pp. 85–90.

Edel, J.B., Schulmann, K., Holub, F.V., 2003. Anticlockwise and clockwise rotations of the Eastern Variscides accommodated by dextral lithospheric wrenching: paleomagnetic and structural evidence. J. Geol. Soc. London 160, 209–218.

Finger, F., Hanzl, P., Pin, C., von Quadt, A., Steyrer, H.P., 2000. The Brunovistulian: Avalonian Precambrian sequence at the eastern end of the Central European Variscides? In: Franke, W., Haak, V., Oncken, O., Tanner, D. (Eds.), Orogenic Processes: Quantification and Modelling in the Variscan Belt. Geol. Soc., London, Spec. Publ., vol. 179, pp. 103–112.

Franke, W., 2006. The Variscan orogen in Central Europe: construction and collapse. Geol. Soc. London, Memoirs 32 (1), 333–343.

Franke, W., Żelaźniewicz, A., 2002. Structure and evolution of the Bohemian Arc. In: Winchester, J.A., Pharaoh, T.C., Verniers, J. (Eds.), Paleozoic Amalgamation of Central Europe. Geol. Soc., London, Spec. Publ., vol. 201, pp. 279–293.

Franke, W., Haak, V., Oncken, O., Tanner, D. (Eds.), 2000. Orogenic Processes: Quantification and Modelling in the Variscan Belt. Geol. Soc., London, Spec. Publ., vol. 179.

Fritz, H., Dallmeyer, R.D., Neubauer, F., 1996. Thick-skinned versus thin-skinned thrusting: rheology controlled thrust propagation in the Variscan collisional belt (the south-eastern Bohemian Massif, Czech Republic–Austria). Tectonics 15, 1389–1413.

Furlong, K.P., Fountain, D.M., 1986. Continental crustal underplating: thermal considerations and seismic–petrologic consequences. J. Geophys. Res. 91, 8285–8294.

Gee, D.G., Zeyen, H. (Eds.), 1996. EUROPROBE 1996 — Lithosphere Dynamics. Origin and Evolution of Continents. . EUROPROBE Secretariat. Uppsala University.

Giese, P., Prodehl, C., 1976. In: Giese, P., Prodehl, C., Stein, A. (Eds.), Main Features of Crustal Structures in the Alps, in Explosion Seismology in Central Europe. Springer, Berlin, pp. 347–363.

Grad, M., Keller, G.R., Thybo, H., Guterch, A., POLONAISE Working Group, 2002. Lower lithospheric structure beneath the Trans-European suture zone from POLONAISE'97 seismic profiles. Tectonpophysics 360, 153–168.

Grad, M., Jensen, S.L., Keller, G.R., Guterch, A., Thybo, H., Janik, T., Tiira, T., Yliniemi, J., Luosto, U., Motuza, G., Nasedkin, V., Czuba, W., Gaczyński, E., Šroda, P., Miller, K.C., Wilde- Piórko, M., Komminaho, K., Jacyna, J., Korabliova, L., 2003a. Crustal structure of the Trans- European suture zone region along POLONAISE'97 seismic profile P4. J. Geophys. Res. 108 (B11), 2541. doi:10.1029/2003JB002426.

Grad, M., Špičák, A., Keller, G.R., Guterch, A., Brol, M., Hegedfls, E., SUDETES Working Group, 2003b. SUDETES 2003 seismic experiment. Stud. Geophys. Geod. 47, 681–689. doi:10.1023/ A:1024732206210.

Grad, M., Guterch, A., Polkowska-Purys, A., 2005. Crustal structure of the Trans-European Suture Zone in Central Poland — reinterpretation of the LT-2, LT-4 and LT-5 deep seismic sounding profiles. Geol. Quart. 49 (3), 243–252.

Grad, M., Guterch, A., Keller, G.R., POLONAISE'97 and CELEBRATION 2000 Working Groups, 2007. Variations in lithospheric structure across the margin of Baltica in Central Europe and the role of the Variscan and Carpathian orogenies. In: Hatcher Jr., R.D., Carlson, M.E., McBride, J.H., Martinez Catalán, J.R. (Eds.), 4-D Framework of Continental Crust. Geological Society of America Memoir, vol. 200, pp. 341–356. doi:10.1130/2007.1200(17).

Grad, M., Guterch, A., Mazur, S., Keller, G.R., Špičák, A., Hrubcová, P., Geissler, W.H., SUDETES 2003 Working Group (in press), Lithospheric structure of the Bohemian Massif and adjacent Variscan belt in central Europe based on Profile S01 from the SUDETES 2003 experiment, J. Geophys. Res., doi: 2007JB005497RR.

Gruntorád, J., Lhotská, Z., 1973. Geophysical research into neovolcanic rocks of the Nízký Jeseník Mts. (in Czech). Geophysical Survey in the Jeseníky Mts. Charles University, Prague, pp. 56–74.

Grygar, R., Gnojek, I., Hubatka, F., Jelínek, J., 2002. Brunovistulian Terrane — synthesis of morphostructural analysis and geophysical data (Moravo-Silesian Area, Czech Republic). Geolines 14, 26–27.

Guterch, A., Grad, M., Materzok, R., Perchuć, E., 1986. Deep structure of the Earth's crust in the contact zone of the Palaeozoic and Precambrian Platforms in Poland (Tornquist–Teisseyre Zone). Tectonophysics 128, 251–279.

Guterch, A., Grad, M., Thybo, H., Keller, G.R., POLONAISE Working Group, 1999. POLONAISE'97 — international seismic experiment between Precambrian and Variscan Europe in Poland. Tectonpophysics 314, 101–121.

Guterch, A., Grad, M., Keller, G.R., Posgay, K., Vozár, J., Špičák, A., Brueckl, E., Hajnal, Z., Thybo, H., Selvi, O., CELEBRATION 2000 Experiment Team, 2003. CELEBRATION 2000 Seismic Experiment. Stud. Geophys. Geod. 47, 659–670.

Handy, M.R., Streit, J.E., 1999. Mechanics and mechanism of magmatic unerplating: inferences from mafic veins in deep crustal mylonite. Earth Planet. Sci. Lett. 165, 271–286.

Hole, J.A., 1992. Non-linear high-resolution three-dimensional seismic travel time tomography. J. Geophys. Res. 97, 6553–6562.

Hrubcová, P., Šroda, P., Špičák, A., Guterch, A., Grad, M., Keller, R., Brückl, E., Thybo, H., 2005. Crustal and uppermost mantle structure of the Bohemian Massif based on data from CELEBRATION 2000 experiment. J. Geophys. Res. 110, B11305. doi:10.1029/2004JB003080.

Hubatka, F., Švancara, J., 2002a. Geologicko-geofyzikální model zemské kůry v místě křížení profilů 8HR/85 a CEL10. Internal Report, Archive of the Geophysical Institute ASCR, in Czech. .

Hubatka, F., Švancara, J., 2002b. Geologicko-geofyzikální model zemské kůry v místě křížení profilů KII a CEL10. Internal Report, Archive of the Geophysical Institute ASCR, in Czech.

Humphreys, E., Clayton, R.W., 1988. Adaptation of backprojection tomography to seismic travel time problems. J. Geophys. Res. 93, 1073–1085.

Hurich, C.A., Deemer, S.J., Indares, A., Salisbury, M., 2001. Compositional and metamorphic controls on velocity and reflectivity in the continental crust: an example from the Grenville Province of eastern Québec. J. Geophys. Res. 106, 665–682.

Janik, T., Yliniemi, J., Grad, M., Thybo, H., Tiira, T., POLONAISE P2 Working Group, 2002. Crustal structure across the TESZ along POLONAISE'97 seismic profile P2 in NW Poland. Tectonophysics 360, 129–152.

Jensen, S.L., Janik, T., Thybo, H., POLONAISE'97 Working Group, 1999. Seismic structure of the Palaeozoic platform along POLONAISE'97 profile P1 in southwestern Poland. Tectonophysics 314, 123–143.

Komminaho, K., 1997. Software manual for programs MODEL and XRAYS — graphical interface for SEIS83 Program package. Rep. 20, 31, pp Dept. of Geophys., Univ. of Oulu, Oulu, Finland.

Krs, M., Krsová, M., Pruner, P., 1995. Paleomagnetism and paleogeography of Variscan formations of the Bohemian Massif: a comparison with other regions in Europe. Stud. Geophys. Geod. 39, 309–319.

Majdański, M., Grad, M., Guterch, A., SUDETES 2003 Working Group, 2006. 2-D seismic tomographic and ray tracing modelling of the crustal structure across the Sudetes Mountains basing on SUDETES 2003 experiment data. Tectonophysics 413, 249–269. doi:10.1016/j.tecto.2005.10.042.

Majdański, M., Kozlovskaya, E., Grad, M., SUDETES 2003 Working Group, 2007. 3D structure of the Earth's crust beneath the northern part of the Bohemian Massif. Tectonophysics 437, 17–36. doi:10.1016/j.tecto.2007.02.015.

Majerová, M., Novotný, M., (1986), Výzkum zemské kůry pomocí hlubinné sondáže. In: Geofyzikální model litosféry, eds. M. Blížkovský, MS Geofyzika n.p. Brno, GFÚ ČSAV Praha, GFÚ SAV Bratislava, in Czech.

Málek, J., Brož, M., Fischer, T., Horálek, J., Hrubcová, P., Janský, J., Novotný, O., Růžek, B., 2001. Seismic measurements along short profiles in western Bohemia during the Celebration 2000 experiment. Acta Mont., A 18 (121), 15–28.

Malinowski, M., Żelaźniewicz, A., Grad, M., Guterch, A., Janik, T., CELEBRATION Working Group, 2005. Seismic and geological structure of the crust in the transition from Baltica to Palaeozoic Europe in SE Poland — CELEBRATION 2000 experiment, profile CEL02. Tectonophysics 401, 55–77. doi:10.1016/j.tecto.2005.03.011.

Matte, P., 1986. Tectonics and plate tectonic model for the Variscan Belt of Europe. Tectonophysics 126, 329–374.

Matte, Ph., 1991. Accretionary history and crustal evolution of the Variscan belt in Western Europe. Tectonophysics 196, 309–337.

Matte, Ph., 2001. The Variscan collage and orogeny (480–290 Ma) and the tectonic definition of the Armorica microplate: a review. Terra Nova 13, 122–128.

Matte, Ph., Maluski, H., Rajlich, P., Franke, W., 1990. Terrane boundaries in the Bohemian Massif: Result of large-scale Variscan shearing. Tectonophysics 177, 151–170.

Mazur, S., Alexandrowski, P., Krysza, R., Oberc-Dziedzicz, T., 2006. The Variscan Orogen in Poland. Geol. Quart. 50 (1), 89–118.

Morozov, I.B., Smithson, S.B., Chen, J., Hollister, L.S., 2001. Generation of new continental crust and terrane accretion in Southeastern Alaska and Western British Columbia: constraints from P- and S-wave wide-angle seismic data (ACCRETE). Tectonophysics 341, 49–67.

Mueller, H.J., 1995. . Modelling of the lower crust by simulation of the in situ conditions: an example from Saxonian Erzgebirge. Phys. Earth Planet. Inter. 92, 3–15.

Oliver, G.J.H., Corfu, F., Krogh, T.E., 1993. U-Pb ages from SW Poland: evidence for a Caledonian suture zone between Baltica and Gondwana. J. Geol. Soc. London 150, 355–369.

Onken, O., Plesh, A., Weber, J., Ricken, W., Schrader, S., 2000. Passive margin detachment during arc–continent collision (central European Variscides). In: Franke, W., et al. (Ed.), Orogenic Processes: Quantification and Modelling in the Variscan Belt. Geol. Soc. Spec. Publ., vol. 179, pp. 9–20.

Plomerová, J., Babuška, V., Ruprechtová, L., 1984. Velocities of seismic waves propagating through the Bohemian Massif from foci in Poland. Stud. Geophys. Geod. 28, 56–66.

Reinecker, J., Lenhardt, W., 1999. Present-day stress field and deformation in eastern Austria. Int. J. Earth Sci. 88, 532–550.

Růžek, B., Vavryčuk, V., Hrubcová, P., Zedník, J., CELEBRATION Working Group, 2003. Crustal anisotropy in the Bohemian Massif, Czech Republic: observations based on the Central European Lithospheric Experiment Based on Refraction (CELEBRATION) 2000. J. Geophys. Res. 108 (B8), 2392. doi:10.1029/2002JB002242.

Schulmann, K., Gayer, R., 2000. A model for a continental accretionary wedge developed by oblique collision: the NE Bohemian Massif. J. Geol. Soc. London 157, 401–416.

Schulmann, K., Kröner, A., Hegner, E., Wendt, I., Konopásek, J., Lexa, O., Štipská, P., 2005. Chronological constraints on the pre-orogenic history, burial and exhumation of deep- seated rocks along the Eastern Margin of the Variscan Orogen, Bohemian Massif, Czech Republic. Am. J. Sci. 305, 407–448.

Schulmann, K., Lexa, O., Štípská, P., Racek, M., Tajčmanová, L., Konopásek, J., Edel, J.B., Peschler, A., Lehmann, J., 2008. Vertical extrusion and horizontal channel flow of orogenic lower crust: key exhumation mechanisms in large hot orogens? J. Metamorph. Geol. 26, 273–297. doi:10.1111/j.1525- 1314.2007.00755.x.

Simancas, J.F., Carbonell, R., González Lodeiro, F., Pérez Estaún, A., Juhlin, C., Ayarza, P., Kashubin, A., Azor, A., Martínez Poyatos, D., Almodóvar, G.R., Pascual, E., Sáez, R., Expósito, I., 2003. Crustal structure of the transpressional Variscan orogen of SW Iberia: SW Iberia deep seismic reflection profile (IBERSEIS). Tectonics 22 (6), 1062. doi:10.1029/2002TC001479.

Špaček, P., Sýkorová, Z., Pazdírková, J., Švancara, J., Havíř, J., 2006. Present-day seismicity of the south-eastern Elbe Fault System (NE Bohemian Massif). Stud. Geophys. Geod. 50, 233–258.

Środa, P., Czuba, W., Grad, M., Guterch, A., Tokarski, A.K., Janik, T., Rauch, M., Keller, G.R., Hegedüs, E., Vozár, J., CELEBRATION 2000 Working Group, 2006. Crustal and upper mantle structure of the Western Carpathians from CELEBRATION 2000 profiles CEL01 and CEL04: seismic models and geological implications. Geophys. J. Int. 167, 737–760. doi:10.1111/j.1365-246X.2006.03104.x.

Tait, J.A., Schätz, M., Bachtadse, V., Soffel, H., 2000. Palaeomagnetism and Paleozoic palaeogeography of Gondwana and European terranes. In: Franke, W., Haak, V., Oncken, O., Tanner, D. (Eds.), Orogenic Processes: Quantification and Modelling in the Variscan Belt. Geol. Soc. Spec. Publ., vol. 179, pp. 21–34.

Thybo, H., Janik, T., Omelchenko, V.D., Grad, M., Garetsky, R.G., Belinsky, A.A., Karatayev, G.I., Zlotski, G., Knudsen, M.E., Sand, R., Yliniemi, J., Tiira, T., Luosto, U., Komminaho, K., Giese, R., Guterch, A., Lund, C.E., Kharitonov I, O.M., Ilchenko, T., Lysynchuk, D.V., Skobelev, V.M., Doody, J.J., 2003. Upper lithospheric seismic velocity structure across the Pripyat Trough and the Ukrainian Shield along the EUROBRIDGE'97 profile. Tectonophysics 371, 41–79.

Vavryčuk, V., Hrubcová, P., Brož, M., Málek, J., ALP 2002 Working Group, 2004. Azimuthal variation of Pg velocity in the Moldanubian, Czech Republic: observations based on a multi-azimuthal common-shot experiment. Tectonophysics 387/ 1–4, 189–203. doi:10.1016/j.tecto.2004.06.015.

Vidale, J.E., 1990. Finite-difference calculation of travel times in three dimensions. Geophysics 55, 521–526.

Wessel, H., Smith, W.H.F., 1995. New version of Generic Mapping Tools released. Eos Trans. AGU 76, 329.

Wilde-Piórko, M., Saul, J., Grad, M., 2005. Differences in the crustal and uppermost mantle structure of the Bohemian Massif from teleseismic receiver functions. Stud. Geophys. Geod. 49, 85–107.

Winchester, J.A., Pharaoh, T.C., Verniers, J., 2002. Paleozoic Amalgamation of Central Europe. J. Geol. Soc. London, Spec. Publ., vol. 201.

Winchester, J.A., Pharaoh, T.C., Verniers, J., Ioane, D., Seghedi, A., 2006. Palaeozoic accretion of Gondwana-derived terranes to the East European Craton: recognition of detached terrane fragments dispersed after collision with promontories. J. Geol. Soc. London, Memoirs 32 (1), 323–332.

Zelt, C.A., 1994. ZPLOT — an interactive plotting and picking program for seismic data. Bullard Lab. Univ. of Cambridge, Cambridge UK.

P3

Hrubcová, P., and W.H. Geissler

**The Crust-Mantle Transition and the Moho beneath the Vogtland/West Bohemian
Region in the Light of Different Seismic Methods**

THE CRUST-MANTLE TRANSITION AND THE MOHO BENEATH THE VOGTLAND/WEST BOHEMIAN REGION IN THE LIGHT OF DIFFERENT SEISMIC METHODS

PAVLA HRUBCOVÁ[1] AND WOLFRAM H. GEISSLER[2]

1   Institute of Geophysics, Acad. Sci. Czech Republic, Boční II/1401, 141 31 Praha 4, Czech Republic (pavla@ig.cas.cz)

2   Alfred Wegener Institute for Polar and Marine Research, Columbusstrasse, 27568 Bremerhaven, Germany (wolfram.geissler@awi.de)

ABSTRACT

The structure of the crust and the crust-mantle boundary in the Vogtland/West Bohemian region have been a target of several seismic measurements for the last 25 years, beginning with the steep-angle reflection seismic studies (DEKORP-4/KTB, MVE-90, 9HR), the refraction and wide-angle experiments (GRANU'95, CELEBRATION 2000, SUDETES 2003), and followed by passive seismic studies (receiver functions, teleseismic tomography). The steep-angle reflection studies imaged a highly reflective lower crust (4 to 6 km thick) with the Moho interpreted in a depth between 30 and 32 km and a thinner crust beneath the Eger Rift. The refraction and wide-angle reflection seismic studies (CELEBRATION 2000) revealed strong wide-angle reflections in a depth of 26−28 km interpreted as the top of the lower crust. Long coda of these reflections indicates strong reflectivity in the lower crustal layer, a phenomenon frequently observed in the Caledonian and Variscan areas. The receiver function studies detected one strong conversion from the base of the crust interpreted as the Moho discontinuity at a depth between 27 and 37 km (average at about 31 km). The discrepancies in the Moho depth determination could be partly attributed to different background of the methods and their resolution, but could not fully explain them. So that new receivers function modelling was provided. It revealed that, instead of a first-order Moho discontinuity, the observations can be explained with a lower crustal layer or a crust-mantle transition zone with a maximum thickness of 5 km. The consequent synthetic ray-tracing modelling resulted in the model with the top of the lower crust at 28 km, where highly reflective lower crustal layer can obscure the Moho reflection at a depth of 32−33 km.

Key words: Bohemian Massif, Vogtland/West Bohemia, crustal structure, Moho, refraction and wide-angle reflection, receiver function, seismic methods, Eger Rift

1. INTRODUCTION

The crust-mantle boundary, the Moho (*Mohorovičić, 1910*), has been a major target for the Earth scientists for the last one hundred years, since its first observation from an

earthquake in 1909. Since then, our knowledge of this prominent boundary has improved. From seismic reflection profiling the crust-mantle transition can be divided into three categories: no distinct reflections at the Moho level, one or more sub-horizontal reflections, and reflections that project from the crust into the mantle (*Cook, 2002*). On the other hand, the reflection Moho can differ from the crust-mantle boundary obtained by other geophysical surveying. In petrologic conception, the Moho can be attributed either to changes in the bulk chemical composition or to the transition in mineral phases (*Mengel and Kern, 1991*). It is clear that various methods sample this boundary in a different way, measure different physical properties and have different spatial resolution (e.g. *Hammer and Clowes, 1997*). Thus some elements of the Moho obtained by several methods are not seen, as well as contrasting definitions may lead to different understanding of this prominent boundary.

This is just the case for the Vogtland/West Bohemian region in the western part of the Bohemian Massif. The area is situated in the transition between different Variscan structural units: the Saxothuringian zone in the northwest, the Teplá-Barrandian and Moldanubian zones in the southeast (see Fig. 1). The whole region was affected by the Permo-Carboniferous post-orogenic extension as well as the alkaline magmatism during the Cenozoic evolution of the Eger Rift. This geodynamically active zone belongs to the European Cenozoic Rift System (*Prodehl et al., 1995*). The most recent expressions of the geodynamic activity are represented by the widespread CO_2 emanations and Quaternary volcanism (*Bräuer et al., 2005a,b*). It is also a region of a frequent occurrence of seismic activity manifested by the intraplate earthquake swarms with magnitudes up to 4.6 (*Horálek et al., 1996, 2000*; *Fischer and Michálek, 2008*). *Fischer and Horálek (2003)* locate the hypocenters of these swarms to the upper and middle crust down to about 20 km depth with the majority between 5 and 15 km.

Geographically it is a border region between Saxony, Bavaria and Bohemia and its deep structure was a target of several deep seismic measurements in the last 25 years, beginning with the steep-angle reflection seismic studies as DEKORP-4/KTB, MVE-90, 9HR (*DEKORP Res. Group, 1988*; *Behr et al., 1994*; *DEKORP and Orogenic Processes Working Groups, 1999*; *Tomek et al., 1997*) as well as the refraction and wide-angle reflection experiments as GRANU'95 (*Enderle et al., 1998*), CELEBRATION 2000 with CEL09 profile (*Hrubcová et al., 2005*) or SUDETES 2003 with S01 profile (*Grad et al., 2008*). Passive seismic experiments with permanent and temporary seismic stations were carried out to study the major lithospheric discontinuities using the receiver function method (*Geissler et al., 2005*; *Wilde-Piórko et al., 2005*; *Heuer et al., 2006*). Different seismic methods, namely the receiver function and the refraction and wide-angle reflection measurements, sampled the crust-mantle boundary, which resulted in the interpretation of the depth and nature of this major discontinuity with respect to the method applied. The aim of this study is to summarize the existing seismic results and discuss them in the light of the theoretical and methodological constraints of the methods together with their resolution. Synthetic modelling of both methods was performed with the aim to find some indicators for joint interpretation.
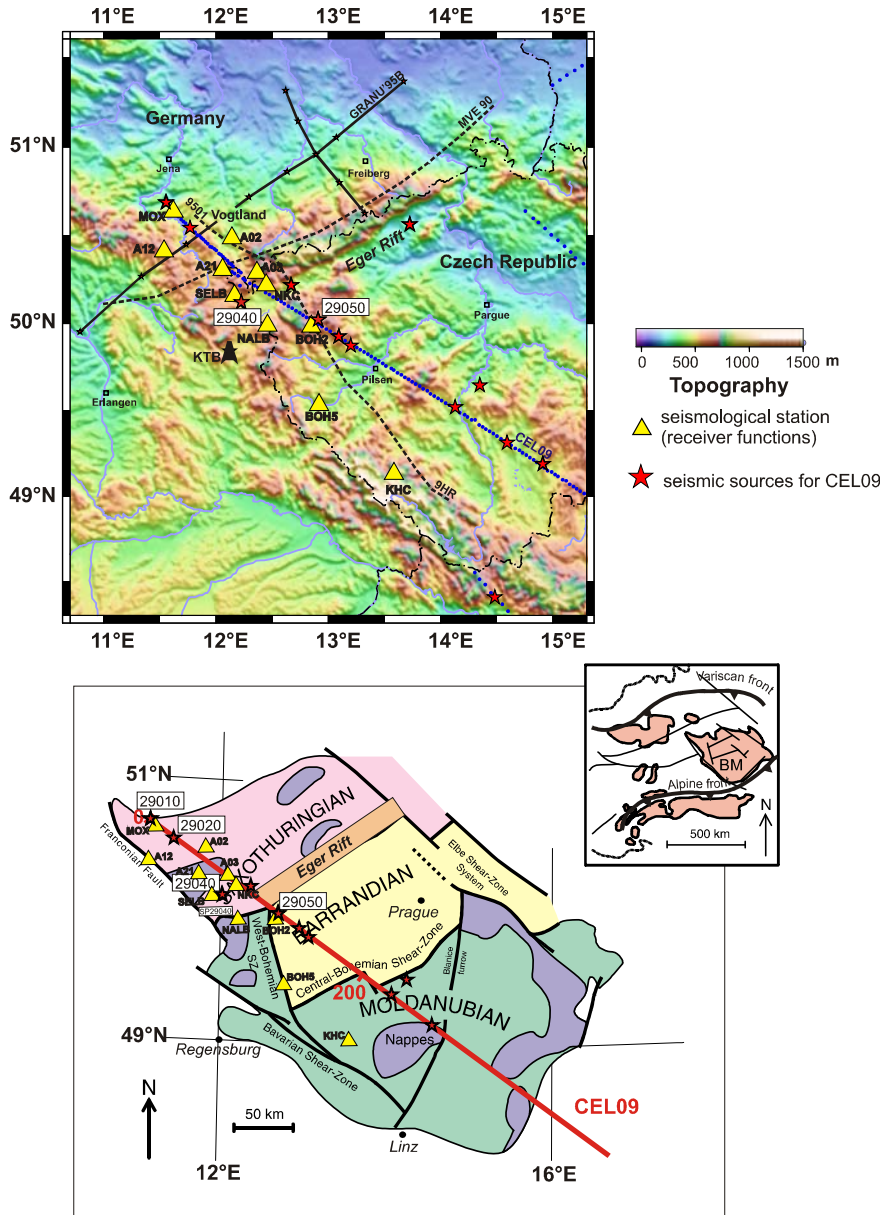
Fig. 1. Topographic and tectonostratigraphic maps of the study area with the location of seismic profiles and seismological stations (yellow triangles). Red stars represent shot points for CEL09 profile. BM, Bohemian Massif (after *Pitra et al., 1999*; *Franke et al., 2000*).

2. GEOPHYSICAL INVESTIGATION
IN THE VOGTLAND/WEST BOHEMIAN AREA

2.1. Refraction and Reflection Studies

The crustal and uppermost mantle velocity structure in the western part of the Bohemian Massif can be inferred from the interpretation of seismic data along the refraction and wide-angle reflection profile CEL09 of the CELEBRATION 2000 experiment (*Guterch et al., 2003*; *Hrubcová et al., 2005*). This profile traverses the Bohemian Massif in the NW-SE direction and was interpreted by trial-and-error forward modelling using a ray-tracing algorithm (*Červený and Pšenčík, 1984*). In this modelling approach, the P-wave velocity distribution was derived using not only first arrivals, but also further phases, i.e. reflected waves and available refractions in later arrivals. The modelling was enhanced by the calculation of synthetic sections and qualitative comparison of the amplitudes of the synthetic and observed seismograms. Since the amplitudes of seismic waves are very sensitive to the velocity gradients and the velocity contrasts at the discontinuities, synthetic seismograms of both reflected and refracted seismic waves can give an additional constraint on the velocity distribution.

The ray-tracing velocity studies of the CEL09 profile in the NW part of the Bohemian Massif (*Hrubcová et al., 2005*) revealed a lower crustal layer with a velocity gradient from 6.9 to 7.5 km s^{-1} above the Moho (Fig. 2). Strong reflection from the top of this layer in a depth of 26−28 km was not attributed to the Moho discontinuity though this reflection was the strongest reflected phase in the NW part of the CEL09 profile and based on its amplitude and shape it might have been interpreted as a reflection from the Moho (PmP phase). But as discussed in *Hrubcová et al. (2005)*, the arrival time of the observed refraction from the upper mantle (Pn phase) did not fit the critical point of the mentioned reflected phase as it should fit in case of refraction and reflection from the same discontinuity (Fig. 2). The Pn mantle refraction occurred 1 s later and did not fit a strong reflection from the top of the lower crust. Moreover, this strong reflection masked a relatively weak PmP Moho reflection arriving later. The character of the reflection from the top of the lower crust showed long and irregular coda, which indicated that the lower crustal layer was highly reflective probably due to a presence of thin layers of the material with contrasting seismic velocities.

The differences in amplitudes and coda length of the reflected phases along the CEL09 profile that were not possible to analyze by the ray-tracing modelling were also studied by the reflectivity method (*Fuchs and Müller, 1971*). The idea was to simulate a variability of the lower crust and the Moho reflections assuming a 1-D seismic velocity-depth structure and especially to test the existence of laminated layers with alternating high and low velocities at the lower crustal level. Section 29040 in Fig. 3 (according to *Hrubcová et al., 2005*) displays a high amplitude reflection from the top of the lower crust, with a long coda suggesting strong reflectivity of the lower crustal layer in the Saxothuringian zone. The coda obscures a relatively weak PmP phase as a reflection from the Moho. The Pn mantle refraction is weak, but observable. The proposed 1-D velocity model explains it by the existence of the lower crustal layer with a background *Vp* velocity of 6.9−7.3 km s^{-1},
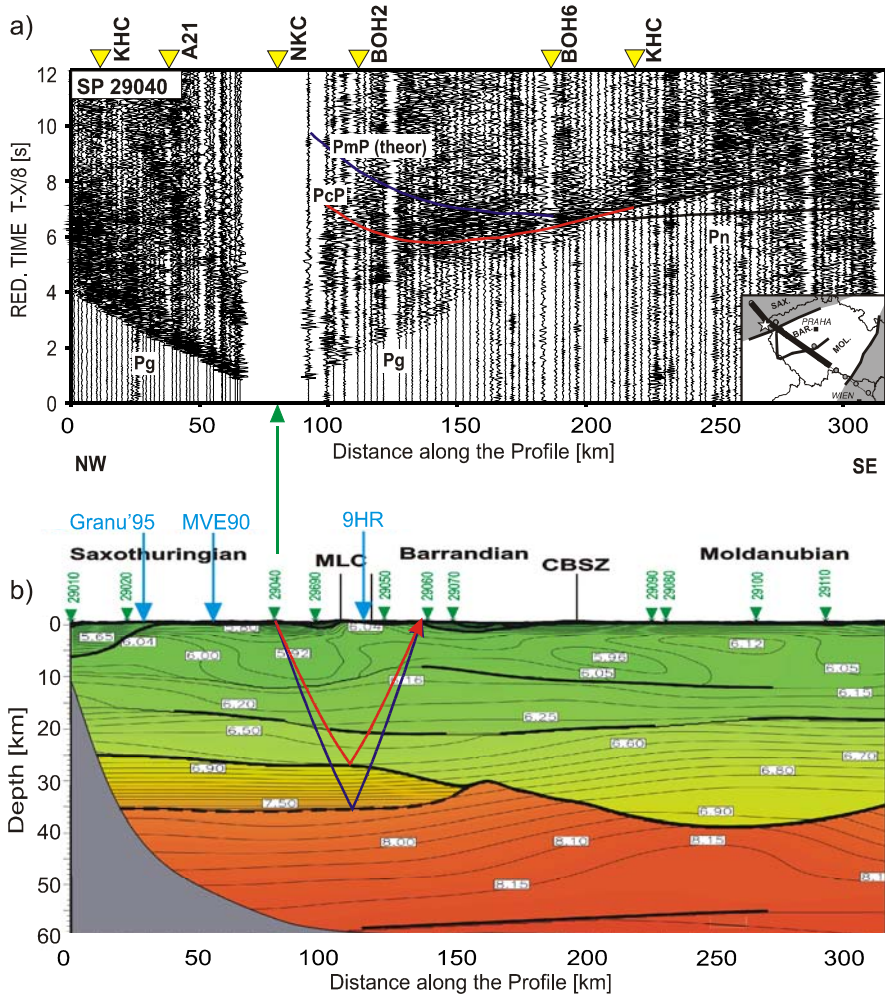
Fig. 2. **a)** Amplitude-normalized vertical-component seismic section of the shot point 29040 in the Saxothuringian with calculated travel times. Strong PcP (reflection from the lower crust) with long coda masks PmP (theor) phase (a theoretical reflection from the Moho) that is not visible in the data. The Pg and Pn are refractions from the crust and mantle, respectively (after *Hrubcová et al.*, *2005*). Yellow triangles show projections of broad-band stations indicated on the top. Sax., Saxothuringian; Bar., Barrandian; Mold., Moldanubian. **b)** The 2-D model of P-wave velocity along the CEL09 profile developed by forward ray-tracing modelling. Bold lines mark boundaries constrained by the reflections and well constrained interfaces; dashed bold lines mark layer boundaries where no reflections were observed. Thin lines represent velocity isolines spaced at intervals of 0.05 km s^{-1}. Triangles show projections of the shot points. Arrows show locations of the other refraction and reflection profiles. Red arrow represents ray reflected from the top of the lower crust; dark blue arrow represents theoretical ray reflected from the bottom of the lower crust. MLC, Mariánské Lázně Complex; CBSZ, Central Bohemian Shear Zone. Vertical exaggeration is 1:2.
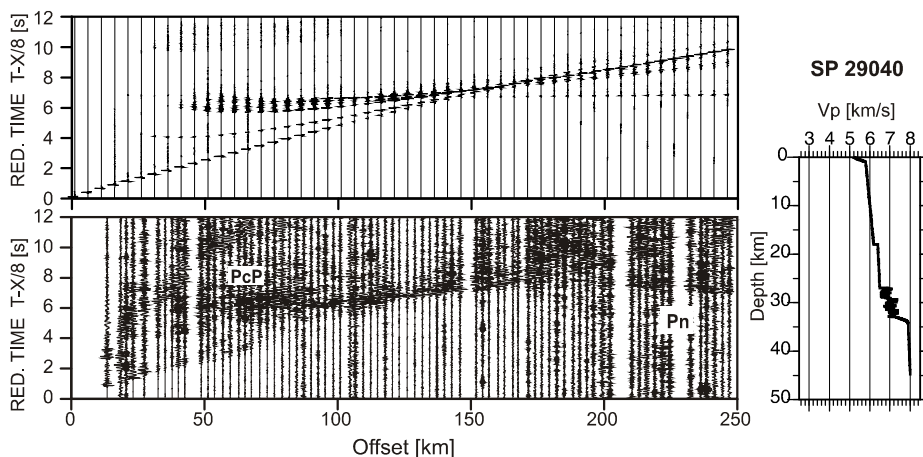
Fig. 3. Modelling of the lower crust and the Moho using the reflectivity method (*Fuchs and Müller, 1971*) for the SP 29040 along the CEL09 profile of the CELEBRATION 2000 experiment. Top - synthetic reflectivity seismogram, bottom - seismic data, right - 1-D velocity model. The synthetic and seismic data sections show amplitude-normalized vertical component plotted with the reduction velocity of 8.0 km s^{-1}. Data have been band-pass filtered by 2–15 Hz. Strong reflections form the top of the lower crust (PcP phase) and from the laminated lower crust with the coda masking the reflections from the Moho (PmP phase is not visible), weak refraction from the mantle (Pn phase) (according to *Hrubcová et al., 2005*).

consisting of layers of randomly alternating high and low velocities with a standard deviation of 4% and correlation length of 300 m. Moho was interpreted as a 1 km thick gradient zone at a depth of 33 km with velocities increasing gradually from 7.3 to 7.9 km s^{-1}, which produced a refracted phase weak enough to fit the data.

Similar results were reported by the wide-angle refraction and reflection profile GRANU'95 and the reflection profile MVE-90. Being perpendicular to the CEL09 profile, they imaged a highly reflective lower crust with a thickness of 4 to 6 km and with an uppermost mantle more or less without reflections. The Moho was interpreted at 10 s of the two-way travel time, which corresponds to a depth from 30 to 32 km, where strong reflectivity dies out. The GRANU'95 results indicate the existence of a high-velocity layer at the base of the crust in the Saxothuringian zone in SE Germany with a velocity increase from 6.5 km s^{-1} in the middle crust to an average value of 7.0 km s^{-1} at a depth of 24 km interpreted as the top of the lower crust (*Enderle et al., 1998*). The MVE-90 profile shows a highly reflective layer in this area at 8–10 s two-way travel time (Fig. 4) corresponding to a depth range of 24–32 km (*DEKORP Research Group, 1994*), which may be viewed as the laminated lower crust. Average P wave velocities in the lower crust and the upper mantle along the CEL09 profile (7.1 and 7.9 km s^{-1}, respectively) are consistent with the velocities along the GRANU'95 and MVE-90 profiles (7.0 and 7.9–8.1 km s^{-1}, respectively). However, the CEL09 crustal thickness of 34 km is slightly bigger than in case of GRANU'95 and MVE-90 where they interpreted the thickness of 30

and 33 km, respectively. The seismic reflection profile 9HR (*Tomek et al., 1997*) indicated a thinner crust of about 29 km with the Moho at 9.2 s the two-way travel time beneath the Eger Rift deepening towards SE and imaged reflectors in the uppermost mantle beneath the rift axis (Fig. 5).

2 . 2 . R e c e i v e r F u n c t i o n S t u d i e s

The receiver function analysis is based on teleseismic recordings of the three-component broad-band seismological stations and show the relative response of the Earth's structure near the receiver (e.g., *Vinnik, 1977*; *Kind et al., 1995*; *Yuan et al., 1997*; *Geissler et al., 2008*). Seismic phases converted from P-to-S (Ps conversions) at discontinuities underneath the receiver are particularly useful for studying seismic structure of the lithospheric discontinuities (Fig. 6). The strongest P-to-S conversions with positive polarity (indicating a velocity increase with depth) are often attributed to the Moho discontinuity that is usually the sharpest seismic velocity contrast near the crust-mantle boundary. The delay time of these P-to-S converted phases in relation to the

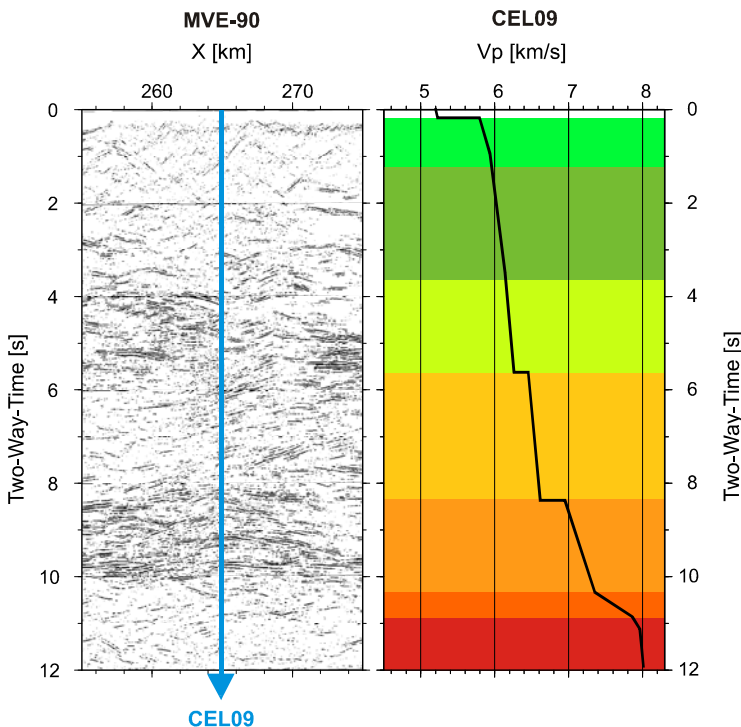**Fig. 4.**   Comparison of the reflections along the seismic reflection profile MVE-90 (*DEKORP Research Group, 1994*) with the 1-D velocity model from the refraction and wide-angle reflection profile CEL09 (converted to two-way travel time) at the crossing point. Note band of reflectors between 8.2 s and 10 s of two-way travel time at the MVE-90 profile corresponding to the high gradient lower crust in the CEL09 profile.
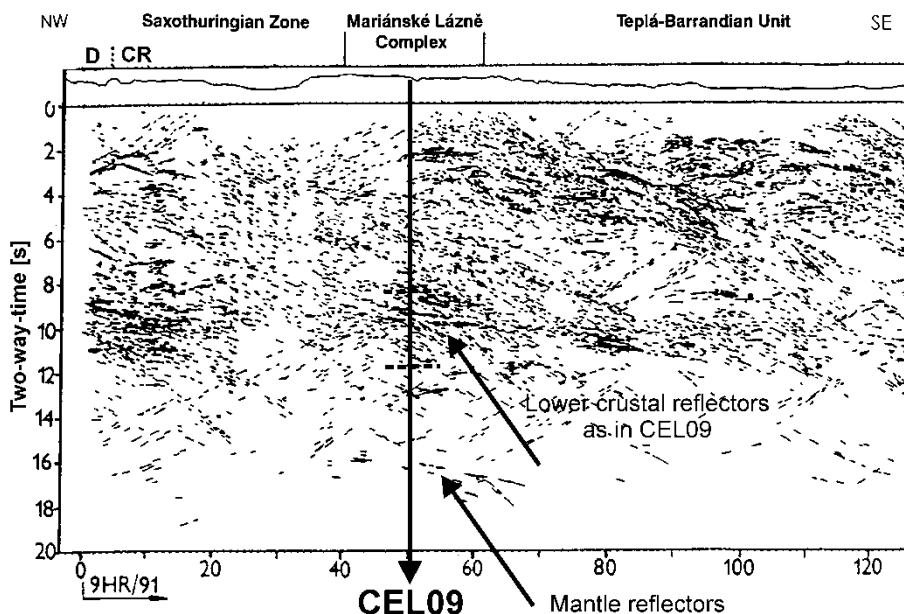
Fig. 5. The reflection seismic profile 9HR (*Tomek et al., 1997*). Note the crossing point with the refraction and wide-angle seismic profile CEL09 and interpreted lower crust.

P waves depends on the depth of the discontinuities and the S wave velocities above them. Their amplitudes depend on the contrast of seismic velocities, densities, and the incidence angle of the impinging P wave.

If a velocity model of the crust is known, the crustal thickness can be calculated from the measured delay times of the Moho P-to-S conversion. However, the crustal thickness estimated only from the delay time of the Moho P-to-S converted phase trades off strongly with the crustal *Vp/Vs* ratio. The ambiguity can be reduced significantly by incorporating the later multiple converted phases, namely, the PpPs and PpSs and PsPs (Fig. 6, see *Geissler et al., 2005* for references).

To separate different types of waves the receiver function studies start with a rotation from the *Z*, N-S and E-W (*ZNE*) components into the P, SV, and SH system (the *LQT* components). For the rotation of the horizontal components, theoretical values of back azimuths are used. The angles of incidence are determined by minimizing the energy on the SV component (*Q*) at a time of the P signal. A time-domain deconvolution method is used to remove the source signal and source-side reverberations from the records in order to allow records from different events to be stacked. The amplitudes of the SV and SH components are normalized in relation to the incident P wave. The arrival times of converted phases are measured as a relative travel time, where zero is the equivalent to the P wave onset. For moveout correction, the IASP91 Earth reference model (*Kennett and Engdahl, 1991*) is used to reduce the time scale of records at any distance to the fixed reference epicentral distance of 67° (slowness: 6.4 s per degree).

The receiver function studies in the Vogtland/West Bohemian region observe converted phases from the base of the crust at about 3.7 s after the P wave onset (Fig. 7, see also *Geissler et al., 2005*; *Heuer et al., 2006*). Multiple conversions follow at about 13 s (positive, PpPs conversion) and 16 s (negative, PpSs and PsPs conversions). The depth to a discontinuity can be estimated from the P-to-S delay times assuming a constant average crustal velocity Vp of 6.3 km s^{-1} and Vp/Vs ratio of 1.73 (*Geissler et al., 2005*; *Heuer et al., 2006*) by multiplying the delay times by a factor of 8.3. Observed delay times of about 3.7 s for the primary P-to-S conversions indicate the depth of this discontinuity at about 31 km. Underneath the western part of the Eger Rift, the delay time of only 3.0−3.3 s indicate the thinning of the crust to about 27 km. As could be shown by *Heuer et al. (2006)* with a dense seismic network, this area of interpreted Moho updoming is restricted to the Cheb basin at the Eger Rift axis and its southwards continuation. Later converted P-to-S arrivals of about 4.3−4.5 s are observed at the stations in the SE part of the Vogtland/West Bohemian region, which suggests the deepening of the Moho in this area to about 36−37 km (station KHC; see *Geissler et al., 2005*).

As was shown by *Geissler et al. (2005)* the primary and multiple Moho conversions observed in the study area could be modelled assuming a rather simple crust-mantle transition with a first-order Moho discontinuity or with a thin gradient zone between the crust and upper mantle. Pronounced lower crustal high-velocity layers seemed not to be adequate to explain the observed waveforms.
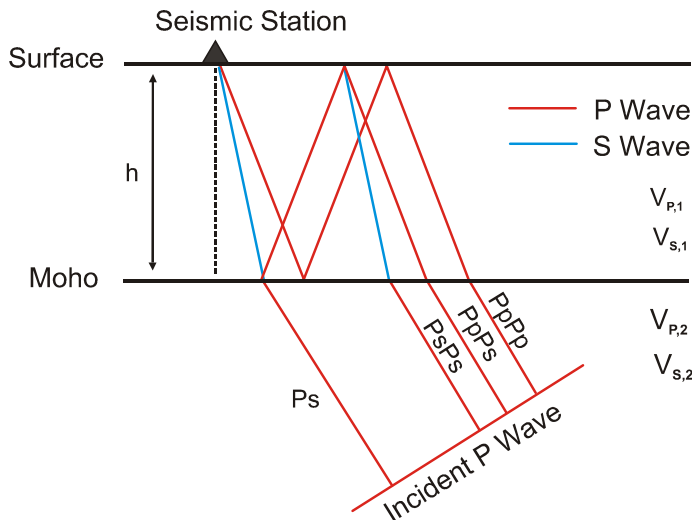

Fig. 6. Schematic model for the receiver function with a horizontal layer at a depth of the Moho over a half space. Plane P wave is incident upon the Moho from below and generates P-to-S converted waves (Ps) and many reverberations between the free surface and the Moho (e.g. PpPp, PpPs, PsPs).
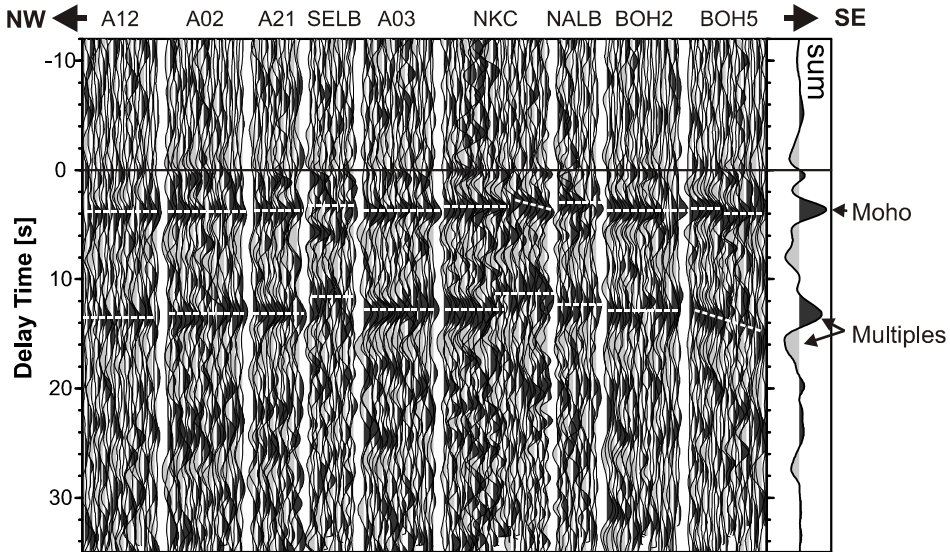
Fig. 7. Single receiver functions for individual broadband seismic stations located close to the CEL09 seismic profile and sorted by backazimuth for each station starting from N (left trace) clockwise. Primary and multiple Moho conversions are indicated. The Moho is observed at about 3.0 to 3.7 s with respect to the arrival time of the teleseismic P wave (indicated as zero), which corresponds to the Moho depths ranging from 27 to 31 km. The differences in the Moho Ps delay times can hardly be seen in the primary conversions (with the exception of stations SELB, NALB and partly NKC; upper dashed lines), but they are obvious from the multiple phases (as indicated for the PpPs phase by lower dashed lines).

2.3. Synthetic Tests for the Receiver Functions

Based on the existing results for Vogtland/West Bohemia, the Moho determination indicated by the active and passive seismic methods show differences in the depth as well as in the character of the transition from the crust to the mantle. To evaluate these differences, first of all we studied the synthetic receiver functions. We extracted 1-D velocity profiles each 10 km along the CEL09 ray-tracing model and calculated their synthetic receiver function response following the plane wave approximation approach of *Kind et al. (1995)*. For such calculation, we assumed a *Vp/Vs* ratio of 1.73 for the upper and middle crust, 1.76 for the lower crust, and 1.79 for the mantle. Then we compared these synthetics with the observed receiver functions (Fig. 8). The first 8 seconds delay time showed more or less good fit with the exception for the amplitudes of the strongest conversion. The observed converted phases showed higher amplitudes than the calculated synthetics, which would indicate a stronger velocity increase at the crust-mantle transition than originally modelled by the CEL09 ray tracing. Another and even bigger discrepancy exists in the amplitudes and delay times of the multiple phases (Fig. 8), where the receiver function data do not fit the synthetics calculated from the CEL09 velocity profile. A prominent feature in the synthetic receiver functions is related to the modelled
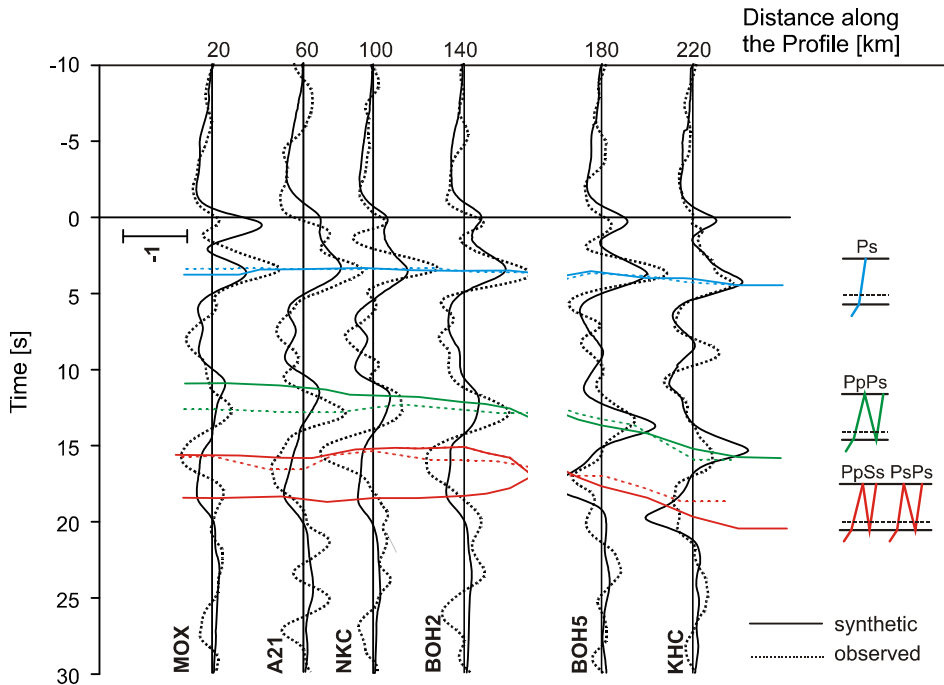
Fig. 8. Comparison of the observed receiver functions (dotted black lines) with the synthetic response of 1-D velocity models extracted from the CEL09 profile (solid black lines) at places close to the stations for the receiver functions. Scale shown corresponds to 10% of the amplitude of the primary P signal. Blue lines mark primary P-to-S conversions from the Moho, green lines are PpPs multiples, red lines represent PpSs and PsPs multiples (for each colour, the dotted lines indicate the observed data, solid lines the responses from the CEL09 model). Note that the responses from the discontinuities at the top and bottom of the CEL09 model almost coincide with the observed data in primary P-to-S conversions (blue lines), but do not coincide for the PpPs multiples (green lines) and even split for PpSs and PsPs multiples (red lines).

discontinuities on the top and at the bottom of the lower crustal layer. For the primary P-to-S conversions the receiver function responses from these two discontinuities almost coincide (Figure 8, blue lines). But they do not coincide for the PpPs multiples (Fig. 8, green lines) and even split for PpSs and PsPs multiples (Fig. 8, red lines). This can be explained in a way that there are interfering multiples from the top and bottom of the lower crustal layer. Looking at the amplitudes, the PpPs multiples seems to be more influenced by the velocity contrast on top of the lower crust whereas the PpSs and PsPs multiples seem to be more influenced by the bottom of the lower crustal layer.

Since we were not able to get a reasonable fit of the receiver function data with the response from the original CEL09 ray-tracing model, we started to alternate the velocity structure. As a reference we look at the station A03 situated at a distance of 70 km along the CEL09 profile. The station A03 showed relatively simple and coherent receiver functions in contrast to some nearby stations (e.g. NKC, Figs. 7 and 8). The upper and

middle crustal velocities were fixed to the CEL09 model. We only changed the lower crustal velocity structure to find better fit with the observed receiver functions. The original CEL09 model converted to S-wave velocity produced reasonable fit in the travel time of the primary conversion but there was no agreement in the amplitudes nor in travel times for the multiples (Fig. 9a, violet line). A model with the first-order Moho discontinuity at a depth of 30 km revealed too strong multiple phases (Fig. 9b, black line). Generally, strong multiples can be reduced by changing the density structure and/or introducing velocity gradient zones. Since we did not have good further constraints to change densities, we tried to get a better fit with further changes of the velocity structure. The best fit in the travel times and amplitudes showed the model with a discontinuity on the top of a velocity gradient zone at the base of the crust (Fig. 9c, orange line). A very good fit was also achieved for the model with a thin lower crustal layer between a depth of 26 and 30 km and a thin Moho transition layer at a depth from 30 to 32 km (Fig. 9d, blue line).
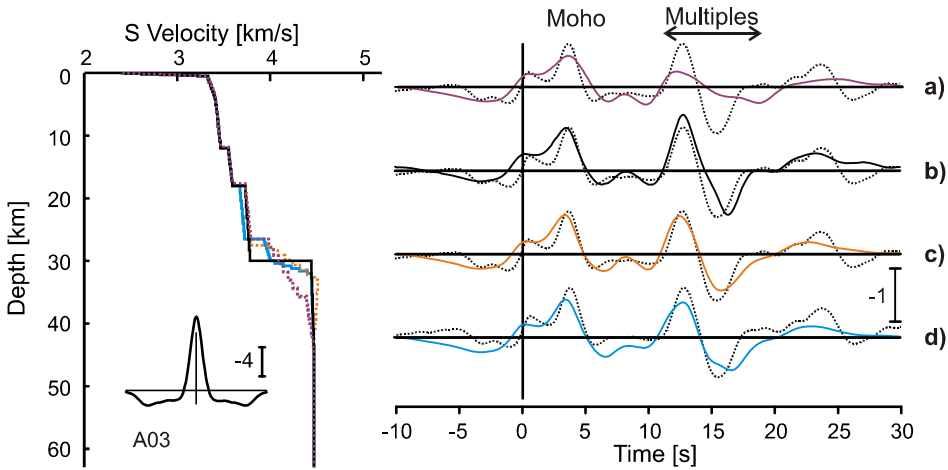

Fig. 9. Receiver functions calculated for different 1-D velocity models using the plane wave method (after *Kind et al.*, *1995*). The arrival time of teleseismic P wave is indicated as zero. A03 represents a form of the initial pulse. Dotted lines show the summed receiver functions for the reference station A03. Coloured lines show the receiver function response of the different velocity models. The upper and middle crustal velocities are the same for all models and are close to the CEL09 model at a distance of 70 km. The lower crustal velocities are changed to get a better fit of the data (see Table 1 for model values). Violet line - CEL09 velocity model at 70 km; black line - sharp Moho velocity contrast at a depth of 30 km; orange line - thinner lower crustal layer with velocity gradient to the Moho level (model with the best fit of the receiver function data); blue line - thin lower crustal layer at a depth of 26–30 km and thin Moho layer at a depth of 30–32 km (model that fits quite well both the receiver function and wide-angle data).

Table 1. Input seismic velocity models for modelling. *n* - number of layers within each interval (*n* = 0, discontinuity). Density was calculated after *Birch (1961)* from *Vp*.

CEL09 original velocity model at km 70			*n*
Depth [km]	*Vp* [m/s]	*Vp/Vs*	
0.0	4.00	1.73	5
0.5	5.75	1.73	5
3.8	5.90	1.73	5
11.8	6.00	1.73	10
11.8	6.14	1.73	0
17.6	6.22	1.73	10
17.6	6.45	1.73	0
26.5	6.56	1.73	10
26.5	6.85	1.73	0
35.8	7.60	1.76	7
35.8	7.85	1.79	0
44.0	8.00	1.79	7
100.0	8.00	1.79	1

2.4. Synthetic Tests for the Ray Tracing

Synthetic receiver function modelling for the station A03 showed that the delay times and amplitudes of the primary and multiple conversions can be explained not only by the first-order discontinuity but also by a maximal 5 km thick gradient zone/lower crustal layer at the base of the crust. Since the ray tracing originally modelled the wide-angle data with a thicker lower crustal zone, pronounced discontinuity on the top of it and less pronounced Moho at a depth of 35 km (see Fig. 2), we tried to change the ray-tracing velocity model and see how it can fit the data.

For such modelling, we did not consider the NW end of the CEL09 profile where the top of the lower crust was interpreted at a depth of 26 km, because the crust-mantle transition in this area was mainly constrained by the crossing profile (GRANU'95) and not that much from the CEL09 refraction data themselves. Instead, we concentrated on Vogtland/West Bohemia, keep the top of the lower crust at a depth of 28 km and tried to model a thinner lower crust. To obtain a reasonable fit in the travel times we ended up with the Moho at a depth of about 32–33 km and the lower crustal zone with the velocities from 6.9 to 7.3 km s^{-1} (Fig. 10).

This model has thinner lower crust and is much closer to the result of the receiver function synthetic modelling (Fig. 9d, blue line). In return, in this approach, the Moho is more pronounced with a velocity increase of 0.5 km s^{-1}. For this reason the Moho reflection is visible in the synthetic sections where we calculate also the amplitudes. This does not fully correspond to the observed wide-angle data where only a response from the top of the lower crust is visible (see Fig. 10). On the other hand, a long coda of the reflection from the top of the lower crust suggests strong reflectivity within this layer as
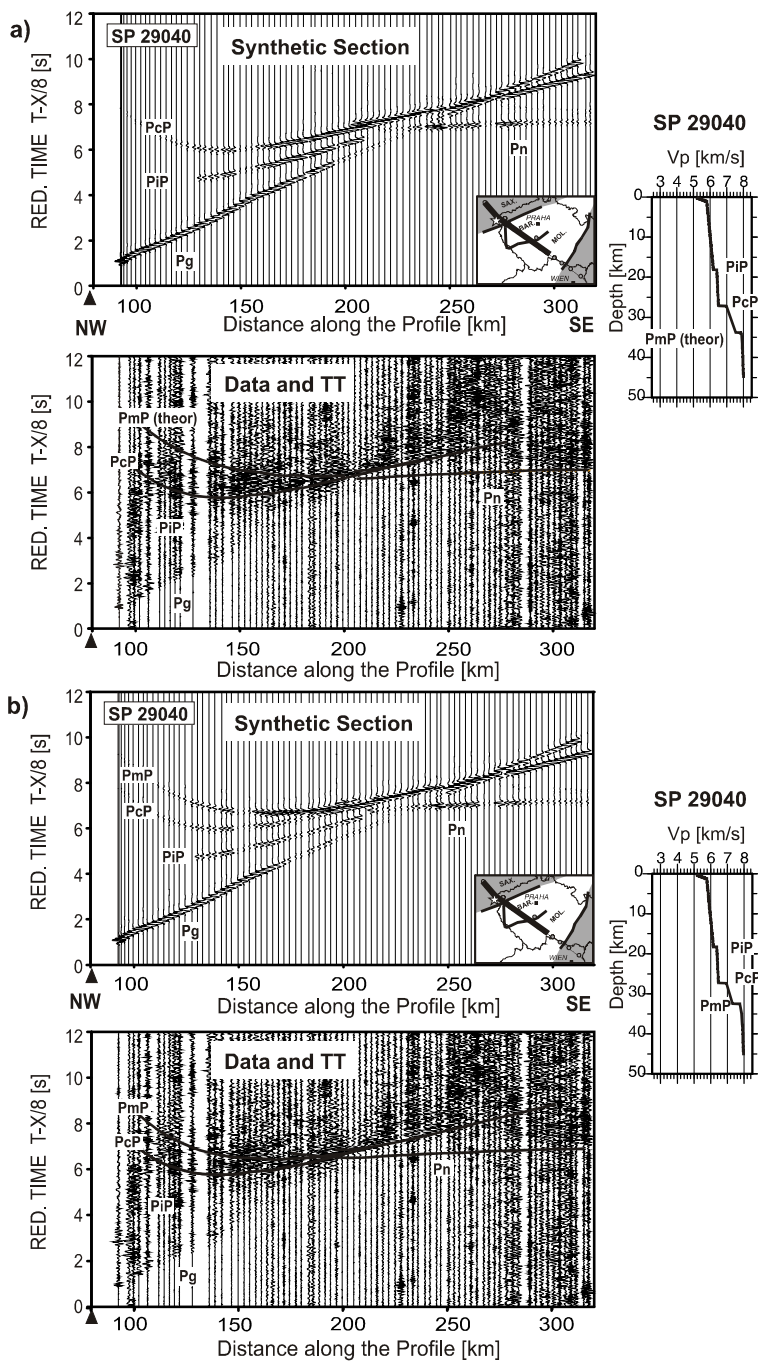
previously modelled with the reflectivity method by *Hrubcová et al. (2005)* and as shown in Fig. 3. The velocity fluctuations in the lower crust correspond to such variations reported by other authors in the Variscan areas, e.g., in Germany (*Sandmeier and Wenzel, 1990*) or in Poland (*Jensen et al., 1999*). *Hrubcová et al. (2005)* simulated the reflectivity of the lower crust and showed that the reflectivity can mask a weak reflection from the Moho. If we follow such approach, we may infer that some reflectivity may also obscure a more pronounced reflection from the Moho.

3. DISCUSSION

In the presented study we concentrated on Vogtland/West Bohemia with the focus on the lower crust and crust-mantle transition in this region. We tried to compare the outcomes from two different seismic methods: the receiver functions and the refraction and wide-angle reflection modelling, and constrained them by previously known results from other seismic investigations. Above, we performed new modelling for the two data sets, receiver function data and refraction and wide-angle data, to get closer to a unified solution. Previously, all methods found indications for a major discontinuity near the base of the crust but differed partly in the depth determination and in the characterization of the crust-mantle transition.

The major question at the beginning was why the original interpretations differed so much. One very important factor addressing this question is the different theoretical background and methodology of both methods as well as their spatial resolution. The receiver function provides near-vertical information on the velocity contrasts and the depth of the seismic discontinuities beneath the stations similar to that of the reflection seismics. In return, the refraction modelling gives smoothened sub-horizontal information on the velocities and depth of discontinuities along large profiles. The comparison of the wide-angle and "reflection" Moho is documented e.g. by *Barton et al. (1984)* or *Braile and Chaing (1986). Jones et al. (1996)* show the differences between near-vertical reflection Moho and the Moho modelled from wide-angle data sets, where they are usually offset from each other, with the wide-angle Moho being shallower to the near-vertical Moho from reflection.

Another important factor is that each method samples the boundary at slightly different place. For the receiver function, the direct P-to-S conversions sample the Moho at a distance of about 5−10 km away from the station and its crustal multiples sample the Moho over a distance of 5−30 km from the station in the direction dependant on the back

---

Fig. 10. (Facing page) Comparison of the ray-tracing forward modelling along the CEL09 profile for SP 29040 illustrating the different velocities in the crust-mantle transition. In each subfigure: top - synthetic sections, bottom - amplitude-normalized seismic sections with calculated travel times, side - 1-D velocity models. Reduction velocity is 8 km s^{-1}, locations of major tectonic units and shot points are indicated. Other description as in Fig. 2. **a)** The velocity model as according to *Hrubcová et al. (2005)*, (see also Fig. 2). Note missing PmP (theor) in the synthetic section. **b)** The velocity model with the top of the lower crust located in the same position. The Moho is shallower and more pronounced. Note PmP phase visible in the synthetic section.

azimuth of the respective incoming teleseismic phase. On the other hand, the refraction and wide angle reflection give the information about the sub-horizontal velocities and discontinuities along the profile mostly from a mid-point between the shot and the receiver. For deeper crustal interfaces and the Moho it is usually more than 30 km away from the shot. From this point of view, the dipping of the reflective lower crustal boundary towards the SE and the whole lower crust edging away in the SE direction may contribute to the different results.

Another important factor there is the *Vp/Vs* ratio and the fact that each method applies this ratio in a different way. For calculation of the depth of the discontinuity from the observed Ps delay times we have to know the average P and S-wave velocities (e.g., average crustal *Vp* and *Vp/Vs*). But the receiver function technique provides information on the near-vertical velocity contrasts constrained by the S-wave velocity distribution in the crust. Thus, it is complementary to the controlled source profiles, in which the P waves are primarily recorded and the S waves are weak or absent.

As far as concern the *Vp/Vs* ratio in West Bohemia, we tried to calculate it from the WEBNET broadband data (e.g. *Fischer and Horálek, 2003*) and wanted to find some depth dependence, but its scatter for the upper and middle crust was quite wide. It ranged from some 1.6 to 1.8, and did not show any simple pronounced relation to the depth. Above, *Kolář and Boušková (2003)* tried to show some indications for its azimuthal variations, which made the task even harder.

The dispersion in the *Vp/Vs* values can indicate possible uncertainty in the depth determination. *Geissler et al. (2005)* interpreted the depth of the Moho at an average depth of 31 km from the P-to-S delay times assuming constant average crustal *Vp* of 6.3 km s^{-1} and *Vp/Vs* ratio of 1.73. If higher values of the *Vp/Vs* were applied then the interface would be shallower, and vice versa. In detail, when considering the *Vp/Vs* of 1.8 we could get the depth of 28 km and for the *Vp/Vs* of 1.6 we get the depth of 37 km. For the delay time of 3.3 s in the Eger Rift, where *Geissler et al. (2005)* interpreted the Moho at 27 km, the depth values can range in-between of 25 km and 33 km for the *Vp/Vs* of 1.8 and 1.6, respectively.

Also, the frequency band of teleseismic body waves covers the range of one to several seconds and thus differs from the controlled source methods with the frequency of several Hz. This determines the resolution of each method and gives the ability to see the details in the determination of the discontinuity. To prove this, we examined the model, which was previously used to explain the reflectivity from wide-angle observations. We calculated a receiver function response for a lower crust with thin (500 m thickness each) internal layers of alternating velocities. However, the frequency content of teleseismic phases does not allow imaging such thin layering and only the average velocity structure in the lower crust can be resolved.

There are some other factors that have not been taken into consideration so far, and which to some extent can influence the achieved results. The effect of anisotropy, reported in this region (*Vavryčuk, 1993*; *Vavryčuk and Boušková, 2008*) and not considered in the above studies, may play an important role in the different interpretation of the crustal thickness as shown by e.g. *Jones et al. (1996)*.

If we look at all the above mentioned aspects, they are quite important though they are inadequate to explain the differences of the results from the active and passive seismic
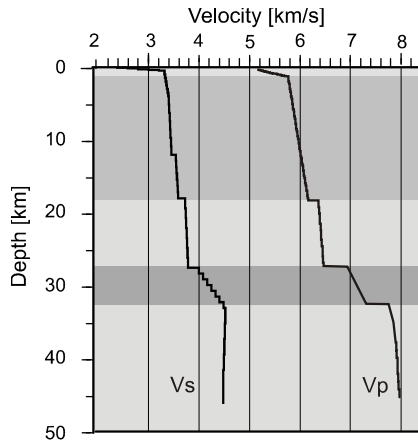
Fig. 11. Final 1-D joint velocity model. *Vs* - S-wave velocity from the receiver functions as for the A3 station, *Vp* - P-wave velocity from the ray-tracing data as for the SP 29040.

methods. For this reason, a special synthetic modelling of both the receiver function and the ray-tracing data was performed with the aim to find the indicators for some joint interpretation. The synthetic modelling of the receiver function observed at the station A03 revealed that an acceptable fit to the data could be achieved for the model with a thin lower crustal layer at a depth of 26–30 km and a thin Moho layer at a depth of 30–32 km (Fig. 9d, blue line). The consequent synthetic ray-tracing modelling showed that such thinner lower crustal layer can fit the data in the travel times, but more pronounced Moho produces a stronger reflection that is not supported by the observations (Fig. 10). On the other hand, a reflectivity of the lower crust recorded by the data and reported also in some other Variscan areas may actually obscure the Moho reflection.

The joint model (Fig. 11) ended up with the top of the lower crust at 28 km, where highly reflective lower crustal layer can obscure the more pronounced Moho at 32–33 km depth. Such model would be in accordance with the wide-angle refraction and reflection profile GRANU'95 and the reflection profile MVE-90 with a highly reflective lower crust of 4–6 km thick and with an uppermost mantle more or less without reflections. The Moho in the MVE-90 data is interpreted at 10 s of the two-way travel time and corresponds to a depth of 30 to 32 km, where the strong reflectivity dies out.

4. CONCLUSIONS

In the presented study we concentrated on Vogtland/West Bohemia with the focus on the lower crust and the crust-mantle transition in this region. We used the outcomes from different seismic methods, namely the receiver functions and the refraction and wide-angle reflection modelling. At the beginning the results of these methods differed since the refraction interpretation attributed the strong reflector at the depths of 26–28 km to the top of the lower crust with a high reflectivity. The Moho was modelled at a depth of

35 km to get a weak contrast on the Moho, compared to the top of the lower crust, in a place where the reflectivity dies out. The receiver function indicated a strong first-order converter at a depth of 31 km, with a local updoming beneath the western Eger Rift to some 27 km.

As discussed, the discrepancies can partly be attributed to different aspects of both methods and their resolution. Among them, the uncertainty in the knowledge of the *Vp/Vs* ratio and the different frequency band of both methods play an important role. Another fact is that the methods sample the boundary at slightly different places. However, these methodological aspects are not enough to explain the observed discrepancies.

New receiver function modelling for a reference station showed that there might be a lower crustal layer (or gradient zone) of maximal 5 km thickness instead of a single first-order discontinuity, which can explain the observed receiver functions. The consequent ray-tracing modelling along the CEL09 profile showed that such thinner lower crust can fit the data in the travel times. The reflectivity within the lower crust recorded by the data and reported also in some other Variscan areas may obscure the Moho reflection. The new model shows the top of the lower crust at a depth of 28 km, where high reflectivity obscures the Moho reflection at a depth of 32–33 km. The new findings of this study provide the base for a future joint mapping/interpretation of the crust-mantle boundary in the whole region, which is known for its complex lithospheric structure. It also shows the necessity for the joint interpretation of different data sets with regard to the resolution and background of each method applied.

References

Barton P.J., Matthews D., Hall J. and Warner M., 1984. Moho beneath the North Sea compared on normal incidence and wide-angle seismic records. *Nature*, **308**, 55–56.

Behr H.-J., Dürbaum H.-J. and Bankwitz P., 1994. Crustal structure of the Saxothuringian Zone: Results of the deep seismic profile MVE-90(East). *Z. Geol. Wiss.*, **22**, 647–769.

Birch F., 1961. The velocity of compressional waves in rocks to 10 kilobars, part 2. *J. Geophys. Res.*, **66**, 2199–2224.

Braile L.W. and Chiang C.S., 1986. The continental Mohorovičić discontinuity: results from near vertical and wide-angle seismic reflection studies. In: Barazangi M. and Brown L. (Eds.), *Reflection Seismology: A Global Perspective*. Amer. Geophys. Union, Geodynamics Series, **13**, 257–272.

Bräuer K., Kämpf H., Niedermann S. and Strauch G., 2005a. Evidence for ascending upper mantle-derived melt beneath the Cheb basin, central Europe. *Geophys. Res. Lett.*, **32**, L08303, doi: 10.1029/2004GL022205.

Bräuer K., Kämpf H., Niedermann S. and Strauch G., 2005b. Correction to "Evidence for ascending upper mantle-derived melt beneath the Cheb basin, central Europe". *Geophys. Res. Lett.*, **32**, L18304, doi: 10.1029/2005GL02434.

Červený V. and Pšenčík I., 1984. SEIS83 - Numerical modelling of seismic wave fields in 2-D laterally varying layered structures by the ray method. In: Engdal E.R. (Ed.), *Documentation of Earthquake Algorithms*. Rep.SE-35, World Data Center A, Boulder, CO, 36–40.

Cook F.A., 2002. Fine structure of the continental reflection Moho. GSA Bull., **114**, 64–79.

Cox K.G., 1980. A model for flood basalt volcanism. *J. Petrol.*, **21**, 629–650.

DEKORP Research Group, 1988. Results of the DEKORP 4/KTB Oberpfalz deep seismic reflection investigations. *J. Geophys.*, **62**, 69–101.

DEKORP Research Group, 1994. The deep reflection seismic profiles DEKORP 3/MVE-90. *Z. Geol. Wiss.*, **22**, 623–824.

DEKORP and Orogenic Processes Working Groups, 1999. Structure of the Saxonian Granulites: Geological and geophysical constraints on the exhumation of high-pressure/high-temperature rocks in the mid-European Variscan belt. *Tectonics*, **18**, 756–773.

Enderle U., Schuster K., Prodehl C., Schultze A. and Briebach J., 1998. The refraction seismic experiment GRANU'95 in the Saxothuringian belt, southeastern Germany. *Geophys. J. Int.*, **133**, 245–259.

Fischer T. and Horálek J., 2003. Space-time distribution of earthquake swarms in the principal focal zone of the NW Bohemia/Vogtland seismoactive region: period 1985–2001. *J. Geodyn.*, **35**, 125–144.

Fischer T. and Michálek J., 2008. Post 2000-swarm microearthquake activity in the principal focal zone of West Bohemia/Vogtland: space-time distribution and waveform similarity analysis. *Stud. Geophys. Geod.*, **52**, 493–511.

Fuchs K. and Müller G., 1971. Computation of synthetic seismograms with the reflectivity method and comparison with observations. *Geophys. J. R. Astron. Soc.*, **23**, 417–433.

Geissler W.H., Kämpf H., Kind R., Klinge K., Plenefisch T., Horálek J., Zedník J. and Nehybka V., 2005. Seismic structure and location of a CO_2 source in the upper mantle of the western Eger rift, Central Europe. *Tectonics*, **24**, TC5001, doi: 10.10292004TC001672.

Geissler W.H., Kind R. and Yuan X., 2008. Upper mantle and lithospheric heteroheneities in central and eastern Europe seen by teleseismic receiver functions. *Geophys. J. Int.*, **174**, 351–376, doi: 10.1111/j.1365-246x.2008.03767.x.

Grad M., Guterch A., Mazur S., Keller G.R., Špičák A., Hrubcová P., Geissler W.H. and SUDETES 2003 Working Group, 2008. Lithospheric structure of the Bohemian Massif and adjacent Variscan belt in central Europe based on Profile S01 from the SUDETES 2003 experiment. *J. Geophys. Res.*, **113**, B10304, doi: 10.1029/2007JB005497.

Guterch A., Grad M., Keller G.R., Posgay K., Vozár J., Špičák A., Brueckl E., Hajnal Z., Thybo H., Selvi O. and CELEBRATION 2000 Experiment Team, 2003. CELEBRATION 2000 seismic experiment. *Stud. Geophys. Geod.*, **47**, 659–670.

Hammer P.T.C. and Clowes R.M., 1997. Moho reflectivity patterns - a comparison of Canadian lithoprobe transects. *Tectonophysics*, **269**, 179–198.

Heuer B., Geissler W.H., Kind R. and Kämpf H., 2006. Seismic evidence for asthenospheric updoming beneath the western Bohemian Massif, central Europe. *Geophys. Res. Lett.*, **33**, L05311, doi: 10.1029/2005GL025158.

Horálek J., Boušková A., Hampl F. and Fischer T., 1996. Seismic regime of the West-Bohemian earthquake swarm region: Preliminary results. *Stud. Geophys. Geod.*, **40**, 398–412.

Horálek J., Fischer T., Boušková A. and Jedlička P., 2000. The Western Bohemia/Vogtland region in the light of the Webnet network. *Stud. Geophys. Geod.*, **44**, 107–125.

Hrubcová P., Šroda P., Špičák A., Guterch A., Grad M., Keller R., Brückl E. and Thybo H., 2005. Crustal and uppermost mantle structure of the Bohemian Massif based on data from CELEBRATION 2000 experiment. *J. Geophys. Res.*, **110**, B11305, doi: 10.1029 /2004JB003080.

Jensen S.L., Janik T., Thybo H. and POLONAISE Working Group, 1999. Seismic structure of the Palaeozoic Platform along POLONAISE'97 profile P1 in northwestern Poland. *Tectonophysics*, **314**, 123–144.

Jones K.A., Warner M.R., Morgan R.P.L., Morgan J.V., Barton P.J. and Price C.E., 1996. Coincident normal-incidence and wide-angle reflections from the Moho: evidence for crustal seismic anisotropy. *Tectonophysics*, **264**, 205–217.

Kennett B.L.N. and Engdahl E.R., 1991. Traveltimes for global earthquake location and phase identification. *Geophys. J. Int.*, **105**, 429–565.

Kind R., Kosarev G.L. and Petersen N.V., 1995. Receiver functions at the Stations of the German Regional Seismic Network (GRSN). *Geophys. J. Int.*, **121**, 191–202.

Kolář P. and Boušková A., 2003. On some anomalies of Vp/Vs ratio of West Bohemain swarm 2000 - preliminary results. *Acta Montana*, **22**, 51–57.

Mengel K. and Kern H., 1991. Evolution of the petrological and seismic Moho – Implications for the continental crust/mantle boundary. *Terra Nova*, **4**, 109–123.

Mohorovičić A., 1910. Das Beben Vom 8. x. 1909. *Jahrbuch Meterologie Observatorie Zagrab*, **9**, 1–63.

Prodehl C., Mueller S. and Haak V., 1995. The European Cenozoic rift system. In: Olsen K.H. (Ed.), *Continental Rifts: Evolution, Structure, Tectonics*. Developments in Geotectonics, Elsevier, Amsterdam, The Netherlands, 133–212.

Sandmeier K.-J. and Wenzel F., 1990. Lower crustal petrology from wide-angle P- and S-wave measurements in the Black Forest. *Tectonophysics*, **173**, 495–505.

Tomek Č., Dvořáková V. and Vrána S., 1997. Geological interpretation of the 9HR and 503M seismic profiles in Western Bohemia. In: Vrána S. and Štedrá V. (Eds.), *Geological Model of Western Bohemia Related to the KTB Borehole in Germany*. *J. Geol. Sci.*, **47**, 43–50.

Vavryčuk V., 1993. Crustal anisotropy from local observations of shear-wave splitting in West Bohemia, Czech Republic. *Bull. Seismol. Soc. Amer.*, **83**, 1420–1441.

Vavryčuk V. and Boušková A., 2008. S-wave splitting from records of local micro-earthquakes in West Bohemia/Vogtland: an indicator of complex crustal anisotropy. *Stud. Geophys. Geod.*, **52**, 631–650.

Vinnik L.P., 1977. Detection of waves converted from P to S in the mantle. *Phys. Earth Planet. Int.*, **15**, 39–45.

Wilde-Piórko M., Saul J. and Grad M., 2005. Differences in the crustal and uppermost mantle structure of the Bohemian Massif from teleseismic receiver functions. *Stud. Geophys. Geod.*, **49**, 85–107.

Yuan X., Ni. J., Kind R., Mechie J. and Sandvol E., 1997. Lithospheric and upper mantle structure of southern Tibet from a seismological passive source experiment. *J. Geophys. Res.*, **102(B12)**, 27491–27500.

P4

Hrubcová, P., P. Środa, M. Grad, W.H. Geissler, A. Guterch, J. Vozár, E. Hegedűs, and Sudetes 2003 Working Group

From the Variscan to the Alpine Orogeny – crustal structure of the Bohemian Massif and Western Carpathians in the light of the SUDETES 2003 seismic data

From the Variscan to the Alpine Orogeny – crustal structure of the Bohemian Massif and the Western Carpathians in the light of SUDETES 2003 seismic data

Hrubcová[1], P., P. Środa[2], M. Grad[3], W.H. Geissler[4], A. Guterch[2], J. Vozár[5], E. Hegedűs[6], and Sudetes 2003 Working Group

[1]Institute of Geophysics, Academy of Science of the Czech Republic, Boční II/1401, 141 31 Prague 4, Czech Republic
[2]Institute of Geophysics, Polish Academy of Sciences, Ks. Janusza 64, 01-452 Warsaw, Poland
[3]Institute of Geophysics, University of Warsaw, Pasteura 7, 02-093 Warsaw, Poland
[4]Alfred Wegener Institute for Polar and Marine Research, Am Alten Hafen 26, D3210, D-27568 Bremerhaven, Germany
[5]Slovak Academy of Sciences, Geological Institute, Bratislava, Slovak Republic
[6]Eötvös Loránd Geophysical Institute, Budapest, Hungary
 (pavla@ig.cas.cz)

The Variscan orogeny is the major Middle to Late Palaeozoic tectonometamorphic event in central Europe with the Bohemian Massif as the largest unit exposed at the surface. Further to the SE, the Western Carpathians form an arc shaped mountain range related to the Alpine orogeny during the Cretaceous to Tertiary. The complex geological structures of the Variscan Bohemian Massif and the Western Carpathians, and especially their contact, were studied using the data of the international seismic refraction experiment SUDETES 2003. The seismic data were acquired along the NW-SE oriented refraction and wide-angle reflection profile S04 starting at the north-west edge of the Bohemian Massif, crossing all its main tectonic units and through the Western Carpathians terminating in the Pannonian Basin. The data were interpreted by 2-D trial-and-error forward modelling of the *P* waves; additional constraint on crustal structure was given by gravity modelling. The differences in seismic velocities reflect, to some extent, the structural variances and tectonic events. Lower velocities of 5.85 km s^{-1} at the contact of the Saxothuringian and Barrandian are caused by low density granites. The lower crust in the Saxothuringian exhibits complicated structure interpreted with the Moho with some lateral topography. The Moho at the northern rim of the Moldanubian is modelled as a first order discontinuity at a slightly shallower depth of 33 km compared to the central part of the Moldanubian in the Bohemian Massif with 39 km. The Moho in the transition between the Bohemian Massif and the Western Carpathians shows strong lateral variations with strongly dipping Moho to the NW from a depth of 26 km at a distance of 415 km to a depth of 37 km. It may be associated with the Pieniny Klippen Belt, a deep-seated boundary between the colliding Palaeozoic lithospheric plate and the microplate ALCAPA, which would suggest a sub-vertical plate boundary in this area. In the upper crust, lower velocities of 4 km s^{-1} to a depth of 6 km represent sedimentary infill of the Carpathian Foredeep and Flysch thinning towards the foreland, which is also expressed as a pronounced gravity low. The Moho in the Carpathians reaches a depth of 32 – 33 km. At contrast, in the Pannonian Basin the Moho rises up to a depth of 25 km, which corresponds with the Pannonian gravity high.

1. Introduction

The Variscan orogeny is the major Middle to Late Palaeozoic tectonometamorphic event in central Europe. It represents the final collision of Gondwana with the northern continent Laurasia and marks the European version of the evolution of the supercontinent of Pangea at the end of the Palaeozoic (*McCann* 2009a). During the Cretaceous to Tertiary, the post-Variscan stage was followed by extensional and compressional tectonics, related to plate motions between Europe and Africa, which resulted in the Alpine orogeny. The largest Variscan unit in central Europe, the Bohemian Massif, represents the most prominent outcrop of pre-Permian rocks. It was formed by the amalgamation of individual Armorican terranes and their final collision with Avalonia and the western margin of the Brunovistulian (*Schulmann & Gayer* 2000). Further to the SE, the Western Carpathians form an arc shaped mountain range originating as a result of convergence of the European and African plates since the Late Jurassic through Quaternary (*McCann* 2009b).

As follows, the region is a complex of tectonic units ranging from Cadomian to Tertiary age with Variscan to Alpine tectonics. To investigate such a structure, central Europe has been covered by a network of seismic refraction experiments (POLONAISE'97, CELEBRATION 2000, ALP 2002, and SUDETES 2003) as a result of a massive international cooperative effort (*Guterch et al.* 1998, 1999, 2003a, 2003b; *Brückl et al.* 2003; *Grad et al.* 2003a, 2003b). This paper focuses on the refraction and wide-angle reflection experiment SUDETES 2003, which involved a consortium of European and North American institutions comprising geophysical groups from the Czech Republic, Poland, the United States, Germany, Slovakia, and Hungary. In this study we present a detailed analysis of data from the main SUDETES 2003 profile S04 (Figure 1 and 2) that extends in the NW-SE direction from Germany, across all main

tectonic units of the Bohemian Massif and continues through the Western Carpathians to the Pannonian Basin in Hungary.

The complex geological structures of the Variscan Bohemian Massif and the Western Carpathians, and especially their contact, are not completely understood or solved in many aspects and are subject to ongoing research and debate. The Bohemian Massif is an excellent example of the Variscan crust exposed to the surface, while the Carpathian crust records the crust forming processes during Mesozoic to Cenozoic. The S04 profile is in a favourable position for studying the individual tectonic units within the Bohemian Massif. Above, its prolongation across the Western Carpathian arc gives an opportunity to study this orogenic belt as well as its contact with the Bohemian Variscan units in the NW. The interpretation of the S04 data gives a new insight into the deep structure and superposition of the tectonic units at depth. Contrasts in seismic properties together with the depth of the Moho discontinuity reflect compositional and structural variances resulting from crust-forming processes during Cadomian, Palaeozoic and Tertiary tectonic development.

2.   Geology and Tectonic Evolution of the Region

The eastern termination of the Variscan belt in central Europe comprises the Bohemian Massif, which developed approximately between 480 and 290 Ma (*Matte et al.* 2001) during a period of large-scale crustal convergence, collision of continental plates and microplates and subduction (*Matte et al.* 1990). It includes the formation of cratonic basement, Cadomian orogenic processes and variable reworking during the Variscan orogeny. In places the massif underwent the highest known Variscan metamorphic overprint, while other units of the massif show only a very low grade tectonometamorphic overprint and well preserved remnants of the Cadomian basement and its Early Palaeozoic overstep sequences. The Bohemian Massif consists mainly of low- to high-grade metamorphic and plutonic Palaeozoic rocks and can be subdivided into several tectonostratigraphic units: the Saxothuringian, the Barrandian, the Moldanubian and the Moravo-Silesian, separated by faults, shear zones or thrusts (see Figure 1).

The Moldanubian unit represents a major crystalline segment within the Bohemian Massif and its boundary with the Saxothuringian in the NW is regarded to be a suture-type discontinuity. A structurally higher unit, the Barrandian, has been thrust over the Saxothuringian rocks towards the northwest (*Dallmeyer et al.* 1995). Reactivation of crustal-scale shear zones during mid-Cretaceous led to the formation of the Bohemian Cretaceous Basin along the NW-SE oriented Elbe Fault Zone reflecting a large-scale zone of crustal weakness. Later, this area was affected by Permo-Carboniferous post-orogenic extension, as well as alkaline magmatism during the Cenozoic evolution of the Eger Rift, a geodynamically active zone belonging to the European Cenozoic Rift System (*Prodehl et al.* 1995).

The Moldanubian/Moravian boundary in the east has the character of a ductile shear zone with a significant translation of the Moldanubian over the Moravian unit during a final stage of the subduction of the oceanic crust and subsequent Variscan collision between the Moldanubian terrane and the Brunovistulian micro-continent to the east (*Dudek* 1980). In this event, the Moldanubian is viewed as a Variscan orogenic root thrust over the Brunovistulian forming together the Moravo-Silesian zone (*Matte* 1991; *Schulmann et al.* 2005). The Moravian unit consists of a Cadomian basement, the Brunovistulian, covered by Devonian to Carboniferous sediments and submerging to the east beneath the Carpathian Foredeep, where it forms the basement reactivated during the Alpine orogeny (*Schulmann & Gayer* 2000). In Mesozoic, the area was subject to a platform development and rifting along the southern/southeastern flank of the Bohemian Massif.

The Western Carpathians form a northward-convex arc as a result of a series of Jurassic to Tertiary subduction and collision events. They represent the northernmost part of the Alpine belt, which evolved during the Alpine orogeny. The geological evolution of individual parts is rather complicated, comprising tectonic processes such as folding, thrusting and the formation of sedimentary basins of various types in the Mesozoic and Tertiary. These processes resulted in superposition of Variscan high-grade crystalline basement and its Late Palaeozoic and Mesozoic cover, overridden by the superficial nappe systems and post-nappe cover formed by Palaeogene, Neogene and Quaternary rocks. Like most of the other collisional fold-belts, the Western Carpathians have been divided into the outer and inner zones based largely on the relative ages of the Alpine events and the intensity of their deformation and metamorphic effects (*McCann* 2008b).

The Outer Western Carpathians include the Carpathian Foredeep, the eastern prolongation of the Alpine Molasse Basin, and the Carpathian Flysch Belt, a Tertiary accretionary complex composed of several north to north-west-verging nappes. They are thrust over the Carpathian Foredeep filled by Neogene strata. The Inner Western Carpathians, covering most of Slovakia, include various pre-Tertiary units and the unconformable Cenozoic sedimentary and volcanic complexes. They are followed by isolated mountains in northern Hungary comprising mainly unmetamorphosed

Palaeozoic and Mesozoic complexes covered by deposits of the Late Cretaceous, Palaeogene and Early Neogene intermontane basins up to 3.5 km thick (*Plašienka et al.* 1997; *Janočko & Jacko* 1999; *Soták et al.* 2001).

From a tectonic point of view, the Outer Western Carpathians correspond to a Tertiary accretionary complex related to the southward subduction of the oceanic to sub-oceanic crust. They are separated from the Inner Western Carpathians by the Pieniny Klippen Belt, a deep-seated boundary between the colliding Palaeozoic lithospheric plate and the microplate ALCAPA. The Pieniny Klippen Belt forms a narrow zone of extreme shortening and wrenching between the accretionary wedge and the Inner Western Carpathians representing the backstop (*Birkenmajer* 1986). According to this interpretation, during Tertiary times, the Carpathian Foredeep was a peripheral foredeep formed due to regional flexure of the descending plate (*Krzywiec* 1997). The subduction-related nappe stacking in the Outer Western Carpathians was followed by regional collapse resulting in the formation of intermontane basins filled by Neogene and Quaternary strata (*Zuchiewicz et al.* 2002).

In the south, the Western Carpathian area also includes the subsurface of the wide flat lowlands of the Pannonian Basin (*Horváth* 1993; *Tari et al.* 1993). The Pannonian Basin System is filled by more than 2 km of Palaeogene and up to 7 km of Neogene and Quaternary sedimentary cover (*Royden et al.* 1983). It was formed within the Inner Carpathians and the Tisza unit due to the back-arc stretching and mantle upwelling (*Konečný et al.* 2002).
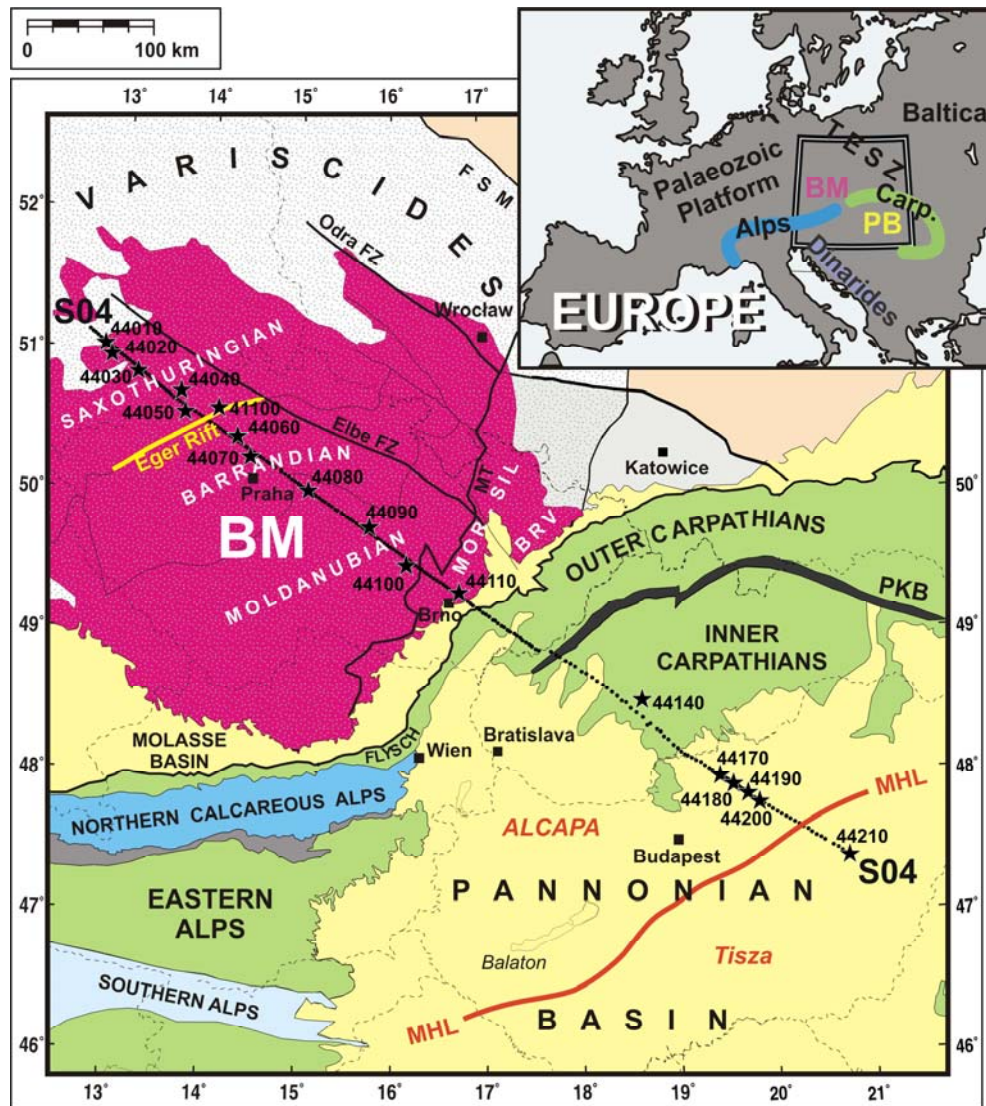

Figure 1. Location of the S04 profile superimposed on a simplified tectonic map. The insert shows major tectonic units in central Europe. BM, Bohemian Massif; Carp., Carpathians; TESZ, Trans-European Suture zone; Mor-Sil, Moravo-Silesian; Brv, Brunovistulian; MT, Moldanubian Thrust; PKB, Pieniny Klippen Belt; MHL, Mid-Hungarian Line.

3

3. Previous Geophysical Investigations in the Study Area

The first attempts to reveal crustal structure of this vast region were associated with the investigation of the Bohemian Massif (*Beránek & Zátopek* 1981) or with the investigation of the Carpathian Foreland (*Majerová & Novotný* 1986; *Bielik et al.* 2004). The interpretation of the refraction measurements indicated a pronounced Moho discontinuity in the central part of the Bohemian Massif with a maximum depth of 39 km and a less pronounced, sometimes blurred, Moho at a depth of about 32 km at the eastern margin of the Bohemian Massif at its contact with the Carpathians (*Beránek & Zounková* 1977). These measurements were complemented by reflection profiling, as well as by other geophysical methods (see, *Bucha & Blížkovský* 1994).

More detailed results were achieved from the refraction and wide-angle reflection experiments CELEBRATION 2000, ALP 2002, and SUDETES 2003 (*Brückl et al.* 2007; *Grad et al.* 2003b; *Guterch et al.* 2003a, 2003b; *Hrubcová et al.* 2005, 2008; *Málek et al.* 2001; *Růžek et al.* 2003, 2007, *Środa et al.* 2006) (Figure 2), which followed previous seismic studies in central Europe (*Guterch et al.* 1999; *Grad et al.* 2002, 2003a; 2006). Two perpendicular profiles, CEL09 and CEL10, crossing the whole Bohemian Massif provided new information about the structure and particularly about the lower crustal properties and the character of the crust-mantle transition. A highly reflective lower crust was associated with the Saxothuringian in the NW, the deepest and the most pronounced Moho was detected in the Moldanubian and a broad crust-mantle transition zone along the eastern edge of the Bohemian Massif (*Hrubcová et al.* 2005; *Hrubcová et al.* 2008). SUDETES 2003 profile S01 provided a good regional picture on the lithospheric structure along the Eger Rift (*Grad et al.* 2008); profiles S02 and S03 gave an insight on the Bohemian Massif in the north-south direction (*Majdański et al.* 2006, 2007). In SE Germany, the seismic refraction and wide-angle reflection profile GRANU'95 (*Enderle et al.* 1998) showed the velocity structure of the Saxothuringian belt. Laminated lower crust was indicated by the deep reflection profile MVE-90 as a part of the DEKORP investigations (*DEKORP Research Group*, 1994) and during a combined investigation of the refraction and receiver function data (*Hrubcová & Geissler* 2009).

An important contribution to the understanding of the geological structure at the transition between the Bohemian Massif and the Carpathians was provided by the interpretation of the regional refraction profile KII extending from the border of the Czech Republic and Poland to Slovakia. In the Silesian zone, two bands of reflections suggested that the Moho is located at a depth of 36-37 km and rising towards the SE to 30-32 km (*Majerová & Novotný* 1986). The deep seismic reflection profile 8HR further to the south (see Figure 2), close to the S04 profile, indicated the Moho at a depth of 35 – 37 km.

The Carpathian Mountains and their foredeep were also subject to the early deep seismic sounding studies, which resulted in a crustal thickness of 40 km. Later, these measurements were complemented by the reflection profiling (*Tomek* 1993; *Tomek, & Hall* 1993; *Vozár et al.* 1999; *Šantavý & Vozár* 2000), as well as by the detailed refraction and wide-angle reflection experiment CELEBRATION 2000 (*Grad et al.* 2006; *Malinowski et al.* 2006, 2007). Profiles CEL01, CEL04, and CEL05 crossed the Carpathian arc in the N-S direction and gave an insight into the main tectonic features associated with the Carpathians and the Pannonian Basin System (*Grad et al.* 2006; *Środa et al.* 2006). In the Pannonian Basin, both refraction and deep reflection profiles recorded since 1970 discovered a thinner crust of about 25 – 30 km and a low-velocity layer in the upper mantle, the top of which is at a depth of 55 km (*Posgay et al.* 1981, 1986, 1995).

Seismic investigations were complemented by other geophysical methods, especially the gravity measurements. The gravitational field pattern of the Bohemian Massif is divided into four positive and negative regional bands in the SW-NE direction (*Bucha & Bližkovský* 1994). They are perpendicular to the S04 profile with a minimum of -60 mGal near the contact of the Saxothuringian and Barrandian at the Eger Rift related to the granitic rocks. The Carpathian gravity low is attributed to low-density porous foredeep sediments covered by nappes of the Outer Western Carpathian accretionary wedge. The Pannonian gravity high results from significant shallowing of the Moho (*Bielik* 2004).

4. Seismic Data

4.1. Acquisition and Processing
The data along the refraction and wide-angle reflection profile S04 were acquired during the international seismic experiment SUDETES 2003 (*Grad et al.* 2003). This experiment was concentrated in the Czech Republic and Poland but also covered portions of Germany, Slovakia, and Hungary. Its NW-SE oriented transect S04 was the longest profile of the SUDETES 2003 experiment and started at the north-west edge of the Bohemian Massif in the Saxothuringian, crossed the Eger Rift, continued along the northern rim of the Barrandian and Moldanubian to the Moravo-Silesian. Then

it continued across the Carpathian Foredeep and Flysch Belt to the Western Carpathians and terminated in the Pannonian Basin. The S04 profile was 740 km long with 18 shot points, of which one was fired twice. About 250 single-channel recorders were deployed along the S04 profile; all recorders were of the Texan type (RefTek 125, Refraction Technology, Inc.) and employed 4.5 Hz vertical geophones. The average distance between shots was 30 km with an verage station spacing of 3 km in the Czech Republic and Germany and 4 km in Slovakia and Hungary. A few stations in Hungary near the Matra Mts. (distance of 610 – 650 km along the profile) were deployed with denser spacing of less than
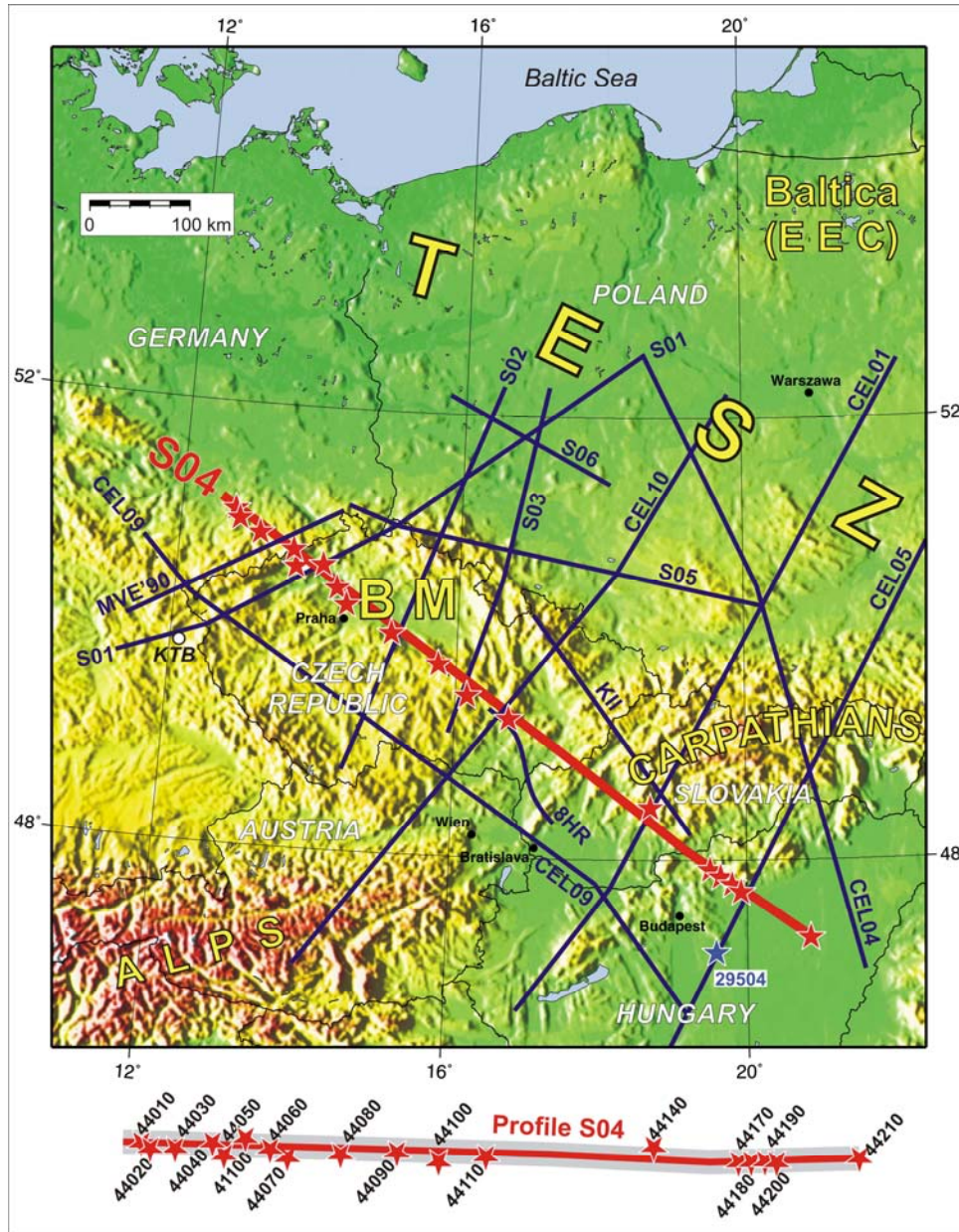

Figure 2. Location of the S04 profile with the shot numbers. Stars mark the positions of individual shot points, small dots refer to the recording positions. Other seismic refraction and reflection profiles (CELEBRATION 2000 – CEL01, CEL04, CEL05, CEL09, CEL10; SUDETES 2003 – S01, S02, S03, S05, S06; MVE-90, and 8HR) are indicated by dark blue solid lines. Blue star refers to the shot point SP 29504 of the CEL09 line. White circle shows the location of the KTB deep borehole. The shots along the S04 profile with their numbers are shown at the bottom of the figure. BM, Bohemian Massif; TESZ, Trans-European Suture zone; EEC, East European Craton.

1 km for shallow structure study. The charges amounted to 400 kg on average. For three shot points larger charges were used. The positions of shot points and stations were measured by GPS and the origin time was controlled by a GPS-

controlled blasting device. Figure 2 shows the field layout of the SUDETES 2003 seismic experiment; for more details on geometry refer to *Grad et al.* (2003), and G*uterch et al.* (2003). The shots along the S04 profile with their numbers are shown at the bottom of Figure 2 and detailed information about the shots is presented in Table 1.

The data from the experiment were recorded with a sampling rate of 0.01 s with a recording time window of 300 s for each shot. Data processing included shot-time corrections to assign a zero time to the exact time of shooting and band-pass filtering of the whole data set (usually 2-15 Hz) in order to remove low- and high-frequency noise. Recordings were sorted into shot gathers; seismic sections were trace-normalized to the maximum amplitude along the trace and cut to a length of 100 s starting at zero reduced time. They were plotted with a reduction velocity of 8 km s^{-1}, a velocity of the upper mantle commonly used for data visualisation in the crustal/upper mantle studies. For plotting, the seismic sections were cleaned and bad quality (noisy) traces (or their parts) were removed. Examples of the recorded wave fields are shown in Figure 3.

4.2. Seismic Wave Field

The seismic data used for the interpretation along the S04 profile have a good signal-to-noise ratio for the *Pg* phases as the refractions from the upper crust, and the *PmP* phases as the reflections from the Moho discontinuity. The *Pn* waves refracted from the upper mantle are sometimes not well-developed and are only visible on a few record sections. Refracted waves from the sedimentary cover (*Psed* phases) are observed in the vicinity of shot points mainly in the SE in the Pannonian Basin. Other phases are complex and sometimes difficult to pick and correlate among shot points. This fact concerns intracrustal reflections P_1P, and upper mantle reflections P^IP.

Clear arrivals of refracted waves from the crystalline crust (*Pg* phase) are typically observed up to offsets of 100 – 120 km. In the area of the Bohemian Massif they show an apparent velocity of 5.8 – 6.1 km s^{-1}. Short-wavelength anomalies of the *Pg* phase reflect the existence of near surface velocity inhomogeneities. Lower apparent velocities of about 5.5 – 5.75 km s^{-1} correlate with the sedimentary basin of the Barrandian unit (the Most Basin at 145 km along the profile) and southern margins of the Bohemian Cretaceous Basin (at about 200 and 280 km along the profile) located along the NW-SE oriented Elbe Fault Zone.

In the middle part of the profile, at the contact of the Bohemian Massif with the Carpathians there are strong differences in the wave fields. The shot points in the Bohemian Massif (Figure 3 – SP 44100, 44110) show an abrupt termination of energy for all phases in the southeast direction from a distance of 400 km along the profile. In contrast, data recorded in the northwest direction from reciprocal shot points in the Pannonian Basin (Figure 3 – SP 44210 and SP 29504) show energy up to offsets of more than 500 km (recorded up to the Barrandian of the Bohemian Massif to a distance of 200 km along the profile). This effect is visible not only in the SUDETES 2003 data but also in the CELEBRATION 2000 data in the same area and reflects strong damping in the upper crust of the Carpathian Flysch and in the nappes of the Inner Carpathians observed in the SE direction. A similar effect was also visible on some sections of the CELEBRATION 2000 experiment along the profiles CEL01, CEL04, and CEL05 in the area of the same tectonic unit (*Grad et al.* 2006; *Środa et al.* 2006). There are two reasons explaining this effect. First, the attenuation of energy is due to porous material of the Carpathian Foredeep and Flysch in the upper crust. When the energy penetrates deeper into the crust and mantle it can propagate well because the damping is mainly constrained to the upper crustal levels. Another reason might be the direction of the energy recording. When recorded to the SE, the energy is damped while when recorded in the opposite direction, to the NW, the energy is visible even for the upper crust as is seen in the data from SP 44140 or SP 44170 in the Carpathians (Figure 3 – SP 44140 and SP 44170, Figure 4 – SP 44170). This may thus be a response due to the direction of the northwest-ward Carpathian nappe thrusting.

4.3. Seismic Wave Field

The seismic data used for the interpretation along the S04 profile have a good signal-to-noise ratio for the *Pg* phases as the refractions from the upper crust, and the *PmP* phases as the reflections from the Moho discontinuity. The *Pn* waves refracted from the upper mantle are sometimes not well-developed and are only visible on a few record sections. Refracted waves from the sedimentary cover (*Psed* phases) are observed in the vicinity of shot points mainly in the SE in the Pannonian Basin. Other phases are complex and sometimes difficult to pick and correlate among shot points. This fact concerns intracrustal reflections P_1P, and upper mantle reflections P^IP.
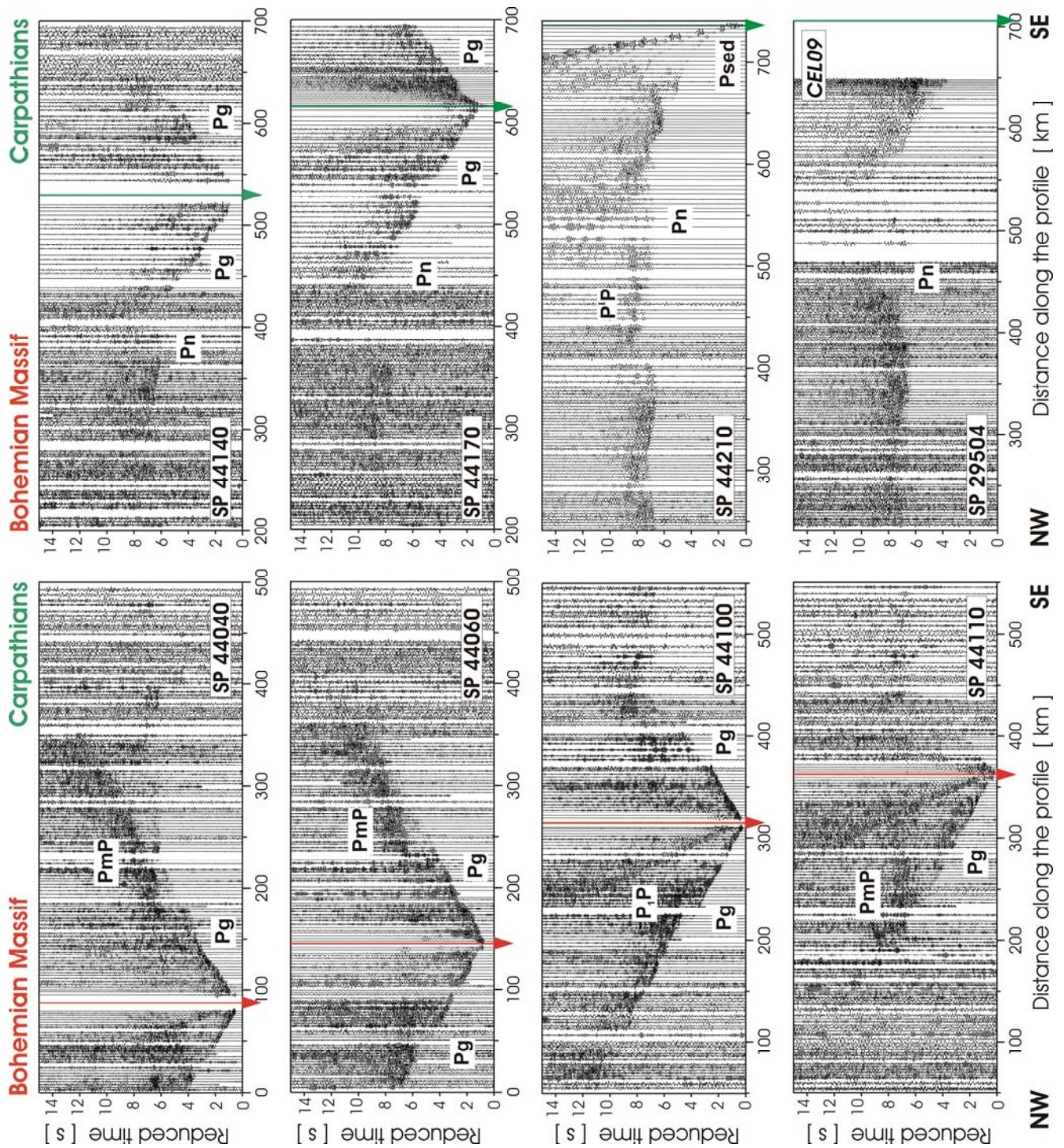
Figure 3. Examples of amplitude-normalized vertical component seismic sections from different parts of the S04 profile plotted with reduction velocity of 8 km s^{-1}. (Left) Shot points in the Bohemian Massif (red arrows). (Right) Shot points in the Carpathians (green arrows). Seismic section from SP 29504 in the Carpathians along the CEL09 profile (see Figure 2) – bottom right. Note differences in the energy propagation in the SE and NW directions, where shot points in the Bohemian Massif show an abrupt termination of energy in the southeast direction at the contact with the Carpathians (distance of 400 km along the profile). In contrary, data recorded in the northwest direction from reciprocal shot points in the Pannonian Basin show the energy up to offsets of more than 500 km (SP 44210, SP 29504).

7

Clear arrivals of refracted waves from the crystalline crust (*Pg* phase) are typically observed up to offsets of 100 – 120 km. In the area of the Bohemian Massif they show an apparent velocity of 5.8 – 6.1 km s^{-1}. Short-wavelength anomalies of the *Pg* phase reflect the existence of near surface velocity inhomogeneities. Lower apparent velocities of about 5.5 – 5.75 km s^{-1} correlate with the sedimentary basin of the Barrandian unit (the Most Basin at 145 km along the profile) and southern margins of the Bohemian Cretaceous Basin (at about 200 and 280 km along the profile) located along the NW-SE oriented Elbe Fault Zone.

In the middle part of the profile, at the contact of the Bohemian Massif with the Carpathians there are strong differences in the wave fields. The shot points in the Bohemian Massif (Figure 3 – SP 44100, 44110) show an abrupt termination of energy for all phases in the southeast direction from a distance of 400 km along the profile. In contrast, data recorded in the northwest direction from reciprocal shot points in the Pannonian Basin (Figure 3 – SP 44210 and SP 29504) show energy up to offsets of more than 500 km (recorded up to the Barrandian of the Bohemian Massif to a distance of 200 km along the profile). This effect is visible not only in the SUDETES 2003 data but also in the CELEBRATION 2000 data in the same area and reflects strong damping in the upper crust of the Carpathian Flysch and in the nappes of the Inner Carpathians observed in the SE direction. A similar effect was also visible on some sections of the CELEBRATION 2000 experiment along the profiles CEL01, CEL04, and CEL05 in the area of the same tectonic unit (*Grad et al.* 2006; *Środa et al.* 2006). There are two reasons explaining this effect. First, the attenuation of energy is due to porous material of the Carpathian Foredeep and Flysch in the upper crust. When the energy penetrates deeper into the crust and mantle it can propagate well because the damping is mainly constrained to the upper crustal levels. Another reason might be the direction of the energy recording. When recorded to the SE, the energy is damped while when recorded in the opposite direction, to the NW, the energy is visible even for the upper crust as is seen in the data from SP 44140 or SP 44170 in the Carpathians (Figure 3 – SP 44140 and SP 44170, Figure 4 – SP 44170). This may thus be a response due to the direction of the northwest-ward Carpathian nappe thrusting.

In the SE, the first arrivals at offsets smaller than 30 km display an apparent velocity of 2.5 – 5 km s^{-1} for the shot points of SP 44170, 44180, 44190, 44200 and especially SP 44210. This reflects a few kilometres thick Neogene and Quaternary sedimentary cover of the Inner Carpathians and the Pannonian Basin.

The local intracrustal reflections are not well developed along the S04 profile. If they exist they are sometimes hard to correlate between the shot points. They are mainly confined to the central part of the Bohemian Massif to a distance of 200 – 300 km along the profile and are visible in the sections from SP 44070, 44080, 44090, 44100 (Figure 3 – SP 44100, *P$_1$P* phase).

As later arrivals, we observe the *P*-wave reflections from the Moho discontinuity (*PmP* phase), usually the strongest phase detected to an overcritical distance of 200 – 250 km. In the Bohemian Massif, these *PmP* phases form relatively long coda, compared to the strong and short *PmP* pulses observed in the southern part of the profile in the Pannonian area (Figure 3 – SP 44210). In the NW, the Moho reflections are visible as strong reflections with long coda. They are sometimes difficult to correlate consistently for all shot points recording the phase, which may indicate a complex Moho structure as, e.g., in the Saxothuringian (Figure 3 – SP 44040).

At long offsets, well-developed overcritical *PmP* phases are observed up to 200 – 250 km. However, phase correlations for this group are difficult, and their travel times are represented by envelopes of high-amplitude arrivals. For SP 44020, 44040, and 44050, these phases show apparent velocities of 6.3 km s^{-1}, which indicates relatively low seismic velocities at lower crustal levels in the central part of the Bohemian Massif (Figure 6).

Only few record sections showed the Moho refractions (*Pn* phases) clear enough for confident correlation. In the Bohemian Massif, they are recorded up to a distance of 250 – 300 km (e.g., Figure 3 – SP44040, Figure 4 – SP 44020). However, they are pronounced in the Carpathians (Figure 3 – SP 44140) and especially from the shot point SP 44210 in the Pannonian Basin, where they are recorded in a northwest direction up to an offset of 530 km (Figure 3 – SP 44210).

The *Pn* phases show an apparent velocity of 8 km s^{-1} on average, especially in the Bohemian Massif. Lower apparent velocities of 7.3 km s^{-1} are detected at the north-western side of the Carpathians and indicate a NW-dipping Moho at a distance of ~400 km along the profile. In a similar way, the undulations of the *Pn* phase visible in the record section of SP 44210 (Figure 3 – SP 44210, Figure 9a) reflect the complicated Moho topography and the delay caused by deep sedimentary strata of the Carpathian Foredeep at the transition between the Bohemian Massif and the Carpathians.
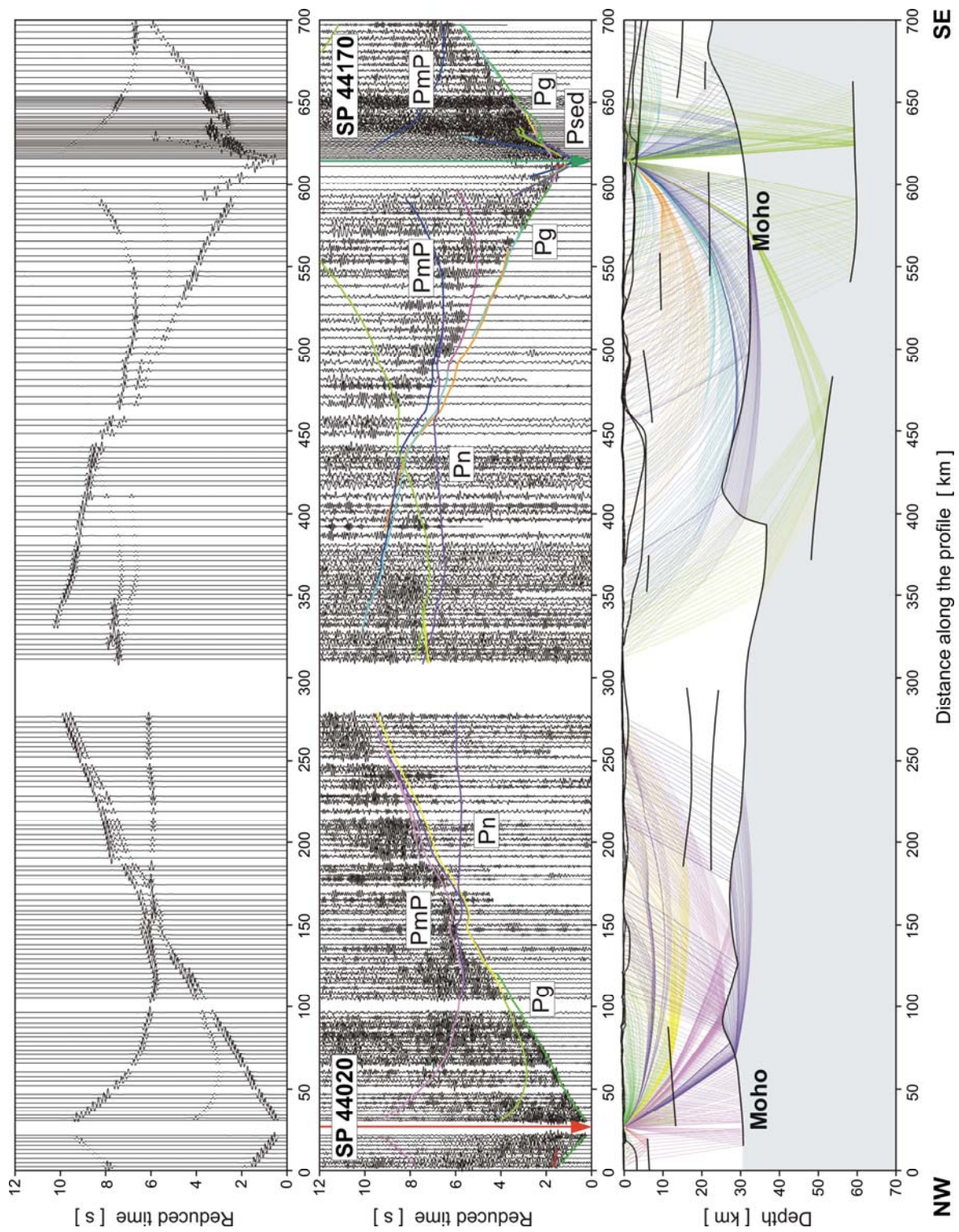
Figure 4. Examples illustrating forward modelling in the Bohemian Massif – the Saxothuringian (SP 44020) and the Carpathians (SP 44170). For both shot points: top – synthetic seismic sections, middle – amplitude normalized record sections with theoretical travel times, bottom – model and ray paths calculated for the final model (Figure 5) using the *SEIS83* ray-tracing technique. Data have been band-pass filtered from 2-15 Hz. Reduction velocity is 8 km s^{-1}. Identification of main seismic phases: *Pg*, refraction within the crust; *Pn*, refraction from the uppermost mantle; *PmP*, reflection from the Moho discontinuity.

9

The crossover distance between the crust and mantle refractions in the Bohemian Massif is 130 – 140 km, whereas in the SE, in the Pannonian Basin, the crossover distance is 110 km, which indicates a thinner crust of about 24 km in the SE compared to 30 – 32 km-thick crust in the NW.

The upper mantle reflections (P^IP phase) are visible on some record sections especially in the recordings from the Carpathians and the Pannonian Basin (Figure 9 – SP 44210) and document upper mantle reflectors in the central part of the S04 profile. Since some lithospheric phases are not very clear there is higher uncertainty in their determination.

5. Seismic Modelling of the Crust and Upper Mantle

To model the structure, we applied forward iterative travel time fitting using the ray-tracing program package *SEIS83* (*Červený & Pšenčík* 1984) supplemented by an interactive graphical interface *MODEL* (*Komminaho* 1997) and *ZPLOT* (*Zelt* 1994). The modelling involved calculation of travel times and synthetic sections to assess variations in amplitude, travel time and duration of both the refracted and reflected seismic phases from the crust and uppermost mantle. The travel times were used to derive the overall velocity structure; the synthetic sections were used for qualitative comparison of the amplitudes of synthetic and observed seismograms, and helped to constrain the velocity gradients and velocity contrasts at discontinuities. Figure 4 shows examples of the forward modelling approach for SP 44020 in the Bohemian Massif and SP 44170 in the Carpathians with calculated travel times and synthetic sections. Such a modelling approach results in a final 2-D velocity model presented in Figure 5.

5.1. Bohemian Massif
In the upper crust of the Bohemian Massif there are following variations in *Vp* velocities. Starting in the NW in the Saxothuringian, a near-surface velocity of 6 km s^{-1} at around a distance of 70 km along the profile corresponds to the Palaeozoic metamorphic rocks at the north-western flank of the Krušné Hory/Erzgebirge Mts. (NW of the Eger Rift) followed by lower near-surface velocities of 5.85 km s^{-1} for the granitoids on the other side of this mountain range. Lower velocities of 3.7 km s^{-1} at a distance of 100 – 150 km along the profile represent Permo-Carboniferous to Tertiary sedimentary successions of local basins down to a depth of 1200 m that are in accordance with the interpretation of *Kopecký* (1978) or *Mlčoch et al.* (2001). At a distance of 110 km these sedimentary successions are penetrated by Tertiary alkaline volcanic rocks of the České Středohoří Mts. with higher near-surface velocities developed at the contact of the Saxothuringian and the Barrandian along the Eger Rift (*Reicherter et al.* 2008). Further to the SE, the velocities of 3.4 km s^{-1} coincide with the embayments of the Bohemian Cretaceous Basin (200 and 280 km along the profile) alternating with the Permo-Carboniferous rocks with velocities of 5.9 – 6.0 km s^{-1} forming the basement of the Barrandian. The velocity structure reflects the tectonic setting in this area, since the profile runs along the contact of the Barrandian with the northern rim of the Moldanubian, sometimes buried beneath the Mesozoic sedimentary successions of the Bohemian Cretaceous Basin parallel with the southern strand of the Elbe Fault zone (Železné Hory Fault).

Velocities of 6.0 km s^{-1} at a distance of 320 km along the profile represent the metamorphic rocks of the northern rim of the Moldanubian exposed at the surface. They are similar to velocities modelled by *Hrubcová et al.* (2005) in the central part of the Moldanubian. Lower velocities of 5.7 – 5.8 km s^{-1} beyond 320 km along the profile correspond to the Palaeozoic metasediments of the Moravo-Silesian unit also observed along the perpendicular CEL10 profile at the eastern edge of the Bohemian Massif (*Hrubcová et al.* 2008).

Deeper parts of the crust in the Bohemian Massif exhibit a very low vertical gradient. This concerns especially the NW end, the Saxothuringian, where the crust was modelled with a *Vp* velocity of 6.1 – 6.35 km s^{-1} in a depth range of 3 – 22 km and constrained by overcritical phases of the intracrustal and Moho reflections. An intracrustal reflector in the Saxothuringian was identified at a depth of 12 km; in the Moldanubian, two mid-crustal reflectors were identified at depths of 17 and 22 km, respectively.

The velocities in the lower crust can be constrained by well-developed overcritical *PmP* phases usually observed up to 200 – 250 km offsets. In the central part of the Bohemian Massif, beneath the Barrandian and Moldanubian (SP 44020, 44040, 44050, and reciprocally SP 44090), the apparent velocities of 6.4 km s^{-1} of these phases indicate low velocities at lower crustal levels (170 – 230 km along the profile). This is documented for data of SP 44040 in Figure 6, which shows the response of a 1-D velocity model with such velocities in the lower crust (Figure 6a) and compares it with the response from a model with higher velocity in the lower crust (Figure 6b) or a model with decreased velocities in the whole crust (except the uppermost part) (Figure 6c).

The *PmP* phases are visible as strong reflections with long coda, which are sometimes hard to fit consistently for all shot points, especially in the NW part in the Saxothuringian. To explain such data, several interpretations are, to some extent, possible. First of all, we introduced a higher velocity lower crust similar to that modelled by *Hrubcová et al.* (2005) for the same unit some 70 km further to the SW. This layer with a velocity of about 7 km s^{-1} was located in a depth range of 23 – 31 km. Compared to *Hrubcová et al.* (2005), where the strongest reflector was from the top of the high-velocity lower crust, in the present study the Moho is quite dominant. Figure 7a shows the effect of such a structure in the data, where it was possible to fit the travel times but there were difficulties to fit the synthetic seismograms. This gave an indication that the velocity contrasts at the top and bottom of the high-velocity lower crust for the S04 data were not accurate. Another way to explain the data was to model the structure by a double Moho, where some parts of the profile showed reflections from the upper Moho, and some other parts from the lower one. Such an interpretation resulted in a reasonable fit in travel times for reflections but there was no good fit for the *Pn* phase. The best fit for both the *PmP*, and *Pn* phases is obtained for a simple Moho with some undulations. Such an interpretation corresponds well with the result of the perpendicular profile S01 (*Grad et al.* 2008) and gives good agreement in travel times and synthetics (Figure 7b).

In the central part of the Bohemian Massif beneath the Barrandian and Moldanubian, the Moho is modelled as a sharp discontinuity at a depth of 28 – 32 km dipping to the SE. The uppermost mantle velocities are in the range of 8.0 – 8.05 km s^{-1}.

At the SE end of the Bohemian Massif beneath the Moravo-Silesian, the lower crust shows slightly elevated velocities of 6.6 km s^{-1} compared to those in the Moldanubian with the Moho at a depth of 32 – 34 km. In the same area, the perpendicular profile CEL10 (*Hrubcová et al.* 2008) showed a gradient zone with velocities of 6.9 – 7.4 km s^{-1} over a depth range of 26 – 36 km. Figure 8 illustrates two possible interpretations of the crust-mantle transition from reciprocal shot points SP 44090 and SP 44140. It compares the *PmP* and *Pn* for a first-order Moho discontinuity with a sharp velocity contrast with phases originating from a high gradient crust-mantle transition zone (as according to *Hrubcová et al.* 2008). The data in this area are not of high quality and some phases are not visible, which allows a wider range of possible solutions. From the calculated travel times and the synthetics it is clear that both interpretations would, to some extent, satisfy the data. Though the usual approach is to try to reach an agreement between interpretations on crossing profiles, in our case we decided to keep the first order Moho discontinuity in the model. Unlike CEL10, the S04 profile is in a more favourable position with respect to the position of the tectonic units. In such a case, when two interpretations are equal in terms of uncertainty, the model of minimum structure is typically the preferred model. Nevertheless, this is a complicated tectonic area and a gradient zone as has been detected along the refraction profile CEL10 (*Hrubcová et al.* 2008) can still be a matter of debate.

5.2. Transition between the Bohemian Massif and the Carpathians

The upper crustal velocities at the transition between the Bohemian Massif and the Carpathians show pronounced lateral variations compared to the Bohemian Massif. Considerably lower velocities of 3.8 – 4.2 km s^{-1} were modelled down to a depth of 7 km in a distance range of 370 – 460 km. They correspond to the Tertiary sediments of the Outer Western Carpathians namely the Carpathian Foredeep and the Carpathian Flysch. Considering the larger distance between the nearest shot points (SP 44110 at the eastern edge of the Bohemian Massif and SP 44140 in the Carpathians, see Figure 2), this area is not well-constrained by the S04 seismic data. Thus, the velocity values modelled along the S04 profile were compared with the ones from the profiles CEL01 and CEL05 (*Grad et al.* 2006; *Środa et al.* 2006) of the CELEBRATION 2000 experiment crossing the same tectonic units. Since the data for SP 44210 in the Pannonian Basin showed a pronounced *Pn* phase visible up to an offset of 500 km, the thickness variation of the Carpathian Flysch and Foredeep sediments with lower velocities was mainly constrained by the *Pn* wave fluctuations from this shot point (Figure 9). The sedimentary thickness was also constrained by the interpretation of the seismic reflection profile 8HR (*Tomek, & Hall* 1993) and by geological information (e.g., *Vozár et al.* 1999; *Golonka & Krobicki* 2004). Figure 9b documents the effect of lower velocities of the Carpathian Foredeep and Flysch and shows a good fit of the travel times with the data for the model where lower velocities of the Carpathian Foredeep and Flysch were introduced (*Pn* phase – violent line) compared to the effect of missing sedimentary successions where travel times come too early to fit the data (marked by blue). Final results also correspond with the interpretation along the reflection profile 8HR (*Tomek, & Hall* 1993; *Hubatka & Švancara* 2002). Very low velocities of 2.2 km s^{-1} to a depth of 0.5 km at the distance of 425 km reflect Neogene to Quaternary sediments of the Vienna Basin margin.
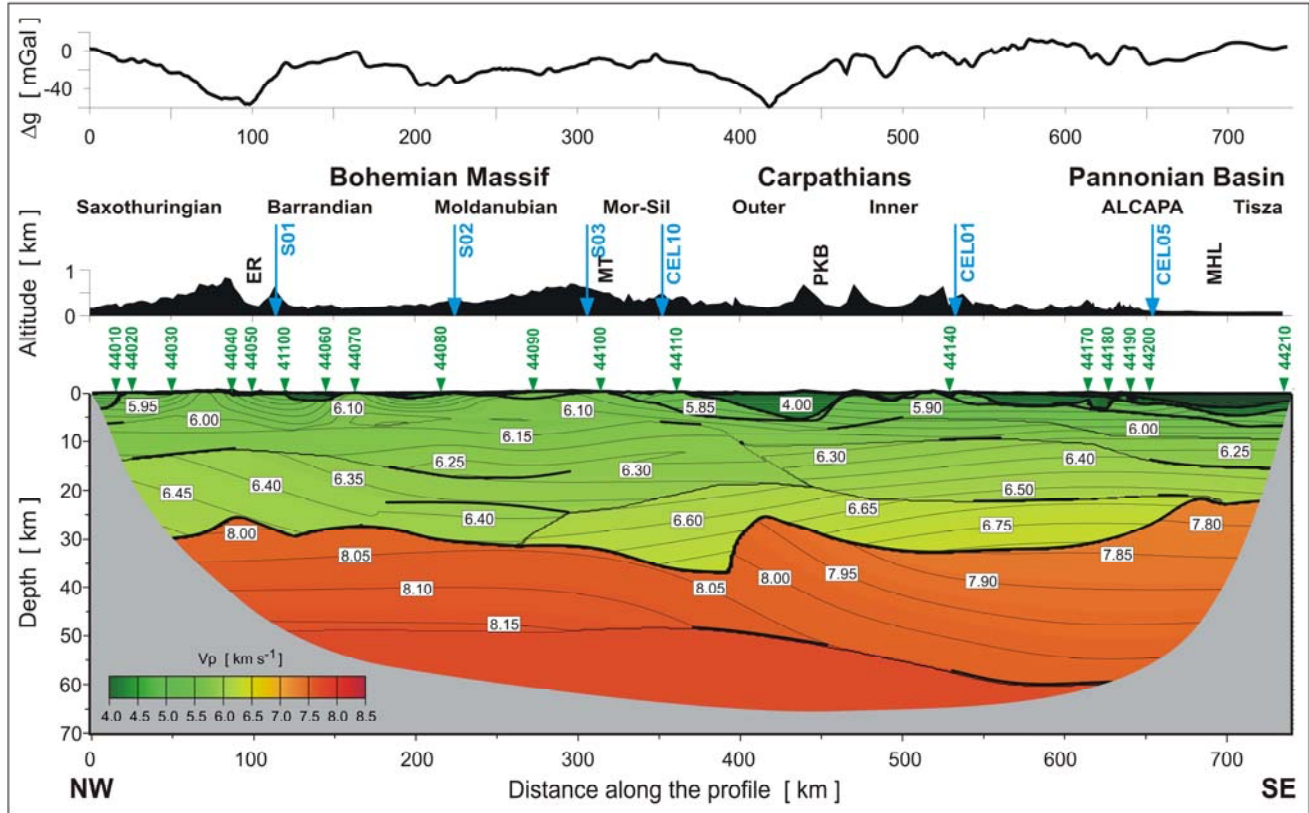
Figure 5. Two-dimensional *P*-wave velocity model for the S04 profile derived from forward ray-tracing modelling with *SEIS83* package (*Červený & Pšenčík*, 1984) with elevations and Bouguer anomaly on the top. The grey covers unconstrained parts of the model. Thick lines mark discontinuities constrained by reflections and well-constrained interfaces in the uppermost crust. Thin lines are isovelocity contours spaced at intervals of 0.05 km s^{-1}. Numbered triangles refer to shot points; blue arrows show locations of other refraction and reflection profiles. ER, Eger Rift; MT, Moldanubian Thrust; PKB, Pieniny Klippen Belt; MHL, Mid-Hungarian Line. Vertical exaggeration is 3:1.

The crust-mantle transition at the contact of the Bohemian Massif and the Carpathians shows strong lateral variations and the Moho in a depth range of 26 – 37 km. The Moho in this area is not constrained by reflections but by refractions from the upper mantle. The apparent velocity of 7.3 km s^{-1} for the *Pn* phase from SP 44140 in the Carpathians indicates a NW-dipping Moho at a distance of 390 – 415 km along the profile (see Figure 8a – SP 44140). A similar effect is visible in the data of SP 44210 where the apparent velocity of 7.3 km s^{-1} at a distance of 315 – 380 km along the profile for the *Pn* phase reflects the Moho dip to the NW in the same area. It is followed by an apparent velocity of 8.5 km s^{-1} at a distance of 210 – 290 km along the profile, which corresponds to the opposite, SE dip of the Moho at 290 – 370 km. To confirm the interpretation, Figure 9 shows the effect of the sharply dipping Moho at the contact of the Bohemian Massif with the Carpathians in contrast to the response from a model with a flat Moho. In the case of the Moho uplift and dip, the fit for *Pn* was achieved for picks at a distance of 325 – 400 km along the profile and also for strong second arrivals at a distance of 290 – 310 km (Figure 9a), which is missing in the case of a flat Moho (Figure 9b, marked by red arrows).

5.3. Western Carpathians and the Pannonian Basin

Leaving the Carpathian Foredeep and Flysch Belt, the profile continues across the Inner Carpathians. Velocities of 5.8 – 5.9 km s^{-1} further to the SE represent the core mountains composed of pre-Alpine basement and its Mesozoic sedimentary cover. At a distance of 490 and 530 km they alternate with lower velocities representing the sediments of the Pannonian Basin. Andesitic and rhyolitic rocks of the Tertiary volcanic edifices are reached at 520 – 545 km along the profile followed by volcano-sedimentary complexes to a distance of 560 km. Elevated velocities at a distance of 610 – 650 km along the profile represent the western slopes of a Tertiary volcanic complex in northern Hungary. Low velocities of 2.2 – 4.2 km s^{-1} down to a depth of 4.5 km from a distance of 650 km reflect the Neogene and Quaternary sediments of the Pannonian Basin in Hungary.
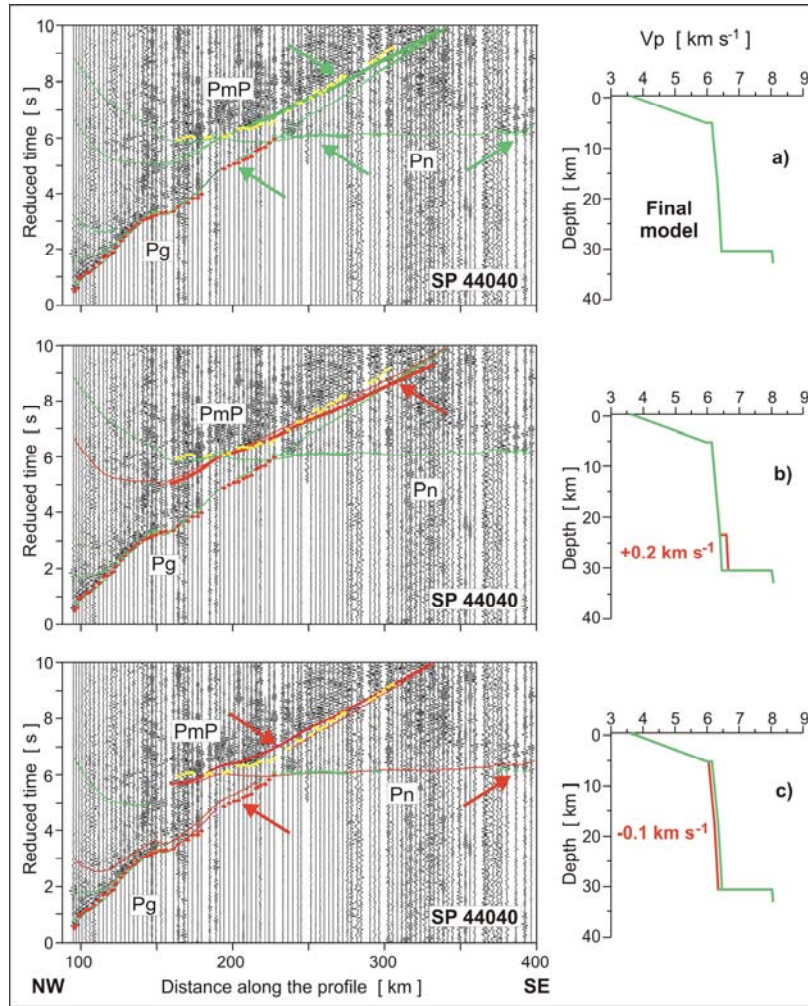
Figure 6. Seismic record sections for SP 44040 with superimposed calculated travel time curves (left) for different velocity models (right) documenting lower Vp velocities in the lower crust interpreted along the S04 profile in the Barrandian and Moldanubian (170 – 230 km along the profile). (a) Response of a velocity model as in Figure 5. Note the fit for the lower crustal, overcritical and Pn phases (see green arrows). (b) Higher velocities in the lower crust. Note a misfit for the overcritical phases (see red arrow). (c) Decreased velocities in the middle and lower crust. Note a misfit for the PmP, overcritical phases, lower crustal and Pn phases (see red arrows).

In the middle crust in the Carpathians, there were detected two isolated reflectors at the depths of 10 km and 20 km in the central part of the Carpathians. The lower crust shows velocities of 6.8 km s^{-1} and the Moho is modelled at 32 – 34 km.

Beneath the Pannonian Basin, the PmP phase is the most pronounced in terms of high amplitude and short coda. The Moho is interpreted as a first-order discontinuity at a depth of 23 km with a sharp velocity increase from 6.5 to 7.8 – 7.9 km s^{-1}. This is in agreement with other geophysical interpretations in this area (*Posgay et al.* 1981; *Bielik et al.* 2004; *Grad et al.* 2006; *Środa et al.* 2006).

Two upper mantle reflectors at the distances of 370 – 460 km and 530 – 630 km along the profile are visible at the depth of 50 – 60 km (Figure 3 – SP 44100, 44140, 44210). They are dipping from the eastern edge of the Bohemian Massif to the central part of the Carpathians. Since some lithospheric phases constraining it are not very clear there is a higher uncertainty in its determination. Velocities beneath this reflector (8.3 km s^{-1}) have even higher uncertainty because there is no reciprocity and they are only constrained by the data of SP 44210.
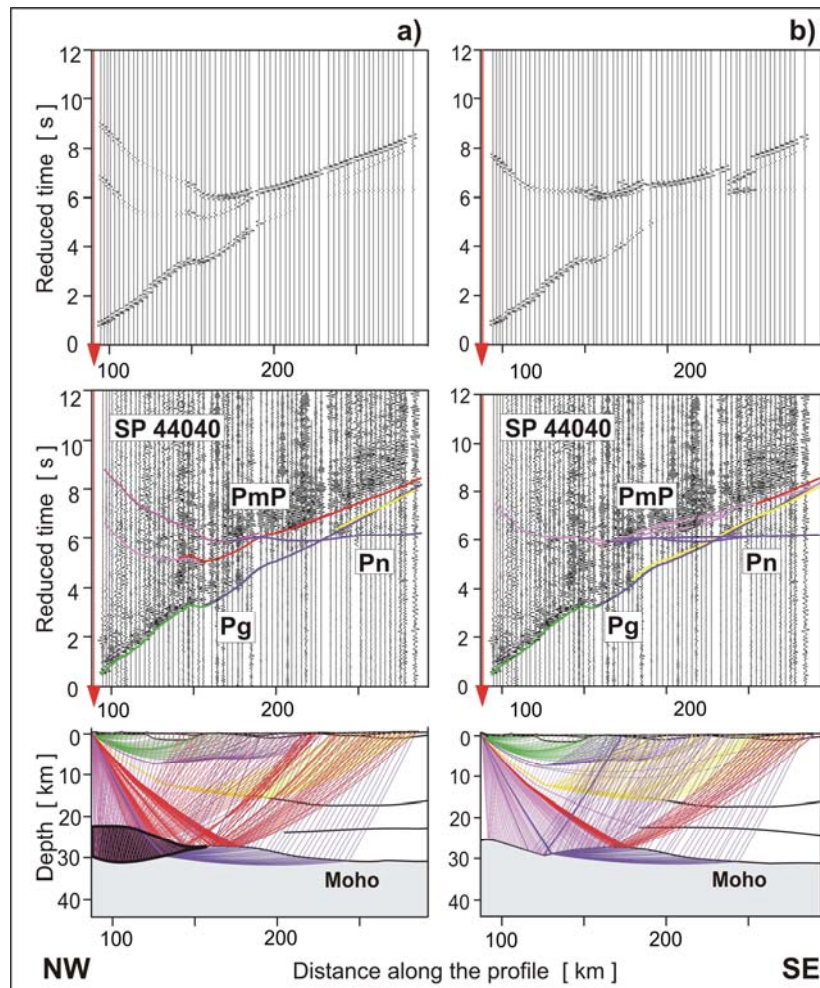
Figure 7. Forward modelling of the lower crust in the Saxothuringian – SP 44040. (a) High velocity lower crust. (b) Final model as in Figure 5. For each part of the figure: top – synthetic seismic sections, middle – amplitude normalized record sections with theoretical travel times, bottom – model and ray paths. Data have been band-pass filtered from 2-15 Hz. Reduction velocity is 8 km s^{-1}. Identification of seismic phases as in Figure 4. High velocity lower crust is marked in brown. Note reflections from the top of the lower crust visible in the synthetic seismic section and not corresponding with the data in (a) compared to a good fit of data with the synthetic section in (b).

6. Analysis of Accuracy, Resolution and Uncertainties

Modelling errors result from a combination of several factors: data timing errors, misidentification of seismic phases, travel time picking, inaccuracy of modelling (misfit between data and modelled travel times) and 2-D geometry of the experiment, not accounting for 3-D effects or anisotropy. Some errors are subjective, introduced by the interpreter during phase correlation, and are not possible to quantify. Their magnitude decreases with increasing quality and quantity of data. Due to the subjective errors, it is not possible to produce a full and systematic error analysis. In this study we attempt to evaluate the errors resulting from picking accuracy and from the misfit between the model and the data. Also, in the process of modelling, the limitations of ray theory must be kept in mind. In addition, two-dimensional modelling does not take into account out-of-plane refracted and reflected arrivals, which must have occurred particularly in such a structurally complex area and at the contacts of several units.

In the interpreted data set, the major phases were correlated with considerable confidence, increased by comparisons of phases picked independently by different interpreters and with the help of reciprocity checking. The following criteria were used to decide whether a given phase can be used for constraining the model: the signal-to-noise ratio high enough to isolate the phase from the noise as series of pulses on neighbouring seismograms, the continuity of the group of pulses over some distance interval and the phase's apparent velocity, which should roughly fit the range of plausible

14

crust/mantle velocities. The important test for credibility of the phases, which significantly reduces the non-uniqueness of the phase identification, was the reciprocity checking: a phase that could be picked consistently (i.e. with the same travel time at the reciprocal shot location) for several shot points was assumed to represent a major structure extending over considerable part of the model and was included in modelling. The phases that could not pass the reciprocity test were not used for modelling. This was mostly the case of short groups of second arrivals with average amplitude, representing most likely reflections (possibly side-reflections) or diffractions from local, relatively small-scale, anomalies or discontinuities. The most credible phases were usually the *Pg* and *Pn* as the first arrivals, characterized by high signal-to-noise ratio. Though, in some areas they were not visible (mainly the *Pn* phase). In the second arrivals, the *PmP* phase was the easiest to correlate due to its high amplitude. Though, for several shot points it could not be reliably correlated reciprocally due to a low signal-to-noise ratio and scatter of its onsets. The mantle phases (*Pn* and *P^{I}P*) from SP 44210 were used for modelling even if they could not be confirmed by reciprocity test – their very high amplitude due to a large charge give the excellent data to confidently model the abrupt changes in Moho topography and thickness of the Carpathians sedimentary foredeep.

The picking accuracy was usually about ±0.05 – 0.1 s for the Pg phases (smaller especially for the near-offset arrivals) and about ±0.1 – 0.2 s for the reflected phases (*PmP*, midcrustal reflections) and the *Pn*. The calculated travel times fit the observed ones with an accuracy for both refracted and reflected phases of ±0.2 s on average. In the ray tracing modelling, we analyze travel time curves rather than single arrivals and in such cases, typical velocity errors were in the range of 0.1 km s^{-1} and errors in the boundary depth determinations were of the order of 1 km. However, in complicated or poorly constrained parts of the model, they might increase up to 0.2 km s^{-1} and 2 km, respectively. In addition, synthetic seismograms generally showed good qualitative agreement with the relative amplitudes of the observed refracted and reflected phases. Figure 10 presents travel time residuals, as well as diagrams of ray coverage and observed reflections along modelled seismic discontinuities. The average of the residuals is close to zero, which means that there is no systematic deviation of the model parameters with respect to the data.

7. Gravity

Following the derivation of the seismic velocity structure, we used gravity modelling to test the seismic model and to obtain additional geophysical constraints on the crustal structure and composition. In a first approximation we converted the *P*-wave velocity model (Figure 5) into densities using the velocity-density relation of *Christensen & Mooney* (1995) for crustal and upper mantle velocities of 6 – 8 km s^{-1} and *Ludwig* (1971) for sedimentary velocities. This resulted in an initial density model. Using the 2-D modelling software GRDGRAVITY developed by *I. Trinks* (internet freeware code), we compared the gravity effect of this initial density model with the Bouguer anomalies (*Bielik et al.* 2006) along the profile. Then we modified densities in the model where needed by the trial-and-error approach in order to obtain a better fit to the corresponding experimental gravity data. The aim was not to obtain a detailed density model but to test the reasonability of the seismic velocities.

Figure 11 shows the observed Bouguer anomaly together with gravity responses of the initial and final density models. From the response of the initial model we can see that the most prominent discrepancies (about 50 mGal) occur in the Saxothuringian in a distance range of 60 – 120 km along the profile and at the contact of the Bohemian Massif with the Carpathian Flysch Belt in a distance range of 380 – 440 km. They are in places where the negative Bouguer anomaly reaches a value of -60 mGal.

The gravity minimum in the Saxothuringian coincides with the location of low density granites in the eastern part of the Krušné Hory/Erzbegirge Mts. (NW of the Eger Rift). There, the differences between the granitoids and orthogneisses and neighbouring metamorphic rocks are more pronounced in densities (about 0.1 g cm^{-3}) than in seismic velocities. A similar effect was also encountered on the CEL09 profile (*Hrubcová et al.* 2005) in the Karlovy Vary area, where such a discrepancy was due to a larger density difference between the Karlovy Vary granites and the surrounding rocks than estimated from the seismic velocity-density relationship. To get the fit with the observed Bouguer data, the Saxothuringian anomaly was modelled by lower densities of about 2.60 – 2.65 g cm^{-3} to a depth of 8 –12 km, which is consistent with the results of *Behr et al.* (1994) along the MVE-90 profile. It is also in agreement with the interpretation of *Blecha et al.* (2009) who modelled the same densities and depths for the gravity minimum of the Karlovy Vary pluton further to the SW.
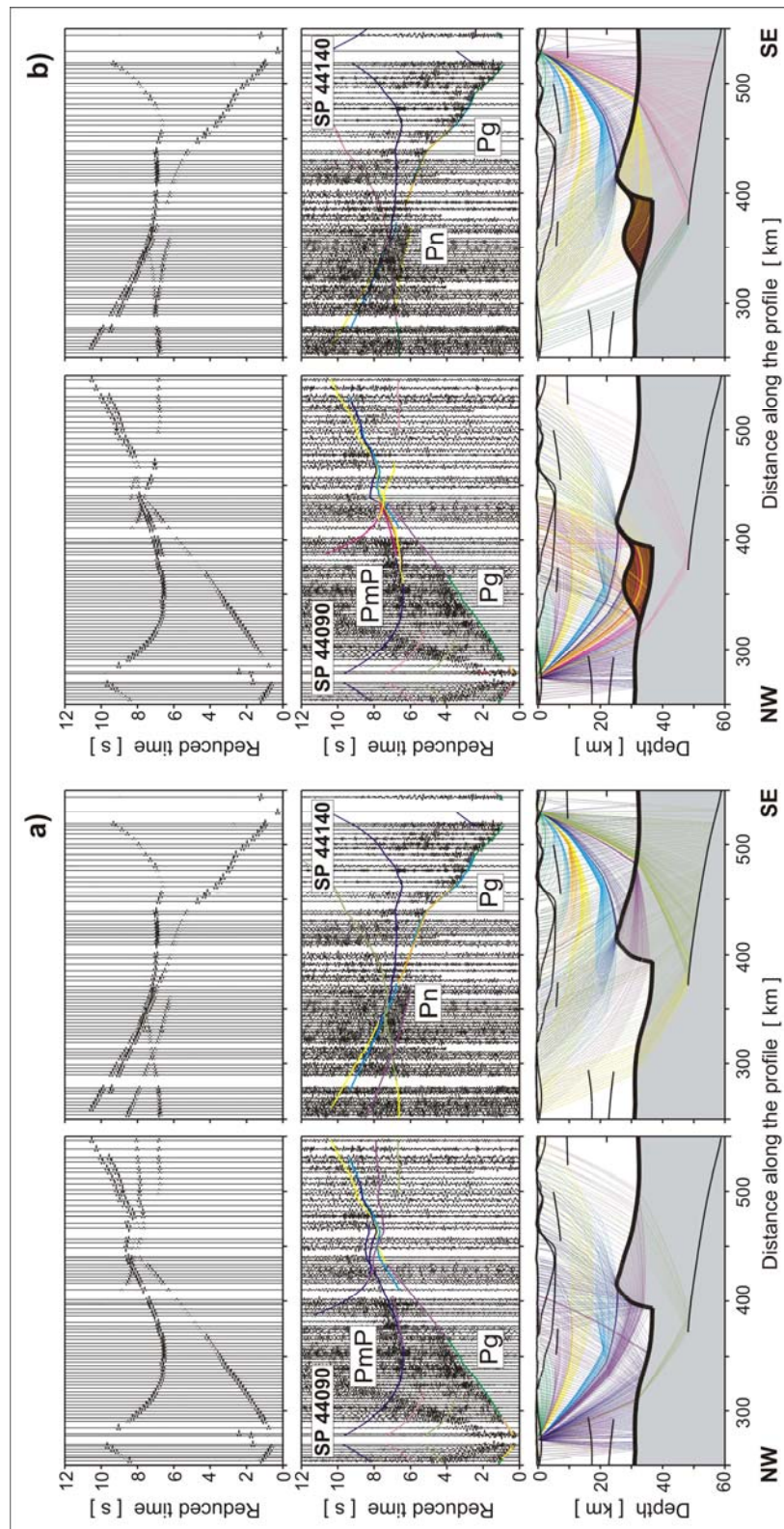
Figure 8. Forward modelling for reciprocal shot points SP 44090 and 44140 illustrating the character of the crust-mantle transition in the Moravo-Silesian. (a) Velocity contrast at the Moho as in Figure 5. (b) High gradient crust-mantle transition zone according to the CEL10 interpretation (*Hrubcová et al.* 2008). For each part of the figure: top – synthetic seismic sections, middle – amplitude normalized record sections with theoretical travel times, bottom – model and ray paths. Data have been band-pass filtered from 2-15 Hz. Reduction velocity is 8 km s^{-1}. High velocity lower crust is marked in brown.

The other pronounced gravity low in the Carpathians is attributed to low-density foredeep and flysch sediments. To achieve the fit in this area it was necessary to introduce lower densities of 2.45 g cm^{-3} than those, which ensued from the velocity-to-density conversion. The discrepancy between the seismic and gravity models can be seen in several factors. Due to the insufficient amount of seismic refraction data as well as seismic attenuation in porous sedimentary rocks, the resolution of the seismic model in the Carpathian Flysch Belt is lower than in some other parts of the profile. Another contributing factor might be a 3-D influence of the Carpathian low anomaly, not taken into account by the 2-D velocity modelling. However, the aim was to test the 2-D velocity results, therefore we confined the gravity modelling to two dimensions. The local gravity minimum at a distance of 425 km was explained with densities of 2.2 g cm^{-3} and coincides with light Neogene to Quaternary sedimentary rocks of the Vienna basin promontory.
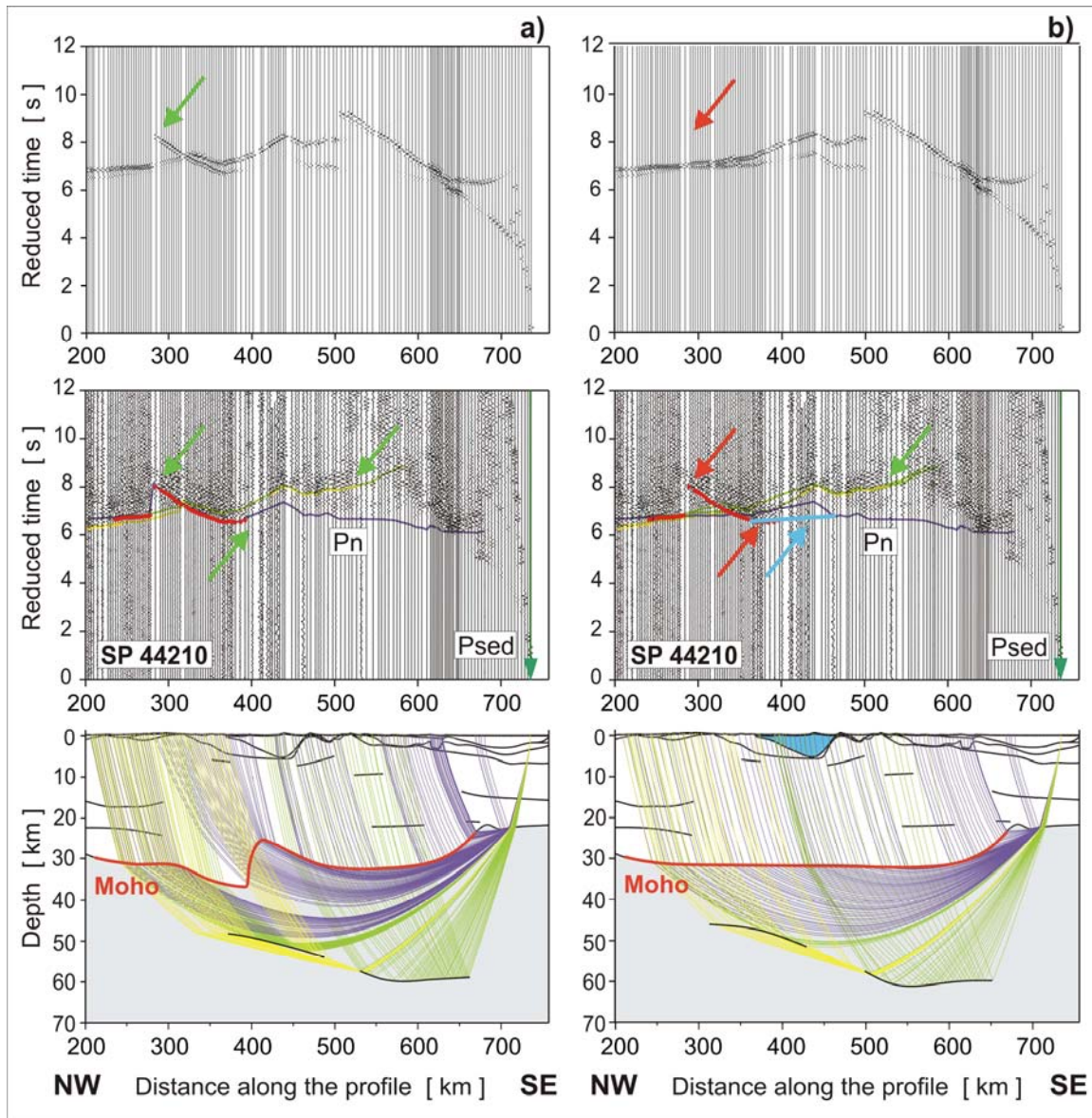

Figure 9. Forward modelling for SP 44210 documenting the Moho at the transition between the Bohemian Massif and the Carpathians. (a) dipping Moho, (b) flat Moho. For each part of the figure: top – synthetic seismic sections, middle – amplitude normalized record sections with theoretical travel times, bottom – model and ray paths. Data have been band-pass filtered from 2-15 Hz. Reduction velocity is 8 km s^{-1}. *Pn*, refraction from the uppermost mantle (violent line). Green arrows mark the Moho effect response. Note good fit for *Pn* and strong second arrivals with picks (marked in red in the middle panel) in the case of the dipping Moho (a) compared to missing response (marked by red arrows) for picks (marked in red in the middle panel) in the case of a flat Moho (b). Note in case (b) good fit of travel times with the data where lower velocities in the Carpathian Flysch were introduced compared to the effect of the model without these velocities that come too early to fit the data (marked by blue line and blue arrow).

17

Other smaller corrections (positive and negative) were made in some other parts of the profile mainly in the upper crust. They explain the anomalies usually caused by numerous granitic, mafic and volcanic rocks occurring along the profile or in its close vicinity and producing gravity effects not accounted for by the velocity modelling. The local gravity lows along the profile were explained by small sedimentary Neogene to Quaternary basins not detected by the refraction seismic data as e.g., the very pronounced anomaly at a distance of 95 km representing the Most sedimentary Basin at the eastern margin of the Krušné Hory/Erzgebirge Mts.
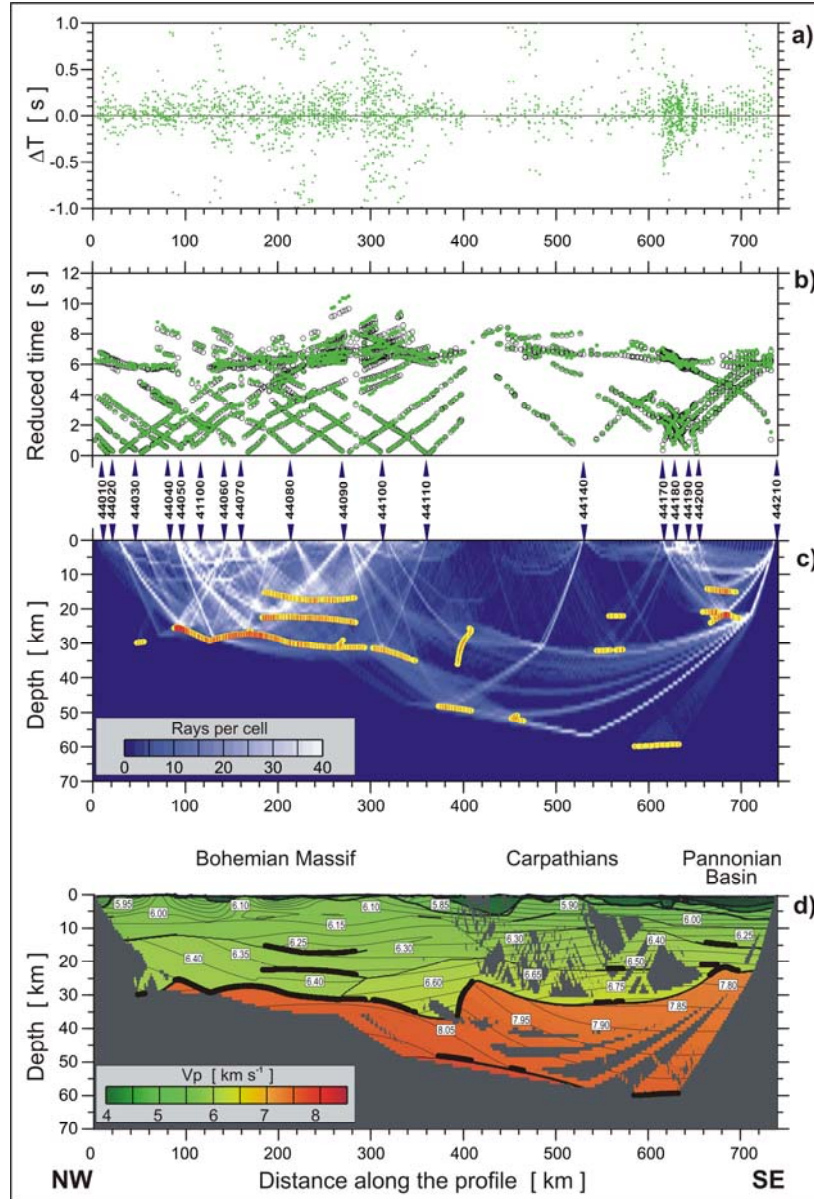

Figure 10. *P*-wave velocity model for the S04 profile (as in Figure 5) with superimposed rays. (a) Travel time residuals. (b) Misfit between the observed (green dots) and calculated (black circles) travel times. (c) Ray coverage and observed reflecting elements along modelled seismic discontinuities. (d) Model with rays.

During gravity modelling different seismic models of the lower crust and Moho were also tested for their gravity effects. In such a way, the high-velocity lower crust in the Saxothuringian revealed a misfit in the gravity data, which was another indication not to promote such a structure in the model. At the eastern side of the Bohemian Massif, the lower crust can be modelled by slightly higher densities than those which ensue from seismic velocities but not that high so as to correspond to the high-velocity zone along the CEL10 profile in the Moravo-Silesian. At the transition between the

Bohemian Massif and the Carpathians, the gravity modelling does not constrain our seismic interpretations, because there is neither an evidence for the Moho dip nor an evidence for a flat Moho and both results show a similar gravity response (Figure 11). However, we choose the model with the dipping Moho, since it fits the seismic data much better with a very good fit for *Pn* and later arrivalsand since the seismic interpretation excludes a flat Moho (see Figure 9 – SP 44210). The Pannonian gravity high results from significant shallowing of the Moho to about 25 – 30 km and corresponds with seismic interpretations as well as the results of *Bielik et al.* (2004).
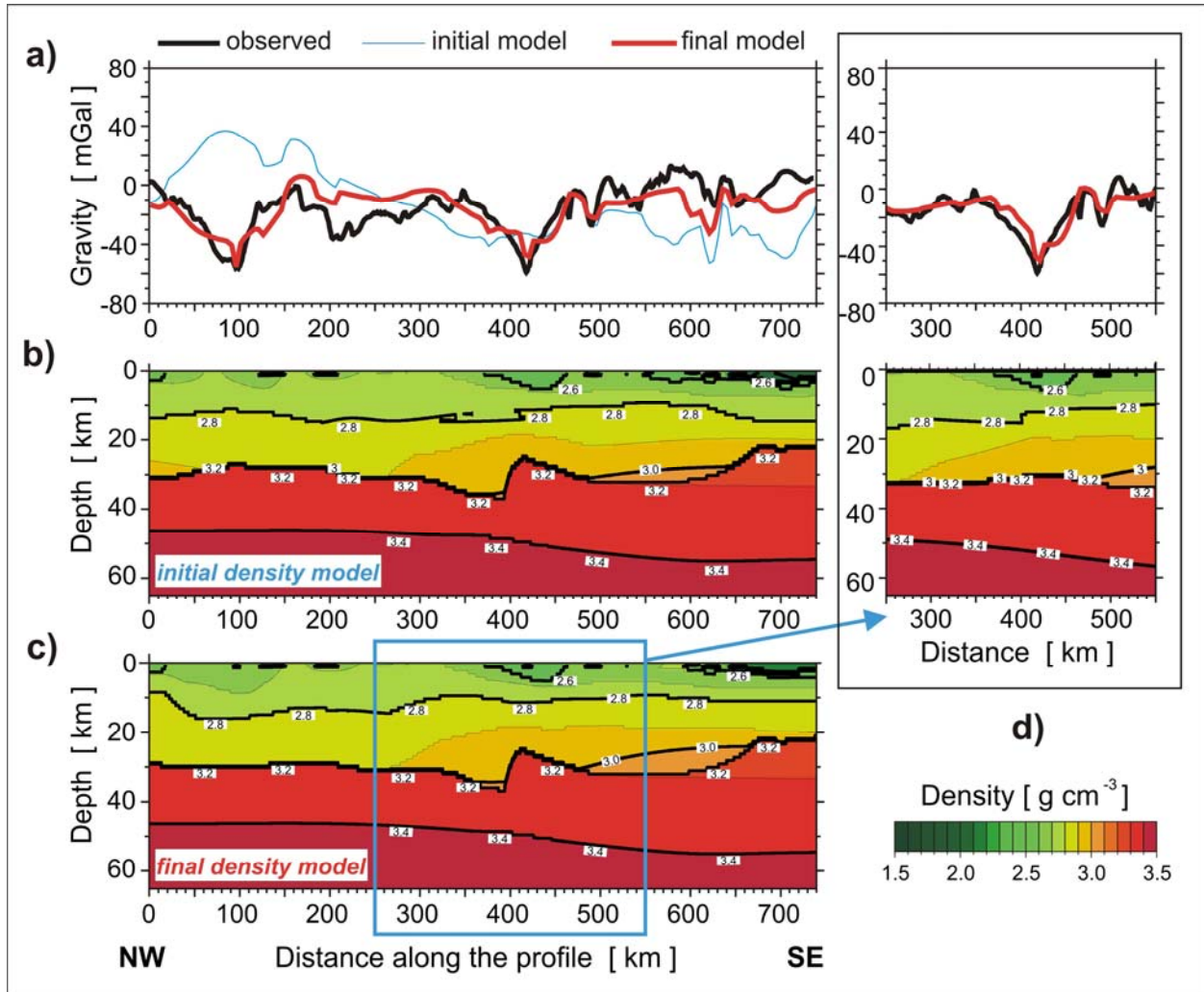

Figure 11. Gravity modelling. (a) Bouguer anomaly (black line), calculated gravity effect from initial density model (blue line) and from final density model (red line). (b) Initial gravity model converted from seismic velocity model in Figure 5. (c) Final gravity model. (d) Insert showing the gravity effect of a flat Moho at the contact of the Bohemian Massif with the Carpathians.

8. Discussion of Geological and Tectonic Implications

In the following discussion, we propose a general tectonic/geological interpretation for the velocity models along the S04 profile. We discuss these units and their contacts based on the *Pg* velocity distribution, character of the lower crust and Moho topography, surface geology and results from other profiles, especially CEL09, CEL10, S01, S02, S03, 8HR and MT-15. Above, we show the additional constraint on the crustal structure given by gravity modelling. We are aware that due to the ambiguity of modelling and data there can be several possible interpretations but because of all the mentioned reasons we believe that our proposed interpretation gives one of the most plausible solutions. In our interpretation we concentrate on velocity variations along the profile. Azimuthal anisotropic studies are a matter of other investigations (e.g., *Růžek et al.* 2003; *Vavryčuk et al.* 2004).
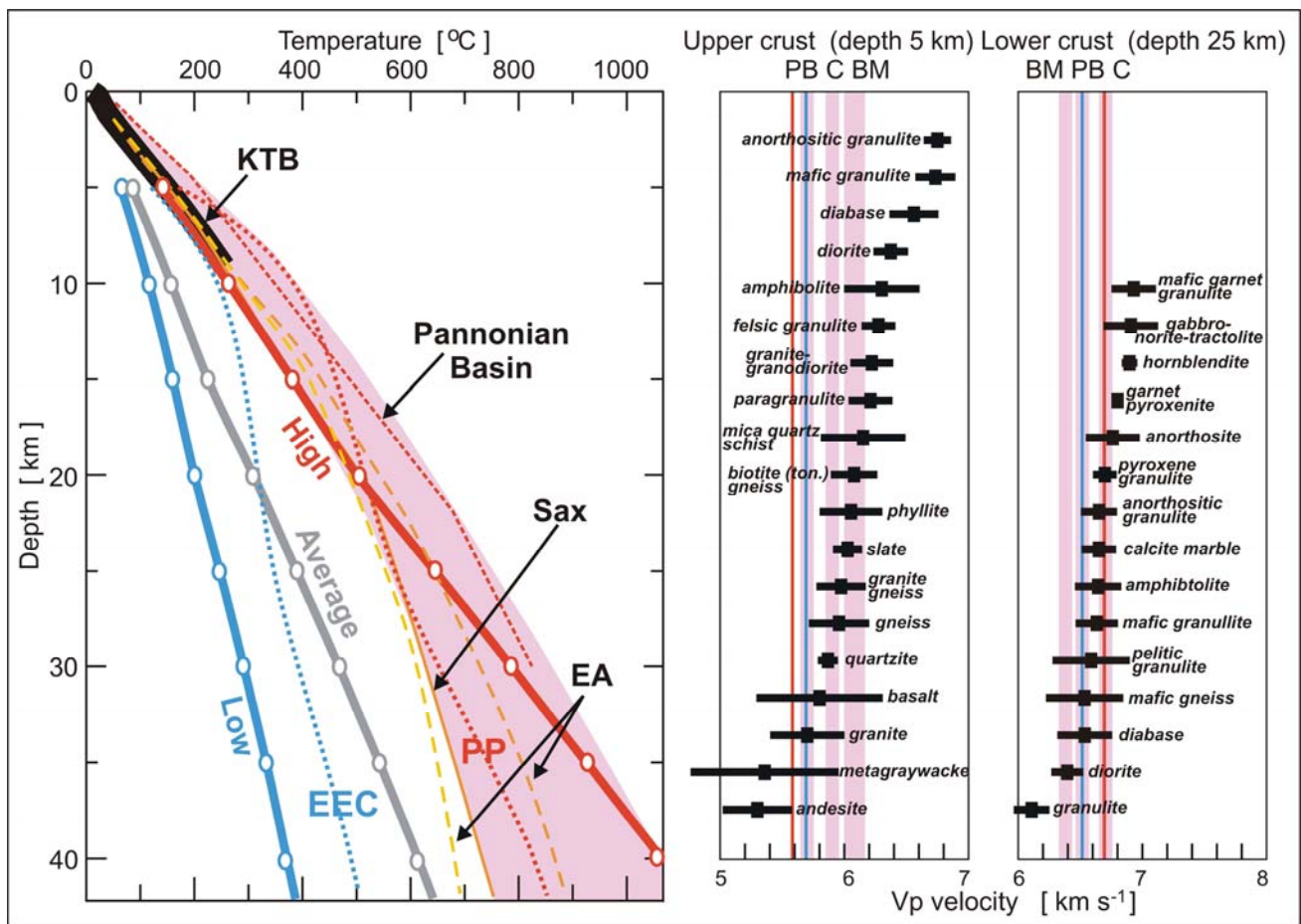
Figure 12. (Left) Geothermal gradients. (Right) Comparison of the *Vp* velocities observed along the S04 profile with laboratory data.
(Left) As a reference, temperature-depth curves are shown for low, average and high heat flow regimes (thick blue, grey and red lines with circles) according to *Christensen & Mooney* (1995). For comparison, temperature-depth curves are shown for the area of the S04 profile, including the Saxothuringian (Sax) (*Čermák* 1995), Palaeozoic Platform (PP) in southwest Poland (*Majorowicz* 1976) and Pannonian Basin (PB) (*Posgay et al.*, 2001), as well as for neighbouring areas, including "hot" Eastern Alps (EA) (*Vosteen et al.,* 2003), and "cold" East European Craton (EEC) in northeast Poland (*Majorowicz* 1976). Thick black line extending to about 10 km shows measured temperature in KTB deep borehole (*Emmermann & Lauterjung* 1997). Shaded pink area represents "hot" crust for the area close to the S04 profile.
(Right) Laboratory data for various rock assemblages (*Christensen & Mooney* 1995; *Christensen* 1974; *Mueller* 1995; *Weiss et al.* 1999; *Grégoire et al.* 2001) are shown for the high temperature model in the crust at 5 km and 25 km depth and plotted as black boxes with black lines representing their error estimates. Anisotropy is not considered. Shaded vertical pink bars represent modelled *Vp* values beneath the S04 profile for the upper crust – 6.0-6.15 km s^{-1} for the Bohemian Massif (BM), 5.9 km s^{-1} for the Carpathians (C) and 5.7 km s^{-1} for the Pannonian Basin (PB), and for the lower crust – 6.4 km s^{-1} for the Bohemian Massif, 6.7 km s^{-1} for the Carpathians and 6.5 km s^{-1} for the Pannonian Basin. The bars are shown with estimated uncertainty of the velocity values of ±0.05 km s^{-1}. Red lines represent average velocities for extended crust (5.59 ± 0.88 km s^{-1} for 5 km depth, 6.69 ± 0.30 km s^{-1} for 25 km depth), while blue lines represent velocities for orogens (5.69 ± 0.67 km s^{-1} for 5 km depth, 6.53 ± 0.39 km s^{-1} for 25 km depth) (*Christensen and Mooney* 1995).

8.1. Crustal Lithology

Interpretation of crustal lithologies along the S04 profile is based on the *P*-wave velocities obtained by 2-D ray tracing modelling. The most plausible lithologies along the profile are inferred from the modelled *Vp* values and compared with global (*Christensen & Mooney* 1995; *Weiss et al.* 1999) and regional (*Christensen* 1974; *Mueller* 1995; *Grégoire et al.* 2001) laboratory data for various crustal rock assemblages. The left part of Figure 12 shows the temperature-depth curves for the low, average and high heat flow thermal regimes according to *Christensen & Mooney* (1995). In the crust of the S04 profile, the published temperature-depth curves for the Saxothuringian (*Čermák* 1995), the Palaeozoic Platform in southwest Poland (*Majorowicz* 1976), the Eastern Alps (*Vosteen et al.* 2003), and the Pannonian Basin (*Posgay et al.* 2001) lie close to the high heat flow curve. This curve also fits the temperatures measured directly in the KTB borehole

20

in the Saxothuringian to a depth of about 10 km (*Emmermann & Lauterjung* 1997). On the other hand, much lower temperatures are observed for the "cold" East European Craton in northeast Poland (*Majorowicz* 1976).

The right part of Figure 12 shows lithological candidates for a high temperature regime in the upper (5 km depth) and lower (25 km depth) crust according to *Christensen & Mooney* (1995) and *Mueller* (1995), where anisotropy has not been taken into account. The original data of *Christensen* (1974), *Weiss et al.* (1999) and *Grégoire et al.* (2001) were corrected downward by 0.3 km s^{-1} to adjust for *in situ* temperature conditions. Various rock assemblages are plotted as black boxes with their error estimates. Shaded vertical pink bars represent modelled *Vp* values beneath the S04 profile: upper crust – from 6.0 to 6.15 km s^{-1} for the Bohemian Massif (BM), 5.9 km s^{-1} for the Carpathians (C) and 5.7 km s^{-1} for the Pannonian Basin (PB); lower crust – 6.4 km s^{-1} for the Bohemian Massif, 6.7 km s^{-1} for the Carpathians and 6.5 km s^{-1} for the Pannonian Basin. For comparison, the average values according to *Christensen & Mooney* (1995) are shown, where red lines represent velocities for extended crust (5.59 ± 0.88 km s^{-1} for 5 km depth, 6.69 ± 0.30 km s^{-1} for 25 km depth), and blue lines represent velocities for orogens (5.69 ± 0.67 km s^{-1} for 5 km depth, 6.53 ± 0.39 km s^{-1} for 25 km depth). The velocities in the Pannonian Basin seem to fit the values for orogens at both 5 and 25 km depth, while those in the Carpathians seem to correspond more to the values for the extended crust. *McCann* (2008b) points that despite being a part of the Alpine-Carpathian Orogen, the Western Carpathians are different from other orogens such as the Alps. The Carpathians underwent diverse tectonic evolution where also an orogenic root typical for the Eastern Alps (*Brückl et al.* 2007) is missing. Our result can, to some extent, reflect this diversity. Also, it should be noted that the values of *Christensen & Mooney* (1995) represent averages of a broad range of velocities for given types of crust.

The upper crystalline crust of the Bohemian Massif (at a depth of 5 km) is characterized by velocities from 6.0 to 6.3 km s^{-1}, which are typical of basement rocks of Cadomian age in the Barrandian unit and the mid-Palaeozoic Variscan granitoids and gneisses in the Moldanubian unit exposed in some places at the surface. The Cadomian basement is also present in the Saxothuringian zone consisting of volcano-sedimentary complexes overlain by Palaeozoic strata. The lower crust of the Bohemian Massif (at a depth from 15 to 30 km) shows velocities of 6.4 – 6.5 km s^{-1}. These relatively low values reflect a continuing predominance of felsic lithologies towards the base of the crust. Similar velocities were obtained along the MVE-90 reflection profile, where they were interpreted as related to gneisses with varying content of metabasites (or mafic gneisses) (see, *Behr et al.* 1994). Pelitic granulites can represent other candidates for the major rock components in the lower crust. Restites from the huge granite bodies of the upper crust are present in the middle-to-lower crust of the Saxothuringian zone and would be in agreement with the modelled velocities. There seems to be no major imprint of the Cenozoic magmatism in the overall velocity structure in the area of the Eger Rift (České Středohoří).

Lower upper crustal velocities of 4.2 – 4.3 km s^{-1} (depth of 5 km) at the transition between the Bohemian Massif and the Carpathians reflect the sedimentary infill of the Carpathian Foredeep as the eastward prolongation of the East Alpine Molasse basin and forming a characteristic clastic wedge thinning towards the foreland. It is followed by rocks of the Carpathian Flysch Belt, composed exclusively of Jurassic to Miocene sediments such as schists, sandstones and their conglomerates that were scraped off the subducted basement of the Carpathian embayment. In the Carpathians, upper crustal velocities of 5.9 km s^{-1} (depth of 5 km) represent various pre-Tertiary units and the unconformable Cenozoic volcanic complexes (rhyolites to dacites) alternating with lower velocities of the sedimentary complexes at the surface (*McCann* 2008b).

Lower crustal *P*-wave velocities of 6.6 to 6.7 km s^{-1} beneath the SE rim of the Bohemian Massif (Moldanubian/Moravo-Silesian) are significantly higher than those further to the northwest indicating slightly more mafic composition and potentially different tectonic origin. The lower crust beneath the Carpathians is characterized by *P*-wave velocities from 6.7 to 6.8 km s^{-1} indicating a more mafic composition than that in the Bohemian Massif (amphibolites, mafic granulites) though the difference is not very high. Lower crustal velocities of 6.5 km s^{-1} are typical for the Pannonian Basin. There, the lower crust might consist of various types of granulites as it is evident from xenoliths, which were brought to the surface by Cenozoic volcanism (e.g., *Kempton et al.* 1997; *Embey-Isztin et al.* 2003) though their composition indicate a more mafic lithology than shown by the S04 P-wave velocities in this area .

Low velocities in the Bohemian Massif lower crust (the Saxothuringian, Teplá-Barrandian and Moldanubian zones) are in agreement with observations all over the Variscan orogenic belt up to the Central Iberian System (*Villaseca et al.* 1999) and maybe even across the Atlantic to the Southern Appalachians (*Taylor & Toksöz* 1982). Xenolith studies (e.g., *Downes* 1993; *Wedepohl* 1995; *Villaseca et al.* 1999) indicate that the lower crust of the Variscan internides might be actually dominated by felsic rock types (felsic/metapelitic granulites, charnockites, restites).

The Moravo-Silesian Zone is more or less equivalent to the Mesozoic Bohemian-Tethyan continental margin. This zone is characterized in its eastern part by strong total magnetic anomalies (*Lenhardt et al.* 2007) which are not too different from anomalies along present-day continental margins. Slightly increased velocities in comparison to the central Bohemian Massif might indicate that the lower crust of the former passive margin was overprinted/modified during the Mesozoic rifting.
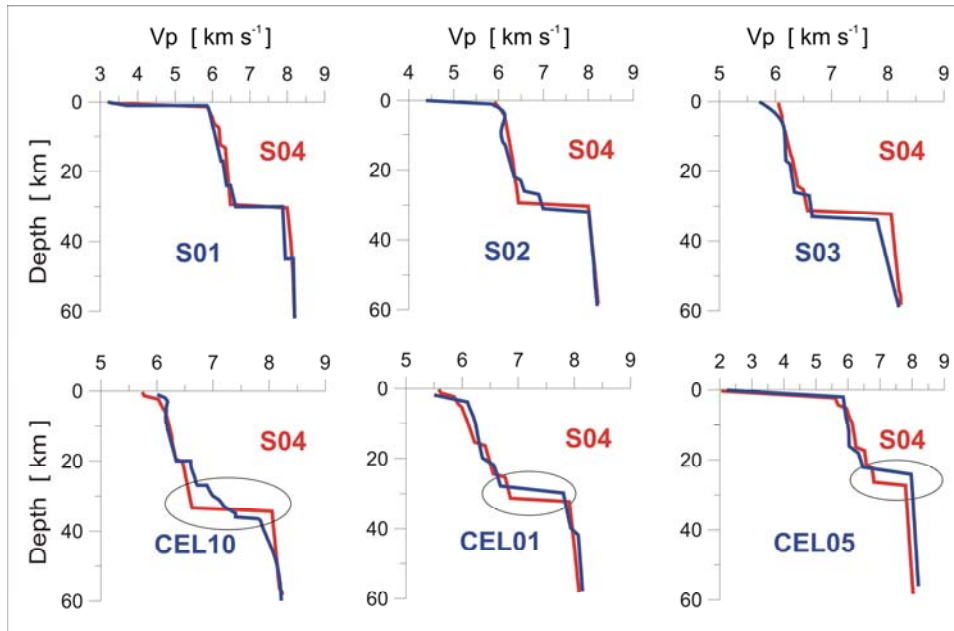

Figure 13. Velocity-depth models from the S04 profile (red lines) with velocity-depth models at intersections with the S01, S02, S03, CEL10, CEL01 and CEL05 profiles (blue lines) (*Grad et al.* 2008; *Majdański et al.* 2006; *Hrubcová et al.* 2008; *Šroda et al.* 2006; *Grad et al.* 2006). Ellipses mark parts of the models discussed in detail in the text.

8.2. Comparison with other refraction lines

One way to decrease the ambiguity of the interpretation was to compare model velocities with other results in the area, especially when there are models for other refraction profiles as is the case for the S04 line (Figure 2). Figure 13 shows the velocity-depth profiles extracted from crossing models (in blue) and compare them to those for S04 (in red) at the intersections. In general, *P*-wave velocities from the S04 model agree with those from the other models. A discrepancy is visible in the Moravo-Silesian where the S04 profile images the Moho discontinuity with a velocity increase from 6.7 to 8.0 km s^{-1} at a depth of 33 km compared to a broad high gradient zone with no sharp discontinuities over a depth range from 26 to 36 km (velocities of 6.9 – 7.4 km s^{-1}) modelled along the CEL10 profile. In the Carpathians, the Moho depth modelled along the S04 profile is slightly deeper (32 and 28 km) than in the case of the crossing profiles CEL01 and CEL05 (30 and 25 km). A final tectonic sketch based on the geophysical modelling along the S04 profile is shown in Figure 14.

8.3. Geology and tectonic development of the Bohemian Massif

The Saxothuringian shows a near-surface velocity of 6 km s^{-1} representing the Palaeozoic metamorphic rocks at the north-western flank of the Krušné Hory/Erzgebirge Mts. (NW of the Eger Rift). Lower velocities of 5.85 km s^{-1} in the upper crust at the contact of the Saxothuringian and Barrandian correspond to the gravity minimum of the low density granites. The contrast between the granites and neighbouring rocks is more pronounced in densities than in seismic velocities and according to the gravity modelling the granites are seated 8-12 km deeper than anticipated from the seismic interpretation. Such a result is in agreement with the interpretation of *Blecha et al.* (2009) who modelled the same densities and depths for the gravity minimum of the Karlovy Vary Pluton further to the SW.

The structure of the lower crust and the Moho in the Saxothuringian is difficult to determine unequivocally with the available seismic information. The data in this area allow several possible interpretations, some of them more favourable than others, though none of them fits all the seismic data. We tested a higher velocity lower crust similar to that modelled by *Hrubcová et al.* (2005) where its extent indicated the continuation of the Saxothuringian unit at depth. However,

compared to *Hrubcová et al.* (2005) where the strongest reflector was from the top of the high-velocity lower crust, in our data the Moho was quite pronounced. A similar way to explain the data was to model the structure by a double Moho where some parts showed reflections from the upper Moho, and some from the lower one. This interpretation resulted in a reasonable fit in travel times for the reflections but not for the upper mantle refraction. Also, the high-velocity lower crust revealed a misfit in the gravity data, which was another indication not to promote such a structure in the model. In our interpretation as in Figure 5, we tend to model the Moho as a sharp velocity contrast with some undulations which might indicate some young tectonic processes at the Moho level. Such an interpretation corresponds well with the result of the perpendicular profile S01 (*Grad et al.* 2008) (Figure 13) and gives good agreement in travel times and synthetics.
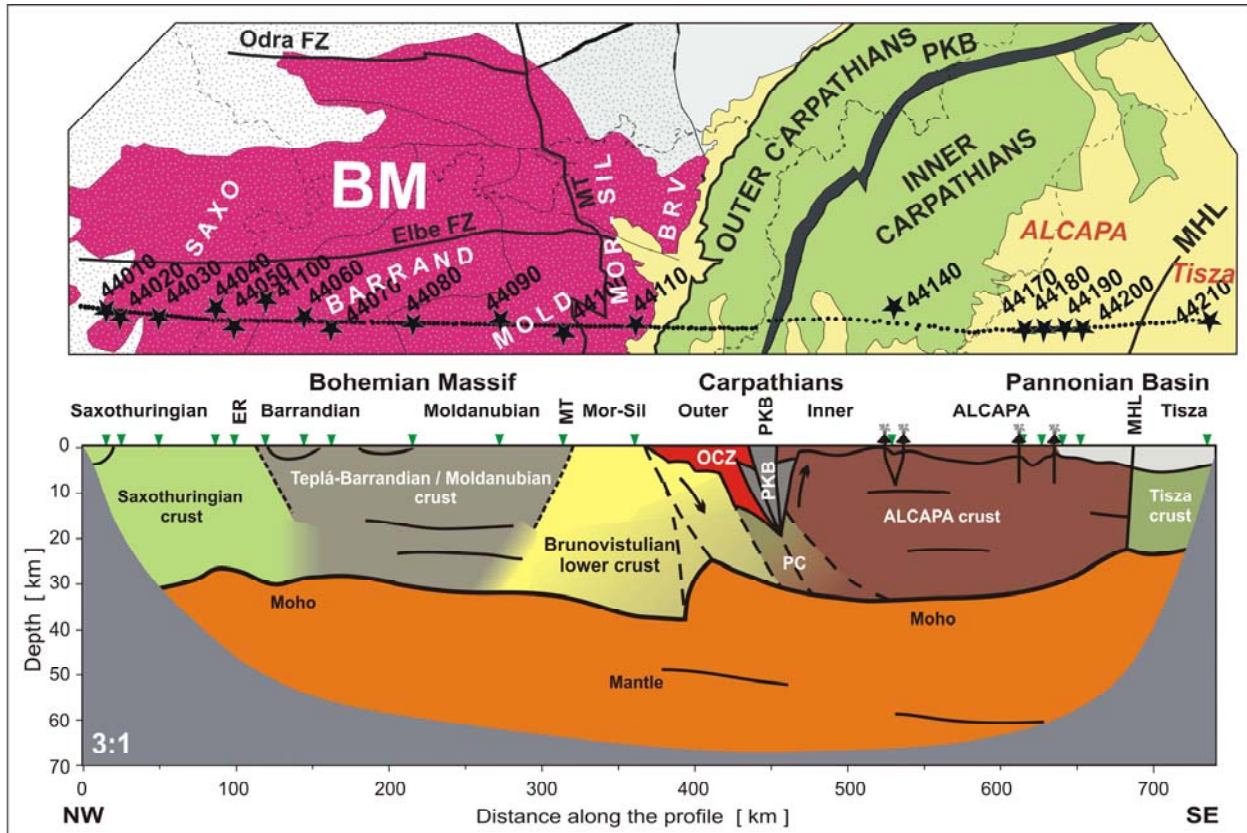

Figure 14. Schematic sketch indicating possible tectonic development along the S04 profile with geological surface map on the top. Vertical exaggeration is 3:1. SAXO, Saxothuringian; BARRAND, Barrandian; MOLD, Moldanubian; MT, Moldanubian Thrust; Mor-Sil, Moravo-Silesian; ER, Eger Rift; PKB, Pieniny Klippen Belt; OCZ, Outer Carpathians Zone; MHL, Mid-Hungarian Line; PC, Pieniny crust. The subdivision to the Outer Carpathians, the Pieniny Klippen Belt and the Pieniny crust is based on the results of the reflection seismics (*Tomek & Hall* 1993) and geological interpretation (*Vozár et al.* 1999; *Golonka & Krobicki* 2004).

The upper crust at the northern rim of the Moldanubian shows velocities of 6.0 km s^{-1} representing the metamorphic rocks exposed at the surface. Their seismic velocities are similar to those modelled by *Hrubcová et al.* (2005) in the central part of the Moldanubian. Gravity highs in this area are caused by metamorphosed Proterozoic and lower Palaeozoic rocks containing abundant mafic bodies (*McCann* 2008a). The profile intersects the area parallel to the contact of the Moldanubian and Barrandian, which is partly buried beneath the Bohemian Cretaceous Basin. The margins of this basin are seen with slightly lower velocities reflecting the Mesozoic sedimentary sequences. The lower crust in the central part of the Bohemian Massif beneath the Barrandian and Moldanubian shows velocities of 6.4 km s^{-1} constrained by well-developed overcritical crustal phases usually observed up to offsets of 200 – 250 km. The Moho is modelled as a first order discontinuity at a depth of 28 – 34 km, slightly dipping to the SE.

At the SE end of the Bohemian Massif beneath the Moravo-Silesian, the lower crust along the S04 profile shows slightly elevated velocities of 6.6 km s^{-1} compared to those in the Moldanubian with the Moho at a depth of 33 km. In this area, the perpendicular profile CEL10 of the CELEBRATION 2000 experiment (*Hrubcová et al.* 2008) shows a gradient zone

with velocities of 6.9 – 7.4 km s^{-1} in a depth range of 26 – 36 km. This gradient zone was interpreted along the whole eastern edge of the Bohemian Massif (profile CEL10), where strong lower crustal reflectivity with a long coda and weak *PmP* phases with unusually high apparent velocity suggested its existence. A slightly different character of the wave field in the CEL10 data suggested differences between the Moravian and Silesian units. While in the Moravian part in the SW, the gradient zone has no distinct velocity contrast either at the top or bottom, more to the NE, in the Silesian unit, the *PmP* is more pronounced, though it is usually not the strongest reflection and is masked by reflections from the top of the lower crust.

The Moravo-Silesian unit as a narrow SW-NE-trending zone of sheared and metamorphosed rocks was formed during the imbrication of the Brunovistulian. The S04 profile intersects it perpendicularly close to the contact of the Moravian and Silesian units. With the S04 data it is not possible to distinguish which of the aforementioned interpretations is more reliable. The travel time residuals, as well as the synthetics for both cases show similar responses (see Figure 8). From the gravity modelling, the lower crust at the eastern side of the Bohemian Massif along the S04 profile can be modelled by slightly higher densities than those which ensue from seismic velocities but not that high so as to correspond to the high velocity zone along the perpendicular CEL10 profile. For all such reasons it might be better to keep the simpler interpretation with the Moho as a first order discontinuity though a gradient zone can still be open to debate.

8.4. Geology and tectonic development of the transition between the Bohemian Massif and the Carpathians
The area at the contact of the Bohemian Massif and the Carpathians is unique because it represents tectonic development through three orogenic cycles (*Grygar et al.* 2002). The oldest cycle is the Cadomian orogeny, which led to the formation of the Brunovistulian unit. The second cycle, the Variscan orogeny, created the accretionary wedge, represented by volcano-sedimentary formations of the Rhenohercynian Foredeep and the Sub-Variscan foreland. Finally, sequences of the West Carpathian Foredeep and the Outer West Carpathian nappes formed the Alpine accretionary wedge. The Brunovistulian is the oldest crustal segment and represents a foreland of both the above-mentioned accretionary wedges: the older Variscan one with generally NE directed kinematics and the younger Alpine wedge with northward tectonics.

The Moho in this area features strong lateral variations in a depth range of 26 – 37 km. It is constrained by the refraction from the upper mantle and shows an abrupt change from a depth of 26 km at a distance of 415 km followed by a steeply dipping portion to a depth of 37 km in a distance range of 390 – 415 km. *Bielik et al.* (2006) discuss the tectonic position of the Brunovistulian upper crust subducted into the lower-crustal position beneath the accretionary wedge. Slightly elevated seismic velocities of 6.6 – 6.75 km s^{-1} compared to the Moldanubian with velocities of 6.4 km s^{-1} can represent the extent of the Brunovistulian lower crust underthrust beneath the Moravo-Silesian.

8.5. Geology and tectonic development of the Western Carpathians
The crust of the Western Carpathians has a complicated structure and is composed of fragments formed during the Variscan, paleo-Alpine and neo-Alpine orogenic events (*McCann* 2008b). The S04 profile is in a favourable position and cuts all main tectonic units of the Western Carpathians. At 400 km along the profile it reaches the sedimentary infill (velocities of ~4 km s^{-1} to a depth of 6 km) of the Carpathian Foredeep forming a characteristic clastic wedge thinning towards the foreland followed by the Tertiary accretionary complex, the Carpathian Flysch Belt. This corresponds to the pronounced gravity low in the Carpathians. However, during modelling it was necessary to introduce lower densities of 2.45 g cm^{-3} than those which ensued from the velocity-to-density conversion (2.5 g cm^{-3}). The local gravity minimum at a distance of 425 km (densities of 2.2 g cm^{-3}) represents light Neogene to Quaternary sedimentary rocks of the Vienna basin promontory, not distinguishable in the seismic data because of larger distance to the nearest shot points in this area.

The Inner Western Carpathians are composed of tectonic units that originated during the paleo-Alpine Orogeny in the Mesozoic. They comprise numerous nappes composed of low- to high-grade metamorphic and plutonic Palaeozoic rocks and largely unmetamorphosed Palaeozoic to Cretaceous strata, which in the area of our investigation are largely north-west verging. Lower velocities of 3.9 km s^{-1} at about 460 km along the profile reflect the Neogene to Quaternary sediments of the Pannonian Basin margin. Increased velocities of 5.8 – 5.9 km s^{-1} further to the SE represent the core mountains (Považský Inovec and Tríbeč) composed of pre-Alpine basement and its Mesozoic sedimentary cover. Higher velocities (5.6 – 5.8 km s^{-1}) of andesitic and rhyolitic rocks of the Tertiary volcanic edifices (Štiavnica stratovolcano) are reached at 520 – 545 km followed by volcano-sedimentary complexes to a distance of 560 km. Elevated velocities at a distance of 610 – 650 km along the profile represent the western slopes of a Tertiary volcanic complex in northern Hungary (Matra stratovolcano) with mainly andesitic volcanism of the Miocene age (*Seghedi et al.* 2004). This is in agreement with the geological interpretation along the MT-15 profile (*Vozár* 2010, personal communications).

The Jurassic/Cretaceous limestones of the Pieniny Klippen Belt (PKB) separating the Outer and Inner Carpathians are the important first-order tectonic structure in the Western Carpathians and can be found at about 450 km along the profile;

however this structure is not obvious in the S04 refraction data at the surface. It represents the contact of the Western Carpathian Internides and the stable European Platform, separating this platform from the microplate ALCAPA in the eastern segment. The abrupt change of the crustal thickness and the dipping Moho (from 37 to 26 km depth at a distance of 400 km along the profile) can represent the contact of these plates at the lower crustal level, which would suggest a sub-vertical plate boundary in this area. The sub-vertical plate boundary may be explained by a steepening of the subduction zone during the final subduction/collision stage as was suggested e.g., by *Lexa & Konečný* (1997) and *Němčok et al.* (1998). Another possible explanation may be due to the fact that the direction of the relative movement of the subducting plates was SW-NE, which is roughly parallel to front of the Carpathian belt in the study area. This would imply a strike-slip movement of the plates parallel to the plate boundary along a (sub-vertical?) shear zone, which might be represented by the PKB at the surface, rather than a dipping subduction-style boundary as it would be in the case of relative movement perpendicular to the orogen strike.

Such a change in crustal thickness is not unusual in the Carpathian crustal structure. Similar effect was modelled along the SW-NE oriented profile CEL11 (*Janik et al.* 2010) at the eastern edge of the Carpathians. Also, *Hauser et al.* (2007) detected the same structure at the south-eastern edge of the Carpathian Belt in Vrancea, the region of a deeper seated present seismicity (*Wenzel et al.* 2002). Though not deep, the seismicity along the Peripieninic lineament (e.g., the area of Dobrá Voda, *Kováč et al.* 2002), indicate geotectonic activity at the western edge of the Western Carpathians.

Considering the Pieniny Klippen Belt as a deep-seated boundary between the colliding Palaeozoic lithospheric plate and the microplate ALCAPA, the zone of the abrupt Moho depth change can represent the continuation of this boundary to the depth. *Vozár et al.* (1999) interpreted the Pieniny Klippen Belt, that forms the dominant structures of the Western Carpathians, as a sub-vertical flower structures reaching a depth of 12 km with its potential extent to a depth of about 16 – 17 km (*Vozár* personal communication). The basement of the Pieniny Klippen Belt reflects the Jurassic-Cretaceous development (see e.g., *Golonka & Krobicki* 2004) and is interpreted as the Pieniny crust. It is presented as an individual Pieniny terrane forming a part of the ALCAPA foredeep with independent tectonic history during the Alpine orogeny (*Janik et al.* 2010).

Considering the larger distance between the nearest shot points (SP 44110 at the eastern edge of the Bohemian Massif and SP 44140 in the Carpathians), the seismic data in this area were not sufficient to constrain the surface structure and the exact shape and position of the individual units at depth. The subdivision into the Outer Carpathians, the Pieniny Klippen Belt and the Pieniny crust, marked in Figure 14, is based on the results from the reflection seismic interpretation (*Tomek, & Hall* 1993; *Hubatka & Švancara* 2002) and geological interpretation (e.g., *Vozár et al.* 1999; *Golonka & Krobicki* 2004).

Crustal thickness and the Moho depth in the Carpathian region clearly tend to decrease from west to east. The Western Carpathians are characterized by crustal thicknesses of 32 – 33 km, while in the regions influenced by Tertiary extension such as the Pannonian Basin the Moho rises up to a depth of 25 km. This is in agreement with the reflection seismic results (*Tomek et al.* 1987; *Tomek & Hall* 1993), as well as the investigations of *Bielik* (2004) who modelled the Pannonian gravity high. However, such thicknesses are small in comparison to those of many other orogens, e.g. in the Alps (*Brückl et al.* 2007). Based on gravity observations, *Lillie et al.* (1994) suggests that collision stopped at an early stage in the Western Carpathians while the collision in the Eastern Alps progressed to an advanced stage such that the orogen is underlain by the full thickness of the European continental crust.

Two mantle reflectors in a depth range of 50 – 60 km are documented below the Carpathians dipping SE. In the Pannonian Basin, *Posgay et al.* (1981) interpreted a low-velocity layer in the upper mantle, the top of which is at a depth of 55 km, which might be associated with the deeper mantle reflector in the SE. Since the lithosphere in the Pannonian Basin is quite shallow, *Posgay et al.* (1981) suggest that the top of this layer is associated with the lithosphere-asthenosphere boundary. The SE mantle reflector modelled from the S04 seismic data cannot contribute to such a discussion as it is constrained by only a few shot points. The shallower mantle reflector more to the NW close to the contact with the Bohemian Massif cannot be associated with such boundary because the lithosphere deepens to the Bohemian Massif (e.g., *Bielik et al.* 2004).

9. Summary and Conclusions

The SUDETES 2003 profile S04 was designed to study the main features from the Variscan to the Tertiary, represented by the Bohemian Massif and the Western Carpathians. The S04 seismic model (Figure 5) reveals diverse and complex structure not only within the tectonic units but also at their contacts (see Figure 14). The differences in seismic velocities

can reflect, to some extent, the structural variances and tectonic events. The main features of the interpretation are summarized below and we hope that these results will be the basis for further integrated geophysical and tectonic analyses.

1. In the Bohemian Massif, the Saxothuringian shows higher near-surface velocities represented by the Palaeozoic metamorphic rocks compared to lower velocities at the contact of the Saxothuringian and Barrandian caused by low density granites. The contrast is even more pronounced in densities than in seismic velocities suggesting deeper seated granites than ensue from seismic modelling.

2. The lower crust in the Saxothuringian exhibits a complicated structure. The allowable models range from a higher velocity lower crust, double Moho or, as in the S04 final interpretation, the Moho with a velocity contrast with some lateral topography. As such, it reveals that the northern termination of the Saxothuringian is not a simple structure.

3. The major crystalline segment within the Bohemian Massif, the Moldanubian, shows velocities representing the metamorphic rocks exposed at the surface. The Moho is modelled as the first order discontinuity, the depth of which is slightly shallower (33 km) at the northern rim of the Moldanubian compared to the central part of the Moldanubian in the Bohemian Massif with the depth of 39 km.

4. Compared to the Moldanubian unit, the lower crust in the Moravo-Silesian shows slightly elevated velocities (6.6 – 6.75 km s^{-1}) though the area is not modelled by a gradient zone as in the case of the perpendicular profile CEL10 along the eastern edge of the Bohemian Massif. Also gravity modelling does not confirm the gradient zone at lower crustal levels. The slightly elevated seismic velocities of the Moravo-Silesian unit can represent the extent of the Brunovistulian lower crust underthrust beneath the Moravo-Silesian.

5. At the contact of the Bohemian Massif with the Western Carpathians the Moho depth shows strong lateral variations. Going from the SE, at the western side of the Carpathians the Moho shallows from 32 km to a depth of 26 km at a distance of 415 km along the profile and steeply dips to the NW to a depth of 37 km. Such a steeply dipping Moho was also modelled along the SW-NE oriented profile CEL11 at the eastern edge of the Carpathians or at the south-eastern edge of the Carpathian Belt in Vrancea (*Janik et al.* 2010; *Hauser et al.* 2007).

6. Considering the Pieniny Klippen Belt as a deep-seated boundary between the colliding Palaeozoic lithospheric plate and the microplate ALCAPA, the abrupt change of the crustal thickness can represent the continuation of this boundary to the depth suggesting a sub-vertical plate boundary in this area. This sub-vertical boundary may be explained by a steepening of the subduction zone during the final subduction/collision stage. Another explanation may be connected with the fact that the relative sinistral plate movement in this area was roughly parallel to the front of the Carpathian belt, rather than perpendicular to the orogen strike as it would be in the case of a dipping subduction-style plate boundary.

7. In the Carpathians, lower velocities of 4 km s^{-1} to a depth of 6 km represent sedimentary infill of the Carpathian Foredeep and Flysch thinning towards the foreland, which is a source of a pronounced gravity low.

8. Further to the SE, in the Carpathians, higher near-surface velocities correspond to the Tertiary volcanic complexes exposed at the surface.

9. The Moho in the Carpathians reaches a depth of 32 – 33 km. This relatively small thickness compared to those of many other orogens, e.g. the Alps, reflects a different tectonic evolution of the Carpathians with the internal Carpathians being parts of two consolidated paleo-Alpine lithospheric fragments or microplates Alcapa and Tisza.

10. At contrast, in the region influenced by Tertiary extension, in the Pannonian Basin, the Moho rises up to a depth of 25 km, which corresponds to the Pannonian gravity high and the Pannonian lithospheric thinning.

References

Arkai, P., 1991. Alpine regional metamorphism of the different tectonic domains in the Hungarian part of the Pannonian Basin.- In: Bauda, A., P. Thélin, and G. Stampfli (eds.): Palaeozoic geodynamic domains and their alpidic evolution in the Tethys. IGCP Project No. 276, Newsletter No. 2, Mémoires de Géologie (Lausanne), 10**,** 5–13.

Behr, H.J., Dürbaum, H.J. & Bankwitz, P. (Eds.), 1994. Crustal structure of the Saxothuringian zone: Results of the deep seismic profile MVE-90 (East). *Z. Geol. Wiss*., 22, 647−769.

Beránek, B. & Zátopek, A., 1981. Earth's crust structure in Czechoslovakia and central Europe by methods of explosion seismology, in Geophysical Synthesis in Czechoslovakia, edited by A. Zátopek, 253–264, Veda, Bratislava, Slovakia.

Beránek, B. & Zounková, M., 1977. Investigations of the Earth's crust in Czechoslovakia using industrial blasting, *Stud. Geophys. Geod., 21*, 273– 280.

Bezák, V., Šefara, J., Bielik, M. & Kubeš, P., 1997. Models of the Western Carpathian lithosphere. In Grecula, P., D. Hovorka, and M. Putiš (Eds.). Geological evolution of the Western Carpathians. Geocomplex, Bratislava.

Bielik, M., Kloska, K., Meurers, B., Švancara, J., Wybraniec, S., Fancsik, T., Grad, M., Grand, T., Guterch, A., Katona, M., Królikowski, C., Mikuska, J., Pasteka, R., Petecki, Z., Polechonska, O., Ruess, D., Szalaiova, V., Šefara, J. & Vozár, J., 2006. Gravity anomaly map of the CELEBRATION 2000 region, *Geologica Carpathica, 57, 3*, 145–156.

Bielik, M., Šefara, J., Kováč, M., Bezák, V. & Plašienka, D., 2004. The Western Carpathians – interaction of Hercynian and Alpine processes, *Tectonophysics, 393,* 63–86.

Birkenmajer, K., 1986. Stages of structural evolution of the Pieniny Klippen Belt, Carpathians. Stud. Geol. Pol. 88, 7–32.

Blecha, V., Štemprok, M. & Fischer, T., 2009. Geological interpretation of gravity profiles through the Karlovy Vary granite massif (Czech Republic), *Stud. Geophys. Geod., 53*, 295–314.

Brückl, E., Bleibinhaus, F., Gosar, A., Grad, M., Guterch, A., Hrubcová, P., Keller, G.R., Majdański, M., Sumanovac, F., Tiira, T., Yliniemi, J., Hegedűs, E. & Thybo, H., 2007. Crustal structure due to collisional and escape tectonics in the Eastern Alps region based on profiles Alp01 and Alp02 from the ALP 2002 seismic experiment, *J. Geophys. Res., 112*, B06308, doi:10.1029/2006JB004687.

Brückl, E., Bodoky, T., Hegedűs, E., Hrubcová, P., Gosar, A., Grad, M., Guterch, A., Hajnal, Z., Keller, G.R., Špičák, A., Sumanovac, F., Thybo, H., Weber, F. & ALP 2002 Working Group, 2003. ALP 2002 seismic experiment, *Stud. Geophys. Geod., 47*, 71– 679, doi:10.1023/A:1024780022139.

Brückl, E., Mitterbauer, U. & Behm, M., 2006. Studies on crustal structure and gravity in the Eastern Alps, in Geodetic Deformation Monitoring: From Geophysical to Engineering Roles. IAG Symposium, 131, (eds.) F. Sanso and A. J. Gil, 181–192.

Bucha, V. & Blížkovský, M. (Eds.), 1994. Crustal Structure of the Bohemian Massif and the West Carpathians, Academia Praha, Prague.

Čermák, V., 1995. A geothermal model of the Central Segment of the European Geotraverse, *Tectonophysics, 244*, 51–55.

Čermák, V. & Bodri, L., 1998. Heat flow map of Europe revised, *Dtsch. Geophys. Ges. V., II*, 58–63.

Červený, V. & Pšenčík, I., 1984. SEIS83 – numerical modelling of seismicwave fields in 2-D laterally varying layered structures by the ray method. In: Engdal, E.R. (Ed.), Documentation of Earthquake Algorithms. Rep. SE-35,World Data Cent. A for Solid Earth Geophysics, Boulder, Colo., 36–40.

Christensen, N. I., 1974. Compressional wave velocities in possible mantle rocks to pressures of 30 kbars, *J. Geophys. Res*., *79,* 407–412.

Christensen, N. I. & Mooney, W. D., 1995. Seismic velocity structure and composition of the continental crust: A global view, *J. Geophys. Res., 100,* (B6), 97619788, doi:10.1029/95JB00259.

Dallmeyer, R.D. & Urban, M., 1994. Evolution of Variscan (Hercynian) and comparable Palaeozoic orogenic belts. J. Czech Geol. Soc,. 39, 21–22.

Dallmeyer, D., Franke, W. & Weber, K. (Eds.), 1995. *Pre-Permian Geology of Central and Eastern Europe*, Springer-Verlag, New York.

DEKORP Research Group, 1994. The deep seismic reflection profiles DEKORP 3/MVE-90, *Z. Geol. Wiss., 22* (6), 623–825.

Downes, H., 1993. The nature of the lower continental crust of Europe: petrological and geochemical evidence from xenoliths, *Phys. Earth Planet. Int., 79*, 195–218.

Embey-Isztin, A., Downes, H., Kempton, P.D., Dobosi, G. & Thirwall, M., 2003. Lower crustal granulite xenoliths from the Pannonian Basin, Hungary: Part 1. mineral chemistry, thermobarometry and petrology, *Contrib. Mineral. Petrol., 144*, 652–670.

Emmermann, R. & Lauterjung, J., 1997. The German Continental Deep Drilling Program KTB: overview and major results, *J. Geophys. Res*., *102(B8)*, 18179–18201.

Enderle, U., Schuster, K., Prodehl, C., Schulze, A. & Bribach, J., 1998. The refraction seismic experiment GRANU95 in the Saxothuringian belt, southeastern Germany, *Geophys. J. Int., 133*, 245–259, doi:10.1046/j.1365-246X.1998.00462.x

Finger, F., Hanzl, P., Pin, C., von Quadt, A. & Steyrer, H.P., 2000. The Brunovistulian: Avalonian Precambrian sequence at the eastern end of the Central European Variscides? In: Franke, W., Haak, V., Oncken, O., Tanner, D. (Eds.), Orogenic Processes: Quantification and Modelling in the Variscan Belt. *Geol. Soc., London, Spec. Publ., 179*, 103–112.

Fritz, H., Dallmeyer, R.D. & Neubauer, F., 1996. Thick-skinned versus thin-skinned thrusting: rheology controlled thrust propagation in the Variscan collisional belt (the south-eastern Bohemian Massif, Czech Republic–Austria), *Tectonics, 15*, 1389–1413.

Golonka, J. & Krobicki, M., 2004. Jurassic paleogeography of the Pieniny and Outer Carpathian basins, *Riv. It. Pal. strat., 110*, 5–14.

Golonka, J. & Pícha, F.J. (Eds.) 2006. *The Carpathians and Their Foreland*, American Association of Petroleum Geologists.

Grad, M., Keller, G.R., Thybo, H., Guterch, A. & the POLONAISE Working Group, 2002. Lower lithospheric structure beneath the Trans European Suture Zone from POLONAISE'97 seismic profiles, *Tectonophysics, 360*, 153–168, doi:10.1016/S0040-1951(02)00350-5.

Grad, M., Jensen, S.L., Keller, G.R., Guterch, A., Thybo, H., Janik, T., Tiira, T., Yliniemi, J., Luosto, U., Motuza, U., Nasedkin, V., Czuba, W., Gaczynski, E., Środa, P., Miller, K.C., Wilde-Piorko, M., Komminaho, K., Jacyna, J. & Korabliova, L., 2003a. Crustal structure of the Trans-European suture zone region along POLONAISE'97 seismic profile P4, *J. Geophys. Res., 108* (B11), 2541, doi:10.1029/2003JB002426.

Grad, M., Špičák, A., Keller, G.R., Guterch, A., Brož, M., Hegedűs, E. & Working Group, 2003b. SUDETES 2003 seismic experiment, *Stud. Geophys. Geod., 47*, 681–689, doi:10.1023/A:1024732206210.

Grad, M., Guterch, A., Keller, G.R., Janik, T., Hegedűs, E., Vozár, J., Ślaczka, A., Tiira, T. & Yliniemi, J., 2006. Lithospheric structure beneath trans-Carpathian transect from Precambrian platform to Pannonian basin: CELEBRATION 2000 seismic profile CEL05, *J. Geophys. Res., 111*, B03301, doi:10.1029/2005JB003647.

Grad, M., Guterch, A., Mazur, S., Keller, G.R., Špičák, A., Hrubcová, P. & Geissler, W.H., 2008. Lithospheric structure of the Bohemian Massif and adjacent Variscan belt in central Europe based on profile S01 from the SUDETES 2003 experiment, *J. Geophys. Res., 113*, B10304, doi:10.1029/2007JB005497.

Grégoire, M., Jackson, I., O'Reilly, S.Y. & Cottin, J.Y., 2001. The lithospheric mantle beneath the Kerguelen Islands (Indian Ocean): petrological and petrophysical characteristics of mantle mafic rock types and correlation with seismic profiles, *Contrib. Mineral Petrology, 142*, 244–259.

Grygar, R., Gnojek, I., Hubatka, F. & Jelínek, J., 2002. Brunovistulian Terrane – synthesis of morphostructural analysis and geophysical data (Moravo-Silesian Area, Czech Republic). *Geolines, 14,* 26–27.

Guterch, A., Grad, M., Thybo, H., Keller, G.R. & Miller, K.C., 1998. Seismic experiment spreads across Poland, Eos Trans. *AGU, 79*, (26), 302–305.

Guterch, A., Grad, M., Thybo, H., Keller, G.R. & the POLONAISE Working Group, 1999. POLONAISE'97 – International seismic experiment between Precambrian and Variscan Europe in Poland, *Tectonophysics, 314*, 101– 121, doi:10.1016/S0040-1951(99)00239-5.

Guterch, A., Grad, M., Špičák, A., Brückl, E., Hegedűs, E., Keller, G.R., Thybo, H. & CELEBRATION 2000, ALP 2002, SUDETES 2003 Working Groups, 2003a. An overview of recent seismic refraction experiments in central Europe, *Stud. Geophys. Geod., 47*, 651–657, doi:10.1023/A:1024775921231.

Guterch, A., Grad, M., Keller, G.R., Posgay, K., Vozár, J., Špičák, A., Brückl, E., Hajnal, Z., Thybo, H., Selvi, O. & the CELEBRATION 2000 Experiment Team, 2003b. CELEBRATION 2000 seismic experiment, *Stud. Geophys. Geod., 47*, 659–669, doi:10.1023/A:1024728005301.

Hauser, F., Raileanu, V., Fielitz, W., Dinu, C., Landes, M., Bala, A. & Prodehl, C., 2007. Seismic crustal structure between the Transylvanian Basin and the Black Sea, Romania, *Tectonophysics, 430*, 1–25, doi:10.1016/j.tecto.2006.10.005.

Horváth, F., 1993. Towards a mechanical model for the formation of the Pannonian Basin, *Tectonophysics, 226*, 333–357.

Hrubcová, P., Šroda, P., Špičák, A., Guterch, A., Grad, M., Keller, R.G., Brückl, E. & Thybo, H., 2005. Crustal and uppermost mantle structure of the Bohemian Massif based on data from CELEBRATION 2000 experiment. *J. Geophys. Res., 110*, B11305. doi:10.1029/2004JB003080.

Hrubcová, P., Šroda, P. & CELEBRATION 2000 Working Group, 2008. Crustal structure at the easternmost termination of the Variscan belt based on CELEBRATION 2000 and ALP 2002 data, *Tectonophysics, 460*, 55–75, doi:10.1016/j.tecto.2008.07.009.

Hrubcová, P. & Geissler, W. H., 2009. The Crust-Mantle Transition and the Moho beneath the Vogtland/West Bohemian Region in the Light of Different Seismic Methods, *Stud. Geophys. Geod.*, 53, 275–294,

Hubatka, F. & Švancara, J., 2002. Geologicko-geofyzikální model zemské kůry v místě křížení profilů 8HR/85 a CEL10. Internal Report, Archive of the Geophysical Institute ASCR, in Czech.

Janik, T., Grad, M., Guterch, A., Vozár, J., Bielik, M., Vozárová, A., Hegedűs, E., Kovác, C.A., Kovács, I. & CELEBRATION 2000 Working Group, 2010. Crustal structure of the Western Carpathians and Pannonian Basin System: seismic models from CELEBRATION 2000 data and geological implication, *J. Geodyn.,* in press.

Janočko, J. & Jacko, S., 1999. Evolution of the Central Paleogene Basin in the Spiska Magura region, Slovakia, *Geologica Carpathica, 50*, 36–37.

Kempton, P.D., Downes, H. & Embey-Isztin, A., 1997. Mafic granulite xenoliths in Neogene alkali basalts from the western Pannonian Basin: insights into the lower crust of a continental back-arc setting. *J. Petrol., 38,* 941–970.

Komminaho, K., 1997, Software manual for programs MODEL and XRAYS – A graphical interface for SEIS83 program package, Rep. 20, 31, Dep. of Geophysics Univ. of Oulu, Oulu, Finland.

Konečný, V., Kováč, M., Lexa, J., & Šefara, J., 2002. Neogene evolution of the Carpatho-Pannonian region. An interplay of subduction and back-arc diapiric uprise in the mantle. *EGS Stefan Mueller Special Publication Series, 1*, 165–194.

Kopecký, L., 1978. Neoidic taphrogenetic evolution and young alkaline volcanism of the Bohemian Massif, *Czech Geological Survey*, *Geol. 31*, 91–107.

Kováč, M., Bielik, M., Hók, J., Kováč, P., Kronome, B., Labák, P., Moczo, P., Plašienka, D., Šefara, J. & Šujan, M., 2002. Seismic activity and neotectonic evolution of the Western Carpathians (Slovakia), *EGU Stephan Mueller Special Publication Series*, *3*, 167–184.

Krzywiec, P., 1997. Large-scale tectono-sedimentary Middle Miocene history of the central and eastern Polish Carpathian Foredeep Basin – results of seismic data interpretation, *Przeglad Geologiczny, 45*, 1039–1053.

Lenhardt, W.A., Švancara, J., Melichar, P., Pazdírková, J., Havíř, J. & Sýkorová, Z., 2007. Seismic activity of the Alpine-Carpathian-Bohemian Massif region with regard to geological and potential field data*, Geol. Carpathica, 58*, 397–412.

Lexa, J. & Konečný, V., 1998. Geodynamic aspects of the neogene to quaternary volcanism, *In* Rakús, M. (Ed.), *Geodynamic development of the Western Carpathians,* GSSR, Bratislava, 143–154.

Lillie, J.R., Bielik, M., Babuška, V. & Plomerová, J., 1994. Gravity modelling of the lithosphere in the Eastern Alpine–Western Carpathian–Pannonian Basin region. *Tectonophysics, 231*, 215–235.

Linnemann, U., D'Lemos, R., Drost, K. Jeffries, T., Gerde, A., Romer, R.L., Samson, S.T. & Strachan, R.A., 2008. Cadomian Tectonics. In McCann, T. (ed.), 2008. *The Geology of Central Europe. Volume 1: Precambrian and Palaeozoic*. Geological Society of London.

Ludwig, W. J., Nafe, J. E. & Drake, C. L., 1971. Seismic refraction. *In* Maxwell, A. E. (Ed.), The sea, v. 4, New York, (Interscience), 53–84.

Majdański, M., Grad, M., Guterch, A. & SUDETES 2003 Working Group, 2006. 2-D seismic tomographic and ray tracing modelling of the crustal structure across the Sudetes Mountains basing on SUDETES 2003 experiment data. *Tectonophysics, 413*, 249–269. doi:10.1016/j.tecto.2005.10.042.

Majdański, M., Kozlovskaya, E., Grad, M. & SUDETES 2003 Working Group, 2007. 3D structure of the Earth's crust beneath the northern part of the Bohemian Massif. *Tectonophysics, 437*, 17–36, doi:10.1016/j.tecto.2007.02.015.

Majerová, M. & Novotný, M., 1986, Výzkum zemské kůry pomocí hlubinné sondáže. *In* Blížkovský, M. (Ed.) Geofyzikální model litosféry, MS Geofyzika n.p. Brno, GFÚ ČSAV Praha, GFÚ SAV Bratislava, in Czech.

Majorowicz, J., 1976. Heat flow map of Poland on the background of geothermal field of Europe and some aspects of its interpretation, *Acta Geophysica Polonica, 24,* 147–156.

Málek, J., Brož, M., Fischer, T., Horálek, J., Hrubcová, P., Janský, J., Novotný, O. & Růžek, R., 2001. Seismic measurements along short profiles inWestern Bohemia during the CELEBRATION 2000 experiment, *Acta Montana*, Ser. A, 18, 15–28.

Malinowski, M., Żelaźniewicz, A., Grad, M., Guterch, A., Janik, T. & CELEBRATION Working Group, 2005. Seismic and geological structure of the crust in the transition from Baltica to Palaeozoic Europe in SE Poland – CELEBRATION 2000 experiment, profile CEL 02, *Tectonophysics, 401*, (1–2), 55–77.

Malinowski, M., Grad, M., Guterch, A. & the CELEBRATION 2000 Working Group, 2008. 3-D seismic modelling of the crustal structure between East European craton and the Carpathians in SE Poland based on CELEBRATION 2000 data, *Geophys. J. Int., 173*, 546–565, doi:10.1111/j.1365-246X.2008.03742.x

Matte, P., Maluski, H., Rajlich, P. & Franke, W., 1990. Terrane boundaries in the Bohemian Massif: Result of large-scale Variscan shearing, *Tectonophysics, 177*, 151–170, doi:10.1016/0040-1951(90)90279-H.

Matte, Ph., 1991. Accretionary history and crustal evolution of the Variscan belt in Western Europe. *Tectonophysics, 196*, 309–337.

Matte, Ph., 2001. The Variscan collage and orogeny (480–290 Ma) and the tectonic definition of the Armorica microplate: a review. *Terra Nova, 13*, 122–128.

McCann, T. (Ed.), 2008a. *The Geology of Central Europe. Volume 1: Precambrian and Palaeozoic*. Geological Society, London.

McCann, T. (Ed.), 2008b. *The Geology of Central Europe. Volume 2: Mesozoic and Cenozoic*. Geological Society, London.

Mlčoch, B., 2001. Výzkum krystalických formací v hlubokých strukturách Doupovského komplexu a jeho širšího okolí. Český geologický ústav, Final report, in Czech.

Mueller, H.J., 1995. Modelling of the lower crust by simulation of the in situ conditions: an example from Saxonian Erzgebirge, *Phys. Earth Planet. Inter.*, *92,* 3–15.

Němčok, M., L. Pospíšil, J. Lexa, & R.A. Donelick, 1998. Tertiary subduction and slab break-off model of the Carpathian–Pannonian region, *Tectonophysics, 295*, 307–340.

Plašienka, D., Grecula, P., Putiš, M., Hovorka, D. & Kováč, M., 1997. Evolution and structure of the Western carpathians: an overview. In Grecula, P., D. Hovorka, and M. Putiš (eds.). Geological evolution of the Western Carpathians. Geocomplex, Bratislava.

Posgay, K., Albu, I., Petrovics, I. & Ráner, G., 1981. Character of the Earth's crust and upper mantle on the basis of seismic reflection measurements in Hungary, Earth Evol. Sci., 1, 272–279.

Posgay, K., Albu, I., Ráner, G. & Varga, G., 1986. Characteristics of the reflecting layers in the Earth's crust and upper mantle in Hungary, in Reflection Seismology: A Global Perspective, *Geodyn. Ser., vol. 13*, (eds.) M. Barazangi and L. Brown, 55– 66, AGU, Washington, D. C.

Posgay, K., Bodogy, T., Hegedűs, E., Kováczsvölgyi, S., Lenkey, L., Szafián, P., Takács, E., Tímár, Z. & Varga, G., 1995. Asthenospheric structure beneath a Neogene Basin in SE Hungary. *Tectonophysics, 252,* 467–484.

Posgay, K., Fancsic, T., Hegedűs, E., Pápa, A., Bodoky, T. & Takács, E., 2001. Metamorphic and geologic effects shown by seismic data in the Carpathian Basin, *Acta Geologica Hungarica, 44,* 113–134.

Prodehl, C., Mueller, S. & Haak, V., 1995. The European Cenozoic Rift System, in Continental Rifts: Evolution, Structure, Tectonics, Dev. Geotectonics, vol. 25, (eds) K. H. Olsen, 133–212, Elsevier, New York.

Reicherter, K., Froitzheim, N., Jarosiński, M., Badura, J., Franzke, H., Hansen, M., Hübscher, Ch., Müller, R., Poprawa, P., Reinecker, J., Stackebrandt, W., Voigt, T., von Eynatten, H. & Zuchiewicz, W., 2008. Alpine tectonics north of the Alps. *In* McCann, T. (ed.) *The Geology of Central Europe. Volume 2: Mesozoic and Cenozoic.* Geological Society, London, 1233–1285.

Royden, L., Horváth, F. & Rumpler, J., 1983. Evolution of the Pannonian basin system, *Tectonics, 2,* 63-90.

Růžek, B., Vavryčuk, V., Hrubcová, P., Zedník, J. & the CELEBRATION Working Group, , 2003. Crustal anisotropy in the Bohemian Massif, Czech Republic: Observations based on Central European Lithospheric Experiment Based on Refraction (CELEBRATION) 2000, *J. Geophys. Res., 108(B8)*, 2392, doi:10.1029/2002JB002242.

Růžek, B., Hrubcová, P., Novotný, M., Špičák, A., & Karousová, O., 2007. Inversion of travel times obtained during active seismic refraction experiments Celebration 2000, Alp 2002 and Sudetes 2003, *Stud. Geophys. Geod.*, 51, 141–164, doi:10.1007/s11200-007-0007-6.

Šantavý, J. & Vozár, J., 2000. Electronical Atlas of Deep Reflection Seismic Profiles of the Western Carpathians, Minist. of Environ. and Geol. Surv. of the Slovak Repub., Geocomplex, Bratislava.

Schulmann, K. & Gayer, R., 2000. A model for a continental accretionary wedge developed by oblique collision: the NE Bohemian Massif. J. Geol. Soc. London 157, 401–416.

Schulmann, K., Kröner, A., Hegner, E., Wendt, I., Konopásek, J., Lexa, O. & Štipská, P., 2005. Chronological constraints on the pre-orogenic history, burial and exhumation of deep-seated rocks along the Eastern Margin of the Variscan Orogen, Bohemian Massif, Czech Republic. Am. J. Sci. 305, 407–448.

Seghedi, I., Downes, H., Vaselli, O., Szakacs, A., Balogh, K. & Pécskay, Z., 2004. Post-collisional Tertiary–Quaternary mafic alkalic magmatism in the Carpathian–Pannonian region: a review, *Tectonophysics*, 393, 43–62, doi:10.1016/j.tecto.2004.07.051.

Soták, J., Pereszlenyi, M., Marchalko, R., Milicka, J. & Starek, D., 2001. Sedimentology and hydrocarbon habitat of the submarine-fan deposits of the Central Carpathian Paleogene Basin (NE Slovakia), *Marine and Petroleum Geology, 18,* 87–114.

Środa, P., Czuba, W., Grad, M., Guterch, A., Tokarski, A.K., Janik, T., Rauch, M., Keller, G.R., Hegedűs, E., Vozár, J. & CELEBRATION 2000 Working Group, 2006. Crustal and upper mantle structure of the Western Carpathians from CELEBRATION 2000 profiles CEL01 and CEL04: seismic models and geological implications, *Geophys. J. Int., 167,* 737–760, doi: 10.1111/j.1365-246X.2006.03104.x.

Švancara, J., Špaček, P. & Hubatka, F., 2005. Regionální geofyzikální obraz geologické stavby ČR a gravimetrická verifikace rychlostních modelů zemské kůry. *In* Novotný, M. et al., (Eds.), SLICE, Závěrečná zpráva projektu VaV/630/3/02. Manuscript GFÚ AV ČR, in Czech.

Tari, G., Báldi, T. & Báldi-Beke, M., 1993. Paleogene retroarc flexural basin beneath the Neogene Pannonian Basin: a geodynamic model, *Tectonophysics,* 226, 433–455.

Taylor, S.R. & Toksöz, M.N., 1982. Crust and upper-mantle velocity structure in the Appalachian orogenic belt: Implications for tectonic evolution. *Geol. Soc. Am. Bull., 93*, 315–329.

Tokarski, A.K. & Świerczewska, A., 2005. Neofractures versus inherited fractures in structural analysis: a case study from quaternary fluvial gravels (Outer Carpathians, Poland), *Annales Societatis Geologorum Poloniae,*75, 95–104.

Tomek, Č., 1993. Deep crustal structure beneath the central and inner West Carpathians, *Tectonophysics, 226,* 417–431.

Tomek, C. &Hall, J., 1993. Subducted continental margin imaged in the Carpathians of Czechoslovakia, *Geology, 21,* 535–538.

Vavryčuk, V., Hrubcová, P., Brož, M., Málek, J. & the ALP 2002 Working Group, 2004. Azimuthal variation of Pg velocity in the Moldanubian, Czech Republic: observations based on a multi-azimuthal common-shot experiment, *Tectonophysics, 387,* 189– 203.

Villaseca, C., Downes, H., Pin, C. & Barbero, L., 1999. Nature and Composition of the Lower Continental Crust in Central Spain and the Granulite-Granite Linkage: Inferences from Granulite Xenoliths, *J. Petrol., 40,* 1465–1496.

Vosteen, H.-D., Rath, V., Clauser, C. & Lammerer, B., 2003. The thermal regime of the Eastern Alps from inversion analyses along the TRANSALP profile, *Phys. Chem. Earth, 28,* 393–405.

Vozár, J., Šantavý, J., Potfaj, M., Szalaiová, V., Scholtz, P., Tomek, Č., Šefara, J., Machková, N., Hnojem, I., Šály, B., Pereszlényi, M., Hrušecký, I., Hlavatý, I., Juřena, V., Rudinec, R., Magyar, J. & Slávik, M., 1999. Atlas of deep reflection seismic profiles of the Western Carpathians and their interpretation, Geol. Survey of Slovak Rep., Bratislava.

Vozárová, A., Vozár, J., Ebner, F., Pamič, J., Kovács, J., Szederkényi, T.S., Vai, G.B., Venturini, C., Kräutner, H.G., Karamata, S., Krstič, B., Sudar, M. & Mioč, P., 2004. Late Variscan (Latest Carboniferous to Early Permian environments 1:2 500 000 : Tectonostratigraphic terrane and paleoenvironment maps of the Circum-Pannonian region, *Manuskript,* Geological Institute of Hungary, Budapešť, ISBN 963 671 245 X CM.

Wedepohl, K.H., 1995. The composition of the continental crust, *Geochim, Cosmochim. Acta, 59,* 1217–1232.

Weiss, T., Siegesmund, S., Rabbel, W., Bohlen, T. & Pohl, M., 1999. Seismic velocities and anisotropy of the lower continental crust: a review, *Pure appl. geophys., 156,* 97–122.

Wenzel, F., Sperner, B., Lorenz, F. & Mocanu, V., 2002. Geodynamics, tomographic images and seismicity of the Vrancea region (SE-Carpathians, Romania), *EGU Stephan Mueller Special Publication Series, 3,* 95–104.

Zelt, C., 1994. ZPLOT–An interactive plotting and picking program for seismic refraction data, report, Bullard Lab., Univ. of Cambridge, Cambridge, U.K.

Zuchiewicz, W., Tokarski, A.K., Jarosiński, M. & Márton, E., 2002. Late Miocene to present day structural development of the Polish segment of the Outer Carpathians, *Stephan Mueller Special Publication Series,* 3, 185–202.

Table 1. Details of the explosive sources along the S04 profile of the *SUDETES 2003* experiment.

Shot number	Longitude deg E	Latitude deg N	Date [dd.mm.yyyy]	Time UTC [hh:mm:ss.sss]	Charge [kg]
44010	12.762560	51.022500	06.06.2003	08:01:00.000	30
44020	12.836900	20.945500	06.06.2003	16:01:00.000	1000
44030	13.143900	50.829500	06.06.2003	12:16:22.680	425
44031	13.143000	50.829000	06.06.2003	12:25:22.929	2930
44040	13.635666	50.697000	04.06.2003	19:00:00.624	400
44050	13.687163	50.548466	04.06.2003	18:49:59.990	400
44060	14.282000	50.378666	04.06.2003	19:20:00.689	400
44070	14.428166	50.234000	05.06.2003	03:50:00.029	260
44080	15.079601	49.998864	05.06.2003	18:09:59.513	400
44090	15.760150	49.734280	04.06.2003	17:50:01.843	400
44100	16.165500	49.463500	06.06.2003	03:11:15.778	400
44110	16.744416	49.266916	06.06.2003	03:50:01.183	400
44140	18.704250	48.474333	07.06.2003	04:30:00.119	400
44170	19.507500	47.916400	06.06.2003	01:20:00.000	350
44180	19.645800	47.849700	06.06.2003	02:20:00.000	60
44190	19.796100	47.780600	07.06.2003	01:20:00.000	60
44200	19.915500	47.714700	07.06.2003	02:20:00.000	60
44210	20.834400	47.301900	05.06.2003	01:40:00.000	700

P5

Růžek, B., V. Vavryčuk, P. Hrubcová, J. Zedník,
and the CELEBRATION Working Group

Crustal anisotropy in the Bohemian Massif, Czech Republic: Observations based on Central European Lithospheric Experiment Based on Refraction (CELEBRATION) 2000

Crustal anisotropy in the Bohemian Massif, Czech Republic: Observations based on Central European Lithospheric Experiment Based on Refraction (CELEBRATION) 2000

Bohuslav Růžek, Václav Vavryčuk, Pavla Hrubcová, Jan Zedník, and the CELEBRATION Working Group[1]

Geophysical Institute, Academy of Sciences of the Czech Republic, Prague, Czech Republic

[1] We study the azimuthal velocity variation of Pg waves in the Bohemian Massif using data collected during Central European Lithospheric Experiment Based on Refraction (CELEBRATION) 2000. We analyze travel times of waves generated by 28 shots and recorded by 256 portable and 19 permanent seismic stations deployed on the territory of the Czech Republic and in adjacent areas. We use recording offset ranging from 30 to 190 km with azimuths covering the whole interval of angles. The observed travel times are inverted for parameters of a velocity model formed by an isotropic low-velocity subsurface layer with a varying depth lying on a homogeneous transversely isotropic half-space with a horizontal axis of symmetry. The recovered velocity displays a systematic azimuthal variation indicating a regional-scale intrinsic or effective anisotropy in the Bohemian Massif. The mean, minimum and maximum values of the velocity are v_{mean} = 6.03 km/s, v_{min} = 5.98 km/s, v_{max} = 6.10 km/s, respectively, indicating an anisotropy of 1.5–2.5%. The direction of the maximum propagation velocity is ~N35°E being approximately perpendicular to the present maximum compression in the Earth crust in central Europe. The observed anisotropy cannot be induced by stress-aligned cracks in the crust, because the crack models predict azimuthal velocity variations completely inconsistent with the observed one. Therefore we suggest the crustal anisotropy to be induced by a preferred orientation of rock-forming minerals and large-scale intrusion fabrics developed during a tectonic evolution of the Bohemian Massif. *INDEX TERMS:* 0905 Exploration Geophysics: Continental structures (8109, 8110); 0935 Exploration Geophysics: Seismic methods (3025); 7205 Seismology: Continental crust (1242); 7218 Seismology: Lithosphere and upper mantle; *KEYWORDS:* anisotropy, Earth crust, seismic waves, refraction

Citation: Růžek, B., V. Vavryčuk, P. Hrubcová, J. Zedník, and the CELEBRATION Working Group, Crustal anisotropy in the Bohemian Massif, Czech Republic: Observations based on Central European Lithospheric Experiment Based on Refraction (CELEBRATION) 2000, *J. Geophys. Res.*, *108*(B8), 2392, doi:10.1029/2002JB002242, 2003.

1. Introduction

[2] Many observations indicate seismic anisotropy as a ubiquitous property of the Earth crust and upper mantle, which is detected on local as well as regional scales using various types of seismic waves [*Babuška and Cara*, 1991; *Savage*, 1999; *Weiss et al.*, 1999]. The anisotropy of the Earth crust is mostly caused by sediment layering, by stress-aligned systems of microcracks, cracks or fractures, by deformation and faulting of the crust, or by textural ordering of rock-forming minerals in the crust. Crustal anisotropy is studied in the laboratory by measuring P and S wave velocities on rock samples, or in situ using arrivals of P and S waves, splitting of S waves or using surface waves.

[3] So far, crustal anisotropy in the Bohemian Massif and adjacent areas has been measured mainly locally at various isolated sites. It has been measured mostly under laboratory conditions on rock samples from West Bohemia [*Pros et al.*, 1998; *Martínková et al.*, 2000; *Chlupáčová et al.*, 2003] and from the KTB drill hole [*Kern and Schmidt*, 1990; *Kern et al.*, 1991; *Jahns et al.*, 1996; *Berckhemer et al.*, 1997]. These measurements show a rather high scatter of P wave anisotropy and orientation of its axes in dependence on the site and type of rock measured. Also, results for shear wave anisotropy obtained from in situ experiments based on shear wave splitting analysis in West Bohemia [*Vavryčuk*, 1993, 1995] and at the KTB site [*Rabbel*, 1994; *Rabbel and Mooney*, 1996] indicate that the strength of anisotropy can vary significantly within the area under study. Nevertheless, the orientation of anisotropy axes from in situ experiments

---

[1]A. Guterch, M. Grad, G. R. Keller, K. Posgay, J. Vozár, A. Špičák, E. Brueckl, Z. Hajnal, H. Thybo, and O. Selvi.
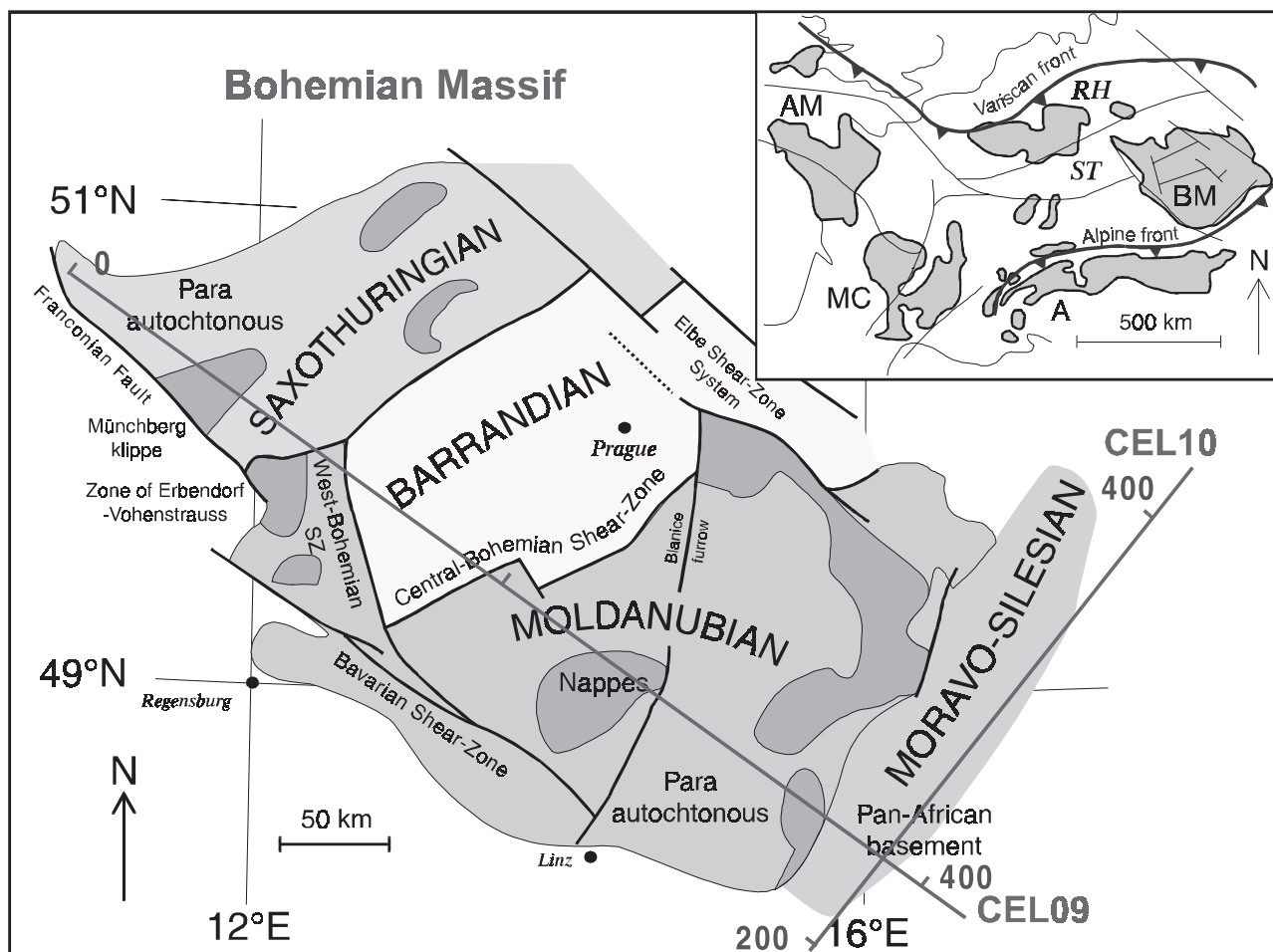
Figure 1. Major tectonic units of the Bohemian Massif and its setting within the European Variscides. BM, Bohemian Massif; AM, Armorican Massif; MC, Massif Central; A, Alps; ST, Saxothuringian Zone; RH, Rhenohercynian Zone [after *Pitra et al.*, 1999; *Franke et al.*, 2000].

seems to be more consistent being related to the direction of the maximum horizontal compressive stress in the region. A similar observation has also been made by *Plomerová et al.* [1981, 1984], who studied the regional-scale velocity variation of waves propagating in the Bohemian Massif. They reported some indications of an increase of *Pg* wave velocities in the NE–SW direction, which is roughly perpendicular to the direction of the maximum compression in the region.

[4] In this paper, we study the upper crustal azimuthal anisotropy of the Bohemian Massif from refraction travel time data collected during Central European Lithospheric Experiment Based on Refraction (CELEBRATION) 2000. We use travel times of *Pg* waves generated by explosions recorded at distances ranging from 30 to 190 km. The travel times of *Pg* waves were measured on records of permanent seismic stations, located on the territory of the Czech Republic and in adjacent areas, and of portable seismic stations, deployed during the CELEBRATION 2000 experiment [*Guterch et al.*, 2001; *Málek et al.*, 2001]. Data from the permanent and portable stations were processed separately and the results were compared. The aim of this study is to decide whether the upper crustal azimuthal anisotropy

can be detected on a regional scale, and if so, to estimate its strength and orientation.

2. Geological and Tectonic Settings

[5] The Bohemian Massif is one of largest stable outcrops of pre-Permian rocks in central and western Europe. It forms the easternmost part of the Variscan Belt, which developed approximately between 500 and 250 Ma during a stage of large-scale crustal convergence, collision of continental plates and microplates and possibly also subduction [*Matte et al.*, 1990]. It consists mainly of high-grade metamorphic and plutonic Paleozoic rocks. On the basis of the respective effects of the Cadomian (Pan-African) and Variscan orogenesis, the Bohemian Massif can be subdivided into various zones, Saxothuringian, Barrandian, Moldanubian, and Moravo-Silesian (see Figure 1). Geographically, it comprises the area of the Czech Republic, partly Austria, Germany, and Poland.

[6] The Moldanubian region represents a major crystalline segment within the Bohemian Massif and its boundary with the Saxothuringian in the NW is regarded to be a major suture-type discontinuity. A structurally higher unit, the

Barrandian, has been thrust over the Saxothuringian rocks toward the northwest, while in the SE it has been thrust in southerly directions over the Moldanubian from which it is separated by a major NE–SW trending Variscan dextral fault, the Central Bohemian Shear Zone [*Dallmeyer et al.*, 1994]. The mostly NE–SW striking Moldanubian/Moravo-Silesian boundary in the east has the character of a major ductile shear zone with a predominance of strike-slip movements. The easternmost part of the Bohemian Massif, the Moravo-Silesian, submerges beneath the Carpathian Foredeep, where it reappears as a basement reactivated during the Alpine orogeny.

[7] From a tectonic point of view, one of the major forming effects was during Variscan orogeny when the Bohemian Massif, as part of Armorica plate, was sandwiched between high-grade Variscan metamorphic areas and initially between two oceanic, then continental, opposing subduction zones [*Matte*, 2001]. The boundaries between the Saxothuringian and Barrandian and between the Barrandian and Moldanubian crustal domains to the west, as well as, between the Moldanubian and Brunovistulian platform to the east were of NE–SW trending and indicated the direction of corresponding metamorphic and intrusion activities. The oldest (370–380 Ma) deformational fabrics occur in the Barrandian complex; they trend NE–SW and dip to the SE. The development of these structures is associated with earliest stages of the Saxothuringian eastward subduction and shortening of the plate. The upper plate progressively evolved into a lithospheric scale arc system, which culminated at around 350–345 Ma and was manifested by intrusion of the Central Bohemian Plutonic Complex. The intrusion fabrics of this intrusive complex are steeply dipping into the east and parallel to the western boundary of the Barrandian domain. The crustal root of the Moldanubian shows nearly vertical NE–SW trending fabrics (estimated age of 370–330 Ma) developed mostly in granulites and associated mantle slivers [*Schulmann et al.*, 2002].

[8] The Moldanubian segment contains mainly high-grade gneisses and migmatites of supracrustal origin, orthogneisses, granulites and numerous Variscan posttectonic granitiod intrusions. The Barrandian is composed largely of Precambrian sedimentary and volcano-sedimentary sequences overlain unconformably by Early Paleozoic strata. The easternmost part of the Saxothuringian zone belonging to the Bohemian Massif is dominated by relatively low-grade sedimentary and volcanic rocks controlled by a number of large NE trending synforms and antiforms from a late stage of deformation. The Moravo-Silesian includes autochtonous Cadomian basement, Brunovistulicum, with its Devonian to Carboniferous sedimentary cover.

3. Data

[9] A large-scale seismic refraction experiment CELEBRATION 2000 (C2000) was realized on the territory of Poland, the Czech Republic, the Slovak Republic, Austria, Hungary, Germany, Russia, and Byelorussia in June 2000 with the aim of investigating the deep lithospheric structure of central Europe. During the C2000 experiment 147 shots were fired, 1200 portable seismic

stations were distributed along 5400 km of profiles, and about 160 000 seismic records were gathered. The average distance between shots was 30 km with a station spacing of 2.7 km. The positions of shots and stations were checked by GPS; the origin time was controlled by a DCF77 timer with an accuracy of 3 ms. The sensors of portable stations were 4.5 Hz geophones, recording instruments were TEXAN, REFTEK and PDAS provided by the IRIS Consortium under the PASSCAL program, by the University of Texas at El Paso, USA, and by GeoForschungsZentrum Potsdam, Germany.

[10] As part of the C2000 experiment, the region of the Bohemian Massif was studied along two international profiles: C09 and C10. Profile C09 traverses the whole Bohemian Massif in the NW–SE direction: it starts in the NW in the Saxothuringian, transects mafic amfibolite complex intrusion and continues to the Barrandian. Then it crosses the granitoid intrusions spreading along the Central Bohemian Shear Zone and continues to the Moldanubian, Moravo-Silesian and further SE to the Neogene basins and Carpathian Foredeep. Profile C10 is spreading along the eastern edge of the Bohemian Massif in Moravo-Silesian unit being almost perpendicular to C09. Starting in SW it crosses the Brunovistulic crystalline complex and continues to the NE to Carboniferous Paleozoic cover. The purpose of these profiles was to investigate the structure of the Bohemian Massif (C09) and of the transition zone between the Bohemian Massif and the Carpathians (C10).

[11] A total of 40 shots were fired along the C09 and C10 profiles with charges ranging from 210 kg to 10713 kg of explosives. For our purpose, we have analyzed recordings from 14 shots fired along the C09 profile, from 9 shots fired along the C10 profile, and additionally from 5 shots fired off any profile (see Table 1). Hence the geometry comprises 23 inline and 5 offline shots. All shots used in the computations were recorded by two types of instrumentation: by portable and permanent seismic stations (see Figure 2). As the extent and quality of the respective data sets is different, they were processed separately and the results were compared.

3.1. Data From Permanent Stations

[12] Figure 3 shows the ray path coverage for *Pg* waves observed at permanent stations operated on the territory of the Czech Republic and in adjacent areas. We have used recording offset ranging from 30 to 190 km. A minimum distance of 30 km was applied to eliminate local-scale effects. The upper limit of 190 km represents the maximum distance at which the arrivals of *Pg* waves, excited by the C2000 explosions, were identified and measured on recordings reliably. The total number of rays is 135. The azimuthal distribution of rays is uniform. Most permanent seismic stations are equipped with three-component broadband sensors and recordings are performed with a sampling frequency of 20 Hz. The corner frequency of the analogue antialias Bessel filter was 5 Hz. The accuracy of picking of arrival times is around 200 ms. This value was assured by exploring the differences between travel times corresponding to doubled explosions (shots fired twice at the same site, see Table 1). The travel times provided by the permanent stations form a nearly

Table 1. List of Shots

Day	Time, UT	Shot ID	Charge, kg	H, m	φ, °N	λ, °E	Territory
			Profile C10 Shots				
16	2215:00.000	20092	210	662	49.8716	17.3891	Czech Republic
23	2100:12.320	20070	210	320	49.1449	16.4381	Czech Republic
23	2245:00.000	20100	210	428	50.0757	17.6246	Czech Republic
23	2315:00.000	20080	210	619	49.4464	16.8323	Czech Republic
24	0015:00.000	20081	210	619	49.4464	16.8327	Czech Republic
24	0100:00.000	20090	210	660	49.8721	17.3894	Czech Republic
24	0115:00.000	20091	210	661	49.8719	17.3892	Czech Republic
25	0300:00.223	20060	210	350	48.6033	15.8447	Austria
25	0344:59.730	20050	210	420	48.3404	15.5951	Austria
			Profile C09 Shots				
23	1914:30.133	29020	210	526	50.5444	11.7666	Germany
23	1931:12.417	29010	210	270	50.6875	11.5573	Germany
24	2100:00.000	29100	210	476	49.3124	14.5900	Czech Republic
24	2200:00.000	29090	210	474	49.5182	14.1295	Czech Republic
24	2245:00.000	29120	210	612	49.0191	15.3173	Czech Republic
24	2315:00.000	29121	210	615	49.0191	15.3168	Czech Republic
25	0015:00.000	29110	210	492	49.1892	14.9104	Czech Republic
25	0045:00.000	29111	210	492	49.1896	14.9105	Czech Republic
26	0015:00.000	29051	210	679	50.0210	12.9091	Czech Republic
26	0100:00.000	29060	210	661	49.9251	13.0923	Czech Republic
26	0115:00.000	29061	210	661	49.9249	13.0925	Czech Republic
26	0214:59.997	29130	210	459	48.8526	15.6997	Austria
26	0230:00.396	29140	210	417	48.6723	16.1564	Austria
26	0348:05.896	29070	435	545	49.8725	13.1993	Czech Republic
			Off-Profile Shots				
23	1900:30.767	29040	413	630	50.1212	12.2250	Czech Republic
24	0315:00.735	26900	160	220	50.5629	13.7243	Czech Republic
25	0315:00.113	26910	200	399	50.2166	12.6683	Czech Republic
25	0329:59.895	26911	3954	399	50.2172	12.6677	Czech Republic
26	0315:00.805	29080	910	446	49.6453	14.3491	Czech Republic

linear time-distance curve (see Figure 3). The mean value of the *Pg* velocity obtained by the least squares is 6.075 km/s with a standard deviation of arrival times of 422 ms. The offset at zero distance caused by the low-velocity layer is 496 ms.

3.2. Data From Portable Stations

[13] Figure 4 shows the ray path coverage for *Pg* waves observed at the C2000 portable stations used in our study. The length of the ray paths covers a range of 30 to 150 km. The azimuthal distribution of rays indicates that the distribution is not uniform, because many rays follow the directions of profiles. However, shots fired off the profiles and cross-profile measurements allowed to spread the spatial distribution of rays over the whole range of azimuths. The total number of rays is 1475. The sampling frequency of one-component (vertical) recordings was 100 Hz. The corner frequency of the antialias FIR filter was 40 Hz. The accuracy of the measured arrival times of *Pg* waves was thus around 50 ms, which shows remarkably higher accuracy than for permanent stations. The travel times form a nearly linear time-distance curve. This indicates that the velocity distribution of the Bohemian Massif has no strong vertical velocity gradient. The mean value of the *Pg* velocity obtained by the least squares, the standard deviation of arrival times, and the time offset at zero distance attributed to a low-velocity layer are summarized in Table 2. The values are calculated for the whole data set and for the C09 and C10 profiles separately. The table shows that the mean velocity for the C10 profile is slightly

higher than for the C09 profile. This is an indication of a weak anisotropy or slight lateral inhomogeneity present in the Bohemian Massif.

4. Time-Term Method

[14] We assume a homogeneous anisotropic crust covered by a thin low-velocity isotropic layer with a variable thickness and velocity. The total travel time τ_{ij} between shot i and station j is expressed as follows [*Bamford*, 1977; *Song et al.*, 2001]:

$$\tau_{ij} = a_i + b_j + D_{ij}S, \tag{1}$$

where a_i is the ith shot delay term ("the shot correction"), b_j is the jth station delay term ("the station correction"), D_{ij} is the epicentral distance between shot i and station j, and S is the slowness. The delay terms a_i and b_j represent the time spent by the refracted wave in the low-velocity layer, thus they combine the effect of the thickness of the layer with its

Table 2. Linear Regression of Travel Times

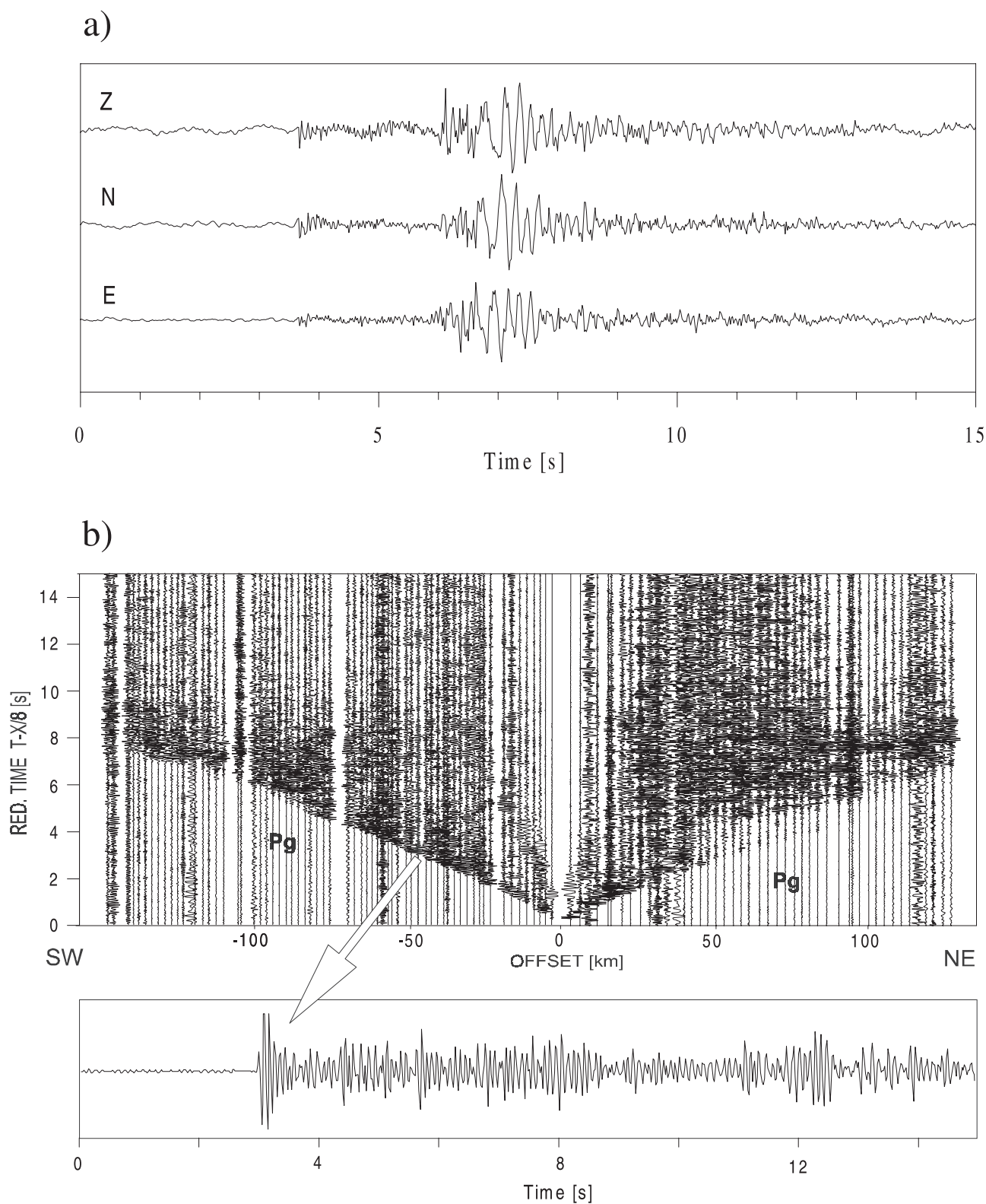| Data Set	Mean Velocity, km/s	Standard Deviation of Time Residuals, ms	Time Offset at Zero Distance, ms
C09 profile	5.964	176	171
C10 profile	6.096	194	446
C09+C10 profiles	6.013	201	279

Figure 2. (a) A three-component velocigram recorded at permanent station PRU (shot 29080, epicentral distance 41 km). (b) Vertical velocigrams recorded at portable stations deployed along profile C10 (shot 20080, time is reduced using $v = 8$ km/s).
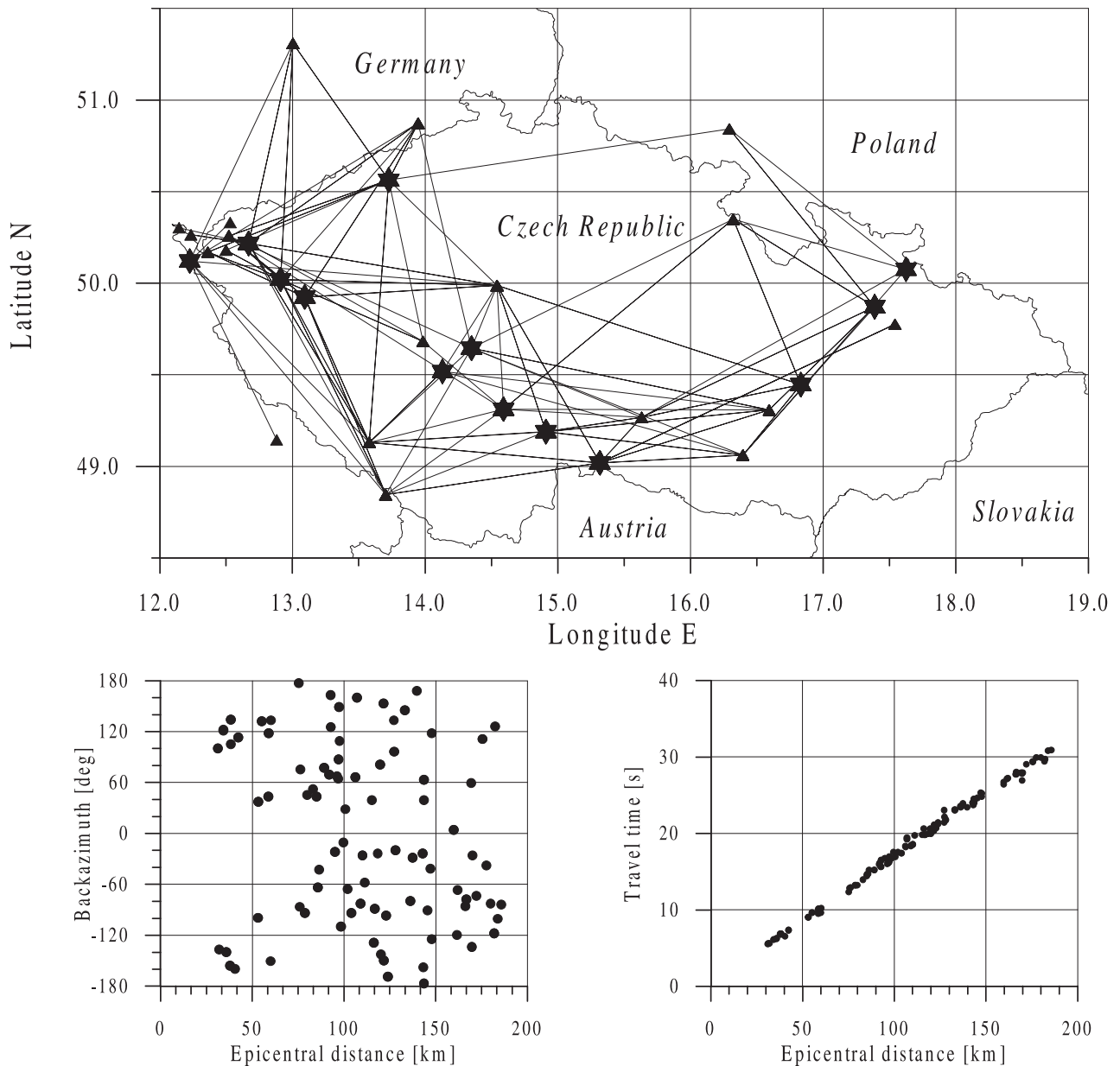
Figure 3. (top) Ray path coverage for waves recorded by permanent seismic stations deployed on the territory of the Czech Republic and in adjacent areas. Shots are marked by stars, and stations by triangles. (bottom left) Azimuth-distance distribution of the data. (bottom right) *Pg* travel times as a function of epicentral distance (the mean velocity is 6.075 km/s, the offset at zero distance is 496 ms).

velocity beneath each shot and station. The properties of the surface layer can probably vary significantly in the area studied and are considered to be unknown. The delay times may also reflect systematic errors in timing or phase identification errors, hence they represent all unknown effects, which should be isolated and removed from the travel times. The shot/station corrections are linearly dependent in equation (1); hence usually only their sum for a given ray (called "the total correction") can be uniquely determined. The separation of shot/station corrections is possible, if at least one of shots is located near a station, so the corresponding corrections can be matched.

[15] The quantity of interest is the slowness S and its azimuthal variation. Assuming mostly horizontal propaga-

tion of refracted waves in a weakly anisotropic crust, we can put [*Backus*, 1965]

$$S = S_0(1 + A\cos 2\varphi + B\sin 2\varphi + C\cos 4\varphi + D\sin 4\varphi), \quad (2)$$

where $S_0 = 1/v_0$ is the slowness in the isotropic reference medium, v_0 is the velocity in the isotropic reference medium, φ defines the azimuth in which the wave propagates, and constants A, B, C, and D are small unknown coefficients which are linear combinations of the elastic parameters defining weak anisotropy. For weak transverse isotropy with a horizontal axis of symmetry, formula (2) simplifies to [*Song et al.*, 2001]

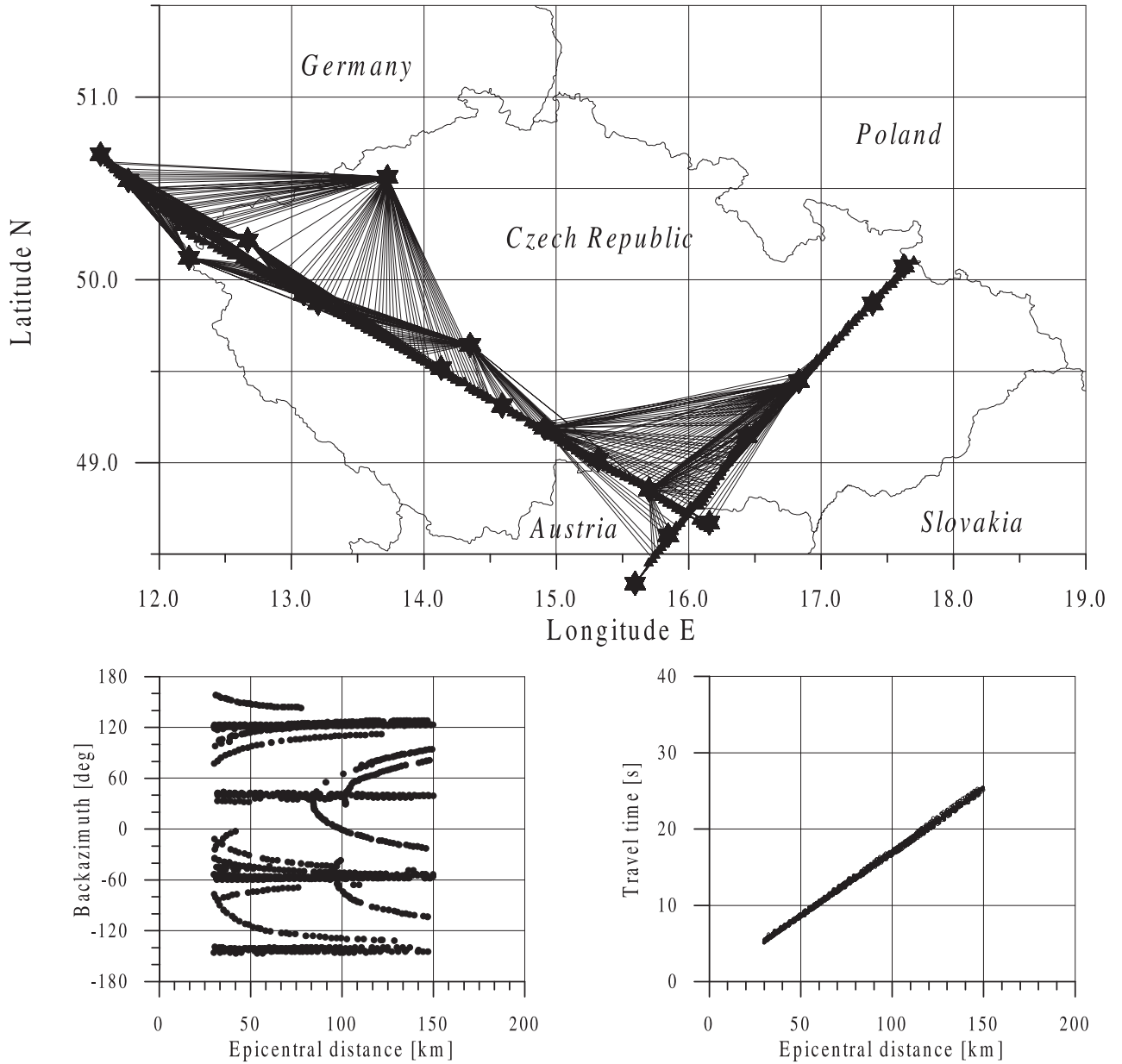$$S = S_0(1 + E\cos 2(\varphi - \varphi_0) + F\cos 4(\varphi - \varphi_0)), \quad (3)$$

Figure 4. Ray path coverage for waves recorded by portable seismic stations. For details, see Figure 3 caption. The mean velocity calculated from the travel times is 6.013 km/s, and the offset at zero distance is 279 ms.

or, equivalently, to [*Vavryčuk*, 1997, equation 15]

$$S = S_0\left(1 + G\cos^2(\varphi - \varphi_0) + H\cos^4(\varphi - \varphi_0)\right), \quad (4)$$

where φ_0 is the angle defining the orientation of the symmetry axis in the horizontal plane, and E, F, G, and H are small unknown coefficients defining transverse isotropy. The azimuthal variation of velocity v can be expressed from equation (4) as

$$v = \frac{1}{S} = \frac{1}{S_0}\left(1 - G\cos^2(\varphi - \varphi_0) - H\cos^4(\varphi - \varphi_0)\right). \quad (5)$$

Equations (2)–(5) are valid only under weak anisotropy; hence they are applicable to anisotropy coefficients less than 0.1.

5. Inverse Problem

[16] The inversion is performed by minimizing two different misfit functions in the L2 norm: we minimize the absolute time residuals,

$$\chi^2_{\text{ABS}} = \frac{1}{n-1}\sum\left(t_{ij} - \tau_{ij}\right)^2 = \min, \quad (6)$$

and the relative time residuals,

$$\chi^2_{\text{REL}} = \frac{1}{n-1}\sum\left(\frac{t_{ij} - \tau_{ij}}{t_{ij}}\right)^2 = \min, \quad (7)$$

where n is the total number of data, t_{ij} are the observed and τ_{ij} are the calculated travel times between the ith shot and

*j*th station. We use the two misfit functions in order to assess the reliability of the results obtained. Misfit function (6) represents a standard minimization procedure. Misfit function (7) reflects a varied quality of the observed data. The travel times measured at large epicentral distances are less accurate because the amplitudes of waves are more attenuated and less identifiable in noise. Hence higher travel times are automatically given lower weights proportional to $1/D_{ij}$.

[17] The minimization is performed with respect to the following sets of parameters: shot/station time corrections a_i and b_j, and parameters defining general weak anisotropy A, B, C, D, and S_0 (equation (2)) or alternatively parameters defining weak transverse isotropy G, H, S_0, and φ_0 (equation (4)). The inverse problem is linear with respect to the shot/station corrections (40 parameters for the data set from permanent stations and 256 parameters for the data set from portable stations) and with respect to the parameters defining general anisotropy (5 parameters), but nonlinear with respect to the parameters defining transverse isotropy (4 parameters). Hence the inversion for general anisotropy is fully linear, but the inversion for transverse isotropy is partly nonlinear. The linear inversion for general anisotropy is performed using the singular value decomposition (SVD) matrix method [*Press et al.*, 1992, p. 51]. The inversion for transverse isotropy is split into two parts: linear ("internal") and nonlinear ("external"). The nonlinear inversion is performed using Powell's optimizing algorithm [*Press et al.*, 1992, p. 406]. The task of this optimization is to find the optimum values of anisotropy parameters G, H, S_0, and φ_0. The linear inversion uses the SVD matrix method and provides an optimum combination of shot/station corrections for each trial set of anisotropy parameters required for the nonlinear optimization.

6. Synthetic Tests

[18] In order to check the robustness of the inversion, we performed a series of synthetic tests for the ray geometries with permanent (see Figure 3) as well as portable (see Figure 4) stations. We preserved the number of stations and shots and their positions and assume a synthetic velocity model of the Earth crust formed by a homogeneous transversely isotropic half-space with the parameters

$$v_0 = 6.0 \text{ km/s}, G = H = -1.266 \times 10^{-2}, \varphi_0 = 60°, \quad (8)$$

covered by a low-velocity isotropic layer. The propagation velocity in the half-space varies from 6.0 km/s in azimuth 150° to 6.152 km/s in azimuth 60°. The mean velocity is 6.066 km/s. The strength of anisotropy is 2.5%. The low-velocity layer is introduced by synthetic shot/station corrections, which are generated randomly with a uniform nonzero probability density in the interval from 0 to 1 s and with zero probability density elsewhere. Moreover, a synthetic Gaussian noise is superimposed on the theoretical travel times in order to simulate the properties of the observed data. The noise is generated with zero mean and with a standard deviation of 300 ms for permanent stations or 200 ms for portable stations, respectively. These values simulate errors present in the observed travel times caused mainly by inaccurate phase picking and by neglecting
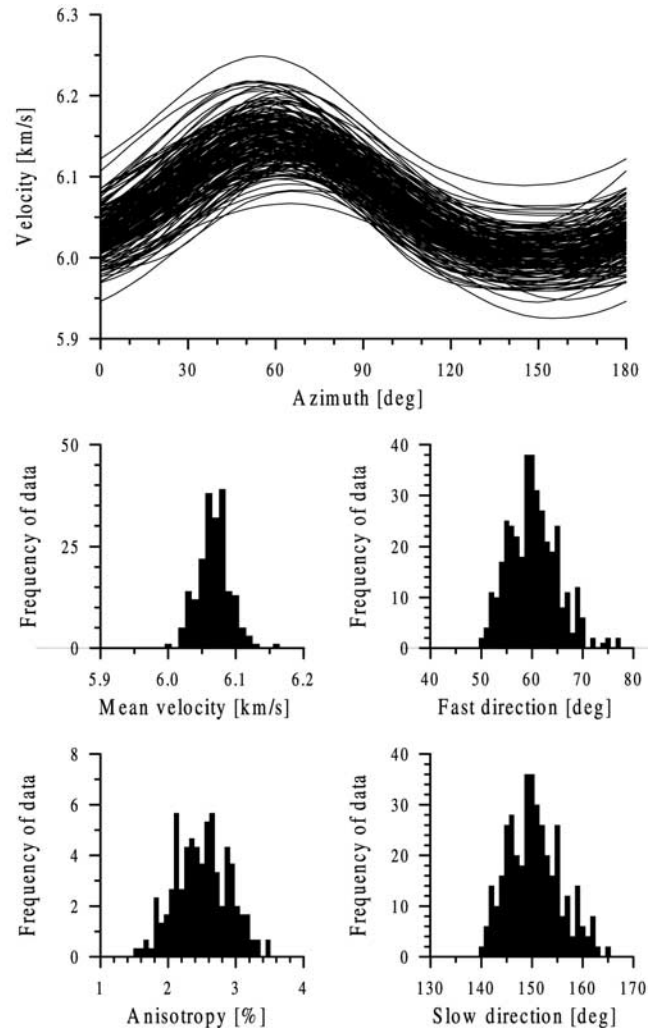

Figure 5. Results of the inversion of synthetic data for the permanent stations. (top) Azimuthal variation of velocity. (bottom) Histograms showing the scatter of the inverted parameters.

inhomogeneities in the crust. The synthetic travel times are inverted for values defined in equation (8). To obtain statistically relevant results, the noise superposition and the subsequent inversion were performed 200 times.

[19] Figures 5 and 6 present the results of the inversion for transverse isotropy (equation (4)) using misfit function (6) for the ray geometry with permanent and portable stations, respectively. The results are also summarized in Table 3. The upper plots in Figures 5 and 6 show the propagation velocity as a function of azimuth. Figures 5 and 6 show 200 inverted curves, each curve corresponding to a particular realization of the noise. It is evident that the family of curves in Figure 5 is much broader than that in Figure 6. This implies that the inversion of data from the portable stations yields remarkably more accurate results than that from the permanent stations. The error for portable stations is ~3 times lower than the error for permanent stations. This is caused mainly by the higher number of rays and by the higher accuracy of picking of arrival times achieved for the portable stations. Nevertheless, the curves surround the true velocity function
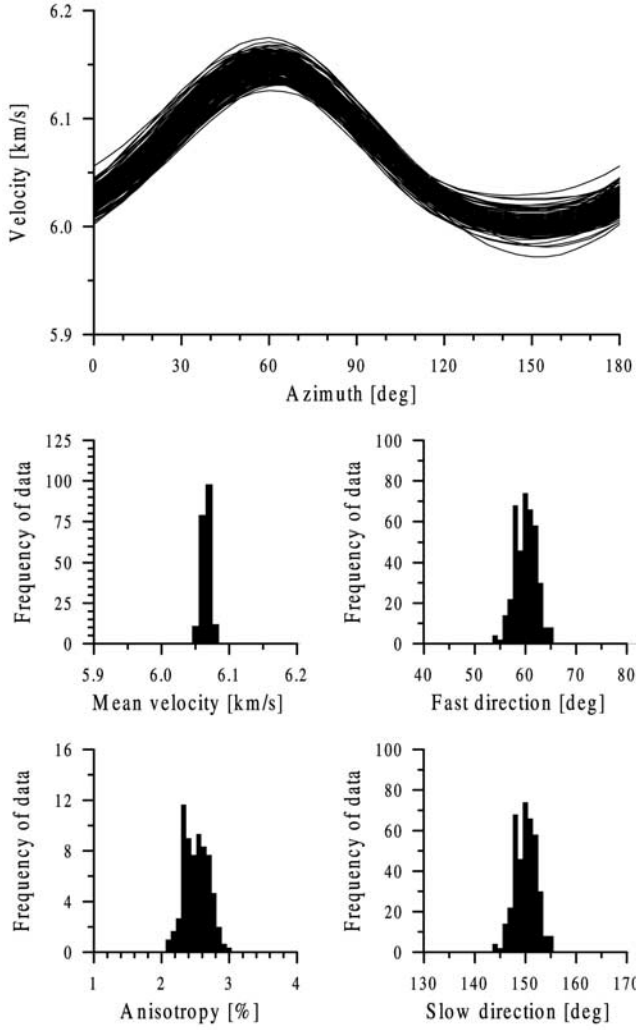
Figure 6. Same as in Figure 5 but for data from the portable stations.

in both cases, and the averaged curves approximate the exact curve quite accurately (see Table 3). The lower plots in Figures 5 and 6 show other statistical properties of the results: histograms of the mean velocity averaged over all azimuths, histograms of the azimuth of maximum and minimum velocities, and histograms of the strength of anisotropy. The mean velocity is calculated by

$$v_{mean} = \frac{1}{S_0}\left(1 - \frac{1}{2}G - \frac{3}{8}H\right), \qquad (9)$$

obtained by averaging equation (5) and using the following identities:

$$\frac{1}{2\pi}\int_0^{2\pi}\cos^2\varphi\,d\varphi = \frac{1}{2}, \quad \frac{1}{2\pi}\int_0^{2\pi}\cos^4\varphi\,d\varphi = \frac{3}{8}. \qquad (10)$$

The strength of anisotropy is defined as

$$\varepsilon = 2\frac{v_{max} - v_{min}}{v_{max} + v_{min}}100\%, \qquad (11)$$

where v_{max} and v_{min} are the maximum and minimum propagation velocities, respectively. Figures 5 and 6 (bottom plots) show that all mentioned quantities approximate the exact values well. Hence the synthetic tests prove that the optimization procedure does not fall into false local minima of equation (6) or (7) corresponding to incorrect or significantly biased results, and that the inversion is well conditioned for both ray geometries. The tests also indicate that when inverting observed data, the azimuth of the maximum velocity should be found with an accuracy of several degrees, and anisotropy with strength of 2–3% should be reliably detected. Therefore we conclude that the ray path coverage, the extent and quality of the input data and the computing tools applied are sufficiently powerful to determine accurately the background isotropic velocity and the strength and orientation of the searched regional-scale anisotropy in the crust.

7. Results

[20] The observed data are inverted in a similar way as those in the synthetic tests. Instead of performing 200 independent perturbations around synthetic travel times, we now perform 200 independent perturbations around travel times calculated from the optimum velocity model found by the inversion. The procedure consists of the following steps: (1) Construction of an optimum velocity model corresponding to the observed travel times and determination of the shot/station corrections, (2) calculation of the theoretical travel times corresponding to the found optimum velocity model and shot/station corrections, (3) superposition of synthetic Gaussian noise with zero mean and with a standard deviation of 300 ms for permanent stations and of 200 ms for portable stations on the theoretical travel times, (4) inversion of the noisy theoretical travel times, and (5) 200 repetitions of steps 3 and 4 for different noise realizations.

Table 3. Inversion of Synthetic Data

| Source of Data	Test Parameters				Test Results		
	Gaussian Noise Level, ms	Number of Stations	Number of Shots	Number of Data	Mean Velocity, km/s	Fast Direction, deg	Anisotropy, deg
Optimization of Absolute Time Residuals							
Portable stations	200	228	28	1475	6.066 ± 0.006	60 ± 2	2.51 ± 0.18
Permanent stations	300	19	21	135	6.068 ± 0.023	60 ± 5	2.47 ± 0.37
Optimization of Relative Time Residuals							
Portable stations	200	228	28	1475	6.065 ± 0.007	60 ± 3	2.47 ± 0.22
Permanent stations	300	19	21	135	6.071 ± 0.025	60 ± 7	2.35 ± 0.44
Exact values					6.066	60	2.5

a)

b)
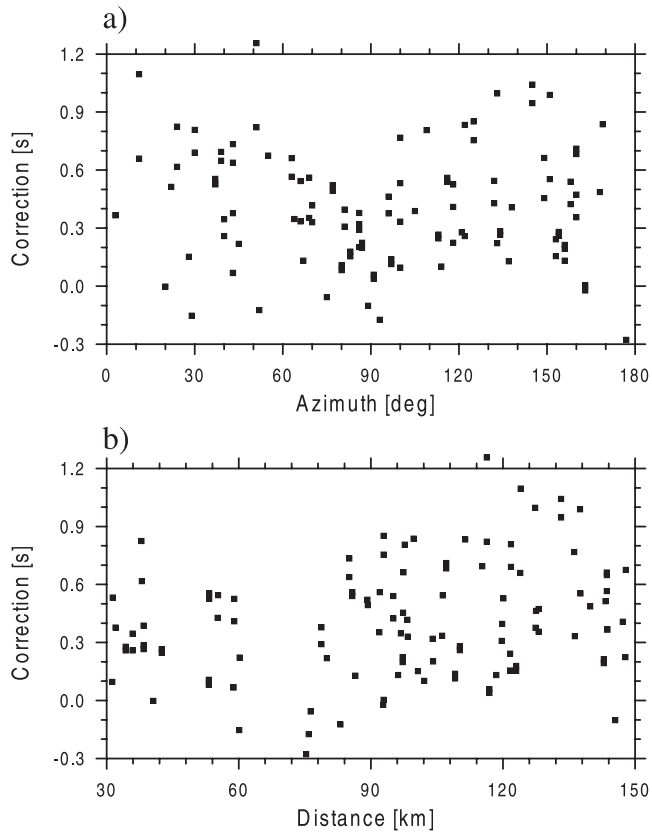
Figure 7. Total time corrections as a function of (a) azimuth and (b) epicentral distance.

[21] The results of the inversion are summarized in Table 4. Figures 7, 8, and 9 show the results if absolute time residuals (6) observed at permanent stations are minimized and a transversely isotropic medium (4) is assumed. Figures 10, 11, and 12 show the same for portable stations. The minimization reduced the standard deviation of time residuals from 422 ms to 271 ms for permanent stations and from 201 ms to 99 ms for portable stations. Nearly the same values are obtained if relative time residuals (7) are minimized (see Table 4).

7.1. Permanent Stations

[22] Figure 7 shows the total time corrections (the sum of the shot and station corrections for a given ray) as a function of azimuth and epicentral distance. We do not show shot/station corrections separately because of their linear dependency. The corrections vary from -0.3 s to 1.2 s and should reflect lateral inhomogeneities and systematic errors in picking of waves. The corrections display no significant trend indicating no or very weak dependence on the azimuth or epicentral distance. Figure 8 shows the retrieved azimuthal variation of the Pg velocity together with histograms quantifying its statistical properties. The figure indicates that the medium is anisotropic with the fast direction in $30-35°$ and with strength of anisotropy of $2-3\%$. Figure 9 shows that the optimum velocity variation is almost independent of the inversion scheme used (linear or nonlinear). Figure 9 also shows that the observed data display a rather high scatter even though the shot/station
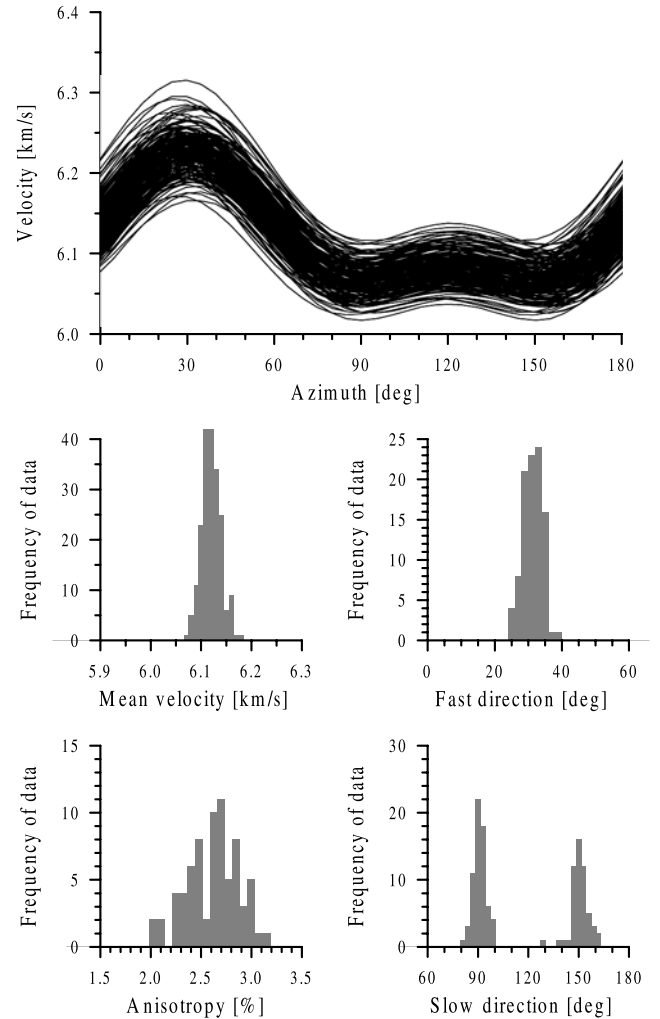

Figure 8. Results of the inversion from data observed at the permanent stations.
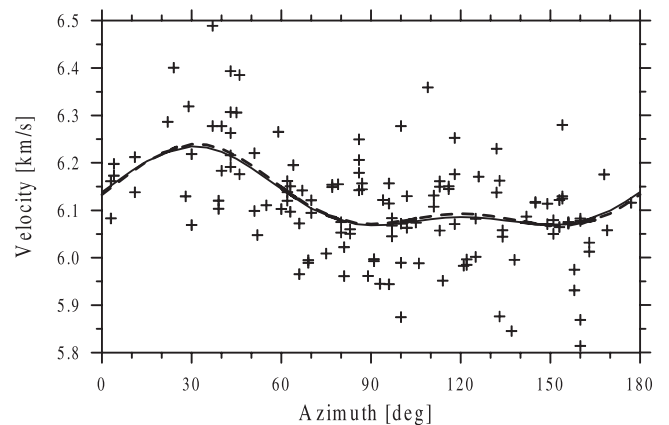

Figure 9. Optimum velocity variations under general weak anisotropy (dashed line) and weak transverse isotropy (solid line) calculated using equations (2) and (4) and data from permanent stations (marked by crosses).
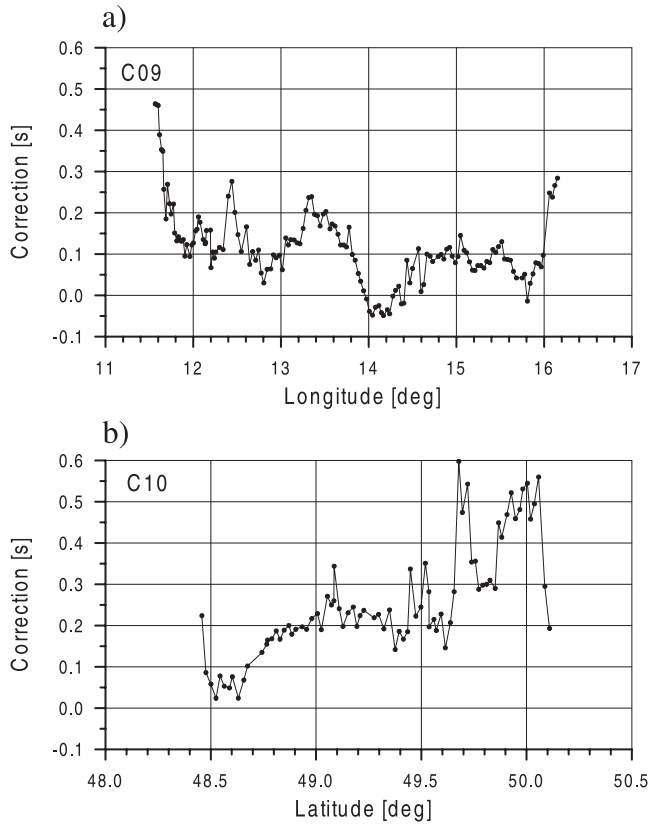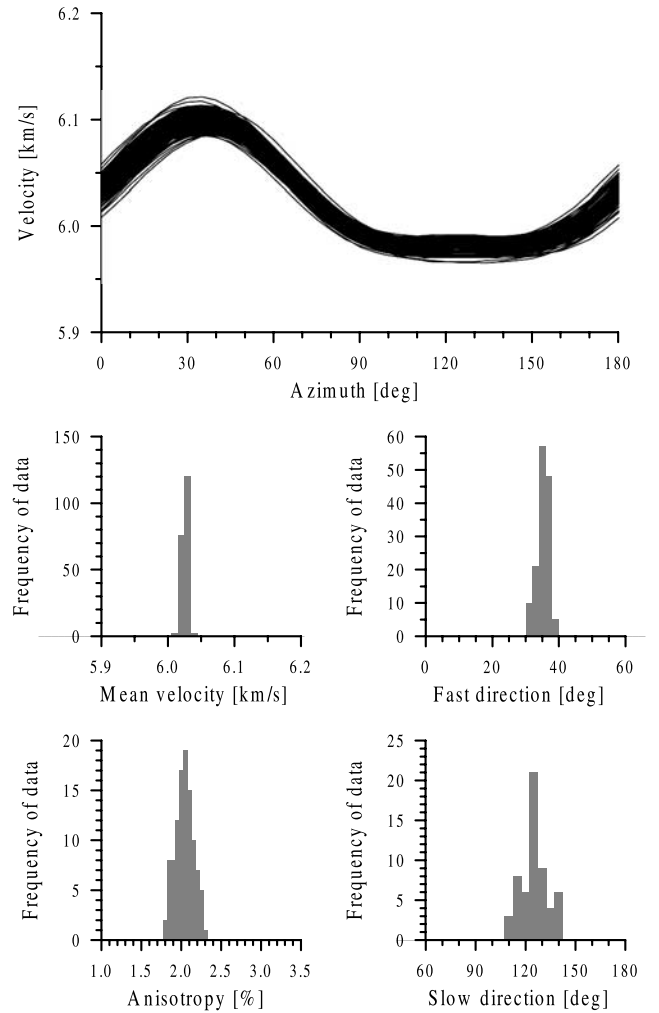
Figure 10. Station corrections along the (a) C09 and (b) C10 profiles.

Figure 11. Results of the inversion from data observed at the portable stations.

corrections have been applied. This might indicate that effects owing to lateral inhomogeneities under a subsurface layer are at least of the same order as those owing to anisotropy.

7.2. Portable Stations

[23] Figure 10 shows the station corrections along the C09 and C10 profiles. We separated the station corrections from the total corrections owing to shots situated on the profiles. The corrections vary from −0.05 s to 0.6 s and display systematic trends, which correlate with a geological structure along both profiles.

[24] Looking at the C09 profile from NW (see Figure 10a), the high corrections (low velocities) at longitude 11.5°E are connected with Saxothuringian Carboniferous rocks. The mafic intrusions are manifested by low corrections (high velocities) around 11.8–12°E. The Saxothuringian crystalline complex (gneisses, migmatites) shows the corrections in 12–12.8°E. High values around 12.5°E coincide with Neogene sedimentary basins. Low values around 12.8°E are connected with mafic intrusions (amfibolite complex). The Barrandian unit (metasediments and Paleozoic strata) extends around 12.8–13.8°E. Low corrections in 13.8–14.3°E can be associated with granitoid plutons with mafic intrusions (amfibolites, diabases, melaphyres) on the Barrandian/Moldanubian contact. The oscillations around 14.5°E can be connected with Tertiary and Quaternary sediments. The Moldanubian unit (gneisses, migmatites and granitoid intrusions) covers the interval 14.5–15.5°E. The Moravo-Silesian unit starts at 15.7°E
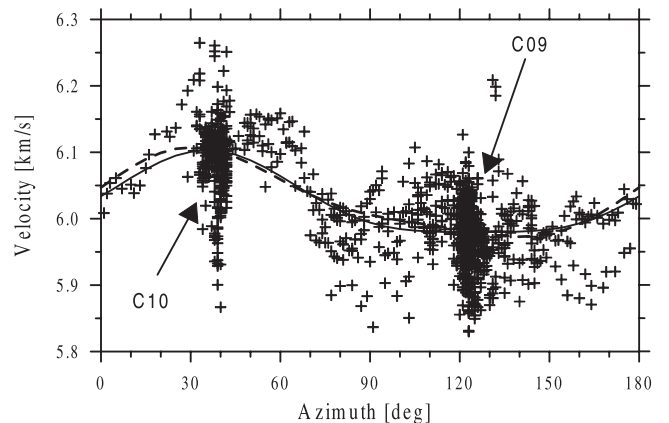

Figure 12. Optimum velocity variations under general weak anisotropy (dashed line) and weak transverse isotropy (solid line) calculated using equations (2) and (4) and data from portable stations (marked by crosses).

Table 4. Inversion of Observed Data

Source of Data	Inversion Parameters			Inversion Results				
	Number of Stations	Number of Shots	Number of Data	Mean Velocity, km/s	Fast Direction, deg	Slow Direction, deg	Anisotropy, %	Standard Deviation of Time Residuals, s
				Optimization of Absolute Time Residuals				
Portable stations	228	28	1475	6.026 ± 0.004	35 ± 2	126 ± 9	2.04 ± 0.12	0.10
Permanent stations	19	21	135	6.121 ± 0.019	31 ± 3	121 ± 30	2.68 ± 0.25	0.27
				Optimization of Relative Time Residuals				
Portable stations	228	28	1475	6.027 ± 0.005	39 ± 3	129 ± 6	1.46 ± 0.15	0.12
Permanent stations	19	21	135	6.041 ± 0.022	35 ± 5	125 ± 26	2.36 ± 0.41	0.31

and extends further to the SE to the Neogene sedimentary basin.

[25] The station corrections along the C10 profile (see Figure 10b) start with high values at latitude 48.4°N attributed to sediments. Then they show a low minimum in 48.5–48.7°N corresponding to a crystalline metamorphic unit. Latitudes 48.7–49.4°N define granitoid intrusions with Neogene sediments around 49.1°N. Paleozoic sediments of Carboniferous age coincide with oscillations in 49.4–49.7°N. The Neogene and Quaternary sediments produce high corrections in 49.7–49.8°N, while mafic intrusions lower the corrections around 49.8°N. High values in 49.8–50.1°N correspond to Paleozoic Carboniferous rocks.

[26] The good correspondence between the station corrections and the geological structure under stations implies that the time term method used in the inversion is capable to effectively separate effects of subsurface inhomogeneities from those of anisotropy. Figure 11 shows the inversion results related to anisotropy. The retrieved anisotropy has the fast direction in 35° and strength of 2%. Figure 12 shows the optimum velocity variations for linear (2) and nonlinear (4) inversion schemes together with observed data after applying shot/station corrections. The figure indicates that the mean value of the *Pg* velocity along the C10 profile is distinctly higher than that for the C09 profile (despite a rather high scatter of the data along both profiles). The high-velocity anomaly is, however, observed not only for the C10 profile traversing the Moravo-Silesian unit but it is observed consistently for all rays in similar azimuths (20–40°) crossing different geological units of the Bohemian Massif (see Figures 1 and 4). This implies that the anomaly can be attributed to anisotropy rather than to different crustal structures beneath the two profiles (e.g., high velocities in the Moravo-Silesian unit). The lateral inhomogeneities under a subsurface layer produce the scatter in the observed data (Figure 12).

7.3. Permanent and Portable Stations

[27] The results demonstrate that the data set from the portable stations (Figure 11) provides much higher accuracy than that from the permanent stations (Figure 8). The scatter of the curves displaying the azimuthal variation of velocity is much larger for the data from the permanent stations than for those from the portable stations. The same is evident from the corresponding histograms: the width of histograms is remarkably larger for the permanent than for the portable stations. The same effect has been observed in synthetic tests (Figures 5 and 6) and can be explained by the low number of travel times and low sampling frequency

for permanent stations. In spite of the different accuracy, the results of the inversion display a good stability and consistency with respect to the data set and the optimizing mode used. Either relative or absolute travel time residuals yield similar values for both data sets: the direction of the maximum velocity varies from 30° to 40°, the direction of the minimum velocity varies from 120° to 130°, and the anisotropy ranges from 1.5% to 2.5%. Also the azimuthal variations of velocity display similar shapes. Intriguingly, the azimuthal variations show well-defined maxima, but shallow and rather indistinct minima. The azimuthal variations retrieved from the permanent stations (Figures 8 and 9) even indicate the existence of two different minima with azimuths around 100° and 150°.

[28] Table 4 presents the retrieved values together with their errors calculated according to the procedure described above. We stress that the procedure is rather simple and able to provide only basic information on the stability of the inversion. The calculated errors, therefore, do not follow the errors of inverted values exactly. The actual errors should reflect many inconsistencies produced by simplifications in the numerical modeling (e.g., non-Gaussian distribution of noise in the observed data, inhomogeneities in deeper parts of the crust, varying orientation and strength of anisotropy, lower symmetry of anisotropy). As a consequence, the actual errors of the retrieved values may be larger than those estimated theoretically.

8. Discussion

[29] We found that the overall azimuthal velocity variation attributed to anisotropy is 1.5–2.5% and the direction of the maximum velocity is ∼N35°E. Interestingly, similar anisotropy values have been detected also for the upper mantle anisotropy studied by *Pn* waves in the west of the Bohemian Massif (so far, no information on *Pn* anisotropy in the Bohemian Massif is available). *Bamford* [1977] studied the uppermost mantle *Pn* velocity beneath southern Germany from a dense network of refraction profiles and reported an anisotropy of 6–7% with the maximum velocity in the direction N20°E. *Enderle et al.* [1996] updated this interpretation and reported an overall *P* wave anisotropy of 3–4% in a horizontal plane immediately below the Moho at a depth of 30 km with the maximum velocity in the direction N31°E. The anisotropy increases to 11% at a depth of 40 km. *Song et al.* [2001] studied the uppermost mantle anisotropy in the western part of the Bohemian Massif and in Germany using regional earthquake *Pn* travel time data and obtained an anisotropy of 3.5–4% with the maximum velocity in the direction ∼N25°E.
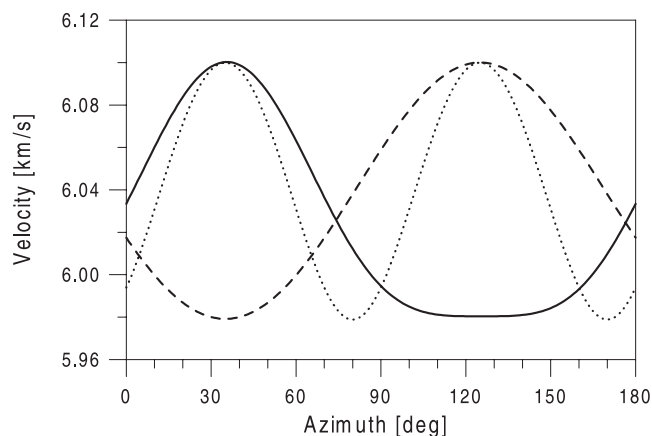
Figure 13. Velocity variations for the dry crack model (dashed line), fluid-filled crack model (dotted line), and for the observed anisotropy (solid line).

[30] The similar fast directions in the horizontal plane for the upper crustal and uppermost mantle anisotropy suggest a stable pattern of anisotropy orientation in the crust and the uppermost mantle in the Bohemian Massif and adjacent areas. However, the strength of the overall anisotropy seems to vary being lower in the crust than in the mantle. This is probably caused by heterogeneities, which are more pronounced in the crust, as well as by a high single-crystal anisotropy of olivine, the dominant component of the upper mantle. Obviously, the low value of crustal anisotropy on the regional scale does not exclude high values of anisotropy on the local scale. Measurements on rock samples frequently show anisotropy even higher than 10% [*Pros et al.*, 1998; *Chlupáčová et al.*, 2003], but a rather high scatter in orientations of the anisotropy axes and in the strength of anisotropy probably causes that the overall anisotropy in the crust is significantly suppressed.

[31] The orientation of the anisotropy axes can be compared with the present-day tectonic stress in the region. The stress measurements in the Bohemian Massif indicate a prevailing direction of the maximum compressive stress in the NW−SE direction with azimuths ranging from 125° to 150° [*Peška*, 1992]. A few exceptions exist in the southern part of the Bohemian Massif where the maximum compressive stress is indicated in the NE−SW direction. However, the NW−SE direction appears to be more reliable because it is more frequent and also consistent with the azimuth of 160° ± 10° determined at the KTB drill hole [*Brudy et al.*, 1997] as well as with the azimuth of 144° ± 26° determined for the overall stress orientation in western Europe [*Müller et al.*, 1992]. Hence the fast *Pg* velocity direction characterized by azimuth 35° is approximately perpendicular to the maximum horizontal compression in the region. A similar relation between anisotropy and tectonic stress has also been observed in other regions, for example in southern California [*Hearn*, 1996].

[32] The relation between anisotropy and present-day stress in the Bohemian Massif excludes the observed anisotropy to be primarily induced by the presence of either dry or fluid-filled stress-aligned cracks or microcracks [*Kaneshima et al.*, 1988; *Crampin*, 1994]. The dry crack model predicts the fast direction parallel to the maximum

compression, and the fluid-filled crack model predicts the fast directions parallel and perpendicular to the maximum compression [*Crampin*, 1984]. However, we observe only the fast direction perpendicular to the maximum compression. Hence the crack models predict azimuthal variations inconsistent with the observed variation (see Figure 13). Consequently, if the crack-induced anisotropy is present in the crust, then its effect should be minor. This could be an indication of a small differential stress in the region that prevents large populations of stress-aligned cracks from forming.

[33] Since the observed crustal anisotropy can hardly be explained by cracks aligned due to present-day stress, we suggest the anisotropy to originate in tectonically induced processes, probably during Variscan orogeny when the Bohemian Massif was sandwiched between opposing subduction zones of NE−SW trending. Such major tectonic activity could imprint the Bohemian Massif some preferentially oriented microstructural and macrostructural features like an alignment of rock-forming minerals (in the Moldanubian unit) or large-scale intrusion fabrics (in the Barrandian unit) responsible for the observed anisotropy at present. The coherent patterns of *Pg* and *Pn* anisotropy might indicate that anisotropy in the crust and uppermost mantle is of a similar origin.

[34] The crustal anisotropy determined from *Pg* waves can also be compared with the mantle anisotropy in the Bohemian Massif studied using the splitting of SKS waves. Assuming a homogeneous transverse isotropy with a horizontal symmetry axis in the crust and upper mantle, the polarization of the fast split *S* wave must be either parallel or perpendicular to the direction of the fast *P* wave velocity. Studies by *Babuška and Plomerová* [2000] and *Plomerová et al.* [2000] however show that the polarizations of split SKS waves do not match the directions of *Pg* or *Pn* anisotropy. This might be explained by the fact that *Pg* and *Pn* waves sample a shallow anisotropic structure, while the SKS results are more sensitive to lithospheric or upper mantle wide structures [*Song et al.*, 2001]. The discrepancy can also arise from an oversimplified anisotropy model, e.g., from the assumptions of a homogeneous transverse isotropy or the horizontal symmetry axis. For example, *Babuška and Plomerová* [2000] suggest dipping anisotropy structures in the lithosphere. The determination of anisotropy from prevailingly horizontally propagating *Pg* or *Pn* waves, which essentially is a 2-D method, cannot yield any such information.

9. Conclusions

[35] The consistency of the results obtained by applying different inversion schemes to different data sets indicates that the upper crust in the Bohemian Massif is anisotropic. The mean propagation velocity of *Pg* waves is 6.03 km/s. This value coincides well with 5.99 km/s obtained by *Růžek et al.* [2000] who studied the velocity model for the same area but from earthquake data. The high-velocity direction has an azimuth of ∼N35°E, approximately perpendicular to the direction of the present-day maximum compression in the Bohemian Massif. The anisotropy is 1.5−2.5% with maximum and minimum velocities v_{max} = 6.10 km/s and v_{min} = 5.98 km/s, respectively. These values

characterize a regional-scale azimuthal anisotropy for ray paths of 30–190 km in length.

[36] The detected crustal anisotropy cannot be primarily caused by the presence of stress-aligned cracks or microcracks in the crust, which is the most common explanation for crustal anisotropy. The crack models predict the maximum velocity in the direction parallel to the maximum compression, but the opposite azimuthal velocity variation is observed. Hence, if the crack-induced anisotropy is present in the crust, then its effect should be minor.

[37] The high-velocity direction in the upper crust determined using *Pg* waves coincides well with that in the uppermost mantle studied using *Pn* waves (depth range 30–40 km). The anisotropy in the uppermost mantle is slightly higher (3–4%) and probably further increases with depth [*Enderle et al.*, 1996]. The coherent patterns of *Pg* and *Pn* anisotropy can indicate that the anisotropy in the crust and uppermost mantle is of similar origin. We suggest that the detected crustal anisotropy is partly intrinsic and partly effective caused by a preferred orientation of rock-forming minerals and large-scale intrusion fabrics developed during the tectonic evolution of the Bohemian Massif.

References

Babuška, V., and M. Cara, *Seismic Anisotropy in the Earth*, Kluwer Acad., Norwell, Mass., 1991.

Babuška, V., and J. Plomerová, Saxothuringian-Moldanubian suture and predisposition of seismicity in the western Bohemian Massif, *Stud. Geophys. Geod.*, 44, 292–306, 2000.

Backus, G. E., Possible forms of seismic anisotropy of the uppermost mantle under oceans, *J. Geophys. Res.*, 70, 3429–3439, 1965.

Bamford, D., *Pn* velocity anisotropy in a continental upper mantle, *Geophys. J. R. Astron. Soc.*, 49, 29–48, 1977.

Berckhemer, H., et al., Petrophysical properties of the 9-km-deep crustal section at KTB, *J. Geophys. Res.*, 102, 18,337–18,361, 1997.

Brudy, M., M. D. Zoback, K. Fuchs, F. Rummel, and J. Baumgärtner, Estimation of the complete stress tensor to 8 km depth in the KTB scientific drill holes: Implications for crustal strength, *J. Geophys. Res.*, 102, 18,453–18,475, 1997.

Chlupáčová, M., Z. Skácelová, and V. Nehybka, P-wave anisotropy of rocks from the seismic area in western Bohemia, *J. Geodyn.*, 35, 45–57, 2003.

Crampin, S., Effective anisotropic elastic constants for wave propagation through cracked solids, *Geophys. J. R. Astron. Soc.*, 76, 135–145, 1984.

Crampin, S., The fracture criticality of crustal rocks, *Geophys. J. Int.*, 118, 428–438, 1994.

Dallmeyer, D., W. Franke, and K. Weber, *Pre-Permian Geology of Central and Eastern Europe*, Springer-Verlag, New York, 1994.

Enderle, U., J. Mechie, S. Sobolev, and K. Fuchs, Seismic anisotropy within the uppermost mantle of southern Germany, *Geophys. J. Int.*, 125, 747–767, 1996.

Franke, W., V. Haak, O. Oncken, and D. Tanner, (Eds.), *Orogenic Processes: Quantification and Modelling in the Variscan Belt*, Geol. Soc. Spec. Publ., 179, 2000.

Guterch, A., M. Grad, and G. R. Keller, Seismologists Celebrate The New Millennium with an Experiment in Central Europe, *Eos Trans. AGU*, 82(45), 529, 534, 536, 2001.

Hearn, T. M., Anisotropic *Pn* tomography in the western United States, *J. Geophys. Res.*, 101, 8403–8414, 1996.

Jahns, E., W. Rabbel, and S. Siegesmund, Quantified seismic anisotropy at different scales: A case study from the KTB crustal segment, *Z. Geol. Wiss.*, 24, 729–740, 1996.

Kaneshima, S., M. Ando, and S. Kimura, Evidence from shear-wave splitting for the restriction of seismic anisotropy to the upper crust, *Nature*, 335, 627–629, 1988.

Kern, H., and R. Schmidt, Physical properties of KTB core samples at simulated in situ conditions, *Scientific Drilling*, 1, 217–223, 1990.

Kern, H., R. Schmidt, and T. Popp, The velocity and density structure of the 4000m crustal segment at the KTB drilling site and their relationship to lithological and microstructural characteristics of the rocks: An experimental approach, *Sci. Drill.*, 2, 130–145, 1991.

Málek, J., M. Brož, T. Fischer, J. Horálek, P. Hrubcová, J. Janský, O. Novotný, and B. Růžek, Seismic measurements along short profiles in western Bohemia during the Celebration 000 experiment, *Acta Montana. A*, 18(12), 15–28, 2001.

Martínková, M., Z. Pros, K. Klíma, T. Lokajíček, and J. Kotková, Experimentally determined P-wave velocity anisotropy for rocks related to the western Bohemia seismoactive region, *Stud. Geophys. Geod.*, 44, 581–589, 2000.

Matte, P., The Variscan collage and orogeny (480–290 Ma) and the tectonic definition of the Armorica microplate: A review, *Terra Nova*, 13, 122–128, 2001.

Matte, P., H. Maluski, P. Rajlich, and W. Franke, Terrane boundaries in the Bohemian Massif: Result of large-scale Variscan shearing, *Tectonophysics*, 177, 151–170, 1990.

Müller, B., M. L. Zoback, K. Fuchs, L. Mastin, S. Gregersen, N. Pavoni, O. Stephansson, and C. Ljunggren, Regional patterns of tectonic stress in Europe, *J. Geophys. Res.*, 97, 11,783–11,803, 1992.

Peška, P., Stress indications in the Bohemian Massif: Reinterpretation of borehole televiewer data, *Stud. Geophys. Geod.*, 36, 307–323, 1992.

Pitra, P., J. P. Burg, and M. Guiraud, Late Variscan strike-slip tectonics between the Tepla-Barrandian and Moldanubian Terranes (Czech Bohemian Massif): Petrostructural evidence, *J. Geol. Soc. London*, 156, 1003–1020, 1999.

Plomerová, J., V. Babuška, and L. Ruprechtová, Travel times of seismic waves propagating to the Bohemian Massif from the south-west direction, *Stud. Geophys. Geod.*, 25, 356–365, 1981.

Plomerová, J., V. Babuška, and L. Ruprechtová, Velocities of seismic waves propagating through the Bohemian Massif from foci in Poland, *Stud. Geophys. Geod.*, 28, 56–66, 1984.

Plomerová, J., M. Granet, S. Judenherc, U. Achauer, V. Babuška, P. Jedlička, D. Kouba, and L. Vecsey, Temporary array data for studying seismic anisotropy of Variscan Massifs-the Armorican Massif, French Massif Central and Bohemian Masif, *Stud. Geophys. Geod.*, 44, 195–209, 2000.

Press, W. H., S. A. Teukolsky, W. T. Vetterling, and B. P. Flannery, *Numerical Recipes in C: The Art of Scientific Computing*, Cambridge Univ. Press, New York, 1992.

Pros, Z., T. Lokajíček, R. Přikryl, A. Špičák, V. Vajdová, and K. Klíma, Elastic parameters of West Bohemian granites under hydrostatic pressure, *Pure Appl. Geophys.*, 151, 631–646, 1998.

Rabbel, W., Seismic anisotropy at the Continental Deep Drilling Site (Germany), *Tectonophysics*, 232, 329–341, 1994.

Rabbel, W., and W. D. Mooney, Seismic anisotropy of the crystalline crust: What does it tell us?, *Terra Nova*, 8, 16–21, 1996.

Růžek, B., J. Zedník, K. Klíma, and L. Ruprechtová, Contribution of local seismic networks to the regional velocity model of the Bohemian Massif, *Stud. Geophys. Geod.*, 44, 175–187, 2000.

Savage, M. K., Seismic anisotropy and mantle deformation: What have we learned from shear wave splitting?, *Rev. Geophys.*, 37, 65–106, 1999.

Schulmann, K., J. Plomerová, V. Babuška, and O. Lexa, A kinematic model of the structural development of the Moldanubian root during the Variscan orogeny based on correlation of crustal and mantle lithosphere fabrics, *Geolines*, 14, 82–84, 2002.

Song, L.-P., M. Koch, K. Koch, and J. Schlittenhardt, Isotropic and anisotropic *Pn* velocity inversion of regional earthquake traveltimes underneath Germany, *Geophys. J. Int.*, 146, 795–800, 2001.

Vavryčuk, V., Crustal anisotropy from local observations of shear-wave splitting in West Bohemia, Czech Republic, *Bull. Seismol. Soc. Am.*, 83, 1420–1441, 1993.

Vavryčuk, V., Reply to comments on "Crustal anisotropy from local observations of shear-wave splitting in West Bohemia, Czech Republic" by G. H. R. Bokelmann and J. Kawahara: Can the Hudson crack model describe behavior of real cracks?, *Bull. Seismol. Soc. Am.*, 85, 661–664, 1995.

Vavryčuk, V., Elastodynamic and elastostatic Green tensors for homogeneous weak transversely isotropic media, *Geophys. J. Int.*, 130, 786–800, 1997.

Weiss, T., S. Siegesmund, W. Rabbel, T. Bohlen, and M. Pohl, Seismic velocities and anisotropy of the lower continental crust: A review, *Pure Appl. Geophys.*, *156*, 97–122, 1999.

————————————————

E. Brueckl, Vienna University of Technology, Gusshausstrasse 27-29, A-1040 Vienna, Austria. (ebrueckl@luna.tuwienac.at)

Z. Hajnal, Department of Geological Sciences, University of Saskatchewan, 114 Science Place, Saskatoon, Saskatchewan, Canada S7N 5E2. (zoltan.hajnal@usask.ca)

M. Grad, Institute of Geophysics, University of Warsaw, Pasteura 7, PL-02-093 Warsaw, Poland. (mgrad@mimuw.edu.pl)

P. Hrubcová, B. Růžek, A. Špičák, V. Vavryčuk, and J. Zedník, Geophysical Institute, Academy of Sciences of the Czech Republic, Bocni II/1401, 141 31 Prague 4, Czech Republic. (pavla@ig.cas.cz; ruzek@ig.cas.cz; als@ig.cas.cz; vv@ig.cas.cz; jzd@ig.cas.cz)

A. Guterch, Institute of Geophysics, Polish Academy of Sciences, Ks. Janusza 64, PL-04-152 Warsaw, Poland. (aguterch@igf.edu.pl)

G. R. Keller, Department of Geological Sciences, University of Texas at El Paso, El Paso, TX 79968, USA. (keller@geo.utep.edu)

K. Posgay, Eötvös Loránd Geophysical Institute, Kolumbusz u. 17-23, H-1145 Budapest, Hungary. (elgi@elgi.hu)

O. Selvi, TUBITAK-MAM, Marmara Research Center, P.O. Box 21, 41470 Gebze/Kocaeli, Turkey. (selvi@yunus.mam.gov.tr)

H. Thybo, Geological Institute, University of Copenhagen, Oster Voldgade 10, DK-1350 Copenhagen, Denmark. (thybo@geol.ku.dk)

J. Vozár, Institute of Geology, Dubravska cesta 9, P.O. Box 106, 840 05 Bratislava 45, Slovakia. (geoljovo@savba.sk)

P6

**Vavryčuk, V., P. Hrubcová, M. Brož, J. Málek,
and the ALP 2002 Working Group**

**Azimuthal variation of Pg velocity in the Moldanubian, Czech Republic:
observations based on a multi-azimuthal common-shot experiment**

Azimuthal variation of *Pg* velocity in the Moldanubian, Czech Republic: observations based on a multi-azimuthal common-shot experiment

Václav Vavryčuk[a,*], Pavla Hrubcová[a], Milan Brož[b], Jiří Málek[b]
The ALP 2002 Working Group[1]

[a]*Geophysical Institute, Academy of Sciences of the Czech Republic, Boční II, 141 31 Praha 4, Czech Republic*
[b]*Institute of Rock Structure and Mechanics, Academy of Sciences of the Czech Republic, V Holešovičkách 41, 182 09 Praha 8, Czech Republic*

Abstract

We study the azimuthal velocity variation of *Pg* waves in the Moldanubian, which is a crystalline segment within the Bohemian Massif in the Czech Republic. We use the data from a multi-azimuthal common-shot experiment performed as part of the ALP 2002 refraction experiment, complemented by profile refraction data from the CELEBRATION 2000 experiment. We analyze the travel times of waves recorded by 72 portable seismic stations deployed along two circles with radii of 35 and 45 km around a shot. The observed travel times display an azimuthal variation indicating anisotropy of 2%. The minimum and maximum velocity values are 5.83 and 5.95 km/s, respectively. The direction of the maximum velocity is ~N50°E. These values characterize horizontal anisotropy of the uppermost crust down to 3 km. The strength and orientation of uppermost crustal anisotropy in the Moldanubian is consistent with the overall upper crustal anisotropy in the entire Bohemian Massif. The high-velocity direction is roughly perpendicular to the present-day maximum compressive stress in the Bohemian Massif and Central Europe and coincides with the orientation of structures formed by the main Variscan tectonic events in the area. This indicates that the anisotropy is caused predominantly by alignment of textural elements and minerals in the rocks, which developed in early geological stages

---

rather than by a preferred orientation of cracks or microcracks due to present-day stress. If the crack-induced anisotropy is present in the medium, then its strength should not exceed 1% and the cracks should be water saturated.

1. Introduction

The Earth's crust is often reported to be anisotropic (Babuška and Cara, 1991), which is manifested by azimuthally dependent velocities of seismic waves. Crustal anisotropy in the Bohemian Massif and adjacent areas has so far been measured on rock samples from West Bohemia and from the KTB drill hole (Kern and Schmidt, 1990; Kern et al., 1991; Jahns et al., 1996; Berckhemer et al., 1997; Pros et al., 1998; Martínková et al., 2000; Chlupáčová et al., 2003), from shear-wave splitting observed in records of micro-earthquakes in West Bohemia (Vavryčuk, 1993, 1995) and from shear-wave splitting observed in the VSP records at the KTB site (Rabbel, 1994; Rabbel and Mooney, 1996). The experiments indicate anisotropy of varying magnitude dependent on the site studied. The orientation of anisotropy axes from in situ experiments is rather stable being related to the direction of the horizontal tectonic stress in the region. A similar observation is reported by Plomerová et al. (1981, 1984), who studied a velocity variation of *Pg* waves in the Bohemian Massif from earthquake data. Recently, Růžek et al. (2003) studied a regional-scale upper crustal anisotropy in the Bohemian Massif from *Pg* refraction data collected during the large-scale refraction experiment CELEBRATION 2000 (Guterch et al., 2001, 2003; Málek et al., 2001). They report a systematic azimuthal variation of the *Pg* velocity, indicating an overall anisotropy of 1.5–2.5% with the direction of the maximum propagation velocity in azimuth of ~N35°E. This direction is approximately perpendicular to the direction of the maximum horizontal compression in the earth crust in Central Europe.

Knowing the multisegmental nature of the Bohemian Massif, we wanted to choose just one segment of the Massif in this paper, and study the anisotropy on the local scale. Therefore, we continue the work of Růžek et al. (2003) but study the azimuthal variation of *Pg* waves in the Moldanubian, a crystalline segment of the Bohemian Massif. The aim is to trace a more detailed anisotropy pattern within the Bohemian Massif and to check whether anisotropy of *Pg* waves can be detected even at a local scale. We use data from a multi-azimuthal common-shot experiment performed within the European refraction experiment ALP 2002 (Brückl et al., 2003). A circular geometry of the experiment was chosen to provide an unequivocal check of seismic anisotropy in the studied area. Additionally, we use data from the CELEBRATION 2000 experiment related to the region of interest to obtain more information on velocity distribution in study area and possible heterogeneity corrections.

2. Geological and tectonic setting

The Moldanubian represents a major crystalline segment within the Bohemian Massif, which is one of the largest stable outcrops of pre-Permian rocks in Central Europe, forming the easternmost part of the Variscan Belt. The Bohemian Massif developed approximately between 500 and 250 Ma during a stage of large-scale crustal convergence, collision of continental plates and microplates, and possibly also subduction (Matte et al., 1990), and is subdivided into various units: Saxothuringian, Barrandian, Moldanubian, and Moravo-Silesian (see Fig. 1).

The Moldanubian unit, sometimes viewed as a Precambrian orogenic root surrounded by younger complexes, adjoins the Saxothuringian in the NW and the Moravo-Silesian to the east. The boundary with the Saxothuringian is regarded as a major suture-type discontinuity, whereas the structurally higher unit in the NW, the Barrandian, has been thrust over the Saxothuringian and Moldanubian units. The Moldanubian unit is separated from the Barrandian unit by a major NE–SW trending Variscan dextral fault, the Central Bohemian Shear Zone, which is obscured by
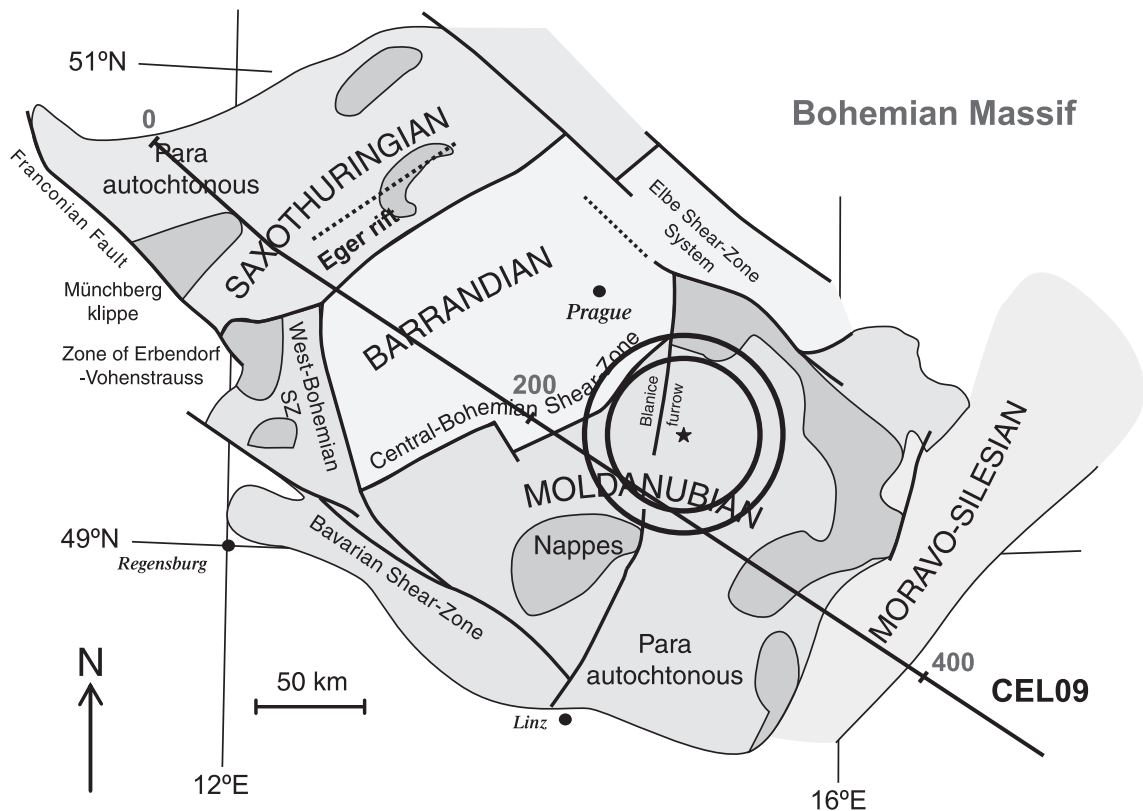
Fig. 1. Major tectonic units of the Bohemian Massif, after Pitra et al. (1999).

Variscan intrusions of the Central Bohemian Pluton. Its eastern boundary with the Moravo-Silesian has the character of a major NE–SW striking ductile shear zone, with a predominance of strike-slip movements. Post-Variscan platform sediments cover the continuation of the Moldanubian unit to the S and SW, where it is bounded by the fault system of the Franconian Line, representing the foreland deformation of the Alpine collision (Dallmeyer et al., 1995).

The Moldanubian segment contains mainly high-grade gneisses and migmatites of supracrustal origin, orthogneisses, granulites, and also numerous Variscan post-tectonic granitoid intrusions, the most prominent of which are the Central Bohemian and Central Moldanubian Plutons. The crustal root of the Moldanubian unit shows nearly vertical NE–SW trending fabrics (estimated age 370–330 Ma) developed mostly in granulites and associated mantle slivers (Schulmann et al., 2002). In detail, the Moldanubian is characterized by an almost missing sedimentary cover

except for two small basins filled with Cretaceous and Tertiary sediments in the SSW.

3. Data

A multi-azimuthal common-shot experiment was performed on the territory of the Czech Republic as part of the ALP 2002 refraction experiment in June 2002. A total of 72 one-component seismic stations were deployed along two concentric circles with radii of 35 and 45 km with an angular step of 10° between stations and 5° angular intercircle shift (see Fig. 2). The radii of circles were delimited both geographically by the extent of the Moldanubian and by the resolution of the method applied. A charge of 500 kg of explosives was detonated at the center of the circles at 49.50493°N latitude, 14.94982°E longitude, and 538-m altitude. The positions of the shot and stations were determined by GPS with an accuracy
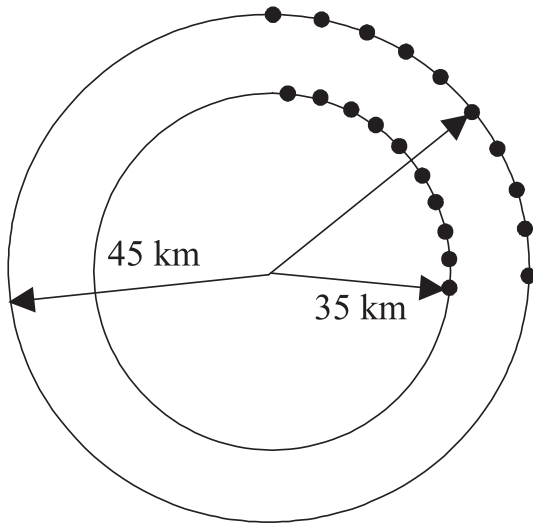
Fig. 2. Geometry of the experiment. Dots mark positions of stations in the azimuth range 0–95°.

better than 20 m; the origin time was controlled by a DCF77 timer with an accuracy of 3 ms. The sensors were 4.5-Hz geophones; the recording instruments were TEXAN.

Fig. 3 shows the *Pg*-wave recordings at the stations. Of the total number of 72 stations, two stations did not record; recordings from four other stations were too noisy to be analyzed. Hence, we analyzed recordings of 66 stations. The sampling frequency of the recordings was 250 Hz. The corner frequency of the anti-alias FIR filter was 100 Hz. The arrival times of *Pg* waves (see Tables 1 and 2) were measured with an accuracy of around 10 ms. The arrival times of *Sg* waves were not analyzed because of high uncertainties in picking in one-component recordings. Fig. 4 shows the azimuthal variation of the *Pg* velocity calculated as distance from the shot divided by travel times. The mean value of the *Pg* velocity is 5.86/5.87 km/s for the inner/outer circle with a standard deviation of 0.06/0.04 km/s.

The calculated velocities show that the crust is not homogeneous or isotropic because the velocity variation is beyond the uncertainty of the measurements. The variation shows the same trend for both circles: It is characterized by high-velocity values for azimuths of 30–60° and by low-velocity values for azimuths of 170–220°. A distinct velocity increase has

also been detected for azimuths of 320–360° at the inner circle, but the corresponding velocities at the outer circle display a different and more complicated pattern. The velocity variation indicates either lateral inhomogeneities or anisotropy in the area. As seen from a detailed geological map of the area (see Fig. 5), some of the velocity anomalies can be readily explained by lateral inhomogeneities. This refers, for example, to a rather high scatter of velocities in the NW to N directions, where the circles exceed the Moldanubian and touch or hit the fragmented structure of the Central Bohemian Shear Zone. Local inhomogeneities can also explain the low velocities in the SSW direction, because the stations were located at or very close to the Tertiary Třeboň Basin characterized by an anomalously low-velocity subsurface layer. Therefore, to assess potential overall anisotropy in the area, we have to first eliminate the subsurface inhomogeneity effects.

4. Station corrections

To eliminate the local inhomogeneities from travel times, we can use the CEL09 profile data collected during the CELEBRATION 2000 experiment (Růžek et al., 2003). This profile intersects both circles and traverses different types of the subsurface structure in the region under study. The profile data can be used to address two points: (1) to approximate the depth extent of rays in the experiment, and (2) to calculate station corrections along the profile, corresponding to delay times induced by a low-velocity subsurface layer. The station corrections along the profile can be used to roughly approximate the station corrections along the circles.

Fig. 6 shows the reduced travel times along the profile in the longitude range of 14–15.5° and at distances between 10 and 100 km. Interpolating upper and lower bounds of the travel times by piecewise linear functions, we can infer 1-D layered models (Shearer, 1999, Fig. 5.5), which are limits for the model in the area (see Fig. 7). The limits should reflect lateral inhomogeneities along the profile. The inferred limits differ down to 8 km, and then they coalesce. This manifests a variability of structure in shallow rather than deep parts of the upper crust. The limits also determine the range of the maximum
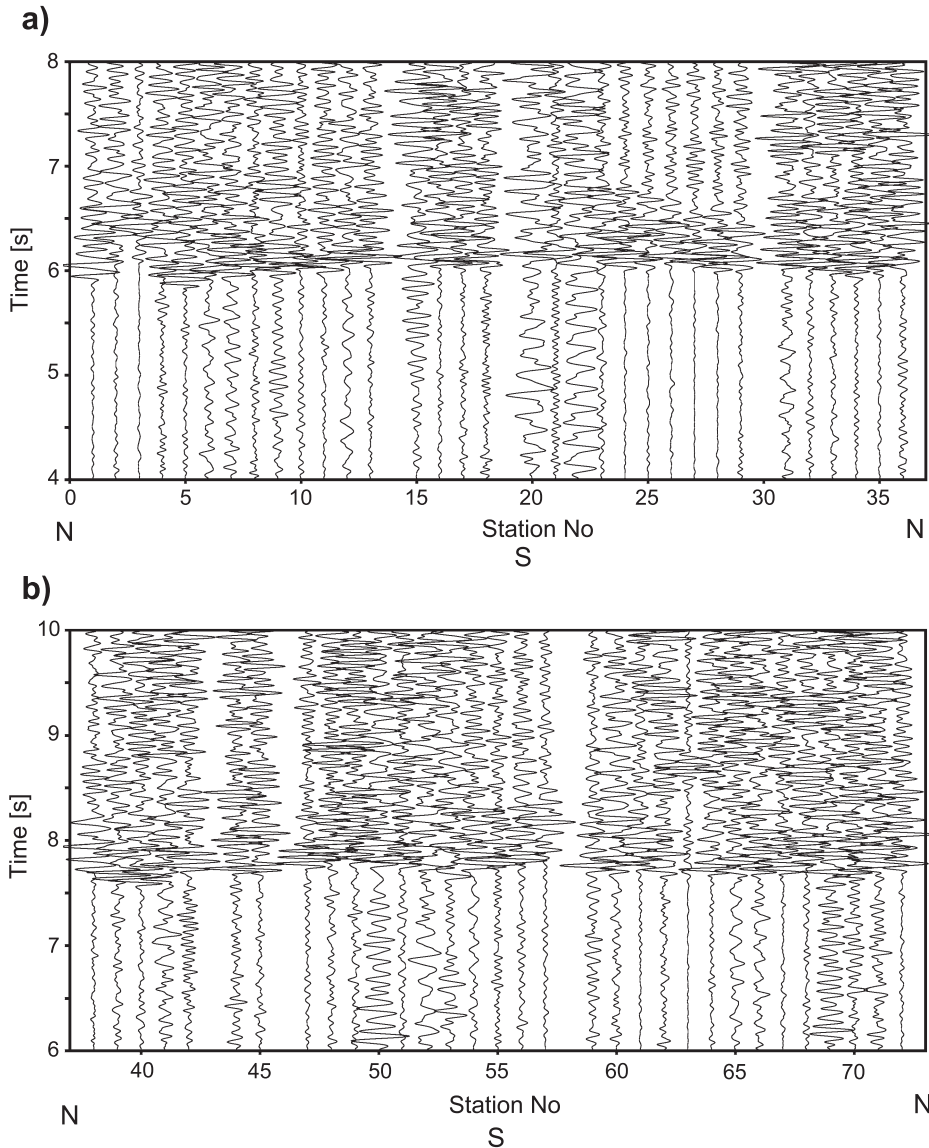
a)

b)

Fig. 3. *Pg*-wave velocity recordings at portable stations deployed along (a) the inner circle at a recording offset of 35 km, and (b) the outer circle at a recording offset of 45 km.

depths reached by rays in the experiment. Fig. 7 shows that the depth is well constrained ranging between 2 and 3 km.

More detailed information on lateral inhomogeneities along the profile can be gained from time station corrections evaluated using the "time-term method" (Bamford, 1977; Enderle et al., 1996; Song et al., 2001). In this method, the measured travel

times are corrected for the delay times due to a low-velocity subsurface layer. The thickness and velocity of the layer can significantly vary within the area and are considered to be unknown. The aim is to isolate and remove these unknown effects from the travel times. The station corrections were calculated using the travel times of the *Pg* waves generated by six shots (Table 3) and measured at 73 stations along the

Table 1
The multi-azimuthal experiment: inner circle

No.	Latitude [°N]	Longitude [°E]	H [m]	D [km]	Azimuth [deg]	T [s]	Type of rock	dt [s]	T^{corr} [s]	Velocity [km/s]
1	49.8131	14.9510	387	34.27	0.1	5.878	B, D	−0.05	5.928	5.78
2	49.8145	15.0347	472	34.97	10.1	6.043	B	0.00	6.043	5.79
3	49.8022	15.1183	510	35.23	20.1	6.058	B	0.00	6.058	5.82
4	49.7786	15.1883	407	34.97	29.4	5.914	B	0.00	5.914	5.91
5	49.7459	15.2640	480	35.12	40.1	5.846	B	0.00	5.846	6.01
6	49.7062	15.3237	515	35.09	50.2	5.924	B	0.00	5.924	5.92
7	49.6599	15.3691	425	34.88	60.2	5.908	A	0.00	5.908	5.90
8	49.6112	15.4054	540	35.02	70.1	5.970	A	0.00	5.970	5.87
9	49.5584	15.4245	600	34.88	80.0	5.920	A	0.00	5.920	5.89
10	49.5039	15.4338	615	35.05	90.0	5.989	A	0.00	5.989	5.85
11	49.4479	15.4215	635	34.76	100.3	5.947	A	0.00	5.947	5.85
12	49.3957	15.4042	632	35.12	110.1	6.014	A	0.00	6.014	5.84
13	49.3471	15.3666	592	34.96	120.0	6.015	A	0.00	6.015	5.81
15	49.2637	15.2590	620	34.98	140.0	6.008	A	0.00	6.008	5.82
16	49.2314	15.1901	620	35.08	150.1	6.003	A	0.00	6.003	5.84
17	49.2098	15.1141	555	34.93	160.0	6.003	A	0.00	6.003	5.82
18	49.1967	15.0341	502	34.83	169.8	6.022	A	0.00	6.022	5.78
19	49.1898	14.9495	548	35.04	180.0	6.054	A	0.00	6.054	5.79
20	49.1940	14.8661	460	35.11	190.0	6.049	A	0.00	6.049	5.80
21	49.2094	14.7850	453	34.98	200.1	6.077	C	0.08	5.997	5.83
22	49.2322	14.7098	415	34.98	210.0	6.049	C	0.08	5.969	5.86
23	49.2615	14.6369	443	35.34	220.1	6.040	C	0.10	5.940	5.95
24	49.3022	14.5810	478	35.00	230.0	5.967	C	0.10	5.867	5.96
25	49.3464	14.5310	468	35.13	240.0	5.950	C	0.08	5.870	5.98
26	49.3950	14.4927	473	35.33	249.9	6.027	C	0.08	5.947	5.94
27	49.4491	14.4732	517	35.10	260.0	5.973	B	0.00	5.973	5.88
28	49.5036	14.4668	580	34.99	269.9	5.944	D	−0.05	5.994	5.84
29	49.5585	14.4727	580	35.05	280.0	5.982	D	−0.05	6.032	5.81
31	49.6611	14.5287	495	35.06	299.9	5.998	D	−0.05	6.048	5.80
32	49.7068	14.5762	440	35.12	309.9	5.985	D	−0.05	6.035	5.82
33	49.7454	14.6368	380	35.02	319.9	5.934	D	−0.05	5.984	5.85
34	49.7770	14.7066	365	34.99	330.0	5.879	D	−0.05	5.929	5.90
35	49.8005	14.7830	465	35.01	339.9	5.903	D	−0.05	5.953	5.88
36	49.8143	14.8653	350	34.95	350.0	5.926	D	−0.05	5.976	5.85

Meaning of quantities: No. is the station number, H is the altitude, D is the distance, T is the travel time, dt is the station correction, $T^{corr}=T-\mathrm{d}t$ is the travel time corrected for the local geology. Types of geological units at the locations of the individual seismic stations: (A) granitoid intrusions of the Central Moldanubian Pluton (station nos. 7–20, 49–54); (B) high-grade gneisses and migmatites, orthogneisses, granulites with intrusions of amphibolites (station nos. 1–6, 27, 38–48, 62); (C) Tertiary and Quaternary sediments (station nos. 21–26, 55–61); (D) granitoid plutons (station nos. 28–36, 63–64); (E) granitoid plutons with mafic intrusions (amfibolites, diabases, melaphyres) of Central Bohemian Pluton (station nos. 65–71); (F) Palaeozoic sediments (station no. 72).

profile with longitudes in the range of 13–15.5°E. We selected stations with the recording offset between 30 and 150 km. On the whole, 245 travel times were inverted for 73 station and six shot corrections.

The station corrections vary from −0.10 to 0.12 s (Fig. 8) and display systematic trends, which correlate with the geological structure along the profile (see Fig. 5). The studied segment of the

CEL09 profile intersects with the contact between the Barrandian in the NW and the Moldanubian (Central Bohemian Shear Zone) and continues across the Moldanubian to the SE. High corrections (low velocities) at longitude 13.6°E are connected with Barrandian Palaeozoic sediments and metasediments (type F). The low corrections (high velocities) at 13.8–14.1°E relate to granitoid plutons with mafic intrusions (amfibolites, diabases, melaphyres) at the

Table 2
The multi-azimuthal experiment: outer circle

No.	Latitude [°N]	Longitude [°E]	H [m]	D [km]	Azimuth [deg]	T [s]	Type of rock	dt [s]	T^{corr} [s]	Velocity [km/s]
38	49.8953	15.1116	448	44.96	15.0	7.676	B	0.00	7.676	5.86
39	49.8709	15.2152	420	44.99	25.1	7.579	B	0.00	7.579	5.94
40	49.8342	15.3096	412	44.89	35.2	7.544	B	0.00	7.544	5.95
41	49.7920	15.3914	426	45.13	44.8	7.572	B	0.00	7.572	5.96
42	49.7362	15.4617	493	45.05	55.0	7.668	B	0.00	7.668	5.88
44	49.6076	15.5517	417	45.02	75.1	7.655	B	0.00	7.655	5.88
45	49.5385	15.5717	527	45.18	85.0	7.676	B	0.00	7.676	5.89
47	49.3985	15.5488	548	45.02	105.0	7.696	B	0.00	7.696	5.85
48	49.2703	15.4612	630	45.38	124.9	7.771	B	0.00	7.771	5.84
49	49.2703	15.4619	603	45.42	124.9	7.761	A	0.00	7.761	5.85
50	49.2183	15.3875	639	45.02	134.9	7.706	A	0.00	7.706	5.84
51	49.1731	15.3043	673	45.01	144.9	7.709	A	0.00	7.709	5.84
52	49.1385	15.2112	578	44.97	154.9	7.690	A	0.00	7.690	5.85
53	49.1185	15.1069	533	44.46	165.1	7.603	A	0.00	7.603	5.85
54	49.1025	15.0036	469	44.93	175.0	7.672	A, C	0.05	7.622	5.89
55	49.1024	14.8967	464	44.93	185.0	7.712	C	0.05	7.662	5.86
56	49.1142	14.7892	434	44.99	195.1	7.746	C	0.10	7.646	5.88
57	49.1383	14.6893	425	44.96	205.0	7.784	C	0.12	7.664	5.87
59	49.2183	14.5124	440	45.01	225.1	7.668	C	0.10	7.568	5.95
60	49.2715	14.4399	396	45.21	235.2	7.662	C	0.08	7.582	5.96
61	49.3331	14.3880	446	45.02	245.1	7.676	C	0.05	7.626	5.90
62	49.3988	14.3507	476	45.02	255.0	7.637	B	0.00	7.637	5.89
63	49.4685	14.3319	516	44.95	265.1	7.619	D	−0.05	7.669	5.86
64	49.5386	14.3294	525	45.08	275.0	7.634	D	−0.05	7.684	5.87
65	49.6080	14.3451	465	45.23	284.9	7.605	E	−0.08	7.685	5.89
66	49.6749	14.3838	380	45.08	295.0	7.639	E	−0.08	7.719	5.84
67	49.7356	14.4373	345	45.05	304.9	7.651	E	−0.08	7.731	5.83
68	49.7899	14.5062	440	45.07	314.9	7.694	E	−0.08	7.774	5.80
69	49.8377	14.5877	280	45.31	324.9	7.633	E	−0.08	7.713	5.87
70	49.8706	14.6841	350	44.96	334.9	7.595	E	−0.08	7.675	5.86
71	49.8943	14.7875	420	44.86	344.9	7.689	E, F	0.00	7.689	5.83
72	49.9074	14.8957	400	44.94	355.0	7.663	F	0.05	7.613	5.90

For the meaning of quantities, see the legend of Table 1.

Barrandian/Moldanubian contact (type E), and the low corrections around 14.3°E reflect high-grade gneisses and migmatites, orthogneisses and granulites (type D). The high corrections around 14.5–14.7°E relate to Tertiary and Quaternary sediments of the Třeboň basin (type C). Granitoid intrusions of the Central Moldanubian Pluton (type A) cover the interval 14.8–15.2°E. The high corrections around 15.0°E could reflect a local sedimentary structure (type G). Places with zero corrections represent the Moldanubian unit (gneisses, migmatites, type B) and the granitoid intrusions of the Central Moldanubian Pluton (type A).

Because the station corrections correspond well to the geological structure under the stations, we con-clude that the evaluation of effects of the subsurface inhomogeneities was successful and that the travel times along the circles can be effectively corrected for them (see Tables 1 and 2).

5. Anisotropy

A circular geometry of the experiment is particularly suitable for studying anisotropy and eliminating or at least suppressing other inhomogeneity effects not accounted for by station corrections. This concerns, for example, effects caused by varying depth of a low-velocity subsurface layer, differences in velocity gradients, or differences in the depth range sampled
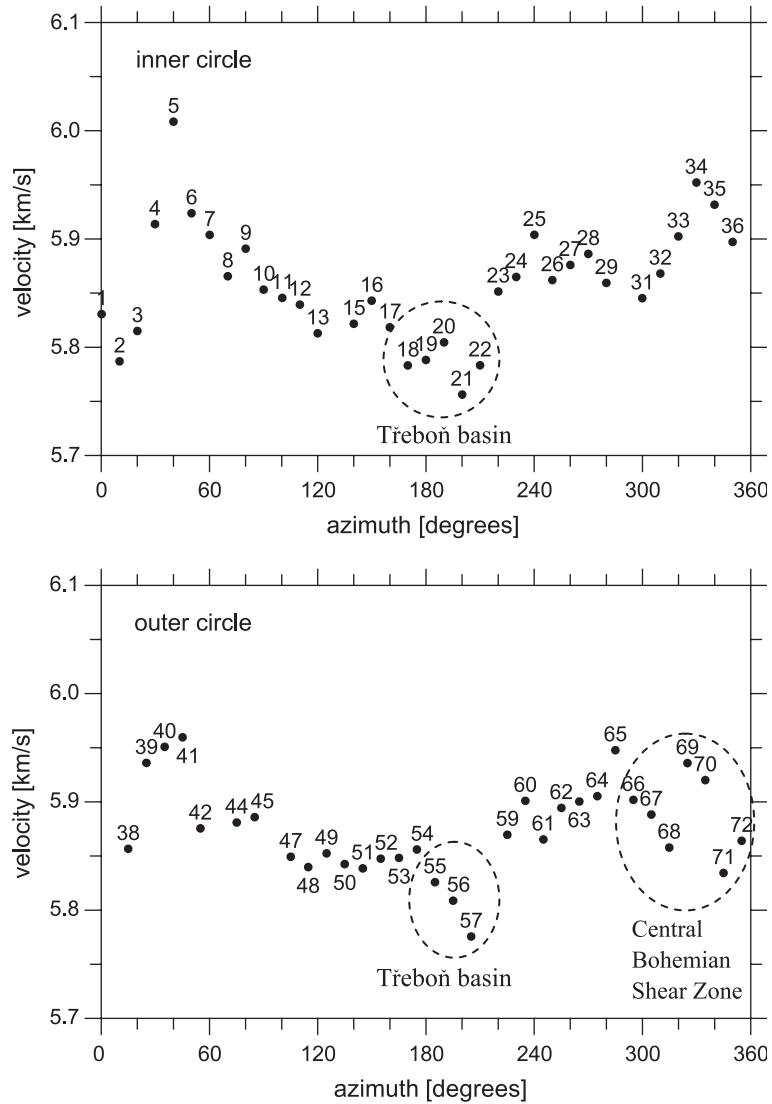
Fig. 4. Uncorrected *Pg* velocity as a function of azimuth for the inner (upper plot) and outer (lower plot) circles.

by the data. To separate anisotropy from the mentioned inhomogeneities, we show the *Pg* velocities calculated from the corrected travel times in the azimuth range 0–180° (Fig. 9). In this range, we compare velocities for the rays being shot in opposite directions and thus sampling different structures. If the velocities retrieved from the opposite rays are consistent and display a pronounced variation with varying azimuth, then it should primarily be the result of anisotropy. The scatter in velocities for the opposite rays quantifies the effects of inhomogeneities not

satisfactorily eliminated by applying the station corrections. Fig. 9 shows a distinct azimuthal variation of the *Pg* velocity and a rough coincidence of this variation along both circles. The variation displays two peaks: a distinct maximum in azimuths of 30–60°, and a less distinct maximum around an azimuth of 150°. The azimuthal velocity variation along both circles indicates that the medium is intrinsically or effectively anisotropic.

Assuming mostly horizontal propagation of refracted waves in a weakly anisotropic crust,
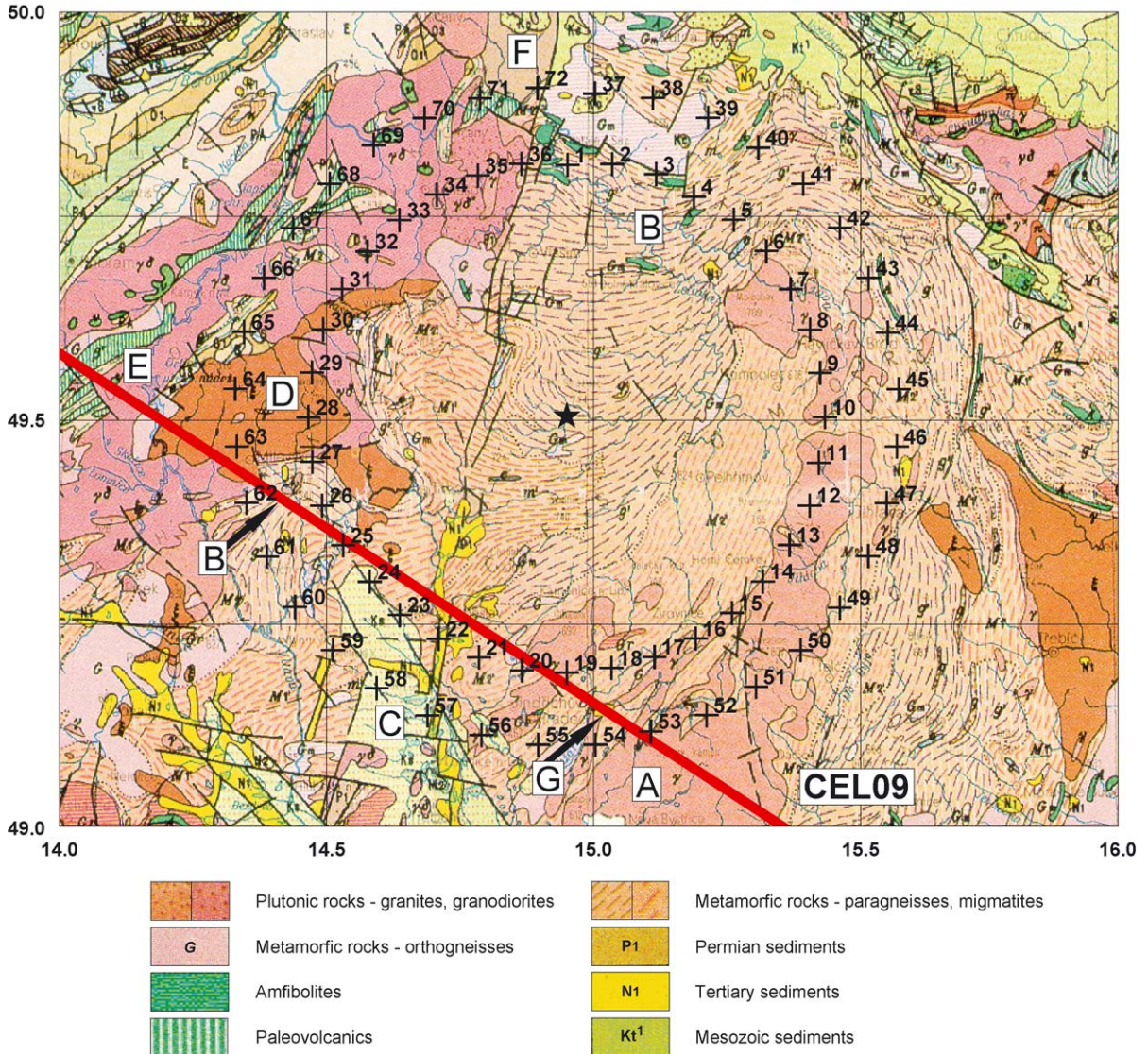
Fig. 5. Geological settings and experiment layout, after Fusán et al. (1993). Crosses mark positions of stations; the star marks the position of the shot.

we can express the velocity as follows (Backus, 1965):

$$v = v_0(1 + A\cos 2\varphi + B\sin 2\varphi + C\cos 4\varphi + D\sin 4\varphi)$$

(1)

where v is the azimuth-dependent velocity, v_0 is the velocity in an isotropic reference medium, φ defines the azimuth in which the wave propagates, and constants A, B, C, and D are small unknown

coefficients that are linear combinations of the elastic parameters defining weak anisotropy. For weak transverse isotropy with a horizontal axis of symmetry, Eq. (1) simplifies to (Song et al., 2001)

$$v = v_0(1 + E\cos 2(\varphi - \varphi_0) + F\cos 4(\varphi - \varphi_0))$$ (2)

where φ_0 is the angle defining the orientation of the symmetry axis in the horizontal plane, and E and F are small unknown coefficients defining weak transverse isotropy.
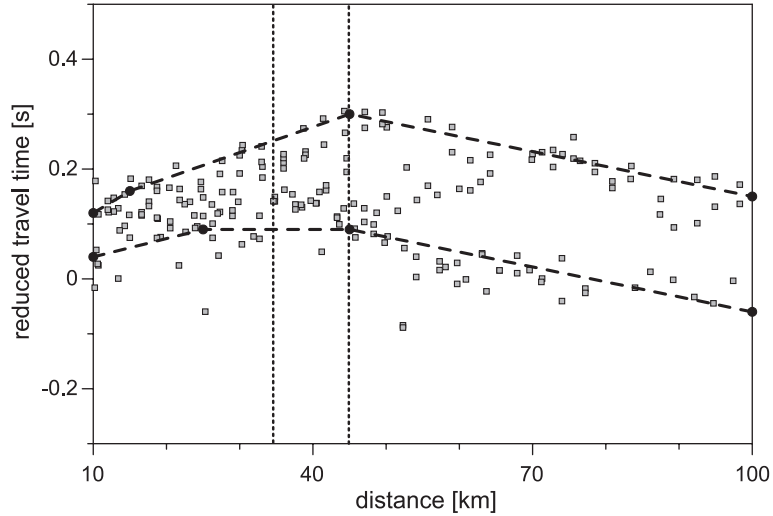
Fig. 6. The reduced travel times along the CEL09 profile as a function of distance. The reduction velocity is 6 km/s. The dashed lines consist of straight-line segments and delineate upper and lower bounds of the travel times. The points between the segments are marked by black dots. Dotted lines show the recording offsets used in the multi-azimuthal common-shot experiment.

Inverting the whole set of the velocity values for an optimum anisotropy model using Eqs. (1) and (2), we obtain v_0=5.87 km/s, A=−0.0019, B=0.0078, C=−0.0044, D=−0.0027, φ_{max}=53°, and ε=2.0% for weak general anisotropy, and v_0=5.87 km/s, E=0.0082, F=0.0049, φ_{max}=50°, and ε=2.0% for weak

transverse isotropy, where φ_{max} is the azimuth of the maximum velocity direction and ε is the strength of anisotropy defined as

$$\varepsilon = 2\frac{v_{max} - v_{min}}{v_{max} + v_{min}}100\% \qquad (3)$$

The velocity variations for the optimum models of general anisotropy and transverse isotropy are very similar (see Fig. 10, lower plot). They are also very similar to the variations obtained when inverting the data of the east semicircles (see Fig. 10, upper plot). For east semicircles, no station corrections were applied because of the absence of distinct subsurface inhomogeneities (see Fig. 5).
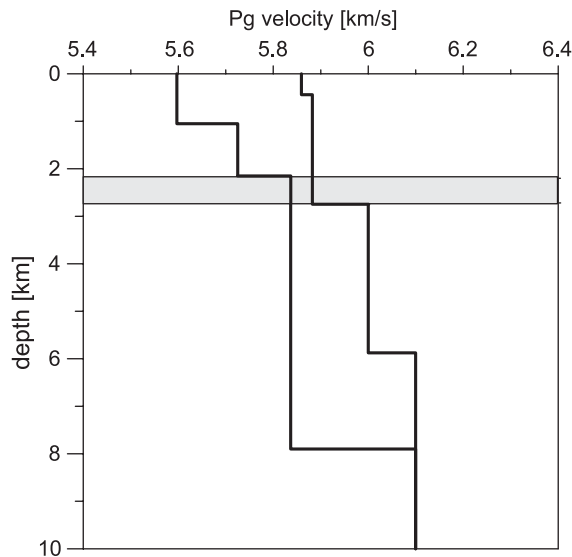
6. Discussion

Růžek et al. (2003) used *Pg* refraction data from the CELEBRATION 2000 experiment to study regional horizontal upper crustal anisotropy in the Bohemian Massif. They used data covering the whole range of azimuths and with recording offsets from 30 to 190 km. They found that the high-velocity direction in the entire Bohemian Massif is ~N35°E, and the overall azimuthal velocity variation is 1.5–2.5%. For studying local scale horizontal anisotropy, we choose the Moldanubian unit, a crystalline segment within the

Fig. 7. The 1-D layered models inferred from the travel times along the CEL09 profile in the longitude range 14–15.5°. The shadow area shows the maximum depths reached by rays in the experiment.

Table 3
Parameters of the CEL09 shots

Date	Time [hh:mm:ss.sss]	Shot ID	Charge [kg]	H [m]	Latitude [°N]	Longitude [°E]	Territory
Jun 24	21:00:00.000	2-910-0	210	476	49.3124	14.5900	Czech Rep.
Jun 24	22:00:00.000	2-909-0	210	474	49.5182	14.1295	Czech Rep.
Jun 24	22:45:00.000	2-912-0	210	612	49.0191	15.3173	Czech Rep.
Jun 24	23:15:00.000	2-912-1	210	615	49.0191	15.3168	Czech Rep.
Jun 25	00:15:00.000	2-911-0	210	492	49.1892	14.9104	Czech Rep.
Jun 25	00:45:00.000	2-911-1	210	492	49.1896	14.9105	Czech Rep.

Bohemian Massif. Based on a multiazimuthal common-shot experiment with recording offsets 35 and 45 km, we found the horizontal anisotropy strength of 2.0% with the high-velocity direction N50°E. These values characterize anisotropy of the uppermost crust down to 3 km. Hence, we conclude that horizontal anisotropy on a local scale in the Moldanubian unit is consistent with that in the entire Bohemian Massif. This might indicate that the horizontal anisotropy pattern for the uppermost crust is stable with no distinct lateral or vertical variations within the Bohemian Massif.

Interestingly, the fast directions in the Moldanubian unit and in the Bohemian Massif are almost perpendicular to the present-day maximum compres-

sive stress in the region, estimated to be in azimuths of N125–150°E (Peška, 1992). The NW–SE direction of the maximum compressive stress is also reported for the KTB drill hole in Germany (Brudy et al., 1997, azimuth of $160° \pm 10°$) and for the overall stress orientation in Western Europe (Müller et al., 1992, azimuth of $144° \pm 26°$). Because the high-velocity direction does not coincide with the direction of the present-day maximum compressive stress in the region, we conclude that the observed anisotropy cannot be primarily affected by the presence of cracks or microcracks in the crust (Kaneshima et al., 1988; Crampin, 1994). The dry crack model predicts the maximum Pg velocity in the direction parallel to the maximum compression,
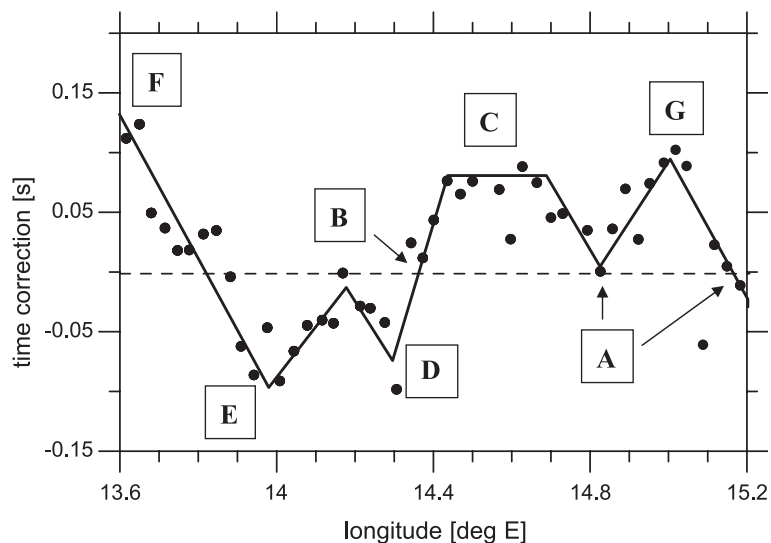

Fig. 8. Station corrections along the CEL09 profile. Types of geological structures: (F) Barrandian Palaeozoic sediments; (E) granitoid plutons with mafic intrusions; (D) granitoid plutons; (B) gneisses and migmatites of the Moldanubian unit; (C) Tertiary and Quarternary sediments (Třeboň basin); (A) granitoid intrusions of the Central Moldanubian Pluton; and (G) local Quarternary sediments.
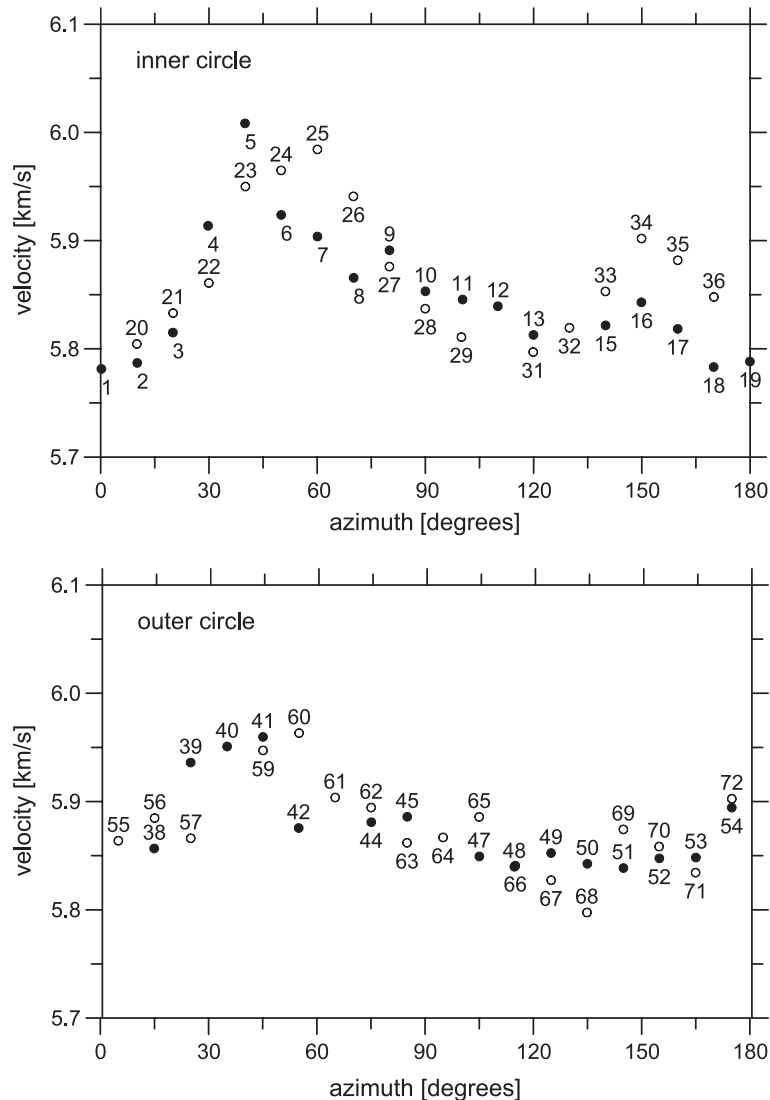
Fig. 9. Corrected *Pg* velocity as a function of azimuth for the inner (upper plot) and outer (lower plot) circles. Open/closed circles mark the stations in the azimuth range 0–180°/180–360°.

and the fluid-filled crack model in the directions parallel and perpendicular to the maximum compression. Obviously, these predictions clearly contradict our observations. This indicates that the observed anisotropy might be caused by preferred orientation of textural elements and minerals or large-scale fabrics imprinted in the crustal rocks during the early tectonic evolution rather than by aligned cracks or micro-cracks induced by the present-day tectonic stress in the region. The

prevailing role of rock-fabric anisotropy is supported by coincidence of the fast direction of *Pg* waves with NE–SW trending of microstructural rock fabric in the part of the Moldanubian covered by the experiment (see Fig. 5). The NE–SW trending coincides with the direction of linear and planar structures in the Bohemian Massif attributed to the Variscan orogeny (Dallmeyer et al., 1995).

The domination of rock-fabric to crack-induced anisotropy is rather surprising, because usually the
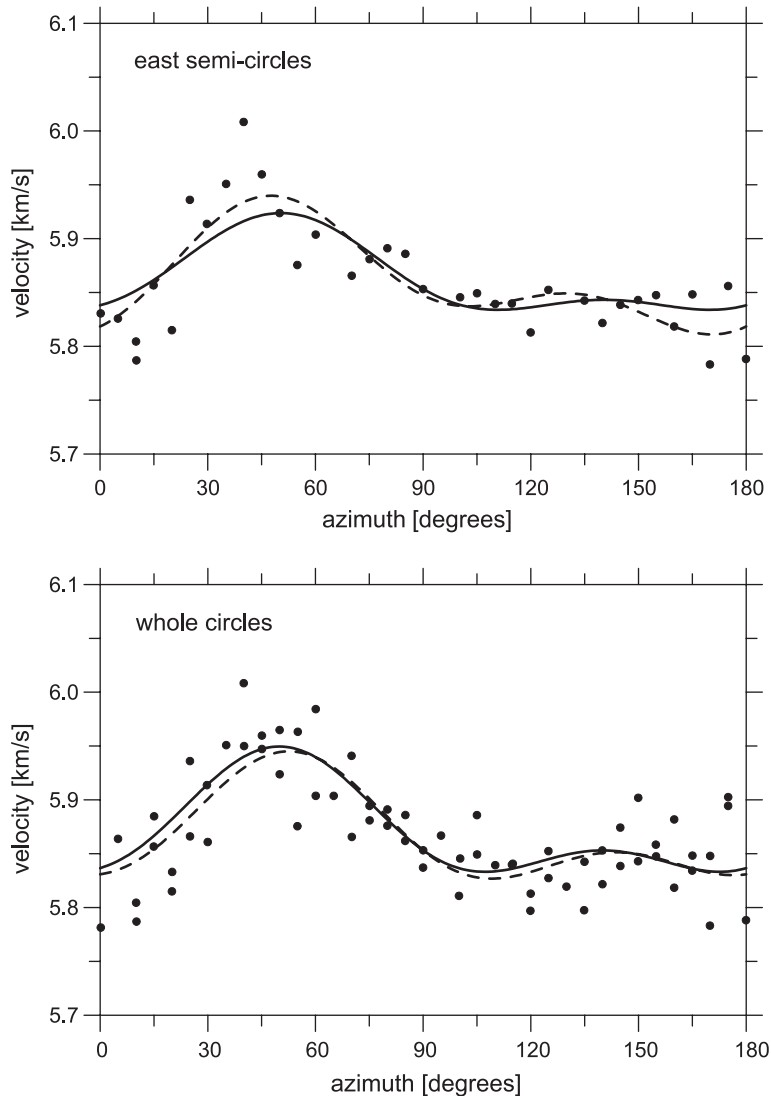
Fig. 10. Optimum anisotropy models. The azimuthal variation of the *Pg* velocity is shown for optimum weak anisotropy (dashed line) and weak transverse isotropy (solid line) models. The models are calculated from original travel times (marked by dots) measured along the east semicircles (upper plot) and from the corrected travel times measured along the whole circles.

crack-induced anisotropy in the uppermost crust is assumed to be at least as significant as the other types of anisotropy (Crampin, 1994; Rabbel, 1994; Rabbel and Mooney, 1996; Rasolofosaon et al., 2000). The minor contribution of the crack-induced anisotropy in the studied area might be explained by the presence of a small present-day deviatoric horizontal stress in the region. This would prevent a remarkable crack-induced anisotropy from devel-

oping. We can also speculate that cracks, oriented perpendicularly to rock foliation, affect the resultant velocity variation and cause its complex form (see Fig. 10). If so, the cracks should be water saturated and the strength of crack-induced anisotropy does not exceed 1%.

Interestingly, similar anisotropy values as found for the upper crust in the Moldanubian and in the entire Bohemian Massif (Růžek et al., 2003) have

been detected also for the uppermost mantle studied by *Pn* waves. So far, the *Pn* anisotropy has not been studied in the Moldanubian part of the Bohemian Massif, but it was studied in the west from the Bohemian Massif. For example, Enderle et al. (1996) updated the interpretation of Bamford (1977) based on refraction experiments, and reported the *Pn* anisotropy of 3–4% immediately below the Moho with the maximum velocity in the direction N31°E. Song et al. (2001) studied the *Pn* anisotropy in the western part of the Bohemian Massif and in Germany using regional earthquakes and found anisotropy of 3.5–6% with the maximum velocity in the direction ~N25°E. Plenefisch et al. (1994) investigated 22 regional earthquakes in SW Germany and northern Switzerland and found anisotropy of 7% with the maximum velocity in the direction ~N50°E. The similar fast directions for the upper crustal and uppermost mantle anisotropy suggest a stable pattern of anisotropy orientation in the crust and the uppermost mantle in the Bohemian Massif and adjacent areas. This might indicate a common tectonic origin of crustal and uppermost mantle anisotropy. The anisotropy was probably induced by processes during Variscan orogeny when the Bohemian Massif was sandwiched between opposing subduction zones of NE–SW trending and when the preferential orientation of micro- and macrostructural fabrics was imprinted.

Acknowledgements

References

Babuška, V., Cara, M., 1991. Seismic Anisotropy in the Earth. Kluwer Academic Publishing, London.

Backus, G.E., 1965. Possible forms of seismic anisotropy of the uppermost mantle under oceans. J. Geophys. Res. 70, 3429–3439.

Bamford, D., 1977. *Pn* velocity anisotropy in a continental upper mantle. Geophys. J. R. Astron. Soc. 49, 29–48.

Berckhemer, H., Rauen, A., Winter, H., Kern, H., Kontny, A., Lienert, M., Nover, G., Pohl, J., Popp, T., Schult, A., Zinke, J., Soffel, H.C., 1997. Petrophysical properties of the 9-km-deep crustal section at KTB. J. Geophys. Res. 102, 18337–18361.

Brudy, M., Zoback, M.D., Fuchs, K., Rummel, F., Baumgärtner, J., 1997. Estimation of the complete stress tensor to 8 km depth in the KTB scientific drill holes: implications for crustal strength. J. Geophys. Res. 102, 18453–18475.

Brückl, E., Bodoky, T., Hegedüs, E., Hrubcová, P., Gosar, A., Grad, M., Guterch, A., Hajnal, Z., Keller, G.R., Špičák, A., Sumanovac, F., Thybo, H., Weber, F., ALP 2002 Working Group, 2003. ALP 2002 seismic experiment. Stud. Geophys. Geod. 47, 671–679.

Chlupáčová, M., Skácelová, Z., Nehybka, V., 2003. *P*-wave anisotropy of rocks from the seismic area in western Bohemia. J. Geodyn. 35, 45–57.

Crampin, S., 1994. The fracture criticality of crustal rocks. Geophys. J. Int. 118, 428–438.

Dallmeyer, D., Franke, W., Weber, K., 1995. Pre-Permian Geology of Central and Eastern Europe. Springer-Verlag, New York.

Enderle, U., Mechie, J., Sobolev, S., Fuchs, K., 1996. Seismic anisotropy within the uppermost mantle of southern Germany. Geophys. J. Int. 125, 747–767.

Fusán, O., Kodym, O., Matějka, A., 1993. Geological map of the Czech Republic 1:1000000, uncovered. Czech Geological Survey.

Guterch, A., Grad, M., Keller, G.R., 2001. Seismologists celebrate the new millennium with an experiment in central Europe, EOS Trans. 82 American Geophysical Union 529, 534, 536.

Guterch, A., Grad, M., Keller, G.R., Posgay, K., Vozár, J., Špičák, A., Brückl, E., Hajnal, Z., Thybo, H., Selvi, O., CELEBRATION 2000 Working Group, 2003. CELEBRATION 2000 seismic experiment. Stud. Geophys. Geod. 47, 659–669.

Jahns, E., Rabbel, W., Siegesmund, S., 1996. Quantified seismic anisotropy at different scales: a case study from the KTB crustal segment. Z. Geol. Wiss. 24, 729–740.

Kaneshima, S., Ando, M., Kimura, S., 1988. Evidence from shear-wave splitting for the restriction of seismic anisotropy to the upper crust. Nature 335, 627–629.

Kern, H., Schmidt, R., 1990. Physical properties of KTB core samples at simulated in situ conditions. Sci. Drill. 1, 217–223.

Kern, H., Schmidt, R., Popp, T., 1991. The velocity and density structure of the 4000 m crustal segment at the KTB drilling site and their relationship to lithological and microstructural characteristics of the rocks: an experimental approach. Sci. Drill. 2, 130–145.

Málek, J., Brož, M., Fischer, T., Horálek, J., Hrubcová, P., Janský, J., Novotný, O., Růžek, B., 2001. Seismic measurements along short profiles in western Bohemia during the Celebration 2000 experiment. Acta Mont., Ser. A Geodyn. 18, 15–28.

Martínková, M., Pros, Z., Klíma, K., Lokajíček, T., Kotková, J., 2000. Experimentally determined *P*-wave velocity anisotropy for rocks related to the western Bohemia seismoactive region. Stud. Geophys. Geod. 44, 581–589.

Matte, Ph., Maluski, H., Rajlich, P., Franke, W., 1990. Terrane boundaries in the Bohemian Massif: result of large-scale Variscan shearing. Tectonophysics 177, 151–170.

Müller, B., Zoback, M.L., Fuchs, K., Mastin, L., Gregersen, S., Pavoni, N., Stephansson, O., Ljunggren, C., 1992. Regional patterns of tectonic stress in Europe. J. Geophys. Res. 97, 11783–11803.

Peška, P., 1992. Stress indications in the Bohemian Massif: reinterpretation of borehole televiewer data. Stud. Geophys. Geod. 36, 307–323.

Pitra, P., Burg, J.P., Guiraud, M., 1999. Late Variscan strike-slip tectonics between the Tepla-Barrandian and Moldanubian Terranes (Czech Bohemian Massif): petrostructural evidence. J. Geol. Soc. (Lond.) 156, 1003–1020.

Plenefisch, T., Faber, S., Bonjer, K.-P., 1994. Investigations of *Sn* and *Pn* phases in the area of the upper Rhine Graben and northern Switzerland. Geophys. J. Int. 119, 402–420.

Plomerová, J., Babuška, V., Ruprechtová, L., 1981. Travel times of seismic waves propagating to the Bohemian Massif from the South-West direction. Stud. Geophys. Geod. 25, 356–365.

Plomerová, J., Babuška, V., Ruprechtová, L., 1984. Velocities of seismic waves propagating through the Bohemian Massif from foci in Poland. Stud. Geophys. Geod. 28, 56–66.

Pros, Z., Lokajíček, T., Přikryl, R., Špičák, A., Vajdová, V., Klíma, K., 1998. Elastic parameters of West Bohemian granites under hydrostatic pressure. Pure Appl. Geophys. 151, 631–646.

Rabbel, W., 1994. Seismic anisotropy at the Continental Deep Drilling Site (Germany). Tectonophysics 232, 329–341.

Rabbel, W., Mooney, W.D., 1996. Seismic anisotropy of the crystalline crust: what does it tell us? Terra Nova 8, 16–21.

Rasolofosaon, P.N.J., Rabbel, W., Siegesmund, S., Vollbrecht, A., 2000. Characterization of crack distribution: fabric analysis versus ultrasonic inversion. Geophys. J. Int. 141, 413–424.

Růžek, B., Vavryčuk, V., Hrubcová, P., Zedník, J., the CELEBRATION Working Group, 2003. Crustal anisotropy in the Bohemian Massif, Czech Republic: observations based on Central European Lithospheric Experiment Based on Refraction (CELEBRATION) 2000. J. Geophys. Res. 108 (B8), 2392.

Schulmann, K., Plomerová, J., Babuška, V., Lexa, O., 2002. A kinematic model of the structural development of the Moldanubian root duing the Variscan orogeny based on correlation of crustal and mantle lithosphere fabrics. Geolines 14, 82–84.

Shearer, P.M., 1999. Introduction to Seismology. Cambridge Univ. Press, Cambridge.

Song, L.-P., Koch, M., Koch, K., Schlittenhardt, J., 2001. Isotropic and anisotropic *Pn* velocity inversion of regional earthquake traveltimes underneath Germany. Geophys. J. Int. 146, 795–800.

Vavryčuk, V., 1993. Crustal anisotropy from local observations of shear-wave splitting in West Bohemia, Czech Republic. Bull. Seismol. Soc. Am. 83, 1420–1441.

Vavryčuk, V., 1995. Reply to comments on "Crustal anisotropy from local observations of shear-wave splitting in West Bohemia, Czech Republic" by G.H.R. Bokelmann and J. Kawahara: Can the Hudson crack model describe behavior of real cracks? Bull. Seismol. Soc. Am. 85, 661–664.